B

Ba

▶ Barium(II) Transport in Potassium(I) and Calcium(II) Membrane Channels

Bacterial Calcium Binding Proteins

Delfina C. Domínguez[1] and Marianna Patrauchan[2]
[1]College of Health Sciences, The University of Texas at El Paso, El Paso, TX, USA
[2]Department of Microbiology and Molecular Genetics, College of Arts and Sciences, Oklahoma State University, Stillwater, OK, USA

Synonyms

Calerythrin; Calmodulin; Calsymin; EF-hand proteins

Definition

Bacterial proteins that bind calcium and are implicated in the regulation of various cellular events. These proteins appear to be involved in a wide variety of functions including chemotaxis, heat shock, pathogenesis, transport (influx and efflux), cell differentiation, and cell signaling.

Background

The calcium ion (Ca^{2+}) is perhaps the most important intracellular messenger in eukaryotes and regulates many cellular processes including cell differentiation, movement, cell cycle, transport mechanisms, and gene expression (Celio et al. 1996). Many effects of Ca^{2+} are mediated by ▶ calcium-binding proteins (CaBPs). Some of these proteins act as Ca^{2+} reservoirs or buffers. More specialized CaBPs such as calmodulin, act as signal transducers activating phosphorylation cascades leading to regulation in gene expression, and control of Ca^{2+} channel activity.

In prokaryotes, a similar role for Ca^{2+} has been proposed but is still not well defined. Ca^{2+} has been implicated in various bacterial physiological processes such as spore formation, chemotaxis, heterocyst differentiation, transport, and virulence. Several reports have shown that bacteria are capable of maintaining intracellular ▶ Ca^{2+} homeostasis, and Ca^{2+} transients are produced in response to adaptation to nitrogen starvation, and environmental stress (reviewed in Dominguez 2004). These findings as well as the demonstrated effect of Ca^{2+} on gene expression suggest a regulatory role of Ca^{2+} in bacterial physiology.

Sequence analyses of prokaryotic genomes indicate the presence of CaBPs proteins with different Ca^{2}-binding motifs (Zhou, et al. 2006). EF-hand containing proteins have been documented in several genera of bacteria (Dominguez 2004; Norris et al. 1996). While the genes of some CaBPs have been cloned and partially characterized, their functional activity remains to be investigated. Although bacterial cells appear to be equipped with the appropriate components (efflux and influx mechanisms, proteins kinases, Ca^{2+} homeostasis) of Ca^{2+} signaling networks, a physiologically integrated signal transduction system(s) remains to be characterized.

V.N. Uversky et al. (eds.), *Encyclopedia of Metalloproteins*, DOI 10.1007/978-1-4614-1533-6,

Bacterial Calcium Binding Proteins, Table 1 Bacterial proteins containing EF-hand- and EF-hand-like motifs

Protein	Organism	Motif	Deviation from EF-hand	References
Calerythrin	*Saccharopolyspora erythrea*	Helix-loop-helix	None	Michiels et al. (2002)
Calsymin	*Rhizobium etli*	Helix-loop-helix	None	Michiels et al. (2002)
Glucanotransferase	*Thermotoga maritime*	Helix-loop-helix	Shorter loop	Zhou et al. (2006)
Slt35	*Escherichia coli*	Helix-loop-helix	Longer loop	Zhou et al. (2006)
Protective antigen	*Bacillus anthracis*	Loop-loop-helix	Entering helix missing	Zhou et al. (2006)
Dockerin	*Clostridium thermocellum*	Loop-loop-helix	Entering helix missing	Zhou et al. (2006)
Galactose-binding protein	*Salmonella typhimurium*	Helix-loop-strand	Exiting helix missing	Zhou et al. (2006)
Alginate-binding protein	*Sphingomonas* sp	Helix-loop-strand	Exiting helix missing	Zhou et al. (2006)
Alkaline protease	*Pseudomonas aeruginosa*	Strand-loop-strand	Entering and exiting helix missing	Zhou et al. (2006)

Structure

EF-Hand Motif and EF-Hand Like Motif Proteins

Sequence analyses of prokaryotic genomes have revealed the presence of 397 putative EF-hand proteins. Most of these proteins with a few exceptions (Calerythrin from *Saccharopolyspora erythrea*, Calsymin from *Rhizobium etli*, the *Brucella abortus* Asp24 and *Streptomyces coelicolor* CabD) are hypothetical proteins (Michiels et al. 2002) and have not been functionally characterized. According to Zhou et al. (2006), most of the predicted EF-hand bacterial proteins contain a single EF-hand motif, while only 39 bacterial proteins have 2–6 EF-hand motifs, 16 of which were previously described in (Michiels et al. 2002).

The superfamily of EF-hand proteins is the largest and best characterized group of CaBPs. Since the description of the EF-hand motif in 1973, more than 66 subfamilies have been reported (Kretsinger 1976: Zhou et al. 2006). All these proteins share a common structural motif that consists of a Ca^{2+}-binding loop flanked by two α-helices. Acidic amino acids in the loop play a very important role in Ca^{2+} binding (Kretsinger 1976).

The canonical EF-hand loop binds Ca^{2+} via side chain oxygen atoms. Residues 1, 3, 5, 7, 9, and 12 of the loop provide the ligands for Ca^{2+} binding in a pentagonal bipyramidal fashion. Residues 1, 3, and 5 act as monodentate ligands, and residue 12, usually a Glu or Asp, is a bidentate Ca^{2+} ligand (Kretsinger 1976). The prokaryotic EF-hand domain shows great sequence and structural diversity. Some of these proteins differ in the length of the Ca^{2+}-binding loop, which may be shorter or longer than 12 residues, while other proteins deviate in the secondary structure flanking the Ca^{2+}-binding loop. However, the structural geometry of these proteins resembles the classical EF-hand motif (Zhou et al. 2006).

Five classes of EF-hand and EF-hand-like motifs have been reported in bacteria (Table 1). They include (1) the typical helix-loop helix EF-hand structure seen in Calerythrin and Calsymin, (2) the extracellular Ca^{2+}-binding region (Excalibur) with a shorter loop containing 10 residue motif DxDxDGxxCE found in various bacteria, (3) the longer 15-residue Ca^{2+}-binding loop seen in the *E. coli* lytic transglycosylase B, and (4) and (5) classes lacking the first or second helix as described in the *C. thermocellum* dockerin and the *Sphingomonas* sp. alginate-binding protein, respectively (Zhou et al. 2006).

Ca^{2+}-Binding ß-Roll Motif

Many Gram-negative bacteria secrete proteins with a ß-roll or parallel ß-helix structure, which contains multiple Ca^{2+}-binding and glycine-rich sequence motifs. These proteins are secreted by the Type 1 secretion system (T1SS) and often have been linked to pathogenesis. Many of these proteins contain a so called repeats-in-toxin (RTX) domain located upstream of the C-terminal uncleaved secretion signal. The RTX is found in several families of proteins including extracellular lipases, proteases, epimerases, and hemolytic toxins.

The RTX domain consists of tandem repeating nonamers of the sequence GGXGXDXUX, in which U is an aliphatic amino acid and X is any amino acid. The first six amino acids bind Ca^{2+} and the last three residues form a ß-strand. The number of tandem repeats varies from 5 to 45. The highly conserved aspartate is required for Ca^{2+} binding and without Ca^{2+} the beta roll structure is not formed. It is important to point out that Ca^{2+} is essential for RTX proteins folding, which takes place outside the cell (Michiels et al. 2002).

Completion of the genome sequence in *Mycobacterium tuberculosis* revealed the presence of a family of proteins with the sequence signature PE_PGRS. The PE domain is linked to a glycine-rich sequence known as the polymorphic GC-rich repetitive sequence (PGRS) region, which has been used in fingerprinting of *M. tuberculosis* clinical isolates. These proteins appear to have multiple Ca^{2+}-binding and glycine-rich motifs (GGXGXD/NXUX) as found in the RTX toxins. It is suggested that these proteins may be involved in host-pathogen interactions (Michiels et al. 2002).

Ca^{2+}-Binding Greek Key Motif

The ß-γ-crystallin superfamily includes Ca^{2+}-binding proteins found in various taxa including eukaryotes, eubacteria, and archea. In eukaryotes, ß-γ-crystallins are the major structural proteins of the lens. The common topological feature of these proteins is a double Greek key motif arranged as four adjacent antiparallel ß-strands sharing the third ß-strand with the opposite motif and forming a domain (Sharma and Balasubramanian 1996). ß-γ-crystallins from all of the three kingdoms showed that Ca^{2+} coordination is conserved in the form of N/D-N/D-#-I-S/T-S, in which the residue occupying the position # provides a main chain carbonyl for direct Ca^{2+} coordination, and the nonpolar residue I contributes to the hydrophobic core of the domain. In contrast to the EF-hand superfamily, ß-γ-crystallins showed Ca^{2+}-binding affinities within the μM range (as often seen in extracellular CaBPs), whereas Ca^{2+}-sensors of the EF-hand superfamily exhibit higher Ca^{2+}-binding affinities in the lower μM to nM range (Kretsinger 1976). The binding of Ca^{2+} produces a variety of physicochemical responses ranging from sequestration to stabilization.

Bacterial proteins with sequence conservation and three-dimensional structure closely related to ß-γ-crystallins include protein S from *Myxococcus xanthus*, *Yersinia pestis*, and the M-crystallin from the archaeon *Methanosarcina acetivorans*. Protein S (PS) is a monomeric CaBP that has two Ca^{2+}-binding domains, each domain consisting of two dissimilar Greek key motifs. PS is a spore-coat-forming protein, whose expression increases during starvation. This protein protects the organism over a long period of desiccation in a Ca^{2+}-dependent manner.

The *Y. pestis* CO92 crystallin is a putative secreted protein. The protein has a unique AA and BB type combination instead of the typical AB or BA found in other members of the ß-γ-crystallin superfamily. In the absence of Ca^{2+} the domains are intrinsically unstructured and only in the presence of Ca^{2+}, acquire their ß-γ-crystallin fold.

The M-crystallin from the archaeon *M. acetivorans* has been recently added to the ß-γ-crystallin superfamily. The protein appears to have a remarkable structural similarity with vertebrate ß-γ-crystallins. M-crystallin has a typical AB-type Greek key motif arrangement with Ca^{2+}-binding properties (packing and conformational changes) more similar to vertebrate lens proteins than to their microbial homologues. Similar to other lens ß- and γ- crystallins, binding of Ca^{2+} produce no noticeable conformational changes (Barnwal et al. 2009). The presence of the Ca^{2+}-binding motifs needs to be tested for functional necessity if not for viability of the organisms.

Evolution

Based on the discovery of bacterial proteins with similarity to calmodulin, the idea that CaBPs originated from prokaryotes was first proposed in 1987 by Swan and coworkers. Later, the prediction and identification of various EF-hands in the genus *Streptomyces* lead to the assumption that CaBPs evolved from Gram positive bacteria. The continued increase of genomic information and computational analyses during the past years have shown that prokaryotic EF-hands exhibit great diversity and high structural variability within the Ca^{2+} loop (Zhou et al. 2006). Based on these observations, it was proposed that the evolution of EF-hand and EF-hand-like proteins in bacteria is far more complex than previously anticipated, and they postulated that the canonical EF-hand motif could be the most visible, but perhaps not the most ancient.

The recent findings of single-handed EF motifs in prokaryotes raised the possibility that the EF-hand motif could be a structural "mobile unit" for Ca^{2+} binding that may have undergone modifications during evolution and had been incorporated into host proteins. Since pseudo-EF-hand proteins are absent from bacterial genomes, they are likely to be phylogenetically younger than canonical EF-hand motifs (Zhou et al. 2006).

Functions

Calcium Transport and Transporters

Three major types of ▶ Ca^{2+} transport systems have been described in prokaryotes: Ca^{2+} exchangers, ▶ Ca^{2+} ATPases, and polyhydroxybutyrate – polyphosphate (PHB-PP) complexes. However, only a few of these have been characterized biochemically, and their physiological significance has yet to be demonstrated.

Calcium Exchangers

In most bacteria Ca^{2+} is exported by Ca^{2+} exchangers, Ca^{2+}/H^+ or Ca^{2+}/Na^+ antiporters. These are low-affinity Ca^{2+} transport systems that use the energy stored in the electrochemical gradient of ions. Depending on the gradient, exchangers can also operate in the reverse (Ca^{2+} entry) direction. Ca^{2+} exchangers differ in ion specificity and have been identified in a number of bacterial genera (Norris et al. 1996). Major examples include *E. coli* proteins ChaA, YrbG, and PitB that have been reported as Ca^{2+}/H^+, Ca^{2+}/Na^+ antiporters (Saaf et al. 2001) and Ca^{2+}/PO_4^{3-} symporter (van Veen et al. 1994), respectively. ChaA may also exhibit Na^+/H^+, and K^+/H^+ antiport activity and play a role in tolerance to high concentrations of Ca^{2+} and Na^+. An acidic motif, EHEDDSDDDD-209 in ChaA is strikingly similar to a motif in ▶ calsequestrin and was proposed to be used as a signature motif for identifying genes encoding Ca^{2+}/H^+ antiporter activity or other Ca^{2+}-dependent activities. YrbG represents a large family of Ca^{2+}/Na^+ exchangers that includes both prokaryotic and eukaryotic proteins. Finally, PitB transports Ca^{2+} as a metal phosphate ($MeHPO_4$) complex in symport with H^+ (Norris et al. 1996).

Ca^{2+} ATPases

Ca^{2+} ATPases are mostly high-affinity Ca^{2+} pumps that export Ca^{2+} from the cytosol to the extracellular environment by using the energy stored in ATP. Several P-type Ca^{2+} translocating ATPases have been described in bacteria and also in the archaeon *Methanobacterium thermoautotrophicum*. These proteins are homologous to the SERCA Ca^{2+} transporter from sacroplasmic reticulum of eukaryotes, and transiently form a phosphorylated intermediate by the transfer of the γ-phosphate of ATP to an aspartic acid residue of the protein (reviewed in Dominguez 2004).

Polyhydroxybutyrate – Polyphosphate (PHB-PP) Complexes

PHB-PP complexes form non-proteinaceous voltage-gated ion channels in planar lipid bilayer. The channels are highly selective for Ca^{2+} over Na^+ at physiological pH (reviewed in Shemarova and Nesterov 2005) and can coexport Ca^{2+} and PP. The complexes are highly abundant in stationary growth phase cells and display many characteristics of protein Ca^{2+} channels: voltage-activated, selective for divalent cations, permeant to Ca^{2+}, Sr^{2+} and Ba^{2+}, and blocked in a concentration-dependent manner by La^{3+}, Co^{2+}, Cd^{2+} and Mg^{2+}.

In addition to translocating Ca^{2+} and maintaining Ca^{2+} homeostasis, Ca^{2+} transporters may play other physiological roles including chemotaxis, sporulation, pathogenesis and survival in a host. These findings provide further support for the idea that Ca^{2+} transport is regulated in bacteria even if the specific transporters and their function(s) remains to be demonstrated unequivocally. Moreover, the data suggest that the Ca^{2+} flux systems may present new targets for future antimicrobial agents.

Calcium Signaling

Ca^{2+} signaling in eukaryotes has long been understood; however, in prokaryotes, it is less well defined. Earlier it has been shown that Ca^{2+} is implicated in the regulation of a number of physiological processes including the expression of virulence factors, chemotaxis, cell division, competence, and autolysis, spore germination, and acid tolerance (reviewed in Dominguez 2004; Shemarova and Nesterov 2005). More recent studies provide further evidence that Ca^{2+} is involved in the regulation of gene expression. The responding processes include iron acquisition, biosynthesis of pyocyanin and proteases, quinolone signaling, nitrogen metabolism, oxidative, and general stress

responses. However, the mechanisms of such regulation are not clear.

Sensing extracellular signals may occur via two different mechanisms: two-component regulators or by signal uptake followed by signal transduction or relay. A two-component *ca*lcium-*r*egulated system *carSR* has been shown to negatively regulate polysaccharide production and biofilm formation in *Vibrio cholera* (Bilecen and Yildiz 2009). The AtoS-AtoC two-component system in *E. coli* was shown to regulate the effect of extracellular Ca^{2+} on biosynthesis of poly-(R)-3-hydroxybutyrate. On the other hand, increased cytosolic Ca^{2+} was shown to alter gene transcription *E. coli* (Naseem et al. 2009).

CaBPs are most likely candidates for binding Ca^{2+} and transducing or relaying Ca^{2+} signal. Thus, for example, a four-EF-hand CaBP CabC has been shown to bind Ca^{2+} and regulate aerial hyphal formation in *Streptomyces coelicolor* (Wang et al. 2008).

Finally, a variety of external stimuli affect cytosolic maintenance of Ca^{2+} in bacteria (reviewed in Shemarova and Nesterov 2005). These include photosensitization in *Propionibacterium acnes* and oxidative stress in *B. subtilis*. Also, butane 2,3-diol, a glycerol fermentation product commonly produced in a human gut, activates Ca^{2+} transients in *E. coli*, thus suggesting the role of Ca^{2+} in bacteria-host cell signaling.

Concluding Remarks

It is clear that evidence in support of the importance of calcium in bacteria is accumulating. However, much work needs to be done to identify and characterize the physiologically important CaBPs. A full assessment of the precise regulatory mechanisms that convert changes in cytosolic free Ca^{2+} into physiological functions awaits further analysis.

Cross-References

- ▶ Biological Copper Transport
- ▶ Calcium ATPase
- ▶ Calcium-Binding Proteins
- ▶ Calmodulin
- ▶ Calsequestrin
- ▶ Penta-EF-Hand Calcium-Binding Proteins

References

Barnwal RP et al (2009) Solution structure and calcium-binding properties of M-crystallin, a primordial betagamma-crystallin from archaea. J Mol Biol 386:675–689

Bilecen K, Yildiz FH (2009) Identification of a calcium-controlled negative regulatory system affecting *Vibrio cholerae* biofilm formation. Environ Microbiol 11: 2015–2029

Celio MR, Tomas P, Shawler B (1996) Guidebook to the calcium-binding proteins. Sambrook & Tooze, Oxford University Press, Oxford

Dominguez DC (2004) Calcium signalling in bacteria. Mol Microbiol 54:291–297

Kretsinger RH (1976) Calcium-binding proteins. Annu Rev Biochem 45:239–266

Michiels J et al (2002) The functions of Ca(2+) in bacteria: a role for EF-hand proteins? Trends Microbiol 10:87–93

Naseem R et al (2009) ATP regulates calcium efflux and growth in *E. coli*. J Mol Biol 391:42–56

Norris et al (1996) "Bacterial calcium-binding proteins". In: Celio MR, Pauls TL, Schwaller B (eds) Sambrook & Tooze. Oxford University Press, pp 209–212

Saaf A et al (2001) The internal repeats in the Na+/Ca^{2+} exchanger-related Escherichia coli protein YrbG have opposite membrane topologies. J biol chem 276:18905–18907

Sharma Y, Balasubramanian D (1996) "Crystallins". In: Celio MR, Pauls TL, Schwaller B (eds) Sambrook & Tooze. Oxford University Press, pp 225–228

Shemarova IV, Nesterov VP (2005) Evolution of mechanisms of calcium signaling: the role of calcium ions in signal transduction in prokaryotes. Zh Evol Biokhim Fiziol 41: 12–17

van Veen HW et al (1994) Translocation of metal phosphate via the phosphate inorganic transport system of Escherichia coli. Biochemistry 33:1766–1770

Wang SL et al (2008) CabC, an EF-hand calcium-binding protein, is involved in Ca2+-mediated regulation of spore germination and aerial hypha formation in *Streptomyces coelicolor*. J Bacteriol 190:4061–4068

Zhou Y et al (2006) Prediction of EF-hand calcium-binding proteins and analysis of bacterial EF-hand proteins. Proteins 65:643–655

Bacterial Mercury Resistance Proteins

Simon Silver and Le T. Phung
Department of Microbiology and Immunology, University of Illinois, Chicago, IL, USA

Synonyms

Microbial toxic mercury resistance; Proteins with mercury as "natural" substrate

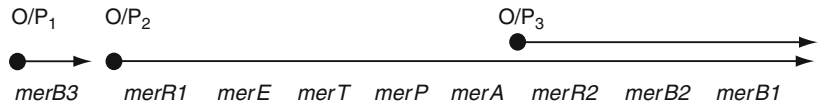

Bacterial Mercury Resistance Proteins, Fig. 1 The genes of the *Bacillus mer* gene complex, i.e., the *mer* operon. OP, operator/promoter mRNA initiation sites; *merR* regulatory gene; *merE* and *merT* genes for membrane transport proteins; *merP* gene for outer surface mercury binding protein; *merA* gene for mercuric reductase enzyme; and *merB* genes for organomercurial lyase enzymes; → direction of mRNA synthesis. GenBank accession AB066362, GI 15076639 (Chen et al. 2008)

Definition

Bacteria carry out chemical transformations of mercury compounds. Often these transformations result from bacterial resistance systems to inorganic mercury (Hg^{2+}) and to organomercurials (such as methylmercury and phenylmercury). There are four types of mercury-specific proteins: detoxifying enzymes producing less toxic products, membrane transport proteins that bring Hg^{2+} into the cells to be detoxified, mercury-binding proteins at the outer cell surface, and DNA-binding transcriptional regulatory proteins governing mRNA synthesis (Barkay et al. 2003; Silver and Phung 2005; Silver and Hobman 2007).

Mercury Resistance (the mer Operon)

The genes for bacterial mercury resistance are clustered in a "*mer* operon" of contiguous genes that are regulated together and are found widely on the plasmids and the chromosomes of both gram-positive and gram-negative bacteria. The number of genes (and therefore corresponding protein products) in different bacteria range from fewer to as many as 9, but in all cases include related protein products (Silver and Phung 2005). Figure 1 shows the genes involved in mercury resistance in *Bacillus*, the most complex of such determinants to have been studied in detail. It includes 3 *merB* genes for organomercurial lyase enzymes, 2 *merR* genes for regulatory proteins, and three operator/promoter mRNA transcriptional control sites (Chen et al. 2008).

Mercuric Reductase Enzyme

Mercuric reductase is a homodimeric protein, whose two active sites lie at the interface between the subunits (Fig. 2a), and include a redox-active cysteine pair, closely homologous to that in the paralogous proteins glutathione reductase and lipoamide dehydrogenase (Ledwidge et al. 2005). The cysteine pair carries electrons transferred from a loosely bound NAD(P)H first to a tightly bound flavin adenine dinucleotide (FAD) next and finally to the active site cysteines, where the substrate Hg^{2+} is reduced to Hg^0 (which is then spontaneously released, Fig. 3) (Silver and Phung 2005). This structural and functional homology raises the question of which enzyme came first in early cell evolution; and we hypothesize that toxic mercury was present early after the origin of life, over three billion years ago, perhaps before the appearance of glutathione and lipoamide. Mercuric reductase is the oldest.

With changing scientific communication, the Wikipedia report (http://en.wikipedia.org/wiki/Mercury%28II%29_reductase) is a good source of current information. Mercuric reductase contains a number of functionally different regions (or domains), starting with a Hg^{2+}-binding domain of approximately 70 amino acids in length (with a cysteine pair dithiol; Fig. 2a) at the N-terminus and ending with a second Hg^{2+}-binding cysteine pair dithiol at the C-terminus of the polypeptide (Ledwidge et al. 2005). In between are the binding determinants of NADPH and FAD, as well as the active site sequence, including a third conserved cysteine pair (Figs. 2a and 3). The substrate Hg^{2+} is initially bound to the N-terminal cysteine pair of one subunit, then transferred to the C-terminal cysteine pair of the opposite subunit, and then to the active site cysteine pair at the interface of the first subunit, for reduction to Hg^0. The currently understood intermediate steps in the binding of Hg^0, electron transfer, and reduction are shown in Fig. 3.

Organomercurial Lyase Enzyme

Organomercurial lyases are small monomeric proteins (just over 200 amino acids in length; determined by the *merB* gene) that function via a biomolecular S_E2 electrophilic substitution reaction mechanism. H^+ originating from aspartic acid residue Asp99 adds to the carbon of the organomercurial (either alkyl such as in methyl- or ethyl-mercuric compounds or aromatic such as in phenylmercury) from the same side as the mercury (Barkay et al. 2003; Miller 2007). Hg-C bond cleavage

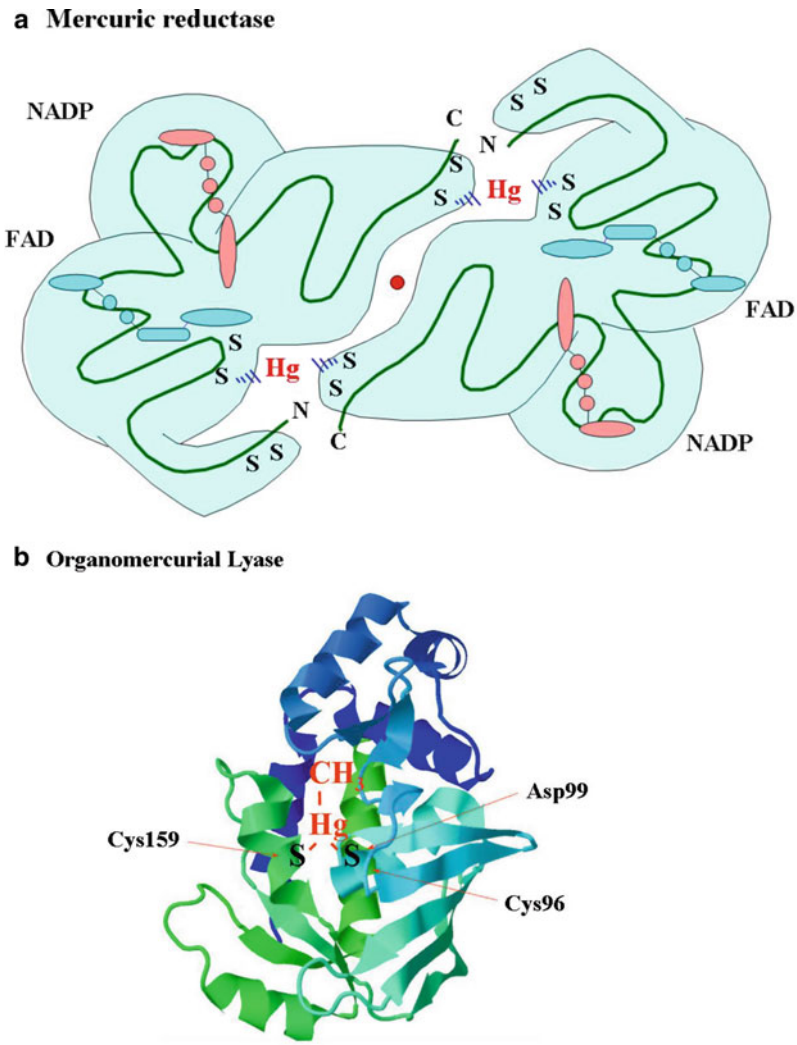

Bacterial Mercury Resistance Proteins, Fig. 2 (**a**) Mercuric reductase showing dimeric structure with bound NADP and FAD and cysteine pair thiols (Silver and Phung 2005) (cartoon adapted from RCSB PDB structure 1ZK7 and 1ZX9; see also Fig. 3) with Hg^{2+} bound at both active sites, although probably only one functions at a time; and (**b**) organomercurial lyase ribbon structure showing active site cysteine pair Cys96 Cys159 thiols and proton donor Asp99, with substrate-binding surface (Lafrance-Vanasse et al. 2009; Miller 2007; Parks et al. 2009) (Adapted from RCSB PDB database ID: 3F0O, viewed in Jmol; see also Fig. 4)

and H^+ addition occur. The currently understood steps of the reaction cycle are shown in Fig. 4 and the protein structure for MerB (which has been independently solved by NMR spectroscopy and by X-ray diffraction from crystalline MerB) is shown in Fig. 2b. An active site cysteine pair (Cys96 and Cys159) covalently binds Hg during the reaction. As a first step, the organomercurial compound enters an internalized active site and forms a Hg-S bond with the thiol from Cys96; the proton released from the Cys96 thiol protonates Asp99 (Fig. 4). Cys159 then forms a second Hg-S bond resulting in a trigonal R-HgS_2 intermediate. Finally, the H donated by Asp99 attacks and releases the RH product, with the addition of a water molecule at the position on the Hg^{2+} previously occupied by the organic R group.

Structural studies provide support for the mechanism proposed in Fig. 4 (Parks et al. 2009; Lafrance Vanasse et al. 2009), in addition to demonstrating the close proximity of Asp99, Cys96, and Cys159 in the protein molecule (Fig. 2b). The binding surface for the organomercurial substrate lies on a hydrophobic surface within the protein molecule. The N-terminal region of the MerB protein appears to function as a "lid" opening to accommodate the organomercurial substrate and then closing over the complex. How the organomercurial lyase substrate-binding surface accommodates different organomercurial groups

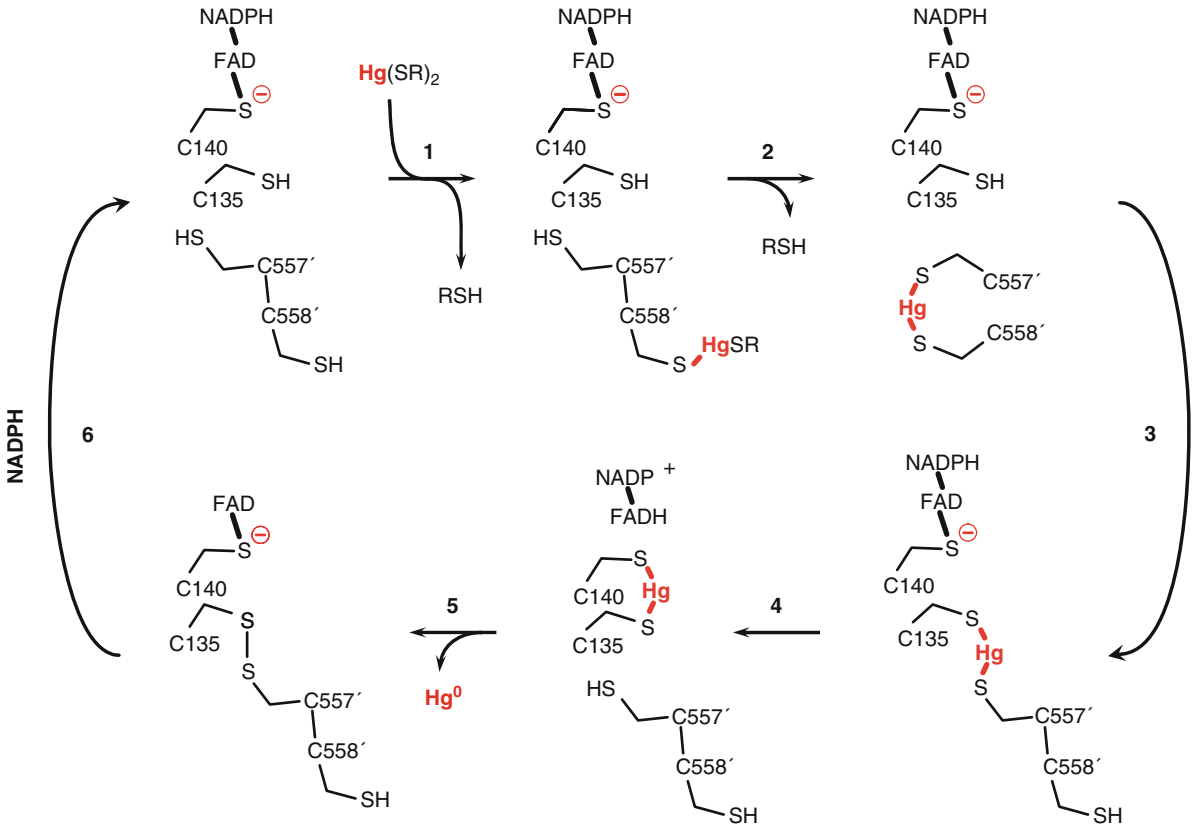

Bacterial Mercury Resistance Proteins, Fig. 3 The steps of mercuric reductase (MerA) activity (Silver and Phung 2005; Barkay et al. 2003). (1) Hg-dithiol substrate binding, *in vivo* directly from MerT protein or in vitro from glutathione or mercaptoethanol. (2) Release of second thiol linkage, and formation of di-cysteine bound Hg^{2+} at C-terminal of second subunit. (3) Transfer of Hg^{2+} to active site Cys135 of one subunit. (4) Formation of Cys135 Cys140 dithiol-bound Hg^{2+} at active site. (5) Reduction of Hg^{2+} to Hg^0 (with electrons from NADPH to FAD) and release of Hg^0. (6) Binding of NADPH to regenerate an active enzyme

[for example, small (methyl) and larger (phenyl)] is not understood. The physical basis for different versions of this MerB having different ranges of organomercurial substrates is also not known.

Whereas mercuric reductase constitutes a "sub-branch" paralogous group within the larger family of enzymes including glutathione reductase and lipoamide dehydrogenase, organomercurial lyases are essentially novel, lacking close homologs (Silver and Phung 2005). Nevertheless, both mercuric reductase and organomercurial lyase enzymes are found broadly among bacterial types, both Gram positive and Gram negative, indicating an ancient origin. There are also less-studied versions of mercuric reductase and organomercurial lyase genes found in a few Archaea; however, these genes and enzymes are not found in eukaryote organisms.

Mercury Transport and Binding Proteins

It seems counter-intuitive for bacteria to have a membrane transport system whose function is to bring the toxic cation Hg^{2+} from a relatively harmless position outside of the bacterial cell to inside the cytoplasm. However, uptake of Hg^{2+} via small membrane proteins is a well-studied process (Silver and Hobman 2007), and is part of all bacterial mercury resistance systems. A functional Hg^{2+} uptake system in the absence (due to mutation) of mercuric reductase causes the cells to be more sensitive ("hypersensitive") to Hg^{2+} than are bacteria lacking all mercury-related genes. The overall logic appears to be that the required electron donor NADPH is a high-energy molecule (like ATP) that cannot be released from the cell. Therefore, evolution resulted in an orderly tight pathway, functioning as a molecular "bucket brigade," starting

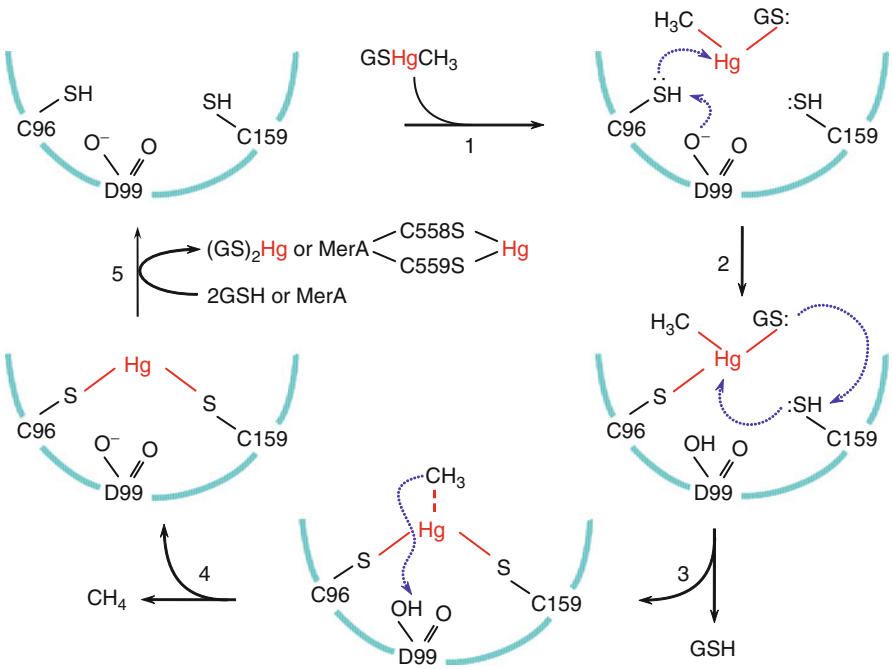

Bacterial Mercury Resistance Proteins, Fig. 4 The steps of organomercurial lyase (MerB) activity. (1) Binding substrate methylmercury coupled to glutathione (GS) to Cys96, and transfer of H^+ to Asp99. (2) Binding to second active site Cys159 thiol. (3) Release of reduced GSH. (4) Transfer of H^+ from Asp99 and release of CH_4. (5) Transfer of Hg^{2+} to GSH or directly to the MerA protein (Miller 2007; Silver and Phung 2005; Parks et al. 2009)

with the binding of Hg^{2+} at the cell surface, to movement across the cell membrane, and ending with binding of Hg^{2+} on mercuric reductase, without freely diffusible Hg^{2+} at any stage. Transport proteins constitute the initial stages of a cysteine pair to cysteine pair cascade, so that Hg^{2+} initially bound outside the cell surface is passed on from one cysteine pair to the next (the exchange frequency can be quite rapid) without ever being released free at any intermediate stage (as the release frequency would be low).

There are three modes of membrane-embedded Hg^{2+}-transport proteins found in the inner membranes of gram-negative bacteria and homologous proteins in gram-positive bacteria. The first one (identified from the genes of transposons Tn*21* and Tn*501*) is MerT, an unusual protein that spans the membrane three times (Fig. 5a) (Silver and Hobman 2007; Brown et al. 2002). There is a closely adjacent di-cysteine dithiol pair in the N-terminal alpha-helical region of MerT and a second di-cysteine dithiol pair in the cytoplasmic loop between the second and third alpha helices (Fig. 5a). All four cysteines are required for function and it is thought that Hg^{2+} is transferred initially from the small periplasmic MerP protein (see below) to the intramembrane cysteine pair, and then to the cytoplasmic cysteine pair in MerT, and finally directly to the N-terminal cysteine pair of a MerP-like domain at the N-terminus of mercuric reductase. The alternative membrane transport proteins, MerF (Howell et al. 2005) and MerC, have respectively two or four transmembrane alpha helices (Fig. 5a). However, both have an intramembrane N-terminal cysteine pair and a cytoplasmic loop cysteine pair, similar to MerT. The functional differences between these three membrane proteins, for example, binding of Hg^{2+} and movement from the membrane protein to mercuric reductase, are not known.

With mercury resistance systems of gram-negative bacteria, Hg^{2+} binding begins with highly specific binding in the periplasm to the small MerP protein (Steele and Opella 1997; Serre et al. 2004), a 72-amino-acid monomer required for transport of MerP across the membrane. The sequence and structure of MerP are unrelated to those of other periplasmic binding proteins. MerP has a tight $\beta1\alpha1\beta2\beta3\alpha2\beta4$ structure (Fig. 5b) with a conserved $GMTC14X_2C17$ Hg^{2+}-binding determinant in the exposed loop between the $\alpha1$ and $\beta1$ segments. Surprisingly a closely homologous approximately 70-amino-acid Hg^{2+}-binding domain is found also at the N-terminus of the larger mercuric reductase enzymes (Silver and Phung 2005), whose subunit contains 560 amino acids with one copy (as with transposons in gram-negative bacteria; Fig. 2a) or 630 amino acids with two tandem

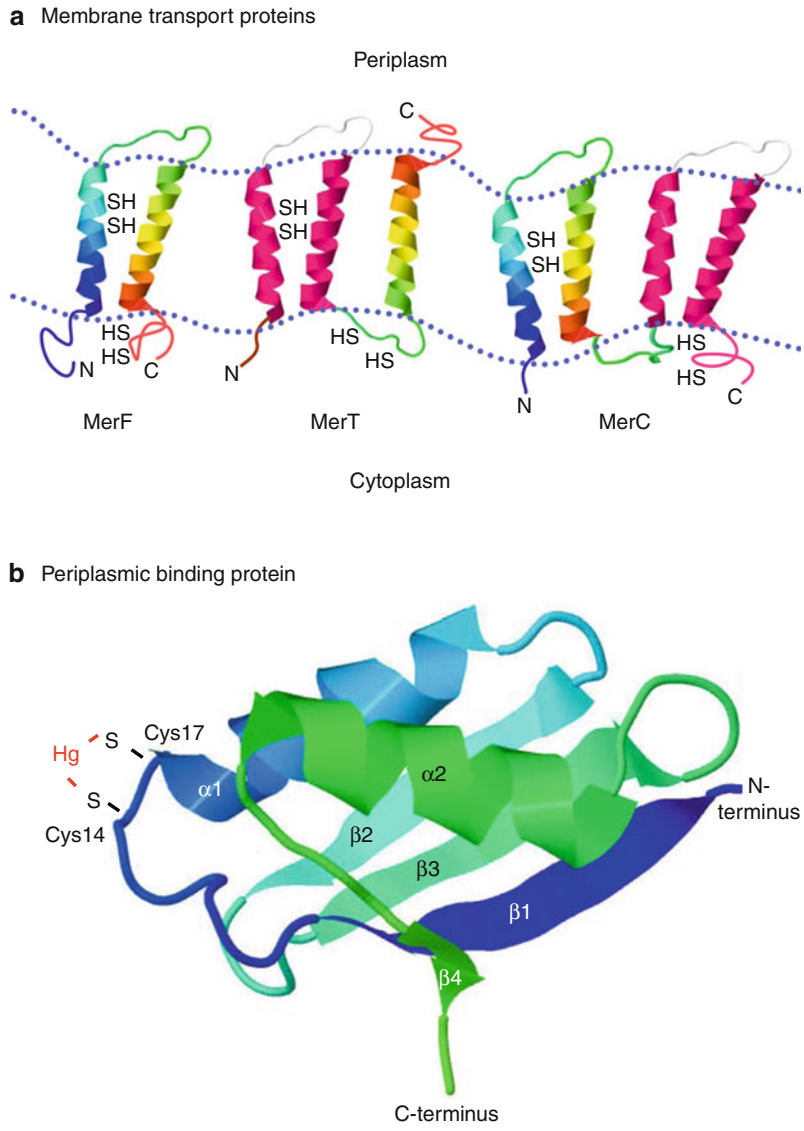

Bacterial Mercury Resistance Proteins, Fig. 5 (**a**) Mercury transport membrane proteins MerT, MerC, and MerF with cysteine pairs (SH) (Brown et al. 2002; Silver and Hobman 2007). The MerF structure is adapted from RCSB PDB database ID: 1WAZ, viewed in Jmol, and used to generate models for MerT and MerC. (**b**) The periplasmic MerP mercury-binding protein with the Cys14 Cys17 Hg^{2+} binding pair (Steele and Opella 1997), adapted from RCSB PDB database ID: 1OSD, viewed in Jmol

Hg^{2+}-binding domains (in gram-positive *Bacillus*). An exception is MerA of *Streptomyces*, which lacks this domain (and has about 480 amino acids). Closely related MerP-like cation-binding domains are found at the N-terminus of Cd^{2+}-resistance P-type ATPases in bacteria and Cu^{+}-transporting P-type ATPases in bacteria and humans (Silver and Phung 2005). The binding of Hg^{2+} by MerP has been well documented in protein structures for MerP with or without Hg^{2+} (Steele and Opella 1997). The basis of cation specificity with Hg^{2+} for MerP or Cd^{2+} or Cu^{2+} for homologs is, however, not known.

Transcriptional Regulatory Protein MerR

MerR, the transcriptional regulatory protein that binds to the DNA (operator/promotor region, OP; Fig. 1), was the first studied of what has subsequently been recognized as a larger class of such regulatory proteins (Barkay et al. 2003; Brown et al. 2003). MerR binds to the OP region of the DNA in both the absence and in the presence of Hg^{2+}. In the absence of Hg^{2+} (Fig. 6a), the −35 and −10 RNA polymerase–binding motifs in the DNA sequence are on opposite faces of the DNA (and in an unusually long nonfunctional distance) making it impossible for RNA polymerase to bind in

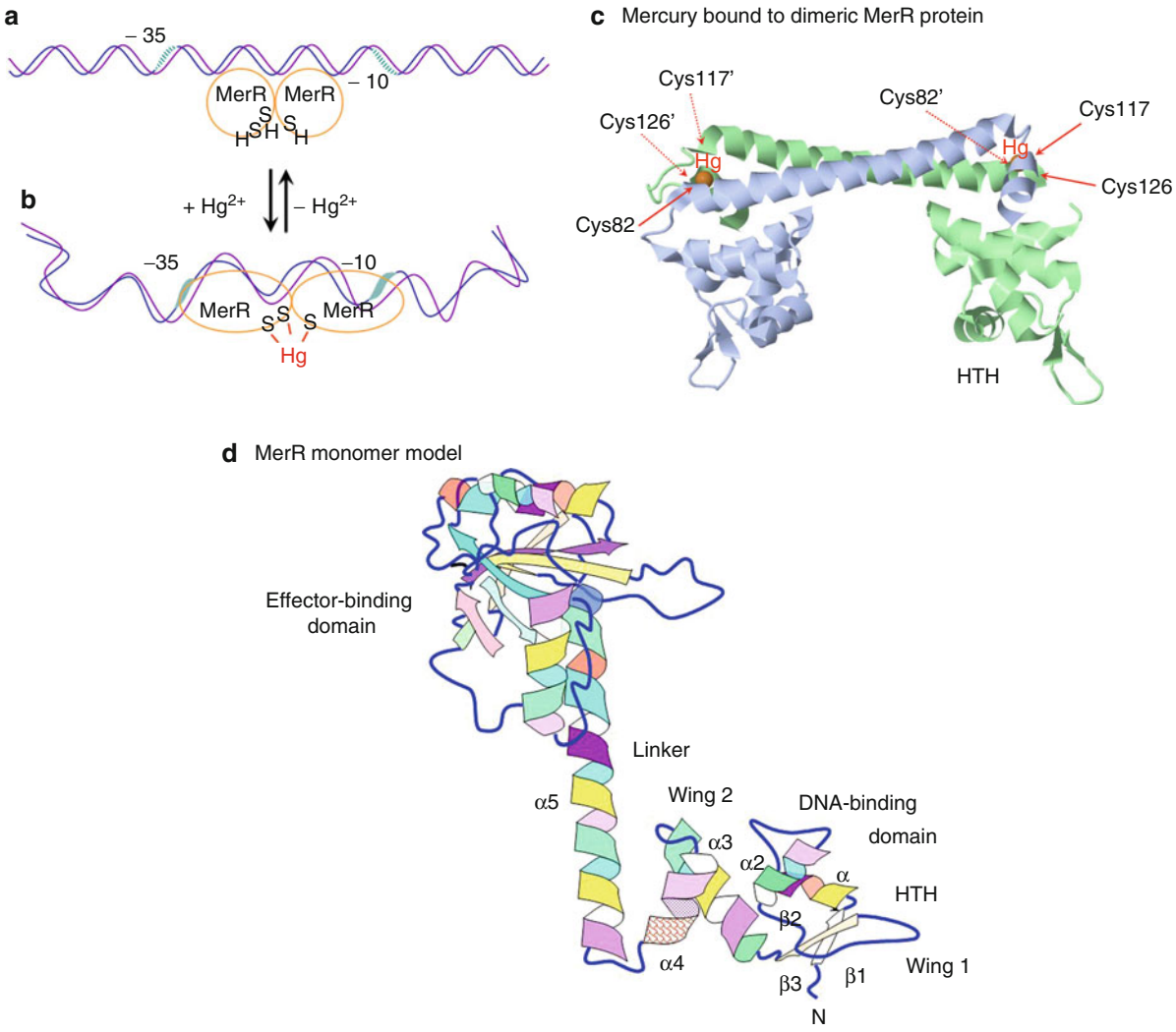

Bacterial Mercury Resistance Proteins, Fig. 6 (**a**) The transcriptional activator protein MerR bound to OP operator/promoter region DNA region without Hg^{2+} and (**b**) with Hg^{2+} with −35 and −10 RNA polymerase–binding sites on the same surface of the DNA with bending and twisting the DNA to "open" for RNA synthesis. (**c**) The structure of the MerR dimer with the three Hg^{2+}-binding cysteines (cysteines 117 and 126 of one monomer and cysteine 82' of the second monomer). One DNA-binding helix-turn-helix site is apparent in the structure (Modified from RCSB PDB database ID: 1Q05 biological assembly, viewed in Jmol for CueR, a close homolog of MerR) (Changela et al. 2003). (**d**) Structure of MerR monomer showing separate domains for Hg^{2+} binding and for binding to DNA (HTH, helix-turn-helix) connected by the long α5 alpha helix

a transcriptionally functional manner. DNA-bound MerR in the absence of Hg^{2+} therefore represses mRNA synthesis about 100-fold. Adding Hg^{2+} to MerR rotates the structure of the protein and results in a twisting and shortening of the DNA so that the −35 and −10 polymerase-binding motifs are properly positioned on the same surface, allowing RNA polymerase binding in a functional manner (Fig. 6b) (Utschig et al. 1995). The presence of Hg^{2+} stimulates mRNA synthesis about 100-fold – together making for an unusual 10,000-fold range of mRNA synthesis, from off to on. In the absence of Hg^{2+}, the MerR protein functions as a repressor, reducing transcription effectively to 0%; in the presence of Hg^{2+}, the unusual "twist and turn" of both the MerR protein and the DNA results in 100% maximum transcription.

Homodimeric MerR is a helix-turn-helix transcriptional regulator with amino acids 9 through 28 from the N-terminus forming an α1 helix-turn-α2 helix (HTH) DNA-binding motif (Fig. 6c and d) (Guo et al. 2010). A pair of long α helices (α5 and α5', one from each subunit) form the dimer subunit interface; and the MerR Hg^{2+}-binding sites are at the ends of helices α5 and α5', away from the DNA-binding HTH (Fig. 6c and d). Three cysteine residues, Cys82 of one subunit together with Cys117' and Cys126' of the other subunit, form one Hg^{2+}-binding site (Fig. 6c), but only one of the two sites binds Hg^{2+} at a time (Kaisa et al. 2011).

Mercury Oxidation by Catalase

The familiar enzyme hydroperoxidase-catalase, whose usual physiological function is to accelerate the rate of conversion of H_2O_2 to H_20, can also catalyze the oxidation of relatively unreactive mono-atomic Hg^0 (which is present in the cell as a gas) to more reactive Hg^{2+} (Smith et al. 1998). This enzyme is found broadly from *E. coli* (encoded by the *katG* gene) to humans and in the environment converts Hg^0 gas to water-soluble Hg^{2+}, completing the mercury cycle. Abiotic nonenzymatic oxidation of Hg^0 is probably responsible for atmospheric Hg^0 being deposited in the sea and lakes (Barkay et al. 2003). However, but catalase in animals is probably responsible for converting the nontoxic Hg^0 (breathed into the lungs and transferred into the red blood cells in the lungs) to Hg^{2+}, which remains in the body and can damage metabolism as a protein thiol poison.

Mercury Methylation

The methylating of inorganic Hg^{2+} to CH_3Hg^+ (methyl mercury) and then to some extent to dimethyl mercury, $(CH_3)_2Hg$, appears to be nonenzymatic and therefore not carried out directly by proteins. Methylation appears to result from cell-released methyl-cobalamin, as an inadvertent side reaction and not a favored process for that abundant cofactor (Silver and Phung 2005; Barkay et al. 2003). Mercury is not methylated with S-adenosylmethionine (SAM), as is inorganic arsenic.

Cross-References

► Arsenic-Induced Stress Proteins

References

Barkay T, Miller SM, Summers AO (2003) Bacterial mercury resistance from atoms to ecosystems. FEMS Microbiol Rev 27:355–384

Brown NL, Shih Y-C, Leang C, Glendinning KJ, Hobman JL, Wilson JR (2002) Mercury transport and resistance. Biochem Soc Trans 30:715–718

Brown NL, Stoyanov JV, Kidd SP, Hobman JL (2003) The MerR family of transcriptional regulators. FEMS Microbiol Rev 27:145–163

Changela A, Chen K, Xue Y, Holschen J, Outten CE, O'Halloran TV, Mondragon A (2003) Molecular basis of metal-ion selectivity and zeptomolar sensitivity by CueR. Science 301:1383–1387

Chen CY, Hsieh JL, Silver S, Endo G, Huang CC (2008) Interactions between two MerR regulators and three operator/promoter regions in the mercury resistance module of *Bacillus megaterium*. Biosci Biotechnol Biochem 72:2403–2410

Guo H-B, Johs A, Parks JM, Olliff L, Miller SM, Summers AO, Liang L, Smith JC (2010) Structure and conformational dynamics of the metalloregulator MerR upon binding of Hg (II). J Mol Biol 398:555–568

Howell SC, Mesleh MF, Opella SJ (2005) NMR structure determination of a membrane protein with two transmembrane helices in micelles: MerF of the bacterial mercury detoxification system. Biochemistry 44:5196–5206

Kaisa M, Hakkila KM, Nikander PA, Junttila SM, Lamminmäki UJ, Virta MP (2011) Cd-specific mutants of mercury-sensing regulatory protein MerR, generated by directed evolution. Appl Environ Microbiol 77:6215–6224

Lafrance-Vanasse J, Lefebvre M, Di Lello P, Sygusch J, Omichinski JG (2009) Crystal structures of the organomercurial lyase MerB in its free and mercury-bound forms. J Biol Chem 284:938–944

Ledwidge R, Patel B, Dong A, Fiedler D, Falkowski M, Zelikova J, Summers AO, Pai EF, Miller SM (2005) NmerA, the metal binding domain of mercuric ion reductase, removes Hg^{2+} from proteins, delivers it to the catalytic core, and protects cells under glutathione-depleted conditions. Biochemistry 44:11402–11416

Miller SM (2007) Cleaving C-Hg bonds: two thiolates are better than one. Nat Chem Biol 3:537–538

Parks JM, Guo H, Momany C, Liang L, Miller SM, Summers AO, Smith JC (2009) Mechanism of Hg−C protonolysis in the organomercurial lyase MerB. J Am Chem Soc 131:13278–13285

Serre L, Rossy E, Pebay-Peyroula E, Cohen-Addad C, Coves J (2004) Crystal structure of the oxidized form of the periplasmic mercury-binding protein MerP from *Ralstonia metallidurans* CH34. J Mol Biol 339:161–171

Silver S, Hobman J (2007) Mercury microbiology: resistance systems, environmental aspects, methylation and human health. In: Nies DH, Silver S (eds) Molecular microbiology of heavy metals. Springer, Heidelberg, pp 357–370

Silver S, Phung LT (2005) A bacterial view of the Periodic Table: genes and proteins for toxic inorganic ions. J Ind Microbiol Biotechnol 32:587–605

Smith T, Pitts K, McGarvey JA, Summers AO (1998) Bacterial oxidation of mercury metal vapor, Hg(0). Appl Environ Microbiol 64:1328–1332

Steele RA, Opella SJ (1997) Structures of the reduced and mercury-bound forms of MerP, the periplasmic protein from the bacterial mercury detoxification system. Biochemistry 36:6885–6895
Utschig LM, Bryson JW, O'Halloran TV (1995) Mercury-199 NMR of the metal receptor site in MerR and its protein-DNA complex. Science 268:380–385

Bacterial Response to Gallium

▶ Gallium in Bacteria, Metabolic and Medical Implications

Bacterial Tellurite Processing Proteins

Raymond J. Turner
Department of Biological Sciences,
University of Calgary, Calgary, AB, Canada

Synonyms

Chalcogen resistance; Metal resistance; Metalloid resistance; Tellurite tolerance

Definition

Tellurite processing proteins from bacteria are those that have been shown to have some biochemical activity and or transformational effect on the tellurite oxyanion (TeO_3^{2-}).

Introduction

Tellurite resistance determinants (groups of genes or an operon specifically responsible) have been isolated and characterized by a number of groups. The Te^r genes first appeared associated with conjugated plasmids and were described in the 1970s (reviewed by Walter and Taylor 1992). However, there have now been many physiological studies that have identified genes, and/or their gene product, that display a basal activity responsible for tellurite oxyanion processing and in many cases detoxification (Zannoni et al. 2008; Chasteen et al. 2009; Turner et al. 2011). It is also not unusual to find multiple genes within a given bacterium that upon deletion, or overexpression, display a tellurite-dependent phenotype. The observations suggest that these genes provide some selective advantage in natural environments (Chasteen et al. 2009), and that these enzymes, although not specific for tellurite, are able to process it and in some cases other oxyanions (Zannoni et al. 2008).

Genes Involved in Basal Tellurite Resistance Levels

Upon studying various genes in bacteria for their physiological contributions, several have been identified to be necessary for the basal resistance to tellurite. Their deletion results in higher sensitivity to tellurite, and in many cases general oxidative stress (reviewed by Zannoni et al. 2008; recent work cited below). Most of this work has been explored in *Escherichia coli*, yet many other organisms are focus of study for tellurite resistance. Such chromosomal determinants in this category include:

NarGHI, *NapA*; These proteins are defined as nitrate reductase. In *E. coli*, NarGHI and its homologue NarXYZ are cytoplasmically localized membrane associated bioenergetic enzymes. These enzymes have demonstrated selenate reductase activity but also tellurite reduction activity (Avazeri et al. 1997). The loss of these enzymes shows a 200-fold decrease in resistance to tellurite, presenting an MIC of 0.03 μg/mL from the wild-type level of 2. Additionally, it has been shown that the periplasmically localized nitrate reductase, NapA, also has this activity.

Trx, *Grx*, *Gor*, *Gsh*; The genes are involved in thiol redox buffering and contribute to the redox poise with the cytoplasm of bacteria. They include thioredoxin (*trx*), glutaredoxin (*grx*), and glutathione reductase (*gor*) and glutathione biosynthetic enzymes (*gsh*). Deletion of any of these genes can lead to a loss of resistance to an MIC of 0.25–0.5 from 2 μg/ml (Turner et al. 1995). It is assumed that a Painter-like reaction, similar to thiol reaction with selenite, is occurring where $2RSH + TeO_3^{2-} \rightarrow RSTeRS$. This reaction is thought to continue to RSSR and Te(0) (Turner et al. 1998; Zannoni et al. 2008). Consistent with this observation is *iscS* (cysteine desulfurase) which was found to confer some of the resistance (Tantalean et al. 2003).

DsbAB; The loss of either *dsbA* or *dsbB* genes coding for disulfide-bond catalyzing enzymes in the periplasm showed a remarkable loss of tellurite tolerance down to 0.008–0.0015 μg/ml from the base level of 2 in wild type. Unexpectedly, the same observation was not observed for the other *dsb* genes (C and D) (Turner et al. 1999). The biochemical mechanism for this observation has been suggested through studies in *Rhodobacter capsulatus* as a reverse electron sink (Borsetti et al. 2007).

Sod; The loss the superoxide dismutase genes of *sodA* and/or *sodB* in *E. coli* displayed a reduction of basil resistance to a level of 0.125–0.25 μg/ml (Turner et al. 1995). This is generally thought to be due to the need of Sod activity to recover from the general oxidative response from the reduction reactions of tellurite to elemental tellurium.

BtuE; a peroxidase (Arenas et al. 2011) displayed a role in tellurite resistance when in a catalase/peroxidase deletion strain. *KatG*; *E. coli* mutants in this catalase/peroxidase gives increased sensitivity and an extract enzyme showed a NAD(P)H-dependent reduction of tellurite (Calderon et al. 2006).

ActP; The acetate permease of *Rhodobacter capsulatus* was defined as the tellurite uptake transporter in this organism and Δ*actP* strains showed a 25-fold increase in tellurite resistance (Borghese and Zannoni 2010). It was concluded that tellurite entrance into the cells is via this monocarboxylate transporter.

LepA; The translational GTPase *lepA* is well conserved in bacteria. It was observed that a Δ*lepA E. coli* strain became sensitive to 0.05 μg/ml tellurite (Shoji et al. 2010).

AceEF/*LpdA*; The pyruvate dehydrogenase (*aceE*), dihydrolipoamide transacetylase (*aceF)*, and dihydrolipoamide dehydrogenase (*lpdA*) from *Aeromonas caviae ST* have been shown to give rise to tellurite resistance when cloned and overexpressed. It is considered that all three of these enzymes have the ability to reduce TeO_3^{2-} to Te(0) (overviewed in Chasteen et al. 2009).

CobA; *Geobacillus stearothermophilus V cobA* gene encoding uroporphyrinogen-III C-methyltransferase utilizes *S*-adenosyl-L-methionine and mediates moderate levels of tellurite resistance when expressed (Araya et al. 2009). However, similar to specific tellurite resistance determinant TehB, no methylated volatile derivatives are found as products suggesting additional reactions must occur.

YqhD; This gene provides tolerance to compounds that generate membrane lipid peroxidation and has a NADPH-dependent aldehyde reduction activity (Perez et al. 2008). As expression of this *yqhD* in *E. coli* provides for tellurite resistance, it implies that peroxidation is a consequence of tellurite exposure.

Summary

Overall the different tellurite processing proteins identified to date are very different at the genetic and protein functional level. The common phenotype of bacteria exposed to tellurite is the reduction of TeO_3^{2-} to Te(0) crystals which is displayed by a blackening of broth cultures and colonies. This activity has directed researchers toward redox biochemistries. Overall, there appears to be many different enzymatic activities involving tellurite, yet it has been difficult to separate direct versus indirect affects. There is a clear dependence on the physiological state of the cells and that the thiol–redox balance is important as tellurite can react with reduced thiol compounds readily at physiological conditions (Turner et al. 1995, 1999). This parallels the observation of general reduction activities that are observed by various metabolic systems as well as the oxidative stress enzymes. However, this is not a consistent observation and likely is species dependent as little reactive oxygen species were observed when *E. coli* is exposed to tellurite compared to other metals (Harrison et al. 2009). A metabolomic study evaluating the hyper-resistance to tellurite in *Pseudomonas pseudoalcaligenes* KF707 is correlated with the induction of oxidative stress response, resistance to membrane perturbation, and general reconfiguration of cellular metabolism (Tremaroli et al. 2009). These observations suggest a pleiotropic biochemistry for the tellurium oxyanion.

Cross-References

- ▶ Bacterial Tellurite Resistance
- ▶ Tellurium and Oxidative Stress
- ▶ Tellurium in Nature
- ▶ Tellurite-Detoxifying Protein TehB from *Escherichia coli*

References

Araya MA, Tantaleán JC, Pérez JM, Fuentes DE, Calderón IL, Saavedra CP, Burra R, Chasteen TG, Vásquez CC (2009) Cloning, purification and characterization of *Geobacillus stearothermophilus* V uroporphyrinogen-III C-methyltransferase: evaluation of its role in resistance to potassium telluirte in *Escherichia coli*. Res Microbiol 160:125–133

Arenas FA, Covarrubias PC, Sandovai JM, Perez-Donoso JM, Imlay JA, Vasquez CC (2011) The *Escherichia coli* BtuE protein functions as a resistance determinant against reactive oxygen species. PLoS One 6:e15979

Avazeri C, Turner RJ, Pommier J, Weiner JH, Giordano G, Vermeglio A (1997) Tellurite and selenate reductase activity of nitrate reductases from *Escherichia coli:* correlation with tellurite resistance. Microbiology 143:1181–1189

Borghese R, Zannoni D (2010) Acetate permease (ActP) is responsible for tellurite (TeO_3^{2-}) uptake and resistance in cells of the facultative phototroph *Rhodobacter capsulatus*. Appl Environ Microbiol 76:942–944

Borsetti F, Francia F, Turner RJ, Zannoni D (2007) The thiol: disulfide oxidoreductase DsbB mediates the oxidizing effects of the toxic metalloid tellurite (TeO_3^{2-}) on the plasma membrane redox system of the facultative phototroph Rhodobacter capsulatus. J Bacteriol 189:851–859

Calderon IL, Arenas FA, Perez JM, Fuentes DE, Araya MA, Saavedra DP, Tantalean JC, Pichuantes SE, Youderian PA, Vasquez CC (2006) Catalases are NAD(P)H-dependent tellurite reductases. PLoS One 20:e70

Chasteen TG, Fuentes DE, Tantalean JC, Vasquez CC (2009) Tellurite: history, oxidative stress, and molecular mechanisms of resistance. FEMS Microbiol Rev 33:820–832

Harrison JJ, Tremaroli V, Stan MA, Chan CS, Vacchi-Suzzi C, Heyne BJ, Parsek MR, Ceri H, Turner RJ (2009) Chromosomal antioxidant genes have metal ion-specific roles as determinants of bacterial metal tolerance. Environ Microbiol 11:2491–2509

Perez JM, Arenas FA, Pradenas GA, Sandoval JM, Vasquez CC (2008) Escherichia coli YqhD exibits aldehyde reductase activity and protects from the harmful effect of lipid peroxidation-derived aldehydes. J Biol Chem 283:7346–7353

Shoji S, Janssen BD, Hayes CS, Fredrick K (2010) Translation factor LepA contributes to tellurite resistance in *Escherichia coli* but plays no apparent role in the fidelity of protein synthesis. Biochimie 92:157–163

Tantalean JC, Araya MA, Saavedra CP, Fuentes DE, Perez JM, Calderon IL, Youderian P, Vasquez CC (2003) The *Geobacillus stearothermophilus* V *iscS* gene, encoding cysteine desulfurase, confers resistance to potassium tellurite in *Escherichia coli* K-12. J Bacteriol 185:5831–5837

Tremaroli V, Workentine ML, Weljie AM, Vogel HJ, Ceri H, Viti C, Tatti E, Zhang P, Hynes AP, Turner RJ, Zannoni D (2009) Metabolomic investigation of the bacterial response to a metal challenge. Appl Environ Microbiol 75:719–728

Turner RJ, Weiner JH, Taylor DE (1995) The tellurite resistance determinants *tehAtehB* and *klaAklaBtelB* have different biochemical requirements. Microbiology 141: 3133–3140

Turner RJ, Weiner JH, Taylor DE (1998) Selenium metabolism in *Escherichia coli*. Biometals 11:223–227

Turner RJ, Weiner JH, Taylor DE (1999) Tellurite-mediated thiol oxidation in *Escherichia coli*. Microbiology 145:2549–2557

Turner RJ, Borghese R, Zannoni D (2011) Microbial reduction of tellurium metalloids as a tool in biotechnology. Biotech Adv. doi 10.1016/j.biotechadv.2011.08.018 (in press)

Walter EG, Taylor DE (1992) Plasmid-mediated resistance to tellurite: expressed and cryptic. Plasmid 27:52–64

Zannoni D, Borsetti F, Harrison JJ, Turner RJ (2008) The bacterial response to the chalcogen metalloids Se and Te. Adv Microbial Physiol 53:1–71

Bacterial Tellurite Resistance

Raymond J. Turner
Department of Biological Sciences, University of Calgary, Calgary, AB, Canada

Synonyms

Chalcogen resistance; Metal resistance; Metalloid resistance; Tellurite tolerance

Definition

Bacteria resistance to tellurite is defined here as specific genes, cluster of genes, or specific genetic operons referred to as resistance determinants. Tellurite (TeO_3^{2-}), redox state Te(IV), is the oxyanion of the chalcogen tellurium (Te; atomic number 52) in group 16 with elements O, S, Se, and Po. In addition to specific determinants a number of bacteria species have been identified to have high levels of resistance to tellurite yet the specific genetics has not been defined; these are referred to as tellurite tolerant.

Introduction

Bacteria treat tellurite quite differently from other antibacterial metal ions. Evolution has seen that a biochemical mechanism of resistance is uniform across species for most all other metal ions other than tellurite. At least five genetically different resistance determinants have been identified with little to no homology between

them. Genes responsible for tellurite resistance (Te^r) in various organisms have been isolated and characterized by a number of groups. The Te^r genes first appeared associated with conjugated plasmids and were described by Anne Summer and Diane Taylor toward the end of 1970s (reviewed by Walter and Taylor 1992); however, several determinants and plasmid homologues have now been found associated with the chromosome as well (Taylor 1999; Zannoni et al. 2008; Chasteen et al. 2009; Turner et al. 2011). Plasmid-encoded resistance determinants are generally associated with plasmids of the H and P incompatibility groups. There are also several Te^r determinants emerging from various bacterial families, suggesting that these determinants provide some selective advantage in natural environments (Chasteen et al. 2009). Such advantages may be unrelated to the Te^r phenotype, as the levels of resistance demonstrated in the laboratory do not always correlate with the levels of tellurium ion species present in the ecological or pathogenic environment. An interesting characteristic of the genes encoding Te^r is they often confer other phenotypes as well, which suggests tellurite-processing proteins could be a form of moonlighting enzymatic activity.

Tellurite is typically sold and used as potassium tellurite; K_2TeO_3. It is difficult to clearly define the ionic species that the bacteria would experience in various growth medium or in the environment. Te can exist in a number of redox states: Telluride (Te^{2-}) → elemental (Te^0) → tellurite (TeO_3^{2-}) → tellurate (TeO_4^{2-}). In aqueous conditions in water Te(IV) at pH 7.0 exists at a ratio of $HTeO_3^-/TeO_3^{2-}$ of $\sim 10^4/1$. Te (VI) would likely be tellurate, TeO_4^{2-}. Thus the standard reduction potential of the Te/TeO_3^{2-} couple (−0.42 V) at basic pHs would be raised to -0.12 V for the couple $HTeO_3^-/TeO_3^{2-}$ at pH 7.0, with no Te^{4+} present due to its instability in water. Although one cannot rule out that the oxyanion of Te could be complexed with organo or metallo cations, the primary species bacteria likely experience for the toxic form that they have developed resistance to is $HTeO_3^-$ (Zannoni et al. 2008).

Tellurite Resistance Determinants

There are now six well-defined Te^r determinants including the Ter, Teh, Tel, Tpm, CysK, and Ars. Their resistance levels toward K_2TeO_3 are summarized in Table 1.

Bacterial Tellurite Resistance, Table 1 Resistance levels mediated by specific tellurite resistance determinants

Te^r	MIC (μg K_2TeO_3/ml)	Mechanism[a, b]
NONE	1–4[c]	
Ter	512–1,024	Reductase[b]
TehAB	128	Methylation[a] and efflux[b]
KlaABTelB	256	Unknown
TpmT	256	Methyltransferase[b]
CysK	1,000	Reductase[b]
ArsABC	64	ATP-dependent efflux[a]

[a]Known mechanism
[b]Proposed or hypothesized
[c]The typical resistance level of most bacteria is in this range. However, highly resistant species do exist and their resistance does not utilize these specific determinants

Ter

Plasmids within the incompatibility group HI-2 and HII confer protection against colicins and resistance to potassium tellurite (Taylor 1999). These resistances are associated with a large cluster of genes (*terZABCDEF*) referred to as the *ter* Te^r determinant (Walter and Taylor 1992). This determinant was also found to be associated with the pathogenicity island of *Escherichia coli* H157:O7, and other pathogenic organisms such as *Yersinia pestis* and *Klebsiella pneumoniae*. A *terZABCDE* operon was also identified in *Proteus mirabilis*, and is common in the *Proteus* genus. Further, *ter* gene homologues are found on the chromosomes of a wide range of bacteria yet little clues are provided to their function. Little is known about the function of each of the genes in the operon. Overall, there is considerable homology between the *ter* genes of the different plasmids and chromosomes, yet the *ter* operon appears to be differently regulated in different organisms.

The biochemical mechanism of the Ter determinant remains unknown. It has been suggested to be involved in tellurite transport, tellurite reduction to Te(0), reduced protein, and glutathione thiol oxidation. The TerD structure has been determined by NMR (PBP: 2KXV), which revealed that this protein binds Ca^{2+} in a common fold that are also thought to be found in TerE and TerZ. TerB NMR structure is also available (PDB 2JXU) yet no clues on the mechanism are provided. There are conflicting reports whether there is increased tellurite uptake or not, yet it is clear that all studies show the accumulation of Te(0) nanocrystals (see Zannoni et al. 2008 and Turner et al. 2011).

TehAB

The *tehAB* genes were first described as a Te^r that was believed to have originated from the IncHII plasmid pHH1508a (Walter and Taylor 1992). However, follow-up studies demonstrated that it was actually on the *E. coli* genome (Taylor et al. 1994), and now homologues are found on many bacteria genomes. The genes mediate resistance only upon overexpression. TehA appears to have sequence characteristics of a transport protein and falls into the C4-dicarboxylate transporter/malic acid family. TehB associates weakly with the membrane. It contains three conserved motifs found in *S*-adenosylmethionine (SAM)-dependent nonnucleic acid methyltransferase (Liu et al. 2000) and has demonstrated SAM binding and methylase activity. Pairs of cysteines in TehA and TehB have been shown to be required for full resistance. Additionally, the resistance is very dependent on many other host metabolic systems (Turner et al. 1995). TehB has the ability to mediate resistance on its own and is partially responsible for the natural resistance of a number of organisms including *Streptococcus*. TehB has been recently crystallized (PDB: 2XVM) and suggests an SN2 nucleophilic attack between the SAM to the telluro oxyanion (Choudhury et al. 2011). Although TehB appears to be a SAM-dependent telluro methylase, methyl telluride does not appear to be the final product in vivo. It is hypothesized that further reactions may occur in the cell before a final organotelluro compound is effluxed out (Zannoni et al. 2008).

kilAtelAB/klaABtelB

The RK2 plasmids have a complex network of co-regulated genes known as the *kil-kor* regulon. A normally cryptic Te^r was identified on some isolates as $RK2Te^R$ and was mapped to the *kilA* locus. The operon is comprised of three genes, *klaA, −B, −C*, which in the Te^r versions are referred to as *kilABTelB*. A single Ser125 to Cys mutation in the integral membrane protein TelB mediates the resistance, and this mutation is solely responsible for the resistance; yet all three of the genes are required for the resistance. The mutation generates a cysteine pair (Cys 125: 132) in an extramembrane loop. Both cysteines are required for resistance and the presence of the determinant protects against cell glutathione oxidation (Turner et al. 2001). The data to date suggests some form of thiol chemistry may be involved in the resistance mechanism. As opposed to the *tehAB* determinant, *kilAtelAB* is much less dependent on the physiological state of the cell to mediate full resistance (Turner et al. 1995). Although there is apparently less "blackening" of cultures' reduced uptake or efflux of tellurite has been ruled out for this determinant as the biochemical mechanism (Turner et al. 1995).

There is some confusion in the literature in that KlaA homologues are found on the chromosome of many organisms, however, it is referred to as TelA and is incorrectly annotated as putative toxic anion resistance protein. It was found that a chromosomal homologue of TelA in *Listeria monocytogenes* demonstrated resistance to antibiotics like nisin, yet no mechanism was proposed. Due to the lethality phenotype associated with the kilA(klaA) gene, very little microbial and biochemical studies are available and thus the biochemical mechanism of this determinant remains elusive.

TpmT

The *tpm* gene was cloned from the tellurite resistant *Pseudomonas syringae* pathovar *pisi* (Cournoyer et al. 1998). Since this observation the gene has been found on a number of other *Pseudomonas spp*. *tpmT* encodes a SAM-dependent thiopurine methyltransferase enzyme, which led the authors to propose that the resistance likely occurs through a volatilization of tellurite into dimethyl telluride.

CysM/CysK

Chromosomally encoded genes, homologous to those involved in cysteine biosynthesis, have been found to mediate tellurite resistance. The *cysM* gene from *Staphylococcus aureus* SH1000 was found to be functionally homologous to the *O*-acetyl serine (thiol)-lyase B family of cysteine synthase proteins. A deletion in this gene gives increased sensitivity to tellurite and could mediate Te^R when transformed into *E. coli*. A homologue of this gene was also identified on an IncHI3 plasmid and was designated *cysK*. This enzyme is a pyridoxal 5′-phosphate-dependent enzyme and catalyzes the transformation of *O*-acetyl-L serine and S^{2-} to L-cysteine and acetate (Ramirez et al. 2006). Somehow this reductase-like enzyme mediates resistance to both pore forming colicins and tellurite, which suggests some parallels toward the Ter determinant yet no homology exists. Homologues of *cysK* have been identified in

Azospririllum brasilense and *Geobacter stearothermophilus*. In the second case, a NADH-dependent reduction of tellurite and an additional gene of *iscS* (cysteine disulfurase) were found to confer some of the resistance (Tantalean et al. 2003). CysK was considered to be a key determinant responsible for the tellurite resistance in *Rhodobacter sphaeroides*, however, other genes such as *trgAB* and a *telA* homologue were also involved (O'Gara et al. 1997). This above work suggests that CysK likely does not mediate the resistance on its own but in concert with other universal systems found in other bacteria as they demonstrate resistance to *E. coli* when cloned.

ArsABC

The arsenate/arsenite resistance determinant *arsABC* which is an arsenate reductase (ArsC) with an ATP-dependent arsenite efflux pump (ArsAB) was also found to mediate moderate levels of tellurite resistance (Turner et al. 1992). It is likely that the pump also recognizes the $HTeO_3^-$ ion. Although the *arsC* gene was required to mediate full resistance, its role is unknown.

Tellurite Tolerant Bacteria

Intrinsic low-level tellurite resistance has been reported for a few Gram positive organisms such as *Corynebacterium diphtheriae, Streptococcus faecalis*, and some *Staphylooccus aureus* strains. Yet increasing number of organisms have been described to have high levels of tellurite resistance and/or processing (reduction), however, the specific genetics and/or the biochemical processes are not completely resolved. Some examples include: *Stenotrophomonas maltophilia Sm777*, *Pseudomonas pseudoalcaligenes* KF707, *Rhodotorula mucilaginosa*. Additionally, there are some "super" tellurite resistant bacteria such as *Pseudoalteromonas telluritireducens, Pseudoalteromonas spiralis*, *Bacillus* sp STG-83 and *Paenibacillus sp*. TeW which is tolerant to ~300–500 μg/ml. A number of obligately aerobic photosynthetic bacteria have been defined with very high levels of tellurite resistance (MIC range from 750 to 2,300 μg/mL) and include: *Erythrobacter litoralis, Erythromicrobium hydrolyticum, E. ursincola, E. ramosum, E. sibiricum, E. ezovicum, Roseococcus thiosulfatophilus* (Yurkov et al. 1996).

Summary

Overall the different determinants are very different at the genetic and protein functional level. However, many of the resistance determinants have at least one gene that is an integral membrane protein (TerC, TehA, TelA). Another common theme is that resistant organisms display increased reduction of tellurite to Te (0) crystals which is displayed by a blackening of broth cultures and colonies. For the most part, the Te^r determinants *ter, klaABtelB, teh*, and *ars* do not mediate resistance to tellurate (Te(VI), TeO_4^{2-}). However, some of the specific determinants and other general metabolite genes involved with tellurite tolerance also mediate some resistance to selenite (SeO_3^{2-}). An example is TpmT. Overall the different Te^r appear to have different dependence on the physiological state of the cells and that the thiol–redox balance is important as tellurite can react with reduced thiol compounds readily at physiological conditions (Turner et al. 1995, 1999). This parallels the observation of general reduction activities that are observed by various metabolic systems as well as the oxidative stress enzymes. Unfortunately, the nature of the chemistry of tellurite reduction makes for challenging biochemistry experiments with the determinants. This and the apparent pleiotropic nature of the physiological targets has not allowed for a clear view of microbiological and biochemical specific mechanisms.

Cross-References

- ▶ Bacterial Tellurite Resistance
- ▶ Catalases as NAD(P)H-Dependent Tellurite Reductases
- ▶ Tellurite-Resistance Protein TehA from *Escherichia coli*
- ▶ Tellurium and Oxidative Stress
- ▶ Tellurite-Detoxifying Protein TehB from *Escherichia coli*

References

Chasteen TG, Fuentes DE, Tantalean JC, Vasquez CC (2009) Tellurite: history, oxidative stress, and molecular mechanisms of resistance. FEMS Microbiol Rev 33: 820–832

Choudhury HG, Cameron AD, Iwata S, Beis K (2011) Structure and mechanism of the chalcogen-detoxifying protein TehB from *Escherichia coli*. Biochem J 435:85–91
Cournoyer B, Watanabe S, Vivian A (1998) A tellurite-resistance genetic determinant from phytopathogeneic pseudomonads encodes a thiopurine methyltransferase: evidence of a widely conserved family of methyltransferases. Biochim Biophys Acta 1297:161–168
Liu M, Turner RJ, Winstone TL, Saetre A, Dyllick-Brenzinger M, Jickling G, Tara LW, Weiner JH, Taylor DE (2000) *Escherichia coli* TehB requires S-adenosylmethionine as a cofactor to mediate tellurite resistance. J Bacteriol 182:6509–6513
O'Gara JP, Gomelsy M, Kaplan S (1997) Identification and molecular genetic analysis of multiple loci contributing to high-level tellurte resistance in *Rhodobacter sphaeroides* 2.4.1. Appl Environ Microbiol 63: 4713–4720
Ramirez A, Castaneda M, Xiqui ML, Sosa A, Baca BE (2006) Identification, cloning and characterization of *cysK*, the gene encoding O-acetylserine (thiol)-lyase from *Azospirillum brasilense*, which is involved in tellurite resistance. FEMS Microbiol Lett 261:272–279
Tantalean JC, Araya MA, Saavedra CP, Fuentes DE, Perez JM, Calderon IL, Youderian P, Vasquez CC (2003) The *Geobacillus stearothermophilus* V *iscS* gene, encoding cysteine desulfurase, confers resistance to potassium tellurite in *Escherichia coli* K-12. J Bacteriol 185:5831–5837
Taylor DE (1999) Bacterial tellurite resistance. Trends Microbiol 7:111–115
Taylor DE, Hou Y, Turner RJ, Weiner JH (1994) Location of a potassium tellurite resistance operon (*tehAtehB*) within the terminus of *Escherichia coli* K-12. J Bacteriol 176:2740–2742
Turner RJ, Hou Y, Weiner JH, Taylor DE (1992) The arsenical ATPase efflux pump mediates tellurite resistance. J Bacteriol 174:3092–3094
Turner RJ, Weiner JH, Taylor DE (1995) The tellurite resistance determinants *tehAtehB* and *klaAklaBtelB* have different biochemical requirements. Microbiology 141: 3133–3140
Turner RJ, Weiner JH, Taylor DE (1999) Tellurite-mediated thiol oxidation in *Escherichia coli*. Microbiology 145:2549–2557
Turner RJ, Aharonowitz Y, Weiner JH, Taylor DE (2001) Glutathione is a target in bacterial tellurite toxicity and is protected by tellurite resistance determinants in *Escherichia coli*. Can J Microbiol 47:33–40
Turner RJ, Borghese R, Zannoni D (2011) Microbial reduction of tellurium metalloids as a tool in biotechnology. Biotechnol Adv. doi:10.1016/j.biotechadv.2011.08.018
Walter EG, Taylor DE (1992) Plasmid-mediated resistance to tellurite: expressed and cryptic. Plasmid 27:52–64
Yurkov V, Jappe J, Vermeglio A (1996) Tellurite resistance and reduction by obligately aerobic photosynthetic bacteria. Appl Environ Microbiol 62:4195–4198
Zannoni D, Borsetti F, Harrison JJ, Turner RJ (2008) The bacterial response to the chalcogen metalloids Se and Te. Adv Microbial Physiol 53:1–71

Barium

▶ Barium(II) Transport in Potassium(I) and Calcium(II) Membrane Channels

Barium and Protein–RNA Interactions

Thirumananseri Kumarevel
RIKEN SPring-8 Center, Harima Institute, Hyogo, Japan

Synonyms

Metal-ion-mediated protein–nucleic acid interactions; Role of metal ions in protein–nucleic acid complexes

Definition

Genomic studies are providing researchers with a potentially complete list of the molecular components present in living systems. It is now obvious that several metal ions are essential to life. More specifically, biological macromolecules (proteins and nucleic acids) that require metal ions to perform their physiological functions are widespread in all organisms. Here, we explored the importance and involvement of one of the alkali earth metals, barium, in the biological system. Based on structural and functional analyses, we clearly demonstrated how the divalent metal ions produce the structural rearrangements that are required for *hut* mRNA recognition. The applications and health risks of barium metal ions are also discussed.

General Background on Barium Metal

The chemical element barium is the 56th element in the chemical periodic table with the symbol of *Ba*, atomic number of 56, and weight of the 137.327. It is the fifth element in group 2, a soft silvery white metallic, and one of the alkaline earth metals. Barium is never found in nature in its pure form due to its reactivity with air. The metal oxidizes very easily and reacts with water or

alcohol. The most commonly occurring minerals containing this element are the very insoluble barium sulfate ($BaSO_4$) and barium carbonate ($BaCO_3$).

The name barium originates from the Greek word "barys," meaning "heavy," which refers to the high density of some common barium ores. It was first discovered by electrolysis of molten barium salts by Sir Humphrey Davy in 1808 in England. Prior to this discovery, Carl Scheele had *distinguished* baryta (barium oxide, BaO) from lime (calcium oxide, CaO) in 1774 but could not isolate barium itself (Mark Winter, "Webelements," www.webelements.com).

Physical and Chemical Properties of Barium Metal

The general, physical, and other important properties of barium are provided in Table 1. Barium is a soft and ductile metal. The barium compounds are notable for their relatively high specific gravity and are also called heavy spar due to their high density. Barium is a highly reducing metal. Thus, the surface of barium metal is covered with a thin layer of oxide that helps protect the metal from attack by air. Once ignited, barium metal burns in air and yields a mixture of white barium oxide (BaO) and barium nitride (Ba_3N_2). In the periodic table, barium is placed three positions below magnesium, indicating that barium is more reactive with air than magnesium.

For example, $2Ba + O_2 \rightarrow 2BaO$

$$B2 + O_2 \rightarrow BaO_2$$

$$3Ba + N_2 \rightarrow Ba_3N_2$$

Barium reacts readily with water to form barium hydroxide and hydrogen gas. The reaction is violent if barium is powdered. Barium also reacts violently with dilute acids, alcohol, and water. It also combines with several metals, including aluminum, zinc, lead, and tin, to form intermetallic compounds and alloys:

$$Ba + 2H_2O \rightarrow Ba(OH)_{2+}H_2 \uparrow$$

The abundance of barium in different environments is shown in Table 2. Naturally occurring barium is a mixture of seven stable isotopes, and the most abundant among these is ^{138}Ba (~72%). There are 22 barium isotopes known, but most of these are highly radioactive and have half-life periods in the range of several milliseconds to several days. The only notable exceptions are ^{133}Ba, which has a half-life of 10.51 years, and ^{137m}Ba with a half-life of 2.55 min. Barium isotopes are used in a variety of applications. Notably, ^{130}Ba is used in the production of $^{131}Ba/^{131}Cs$, which is used in internal radiotherapy to treat tumors/cancers in the cervix, prostate, breast, skin, or other body sites. ^{133}Ba is a standard gamma-ray reference source, which has been used in nuclear physics experimental studies ("Barium in Webelements & Wikipedia" www.webelements.com; http://en.wikipedia.org/wiki/Barium).

Other applications of barium are given below:

1. The most important application of elemental barium is as a scavenger to remove the last traces of oxygen and other gases in vacuum tubes such as TV cathode ray tubes (CRT).
2. An alloy of barium with nickel is used in spark plug wires.
3. Barium sulfate, as a permanent white or blanc fixe, is used in X-ray diagnostics (barium meals or barium enemas).
4. Barium sulfate is important to the petroleum industry, e.g., as drilling mud, a weighting agent in drilling new oil wells.
5. It is also a filler in a variety of products such as rubber.
6. Lithopone, a pigment that contains barium sulfate and zinc sulfide, is a permanent white that has good covering power and does not darken when exposed to sulfides. It is used in interior paints and in some enamels.
7. Barium carbonate is used in glass making and cement. Being a heavy element, barium increases the refractive index and luster of the glass.
8. Barium carbonate is also used as a rat poison.
9. Barium nitrate and chlorates are used to give green color in pyrotechnics.
10. Barium peroxide can be used as a catalyst to start an aluminothermic reaction when welding rail tracks together. It is an oxidizing agent, which is used for bleaching.
11. Barium titanate is a potential dielectric ceramic used for capacitors.
12. Barium fluoride is used as a source material in the manufacture of optical components such as lenses. Barium fluoride is also a common and one of the best scintillators for the detection of X-rays, gamma rays, or other high-energy particles.

Barium and Protein–RNA Interactions, Table 1 Physical, chemical, and other important factors of barium metal

Barium appearance						
 Silver Gray					 Natural Barium Sulfate	
General properties						
Name, symbol, number					Barium, Ba, 56	
Pronunciation					BAIR-ee-əm	
Element category					Alkaline earth metals	
Group period block					2, 6, s	
Standard atomic weight					137.33 g·mol^{-1}	
Electron configuration					[Xe] 6 s2	
Electrons per shell					2, 8, 18, 18, 8, 2	
Physical properties						
Phase					Solid	
Density					(Near r.t.) 3.51 g·cm^{-3}	
Liquid density at mp					3.338 g·cm^{-3}	
Melting point					1,000 K 727°C 1,341°F	
Boiling point					2,170 K 1,897°C 3,447°F	
Heat of fusion					7.12 kJ·mol^{-1}	
Heat of vaporization					140.3 kJ·mol^{-1}	
Specific heat capacity					(25°C) 28.07 J·mol^{-1}·K^{-1}	
Vapor pressure						
P (Pa)	1	10	100	1 k	10 k	100 k
at T (K)	911	1,038	1,185	1,388	1,686	2,170
Atomic properties						
Oxidation states					2 (strongly basic oxide)	
Electronegativity					0.89 (Pauling scale)	
Ionization energies					1st: 502.9 kJ·mol^{-1}	
					2nd: 965.2 kJ·mol^{-1}	
					3rd: 3,600 kJ·mol^{-1}	
Atomic radius					222 pm	
Covalent radius					215±11 pm	
Van der Waals radius					268 pm	
Other properties						
Crystal structure					body-centered cubic	
Magnetic ordering					paramagnetic	
Electrical resistivity					(20°C) 332 nΩ·m	
Thermal conductivity					(300 K) 18.4 W·m^{-1}·K^{-1}	

(*continued*)

Barium and Protein–RNA Interactions, Table 1 (continued)

Other properties				
Thermal expansion				(25°C) 20.6 μm·m^{-1}·K^{-1}
Speed of sound (thin rod)				(20°C) 1,620 m/s
Young's modulus				13 GPa
Shear modulus				4.9 GPa
Bulk modulus				9.6 GPa
Mohs hardness				1.25
CAS registry number				7440-39-3
Most stable isotopes				
Main article: isotopes of barium				
Isotope	Z(p)	N(n)	Mass	Half-life
^{130}Ba	56	74	129.9063208	PRIMORDIAL radioactive [7E+13 a]
^{132}Ba	56	76	131.9050613	STABLE [>300E+18 a]
^{133}Ba	56	77	132.9060075	10.51(5) a
^{134}Ba	56	78	133.9045084	Stable
^{135}Ba	56	79	134.9056886	Stable
^{136}Ba	56	80	135.9045759	Stable
^{137}Ba	56	81	136.9058274	Stable
^{138}Ba	56	82	137.9052472	Stable

Barium and Protein–RNA Interactions, Table 2 Abundance of barium in different environments

Location	ppb[a] by weight	ppb by atoms
Universe	10	0.09
Sun	10	0.1
Meteorite	2,800	410
Crustal rocks	340,000	51,000
Seawater	30	1.4
Stream	25	0.2
Human	300	14

[a]ppb – parts per billion (=10^9), both in terms of weight and in terms of number of atoms are given in the table above

Barium Metal in Biological Systems

Although barium has no biological role, all of its compounds that are soluble in water or acid are toxic. Inhaled dust containing barium compounds can also accumulate in the lungs, causing a benign condition called baritosis. Since barium sulfate is highly insoluble in water as well as stomach acids, it can be ingested as a suspension (barium meal) for body imaging. It is eliminated completely from the digestive tract and does not bioaccumulate, unlike other heavy metals.

The British Pharmaceutical Codex from 1907 indicates that barium chloride [*barii chloridum*, $BaCl_2.2H_2O$] has a stimulating action on the heart and other muscles. It was said that it "raises blood pressure by constricting the vessels and tends to empty the intestines, bladder and gall bladder." Its poisonous nature was also pointed out. Barium sulfide (BaS) was used as a depilatory agent (removes hair). At low doses, barium acts as a muscle stimulant, whereas higher doses affect the nervous system, causing cardiac irregularities, tremors, weakness, anxiety, dyspnea, and paralysis. This may be due to its ability to block potassium ion channels, which are critical to the proper function of the nervous system. However, individual responses to barium salts vary widely, with some being able to handle barium nitrate casually without problems and others becoming ill from working with it in small quantities.

Metal Barium-Ion-Binding Proteins

Barium Interactions with Proteins or Bound Ligands

Barium is less notable in biological systems compared to metals such as iron (Fe) or zinc (Zn). However, there are useful interactions involving barium in biological systems, such as the binding of barium ions to phosphoinositide-specific phospholipase. Barium and calcium are used as mediators by bonding to the active

Barium and Protein–RNA Interactions, Table 3 Metal barium in proteins

Sl. no	PDB code	Name	Ref.	No. Ba^{2+}	Interactions with
1	1DJH	Phospholipase C-delta1	Essen et al. (1997) Biochemistry 36: 2753	3	N312, D343, E390, I651, D653, N677, D706, D708
2	1SOF	Bacterioferritin	Liu et al. (2004) Febs Lett 573:93	2	N148, Q151
3	1WRO	HutP	Kumarevel et al. (2005) Nucleic Acids Res. 33:5494	6	His ligand, H77, H73, E90, H138
4	2ADI	Monoclonal anti-cd4 antibody q425	Zhou et al. (2005) PNAS 102:14575	1	D32, E50, N100
5	2B5E	Disulfide isomerase	Tian et al. (2006) Cell 124:61	1	E194
6	2BOU	EGF domains	Abbott et al. (to be published)	2	D43, N63, D95, E98, N114
7	2CIS	D-hexose-6-phosphate mutarotase	Graille et al. (2006) J Biol Chem 281:30175	1	Glucose-6-phosphate
8	2DNS	D-amino acid amidase	Okazaki et al. (2007) J Mil Biol 368:79	4	D122, nonspecific
9	2ITD	Potassium channel KcsA–Fab complex	Lockless et al. (2007) Plos Biol 5: e121	2	T175
10	2QDE	Mandelate racemase	Agarwal et al. (to be published)	1	D195, N197, E221, D246, E247
11	2 V02	Calmodulin	Kursula and Majava (2007) Acta Cryst. F 63:653	1	N60, D56, D58, E67
12	2V2F	Penicillin-binding protein (PBP1A)	Job et al (2008) J. Biol. Chem. 283:4886	1	T364, S472
13	2W2F	p-Coumaric acid decarboxylase	Rodriguez et al. (2010) Proteins 78:1662s	1	–
14	2 W54	Xanthine dehydrogenase	Dietzel et al. (2009) 284:8764	1	E172, H173, T266
15	2WTR	Beta arrestin-1	Zhou et al. (to be published)	2	–
16	2X6B	Potassium channel	Clarke et al. (2010) Cell 141:1018	1	T96
17	3AA6	Actin capping protein	Takeda et al. (2010) Plos Biol 8: e1000416	1	D38
18	3E8F	NaK channel	Alam & Jiang (2009) Nat. Struct. Mol. Biol. 16,35	2	–
19	3LR4	Sensor protein	Edwards et al. (to be published)	5	D136
20	3NKV	Ras-related protein Rab-1b	Muller et al. (2010) Science 329,946	2	D44, D132, T134
21	3NS4	Vacuolar protein sorting-associated protein 53	Vasan et al. (2010) PNAS 107:14176	3	N620, T720, N727
22	1VBZ	Hepatitis delta virus ribozyme	Ket et al. (2004) Nature 429:201	2	Ura120, Ura163
23	1ZQB	DNA polymerase	Pelletier & Sawaya (1996) Biochemistry 35:12778	3	D190, D192, T101, V102, I106, Gua7, Thy6

sites of the enzymes in the reaction as phospholipase connects phospholipids together to form a membrane. In another example, barium salts were used to determine the packing density of phospholipids in the cellular membrane of certain species of bacteria. Because of its interactions with phospholipids, a third function of barium in biological systems is the modeling of phospholipid head groups. Barium diethyl phosphate is a model compound used to analyze the head groups of phospholipids. From these examples, it is clear that barium is often used in the arrangement and connection of phospholipids in cellular membranes (Essen et al. 1997; Snyder et al. 1999; Herzfeld et al. 1978). Recently, the number of barium metal ion containing crystal structures available is rapidly increasing. We searched the protein databank (Berman et al. 2000, 2002) (PDB www.pdb.org) and found 23 nonhomologous protein structures containing barium metals (Table 3). Based on the analysis of protein–metal ion interactions, barium metal ions appear to prefer to interact with aspartic acid followed by asparagine, glutamic acid, and threonine.

Metal (Barium)-Ion-Mediated Protein–RNA Interactions

General Introduction to HutP

Regulating gene expression directly at the mRNA level represents a novel approach in the control of cellular processes in all organisms. In this respect, RNA-binding proteins, while in the presence of their cognate ligands, play a key role by targeting the mRNA to regulate its expression through attenuation or antitermination mechanisms. The distinction between the attenuation and antitermination pathways is the end result of interactions between the terminator and the activated protein that decides whether transcription is terminated or allowed to continue. In the attenuation process, the regulatory protein, activated by the regulatory molecule, pauses the transcription at the terminator structure, which otherwise permits the readthrough of the transcription apparatus. The best example for this kind of regulation is the tryptophan biosynthetic operon (Yanofsky 2000; Gollnick and Babitzke 2002; Antson et al. 1995, 1999). In contrast to this mechanism, the antitermination process requires the activated protein to bind to the preexisting terminator structure to allow the RNA polymerase to transcribe the downstream genes. An example of this is the BglG/SacY family of antitermination proteins. The target sequences for these antiterminator proteins comprise either single- or double-stranded regions of their respective mRNAs.

HutP (16.2 kDa, 148 aa) is an RNA-binding antiterminator protein that regulates the expression of the *h*istidine *ut*ilization (*hut*) operon in *Bacillus subtilis* by binding to *cis*-acting regulatory sequences on *hut* mRNA. In the *hut* operon, HutP is located just downstream from the promoter, while the five other subsequent structural genes, *hutH*, *hutU*, *hutI*, *hutG*, and *hutM*, are positioned far downstream from the promoter. In the presence of L-histidine and divalent metal ions, HutP binds to the nascent *hut* mRNA leader transcript. This allows the antiterminator to form, thereby preventing the formation of the terminator and permitting transcriptional readthrough into the *hut* structural genes. In the absence of L-histidine and divalent metal ions or both, HutP does not bind to the *hut* mRNA, thus allowing the formation of a stem-loop terminator structure within the nucleotide sequence located between *hutP* and the structural genes. Similar to HutP, many regulatory proteins that involve allosteric regulation by small molecules to modulate their binding to the cognate mRNA have been described for various operons. These proteins must initially be activated by their specific ligands before they can function as antiterminators/attenuators (Oda et al. 1992, 2000; Kumarevel et al. 2002, 2003, 2004a, b).

Requirement of L-Histidine

HutP requires L-histidine (~10 mM) for binding to the *hut* mRNA. To obtain additional insights into the requirement of L-histidine and its important functional groups responsible for activation, we analyzed 15 different L-histidine analogs. Among the analogs tested, L-histidine β-naphthylamide (HBN) and L-histidine benzyl ester showed higher affinity (10-fold) over L-histidine. L-histidine methyl ester and L-β-imidazole lactic acid showed similar affinity as L-histidine (Kd ~300 nM), and urocanic acid, histamine, and L-histidinamide showed only weak activation. D-Histidine, imidazole-4-acetic acid, L-histidinol, α-methyl-DL-histidine, 1-methyl-L-histidine, 3-methyl-L-histidine, and 3-(2-thienyl)-L-alanine failed to show any activation. Based on the analysis of the active analogs, we found that the imidazole group as well as the backbone moiety of L-histidine is essential for activation. Moreover, HutP activation by L-histidine is highly stereospecific since D-histidine prevented *hut* mRNA binding to HutP. This suggests that the correct positioning of the α-amino and carboxy moieties of L-histidine is essential for HutP activation (Kumarevel et al. 2003, 2004a).

Requirement of Divalent Metal Ions for the Activation of HutP

Our previous analyses suggested that HutP binds to its cognate RNA only in the presence of L-histidine. To analyze the ability of HutP to bind to mRNA, the reactions are carried out in the presence of L-histidine (10 mM) and Mg^{2+} ions (5 mM). However, we do not know what function the metal ions play in antitermination complex formation. In order to understand the role of metal ions in the formation of this complex, we used a gel mobility shift assay, and these studies suggested that Mg^{2+} ions are important for the HutP–RNA interactions. When $MgCl_2$ was omitted from the binding reactions, HutP failed to bind to *hut* mRNA. When 0.5 mM of $MgCl_2$ was incorporated in the binding buffer, we clearly observed formation of an antitermination complex. The level of complex formation was concentration-dependent, increasing further

Barium and Protein–RNA Interactions, Table 4 Selected divalent and monovalent metal ions and its properties

	Metal ion (compound used)	Ionic radii	Preferred coordination	Concentration in bacterial cells (mg/kg)
Divalent	Mg ($MgCl_2$)	0.72	6	7×10^3
	Ca ($CaCl_2$)	0.99, 1.12	6, 8	5.1×10^3
	Mn ($MnCl_2$)	0.83	6	260
	Cu ($CuCl_2$)	0.57, 0.73	4, 6	150
	Zn ($ZnCl_2$)	1.02, 1.08	4, 6	83
	Co ($CoCl_2$)	0.74	6	7.9
	Cd ($CdCl_2$)	0.95	4–7	0.31
	Ba ($BaCl_2$)	1.35, 1.38	6, 7	–
	Sr ($SrCl_2$)	1.13	6	–
	Yb ($YbCl_2$)	1.02–1.14	6–8	–
	Ni ($NiCl_2$)	0.69	6	–
	Pb ($PbCl_2$)	1.19–1.49	4–12	–
	Ag ($AgNO_3$)	0.94	6	–
	Hg (Hg $(CN)_2$)	0.69–1.14	2,4,6,8	–
	Pt (K_2PtCl_4)	0.80	6	–
Monovalent	Na (NaCl)	0.99–1.39	4–12	4.6×10^3
	K (KCl)	1.37–1.64	4–12	115×10^3

with higher metal ion and L-histidine concentrations. The metal ion Kd (489 μM) value for the HutP–RNA interactions appeared to be more efficient (>10-fold) compared to the metal ions for other protein–RNA interactions, suggesting the existence of an efficient metal-ion-binding pocket (Kumarevel et al. 2004c; 2005a).

Biochemical Analysis of HutP–RNA Interactions in the Presence of Various Metal Ions

From the aforementioned studies, it is clear that divalent metal ions, Mg^{2+} ions, are essential for mediating the HutP–RNA interactions. To substantiate the requirement for divalent metal ions and also to identify the best divalent metal ions that support the interactions, we performed binding reactions in the presence of various divalent metal ions. The properties of the divalent metal ions used in the present study including their ionic radii, preferred coordination, and concentrations present within the bacterial cells are summarized in Table 4. Of the 15 different divalent metal ions tested, 12 (Mg^{2+}, Ca^{2+}, Mn^{2+}, Zn^{2+}, Co^{2+}, Cd^{2+}, Ba^{2+}, Sr^{2+}, Ni^{2+}, Pb^{2+}, Ag^{2+}, Pt^{2+}) were able to mediate the HutP–RNA interactions. The only metal ions that failed to support the interactions were Cu^{2+}, Yb^{2+}, and Hg^{2+} (Fig. 1). Among the 12 divalent ions that participated in the interactions, Mn^{2+}, Zn^{2+}, and Cd^{2+} were more efficient, followed by Mg^{2+}, Co^{2+}, and Ni^{2+} ions (Fig. 1). Interestingly, the divalent metal ions that are less abundant in the bacterial cell, such as Mn^{2+}, Zn^{2+}, and Cd^{2+}, were the active divalent metal ions, whereas the more commonly found divalent metal ions, Mg^{2+}, Ag^{2+}, and Ca^{2+}, were weakly efficient (Kumarevel et al. 2005b).

Interestingly, Ni^{2+} ions, which are reportedly not present within bacterial cells, also mediate the complex formation more efficiently than Mg^{2+}, and other metals that are not found in bacteria, such as Ba^{2+}, Pb^{2+}, Pt^{2+}, and Sr^{2+}, also participate in the complex. We compared the atomic radii of the metal ions that support the HutP–RNA interactions in order to study the pocket that accommodates the metal ions. When we compared the ionic radii of the metal ions, based on their preferred hexameric coordination, we found that the radii for Cu^{2+}, Mg^{2+}, and Co^{2+} were nearly the same size (Table 4). However, Cu^{2+} failed to interact with the complex. Similarly, although the radii between the Yb^{2+} and Zn^{2+} ions were essentially the same size, Yb^{2+} was noninteractive, whereas Zn^{2+} showed the highest interactions with the protein–RNA complex. The Ba^{2+} ion, which has the longest ionic radius, showed the lowest support for the HutP–RNA interactions. Although these studies suggested that the atomic radii of the divalent metal ions are important for their support in mediating the HutP–RNA interactions, it is possible that the underlying mechanism may be much more complicated.

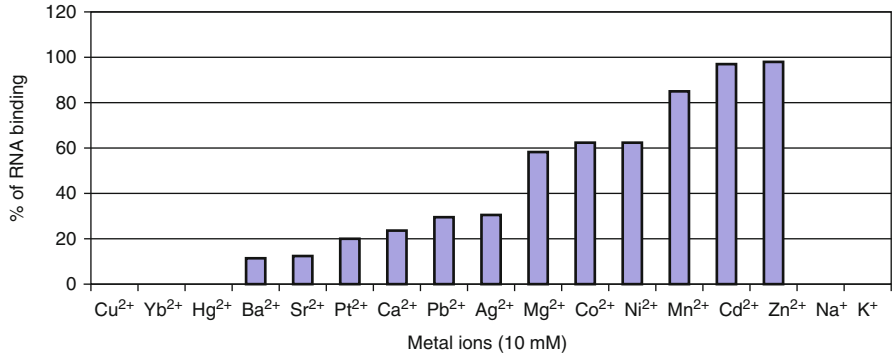

Barium and Protein–RNA Interactions, Fig. 1 Analysis of the abilities of various metal ions to mediate the HutP–RNA interactions. Fifteen divalent and two monovalent cations were analyzed by a gel shift assay. The amounts of complexed and free RNA were used to calculate the percentage of metal ion interactions involved in making the ternary complex

Both tested monovalent cations (Na^+, K^+) failed to mediate the HutP–RNA interactions even at high (10,100 mM) concentrations in the absence of divalent cations. From these analyses, it can be concluded that divalent cations are mandatory for the interactions between HutP and its RNA and cannot be replaced with monovalent cations.

Structural Analysis of HutP–RNA Interactions in the Presence of Ba^{2+} Metal Ions

To clarify the Ba^{2+} metal ion coordinations within the HutP and L-histidine ligand complex, crystallization trials were carried out with HutP, L-histidine, and $BaCl_2$, as well as with other ions, such as $MnCl_2$ or $MgCl_2$. All of the complexes were crystallized successfully, and the structures HutP–L-histidine–Ba^{2+}, HutP–L-histidine–Mn^{2+}, and HutP–L-histidine–Mg^{2+} were solved by molecular replacement with HutP–HBN (PDB id, 1VEA) as a search model (Kumarevel et al. 2004a, 2005a, b; Gopinath et al. 2008). The overall structures of the HutP–L-histidine–Ba^{2+} are shown in Fig. 2a. Each asymmetric unit contains three molecules of HutP and three L-histidines related by non-crystallographic threefold axis, forming a tight trimer, with each monomeric HutP molecule consisting of four α-helices and four β-strands, arranged in the order α- α -β- α - α - β- β- β in the primary structure, and the four antiparallel β-strands form a β-sheet in the order β1- β2- β3- β4, with two α-helices each on the front and the back (Fig. 2a–c). Consistent with previous X-ray and biochemical analyses, these complexes form a hexameric structure along the twofold axis (Fig. 2b).

The exceptional quality of both the experimentally phased electron density map and that obtained with the calculated phases and $2|F_{obs}|-|F_{calc}|$ amplitudes allowed us to identify three specific divalent metal binding sites unambiguously in the complexes. These three specific binding sites were consistent in the present HutP–L-histidine–Ba^{2+} and HutP–L-histidine–Mn^{2+} and our other reported HutP–L-histidine–Mg^{2+} and HutP–L-histidine–Mg^{2+}–21mer RNA complexes. The bound metal ions (Ba^{2+}, Mn^{2+}, Mg^{2+}) were located at the dimer or dimer–dimer interface with a similar recognition motif, critically forming the hexacoordination with the L-histidine ligand and the histidine cluster of the HutP protein (Figs. 2c, 3a). Out of the six coordinations, two were with the amino and carboxyl groups of the L-histidine ligand, and three were with the imidazole nitrogens of His138, His73, and His77. The sixth coordination of the Mg^{2+} ion was that with a water molecule (Fig. 3a). This typical hexacoordination with the L-histidine and histidine cluster may not be possible with the monovalent metal ions (K^+, Na^+), and hence, these metal ions could not mediate the protein–RNA interactions (Figs. 1 and 3a). In the case of the HutP–L-histidine–Ba^{2+} complex, we found three additional nonspecific Ba^{2+} ions located at the center of the HutP trimer (Figs. 2a–b and 3b). However, these three Ba^{2+} are related by a non-crystallographic threefold axis and may occur as alternative positions of a disordered Ba^{2+} ion. A close view of these Ba^{2+} positions and their interactions (Fig. 3b) shows that each Ba^{2+} is bonded with two coordinations derived from the two molecules, i.e., Gly89 of one molecule and Glu90 from the other adjacent molecule.

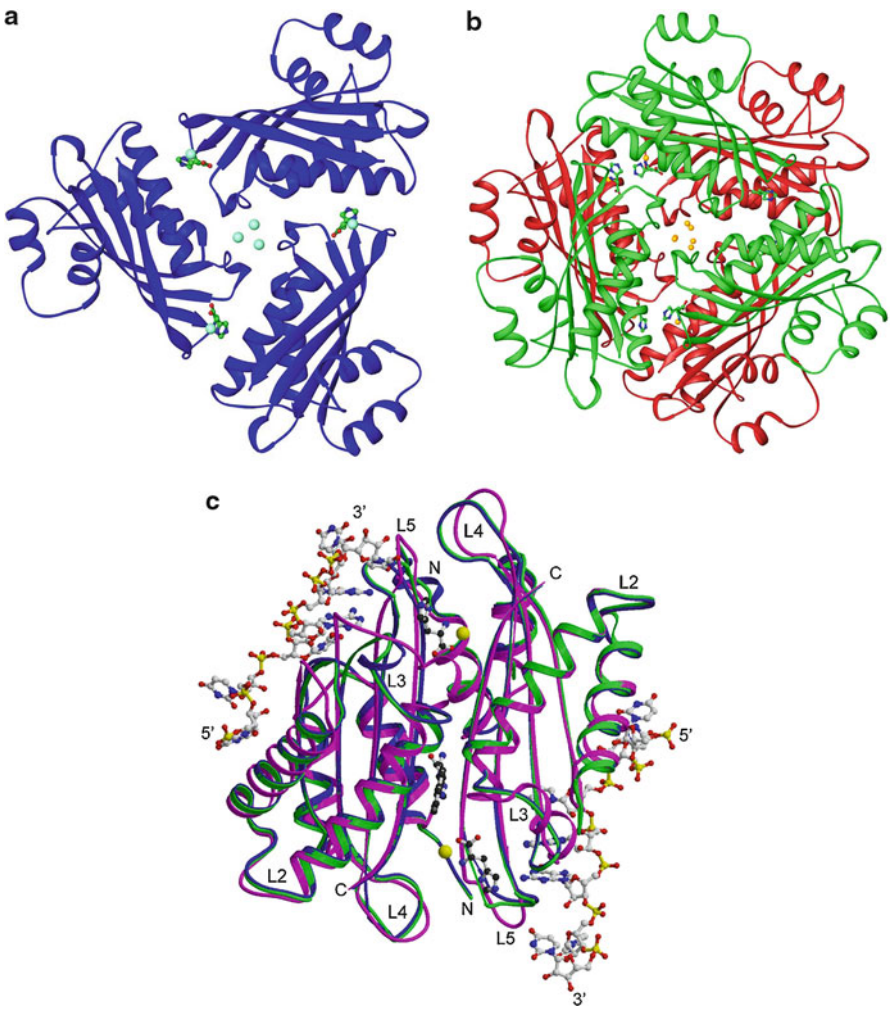

Barium and Protein–RNA Interactions, Fig. 2 Crystal structure of the HutP with divalent metal ion and RNA complexes. (**a**) Structure of the HutP–L-histidine–Ba^{2+} complex shown in a *ribbon* diagram. The bound L-histidines are shown as a *ball*-and-*stick*, and the divalent metal ion is represented by CPK model. (**b**) Hexameric formation of the divalent metal complex (HutP–L-histidine–Ba^{2+}). One trimer is shown in *red*, and the other is *green*. The divalent metal ions represented by the CPK model. (**c**) The crystal structure of the HutP complexes. HutP-histidine β-naphthylamide (HBN, an L-histidine analog) complex (magenta) superimposed along with the divalent metal ion complex (*blue*) and the HutP quaternary (HutP–L-histidine, Mg^{2+}, and RNA) complex (*green*) shown in a *ribbon* diagram with labels for N-, C-terminals, loop regions, and RNA directions. The bound HBN is shown as a *ball*-and-*stick* model colored by atom type (nitrogen, *blue*; carbon, *green*; oxygen, *red*). The L-histidines and HBN are represented by *ball*-and-*stick* models in green, and the Mg^{2+} ions are represented by CPK models, colored in *yellow*

However, this nonspecific Ba^{2+} binding site is not required for protein–RNA interactions, because Mn^{2+} and Mg^{2+} can also mediate the complex formation even without this metal ion interaction.

Site-directed mutational analyses showed that all of the histidines (His73, His77, and His138) involved in the metal ion interactions were required for the coordinations as observed recently with Mg^{2+} ions. When we analyze all three of the divalent metal ion (Ba^{2+}, Mn^{2+}, and Mg^{2+}) complexes, we found that although the metal ion coordinations were essentially the same in all of the cases, however, the coordination distance changed slightly (2.28 Å for Mg^{2+}, 2.26 Å for Mn^{2+}, and 2.60 Å for Ba^{2+}), depending on the metal ion radius (Fig. 4). The maximum difference in coordination distances observed for Ba^{2+} was 0.33 Å, in comparison with Mg^{2+}, and this

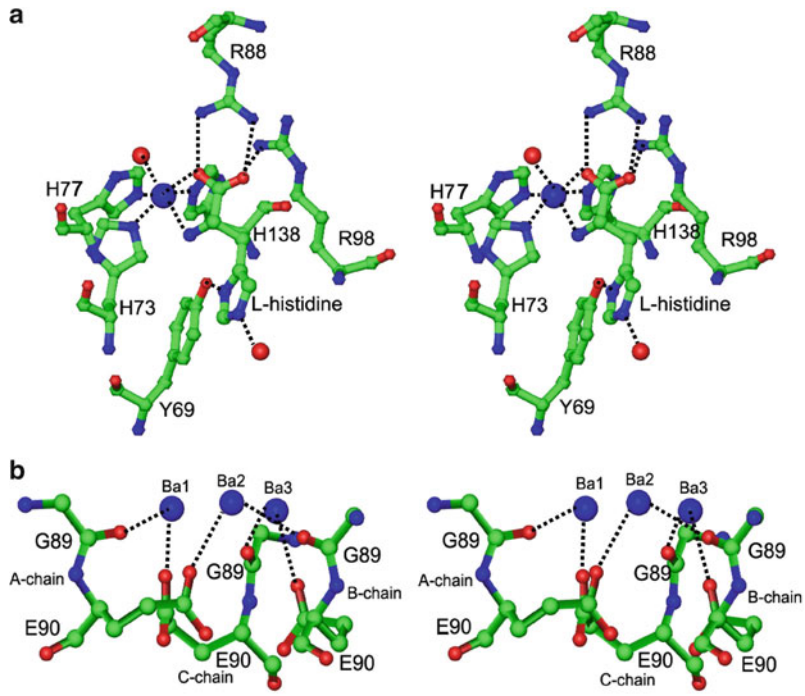

Barium and Protein–RNA Interactions, Fig. 3 Stereo view of divalent metal ion coordinations in the complex structures. (**a**) A close-up view of the Ba^{2+} ion binding site in the HutP–L-histidine–Ba^{2+} complex. Hydrogen bonds are indicated by *broken lines*. The L-histidine ligand and the protein residues are represented by *ball*-and-*stick* models colored by atom type, as shown in Fig. 2c. The Ba^{2+} and water molecules are represented by CPK models in *blue* and *red*, respectively. (**b**) A close-up view of the nonspecific Ba^{2+} ion binding site and its interactions. Hydrogen bonds and the color scheme are described in Fig. 3a

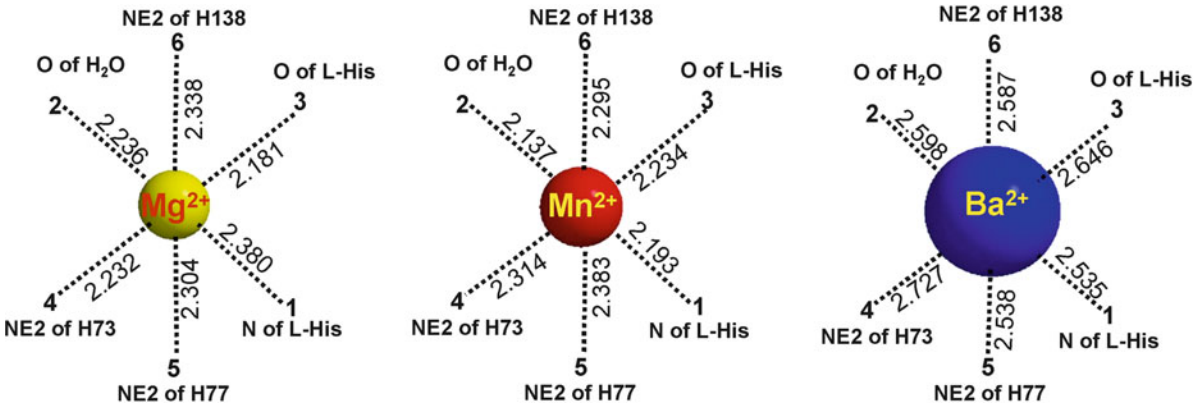

Barium and Protein–RNA Interactions, Fig. 4 Divalent metal ion coordination distance comparison for different metal ions observed in the complex structures. A schematic hexacoordination of the metal ions, drawn and numbered as in Fig. 3a

may be due to the difference in ionic radii (Table 4). Due to the larger ionic radius of the Ba^{2+} ions, all six of the metal-coordinating functional groups displaced around (0.3–0.4 Å) from the center of the ion, as compared with other metal ions (Mn^{2+} and Mg^{2+}). From these analyses, it seems that the metal ion resides in between the HutP monomers and that interface may accept a wide range of divalent metal ions with different ionic radii.

Role of Divalent Metal Ions in the HutP–RNA Interactions

When we analyzed our reported structures of HutP (apo HutP, HutP–Mg^{2+}, HutP–HBN complex, HutP–L-histidine–Mg^{2+}, HutP–L-histidine–Ba^{2+}, HutP–L-histidine–Mn^{2+}, and HutP–L-histidine–Mg^{2+}–21mer RNA complex, HutP–L-histidine–Mg^{2+}–55mer RNA complex), it was quite clear that the specific metal ion

coordinations with the histidine cluster of HutP (His73, His77, His138) and the L-histidine ligand are indispensable for the structural rearrangements, which is required to recognize the RNA. The apo HutP, HutP–Mg^{2+}, and HutP–HBN complexes adopted similar conformations, indicating that the Mg^{2+} ion or L-histidine ligand alone may not be sufficient for the activation of HutP. Two metal ion interactions are lost in the HutP–Mg^{2+} complex in the absence of L-histidine, providing an explanation for why the metal ion itself may not reside in the complex to facilitate the required structural rearrangements. When we introduced the divalent metal ion into the HutP–L-histidine complex, the metal ion bound to the L-histidine and moved approximately 12 Å on either side of the dimer interface (Fig. 2c). This movement of L-histidine along with the metal ions is apparently linked to the many local conformational changes, especially in the loop regions, L3, L4, and L5, in addition to the L-histidine binding site (Figs. 2c and 3a). These conformational changes become evident upon a comparison of the inactive/preactive conformations and the divalent metal ion complexes. The divalent metal ion complex represents the activated conformation of HutP which is required for the recognition of RNA, since there are no further conformational changes observed of the activated HutP protein upon RNA binding. Therefore, we suggest that the divalent metal ions play a major role in activating the HutP protein through the structural rearrangements specifically required for RNA recognition. Thus, HutP represents the first example of a single-stranded RNA-binding protein that requires metal ions for mediating RNA–protein interactions (Kumar et al. 2006; Kumarevel 2007).

Metal Barium Ion and Its Interactions with Nucleic Acids

Metal ions are unavoidably involved in almost every aspect of nucleic acid chemistry. Due to their polyanionic nature, the natural nucleic acids DNA and RNA always occur in combination with cations. In principle, each nucleotide carries one negative charge associated with its phosphate groups, and it needs to be shielded to enable the formation of a stable secondary structure. This shielding can be provided by a variety of cations (polyamines, mono-, or divalent cations). The maintenance of nucleic acid structural integrity is the main role of these metal ions. However, metal ions are also important for the biological action of nucleic acids such as RNA folding, catalytic cofactors in ribozymes, and mediation of protein–RNA interactions.

The most common intracellular metal ion is the potassium ion. Magnesium and calcium are also two other important metal ions for the function of nucleic acids. Although the barium ion is not biologically important for the functions of nucleic acids, it is used as a divalent metal ion during the crystal screening process. When we searched the PDB (Berman et al. 2000, 2002; (www.pdb.org)) for barium metals containing nucleic acid complexes, we found 23 nonhomologous structures containing one or more barium ions (Table 5). Most of the bound barium ions interact with the nucleic acids (DNA/RNA) either through phosphate backbones or predominantly with guanines (Table 5).

Environmental and Health Effects of Barium Metal

The environmental background level of barium is low, ~0.0015 parts per billion (ppb) in air. Most surface water contains about 0.38 ppb or less of barium, and some areas of underground water wells may have up to 1 ppb of barium. High amounts of barium may be found in soils (100 ~ 3,000 ppm) and in some foods, such as nuts, seaweed, fish, and certain plants. The amount of barium found in water and food usually is not high enough to cause any health concern, or at least no related ailments have been registered thus far. However, ongoing investigations are being conducted to determine if long-term exposure to low levels of barium may cause any health concerns.

Extensive use of barium in industries, such as mining processes, refining processes, and the production of barium compounds, can pollute the environment by releasing great amounts of barium waste into the air. As a result, barium concentrations in air, water, and soil may be higher than those naturally occurring at many locations. Additionally, people with the greatest known risk of exposure to high levels of barium are those working in the industries that make or use barium compounds. Most of the health risks that they undergo are caused by breathing in air that contains barium sulfate or barium carbonate. Many hazardous waste sites contain certain amounts of barium compounds,

Barium and Protein–RNA Interactions, Table 5 Metal barium in nucleic acids

Sl. no	PDB code	Name	Ref.	No. Ba^{2+}	Interactions with
DNA					
1	1IHH	Dodecamer duplex	Spingler et al. (2001) Inorg Chem 40:5596	1	ADE10, GUA11
2	1QYK	DNA quadruplex	Cardin et al. (to be published)	2	Only backbones
3	1XCS	Oligonucleotide/ drug complex	Valls et al. (2005) J Biol Inorg Chem 10:476	1	Only backbones
4	220D	DNA decamer	Gao et al. (1995) Biophys J 69:559	1	–
5	284D	Four-stranded DNA	Salisbury et al. (1997) PNAS 94:5515	11	–
6	3FQB	Z-DNA	Mandal et al (to be published)	2	Gua4
7	3GOJ	Holliday junction	Naseer & Cardin (to be published)	4	Gua4 (1)
8	3GOM	Holliday junction	Naseer & Cardin (to be published)	5	Gua4 (1)
9	2DQO	DNA:RNA duplex	Juan et al (2007)Nucleic Acids Res. 35,1969	2	rGua13, rAde17
10	1Y7F	Oligonucleotide racemase	Egli et al. (2005) Biochemistry 44:9045	1	Gua3
11	1IOF	Decamer complex	Tereshko et al. (2001) Nucleic Acids Res 29:1208	1	Gua3
12	2GPX	A-DNA octamer	Jiang et al (2007) Nucleic Acids Res 35:477	1	Gua3
RNA					
13	1J6S	RNA tetraplex	Pan et al. (2003) Structure 11:815	8	Gua8, Gua10, Gua11, Gua16, Gua17, Gua20, Gua22, Gua23
14	1KD4	Polyribonucleotide	Kacer et al. (2003) Acta Cryst Sec D 59:423	2	Gua2, Ura3, Gua8
15	1NTA	Streptomycin RNA-aptamer	Tareshko et al. (2003) Chem Biol 10:175	3	Gua6, Ura10, Ura11, Gua114, Gua115
16	1U9S	Ribonuclease P	Krasilnikov et al. (2004) Science 306:104	21	Gua79, Gua98, Gua99, Gua100, Gua110, Gua123, Gua130, Gua141, Gua157, Ura158, Gua159, Gua161, Gua162, Gua167, Gua171, Cyt175, Gua182, Ura183, Ade192, Ade197, Gua218, Cyt219
17	1Y6S	HIV-1 DIS RNA	Ennifar et al. (2003) Nucleic Acids Res. 31:2671	6	Ura3, Ura6, Gua4, Gua7, Gua9, Gua10
18	2HOL	Thi-box riboswitch	Edwards & Ferre-D'Amare (2006) Structure 14:1459	9	Gua36, Gua40, Ade41, Gua60, Gua66, Gua78
19	3F2W	FMN riboswitch	Serganov et al. (2009) Nature 458:233	16	Gua9, Gua16, Gua19, Gua28, Gua33, Gua41, Gua62, Gua97, Gua101, Ade102 Gua36, Ura52, Gua70, Ura89, Gua93
20	3IQN	SAM-I riboswitch	Stoddard et al. (2010) Structure 18:787	5	–
21	3OXJ	Glycine riboswitch	Huang et al. (2010) Mol Cell 40:774	24	Gua1, Gua8, Ura19, Gua60, Ura61, Gua79, Gua80
22	3P4B	Polyribonucleotide	Pallan et al.(2010) Nucleic Acids Res. (In press)	2	–
23	439D	Polyribonucleotide	Perbandt et al. (2001) Acta Cryst Sec D 57:219	1	Gua81, Gua82

and these sites may be a source of exposure for people living and working near them. Exposure near hazardous waste sites may occur by breathing dust, eating soil or plants, or drinking water that is polluted with barium. Skin contact may also cause health problems. Barium that enters the body by breathing, eating, or drinking is removed mainly in feces and urine. Most of the barium that enters our body is removed within a few days, and almost all of it is excreted within 1–2 weeks. Most of the barium that remains in the body goes to the bones and teeth. However, the long-term health effects of the barium that stays in the body are not known.

The health effects of different barium compounds depend on how well the specific barium compound dissolves in water. For example, barium sulfate does not dissolve well in water and has few adverse health effects. Doctors sometimes give barium sulfate orally or by placing it directly in the rectum of patients for purposes of obtaining X-rays of the stomach or intestines. The use of this particular barium compound in this type of medical test is not harmful to people. However, barium compounds such as barium acetate, barium carbonate, barium chloride, barium hydroxide, barium nitrate, and barium sulfide that dissolve in water can cause adverse health effects. Most of what we know about health risks from barium comes from studies in which a small number of individuals were exposed to fairly large amounts of barium for short periods. Eating or drinking very large amounts of barium compounds dissolved in water may cause paralysis or death in a few individuals. Some people who eat or drink somewhat smaller amounts of barium for a short period may potentially have difficulties in breathing, increased blood pressure, changes in heart rhythm, stomach irritation, minor changes in blood pressure, muscle weakness, changes in nerve reflexes, swelling of the brain, and damage to the liver, kidney, heart, and spleen. One study showed that people who drank water containing as much as 10 ppm of barium for 4 weeks did not have increased blood pressure or abnormal heart rhythms. We have no reliable information about the possible health effects in humans who are exposed to barium by breathing or by direct skin contact. However, many of the health effects may be similar to those seen after eating or drinking barium. There is no information available on the ability of barium to cause birth defects or affect reproduction in humans. Barium has not been shown to cause cancer in humans.

However, the health effects of barium are more well studied in experimental animals than in humans. Rats that ate or drank barium over short periods had buildup of fluid in the trachea (windpipe), swelling and irritation of the intestines, changes in organ weights, decreased body weight, and increased rates of death. Rats that ate or drank barium over long periods had increased blood pressure and changes in the function and chemistry of the heart. Mice that ate or drank barium over a long period had shortened life spans. There is no reliable information about the health effects in experimental animals that are exposed to barium by breathing or by direct skin contact.

Cross-References

- ▶ Barium Binding to EF-Hand Proteins and Potassium Channels
- ▶ Barium, Physical and Chemical Properties
- ▶ Cobalt Proteins, Overview
- ▶ Copper-Binding Proteins
- ▶ Magnesium
- ▶ Magnesium Binding Sites in Proteins
- ▶ Magnesium in Biological Systems
- ▶ Nickel Ions in Biological Systems
- ▶ Nickel-Binding Proteins, Overview
- ▶ Nickel-Binding Sites in Proteins
- ▶ Zinc-Binding Proteins, Abundance
- ▶ Zinc-Binding Sites in Proteins

References

Antson AA, Dodson EJ, Dodson G, Greaves RB, Chen XP, Gollnick P (1999) Structure of the *trp* RNA-binding attenuation protein, TRAP, bound to RNA. Nature 401:235–242

Antson AA, Otridge J, Brzozowski AM, Dodson EJ, Dodson GG, Wilson KS, Smith TM, Yang M, Kurecki T, Gollnick P (1995) The structure of trp RNA-binding attenuation protein. Nature 374:693–700

Barium (2001) In wikipedia, the free encyclopedia. Retrieved 20 Apr 2011, from http://en.wikipedia.org/wiki/Barium

Berman HM, Battistuz T, Bhat TN, Bluhm WF, Bourne PE, Burkhardt K, Feng Z, Gilliland GL, Iype L, Jain S, Fagan P, Marvin J, Padilla D, Ravichandran V, Schneider B, Thanki N, Weissig H, Westbrook JD, Zardecki C (2002) The protein data bank. Acta Crystallogr D Biol Crystallogr 58:899–907

Berman HM, Westbrook J, Feng Z, Gilliland G, Bhat TN, Weissig H, Shindyalov IN, Bourne PE (2000) The protein data bank. Nucleic Acids Res. 28:235–242

Essen L-O, Perisic O, Lynch DE, Katan M, Williams RL (1997) A ternary metal binding site in the C2 domain of phosphoinositide-specific phospholipase C-δ1. Biochemistry 36:2753–2762
Gollnick P, Babitzke P (2002) Transcription attenuation. Biochim Biophys Acta 1577:240–250
Gopinath SCB, Balasubramanian D, Kumarevel TS, Misono TS, Mizuno H, Kumar PKR (2008) Insights into anti-termination regulation of the *hut* operon in *Bacillus subtilis*: importance of the dual RNA-binding surfaces of HutP. Nucleic Acids Res 36:3463–3473
Herzfeld J, Griffin RG, Haberkorn RA (1978) ^{31}P chemical-shift tensors in barium diethyl phosphate and urea-phosphoric acid: model compounds for phospholipid head-group studies. Biochemistry 17:2711–2718
Kumar PKR, Kumarevel TS, Mizuno H (2006) Structural basis of HutP-mediated transcription anti-termination. Curr Opin Struct Biol 16:18–26
Kumarevel TS (2007) Structural insights of HutP-mediated regulation of transcription of the *hut* operon in *Bacillus subtilis*. Biophys Chem 128:1–12
Kumarevel TS, Fujimoto Z, Padmanabhan B, Oda M, Nishikawa S, Mizuno H, Kumar PKR (2002) Crystallization and preliminary X-ray diffraction studies of HutP protein: an RNA-binding protein that regulates the transcription of *hut* operon in *Bacillus subtilis*. J Struct Biol 138:237–240
Kumarevel TS, Mizuno H, Kumar PKR (2003) Allosteric activation of HutP protein, that regulates transcription of hut operon in *Bacillus subtilis*, mediated by various analogs of histidine. Nucleic Acids Res Suppl 3:199–200
Kumarevel TS, Fujimoto Z, Karthe P, Oda M, Mizuno H, Kumar PKR (2004a) Crystal structure of activated HutP; an RNA binding protein that regulates transcription of the hut operon in *Bacillus subtilis*. Structure 12:1269–1280
Kumarevel TS, Fujimoto Z, Mizuno H, Kumar PKR (2004b) Crystallization and preliminary X-ray diffraction studies of the metal-ion-mediated ternary complex of the HutP protein with L-histidine and its cognate RNA. BBA- Prot Proteomics 1702:125–128
Kumarevel TS, Gopinath SCB, Nishikawa S, Mizuno H, Kumar PKR (2004c) Identification of important chemical groups of the *hut* mRNA for HutP interactions that regulate the *hut* operon in *Bacillus subtilis*. Nucleic Acids Res 32:3904–3912
Kumarevel TS, Mizuno H, Kumar PKR (2005a) Structural basis of HutP-mediated anti-termination and roles of the Mg^{2+} ion and L-histidine ligand. Nature 434:183–191
Kumarevel TS, Mizuno H, Kumar PKR (2005b) Characterization of the metal ion binding site in the anti-terminator protein, HutP, of *Bacillus subtilis*. Nucleic Acids Res 33:5494–5502
Oda M, Katagai T, Tomura D, Shoun H, Hoshino T, Furukawa K (1992) Analysis of the transcriptional activity of the hut promoter in Bacillus subtilis and identification of a *cis*-acting regulatory region associated with catabolite repression downstream from the site of transcription. Mol Microbiol 6:2573–2582
Oda M, Kobayashi N, Ito A, Kurusu Y, Taira K (2000) *cis*-acting regulatory sequences for antitermination in the transcript of the *Bacillus subtilis hut* operon and histidine-dependent binding of HutP to the transcript containing the regulatory sequences. Mol Microbiol 35:1244–1254
Snyder S, Kim D, McIntosh TJ (1999) Lipopolysaccharide Bilayer structure: effect of chemotype, core mutations, divalent cations, and temperature. Biochemistry 38:10758–10767
Winter M, The periodic table on the web "WebElements™." Source: WebElements http://www.webelements.com/
Yanofsky C (2000) Transcription attenuation: once viewed as a novel regulatory strategy. J Bacteriol 182:1–8

Barium Binding to EF-Hand Proteins and Potassium Channels

Vladimir N. Uversky
Department of Molecular Medicine, University of South Florida, College of Medicine, Tampa, FL, USA

Synonyms

Ca^{2+}-activated K^+ channels; Calcium-modulated potassium channels; Calmodulin; EF-hand calcium-binding proteins; Potassium channels

Definition

Barium can effectively interact with several EF-hand calcium-binding proteins. This metal ion is also considered as a potent inhibitor of the regulated potassium channels. It also can inactivate some calcium channels.

Some Physicochemical Properties of Barium

The chemical element barium is the 56th element in the chemical periodic table with the symbol of Ba, atomic number of 56, and atomic mass of the 137.33. It belongs to the group 2 (of which it is a fifth element) in the periodic table. Therefore, barium, which is a soft, silvery-white metal, with a slight golden shade when ultrapure, and highly reactive metal, is the heaviest nonradioactive member of the alkaline-earth elements. Barium is a relatively common element in Earth (it has a concentration of 0.0425% in the Earth's crust and 13 μg/L in sea water, being 14th in natural abundance in the Earth's crust), being naturally found only

in combination with other elements in minerals. Since ultrapure barium is hard to prepare, its major physical properties are not well characterized as of yet.

Chemically, barium is rather similar to magnesium, calcium, and strontium, being even more reactive. It always exhibits the oxidation state of +2 and easily and exothermally reacts with chalcogens. Its reactions with water and alcohols are also very exothermic. Due to its ability to react with oxygen and air, barium is stored under oil or inert gas atmosphere.

The most common industrial use of barium metal or barium-aluminum alloys is gettering, that is, the removal of unwanted gases from the vacuum tubes. Barium sulfate is used in the petroleum industry (as the drilling fluid), paint, or as a filler for plastics and rubbers. Due to its low toxicity and relatively high density, barium sulfate is widely used as the radiocontrast agent in the X-ray imaging of the digestive tract. Barium nitrate can be added to fireworks to provide them with a green color.

There is no information on the toxicity of the metallic barium due to its high reactivity. Barium is not carcinogenic and does not bioaccumulate. Although insoluble barium sulfate is not toxic, water-soluble barium compounds are poisonous. At low doses, barium ions act as a muscle stimulant, whereas higher doses affect the nervous system, causing cardiac irregularities, tremors, weakness, anxiety, dyspnea, and paralysis. These effects were attributed to the capability of Ba^{2+} to block potassium ion channels, which are critical to the proper function of the nervous system (Werman and Grundfest 1961; Gilly and Armstrong 1982; Armstrong and Taylor 1980).

Barium and EF-Hand Proteins

Calmodulin and Barium

Since calcium ions are important second messengers in various signaling processes of almost all organisms, cells contain various Ca^{2+}-binding proteins that can sense calcium concentration and often undergo the calcium ion binding-induced conformational changes which alter their ability to interact with other proteins. An illustrative example of such calcium sensor is calmodulin (CaM, an abbreviation for CALcium-MODULated proteIN), which is a prototypic EF-hand calcium-binding protein that acts by sensing calcium levels and binding to target proteins in a regulatory manner. The importance of this protein for all the vertebrates is reflected in its 100% sequence conservation. Calmodulin is a small protein comprising of 148 amino acids long with the molecular mass of 16.7 kDa. It contains four EF-hand motifs, each of which binds a single Ca^{2+} ion. Structurally, CaM has two approximately symmetrical globular domains (the N- and C-domains, each containing two EF-hands), separated by a flexible linker region. EF-hands are characterized by the presence of specific electronegative environment necessary for calcium coordination. Calcium binding induces noticeable conformational changes, where hydrophobic methyl groups of the key methionine residues become solvent exposed, generating specific hydrophobic surfaces, which can in turn bind to basic amphiphilic helices (BAA helices) on the target protein.

In addition to be able to sense calcium, CaM is able to be activated by other metal ions, although the CaM affinities of many metal ions are noticeably lower than that of calcium. For example, the CaM-regulated activation of cerebellar nitric oxide synthase requires an over 200-fold higher concentration of Ba^{2+} than of Ca^{2+}, and the interaction between CaM and caldesmon is weakened by the exchange of Ca^{2+} for Ba^{2+} (Kursula and Majava 2007). Based on the X-ray crystallographic analysis of the calmodulin crystals soaked in barium chloride, it was concluded that Ba^{2+} is able to substitute Ca^{2+} in EF-hand 2 but not in any of the other EF-hands. The coordination of the Ba^{2+} ion was similar to that of Ca^{2+}, and the coordination distances between the ion and the O atoms of CaM EF-hand 2 ranged between 2.5 and 2.8 Å, whereas the coordination distances for Ca^{2+} in CaM are usually 2.3 Å (Kursula and Majava 2007). In addition to the canonical binding within the EF-hand 2, CaM possesses a second Ba^{2+}-binding site in the close vicinity of the EF-hand 2 (Kursula and Majava 2007). The differences in the Ca^{2+} and Ba^{2+} binding to calmodulin were explained by the much larger ionic radius of Ba^{2+} (1.35 Å) when compared with Ca^{2+} (0.99 Å) (Kursula and Majava 2007).

Barium and FhCaBP4

In addition to calmodulin, different organisms are known to contain some additional calcium sensors. In trematodes (which are flatworm parasites), these sensors are presented by a family of proteins which combine EF-hand-containing domains with dynein

light chain (DLC)-like domains. Functional characterization of the member of this protein family, FhCaBP4 from liver fluke (*Fasciola hepatica*), that has an N-terminal domain containing two imperfect EF-hand sequences and a C-terminal dynein light chain-like domain revealed that in addition to calcium this protein can bind barium (Orr et al. 2012).

Barium and KChIPs

KChIPs are Kv channel-interacting proteins that bind to the cytoplasmic N-terminus of Kv4 α-subunits and regulate the ion current of Kv channels. There are four KChIP families, KChIP1, KChIP2, KChIP3, and KChIP4, each is encoded by different genes and contains several splice variants. Although all KChIPs share a high degree of sequence homology at their C-terminal domains that contain four EF-hands, their N-terminal domains are notably diversified (Chang et al. 2003). A representative member of this family of proteins, KChIP1, was shown to possess two types of Ca^{2+}-binding sites, high-affinity and low-affinity Ca^{2+}-binding sites. However, only low-affinity-binding site for Mg^{2+}, Sr^{2+}, and Ba^{2+} was observed in this protein (Chang et al. 2003). Deletion-mutation analysis revealed that EF-hand 4 of KChIP1 is likely to represent the high-affinity-binding site, whereas the intact low-affinity-binding site for metal ions is likely to be located at EF-hand 2 or EF-hand 3. Although in its apo-form KChIP1 has a propensity to form dimers, binding of metal ions promoted structural changes in this protein leading to its tetramerization (Chang et al. 2003).

Ba^{2+}-Dependent Inactivation of L-Type α_{1C} Calcium Channel

The voltage-dependent calcium channels control the calcium ion influx that plays a major role in the excitation-contraction coupling of cardiac myocytes. In the cardiac L-type calcium channel, there are seven to nine distinct α_1-subunits (α_{1A}, α_{1B}, α_{1C}, α_{1D}, α_{1E}, α_{1F}, α_{1G}, α_{1H}, and α_{1S}). The C-terminal region of the α_{1C}, with its EF-hand binding motif, is especially important for a negative feedback mechanism related to the regulating voltage-dependent calcium influx in cardiac cells. This EF-hand binding motif is mostly conserved between the C-termini of six of the seven α_1-subunit Ca^{2+} channel genes. Mutational analysis of the role of the glutamate residue E1537 located in the EF-hand binding motif of the cardiac α_{1C} channel revealed that the whole-cell Ba^{2+} and Ca^{2+} currents proceeded more slowly as the glutamate residue was replaced by more hydrophobic residues in the following order: E > Q > G ≈ S > A (Bernatchez et al. 1998).

Barium as a Modulator of c-Fos Expression and Posttranslational Modification

The analysis of the effect of the exogenous barium on PC12 rat pheochromocytoma cells revealed the existence of the transient induction of the *c-fos* gene and showed that the barium-induced c-fos protein underwent less extensive posttranslational modifications (Curran and Morgan 1986). These effects were specific to barium and were not shared by a range of di- and trivalent cations examined (such as cadmium, cesium, cobalt, magnesium, manganese, lanthanum, strontium, tin, or zinc ions in concentrations up to 10 mM). The unique ability of barium to boost the *c-fos* gene expression was due to the capability of this cation to enter the cell through a voltage-dependent calcium channel and interact with calmodulin to stimulate c-fos expression (Curran and Morgan 1986).

Barium and Potassium Channels

Potassium Channels and Structural Determinants of Their Specificity

Many fundamental biological processes including electrical signaling in the nervous system depend on the rapid diffusion of potassium ions across cell membranes. This diffusion across the cell membranes is determined by the existence of specific proteins, K^+ channels, which use diverse mechanisms of gating (the processes by which the pore opens and closes), but they all exhibit very similar ion permeability characteristics (Doyle et al. 1998). In fact, all K^+ channels show a selectivity sequence of $K^+ \approx Rb^+ > Cs^+$, whereas their permeability for the smallest alkali metal ions Na^+ and Li^+ is very low (Doyle et al. 1998). In fact, all potassium channels are at least 10,000 times more permeable to K^+ than to Na^+. On the other hand, K^+ channels exhibit a throughput rate approaching the diffusion limit (Doyle et al. 1998). This unusual combination of a high K^+ selectivity with a high throughput rate suggested the existence of some specific properties of the ion conductance pore.

The X-ray analysis of the potassium channel from *Streptomyces lividans* (KcsA K^+ channel, which is an integral membrane protein with high sequence

similarity to all known K^+ channels, particularly in the pore region) revealed that the four identical subunits of this protein create an inverted cone that contained the selectivity filter of the pore in its outer end (Doyle et al. 1998). The narrow selectivity filter is only 12 Å long, whereas the remainder of the pore is wider and lined with hydrophobic amino acids.

Structurally, this selectivity filter was shown to be characterized by two essential features. First, the main chain atoms of regions involved in the formation of the selectivity filter create a stack of sequential oxygen rings. This stack of oxygen rings represents numerous closely spaced sites of suitable dimensions for coordinating a dehydrated K^+ ion that therefore has only a very small distance to diffuse from one site to the next within the selectivity filter. The second important structural feature of the selectivity filter is the protein packing around it. Here is how this structural feature is described in the original article (Doyle et al. 1998): "The Val and Tyr side chains from the V-G-Y-G sequence point away from the pore and make specific interactions with amino acids from the tilted pore helix. Together with the pore helix Trp residues, the four Tyr side chains form a massive sheet of aromatic amino acids, twelve in total, that is positioned like a cuff around the selectivity filter. The hydrogen bonding, for example, between the Tyr hydroxyls and Trp nitrogens, and the extensive van der Waals contacts within the sheet offer the immediate impression that this structure behaves like a layer of springs stretched radially outward to hold the pore open at its proper diameter." This intricate spatial organization of the selectivity filter and a region around it in the potassium channel produce structural constraints to coordinate K^+ ions but not smaller Na^+ ions. Since in the crystal structure, the selectivity filter contained two K^+ ions about 7.5 Å apart, it was proposed that such configuration promoted ion conduction by exploiting electrostatic repulsive forces to overcome attractive forces between K^+ ions and the selectivity filter (Doyle et al. 1998).

Structural Basis for the Barium-Induced Inhibition of the Ca^{2+}-Activated K^+ Channels

The effect of barium on the potassium channels is determined by its physicochemical properties. In fact, the atomic, covalent, and van der Waals radii of barium are of 222, 215 ± 11, and 268 pm, respectively. These values compare favorably with those of potassium (227, 203 ± 12, and 275 pm, respectively). Therefore, stereochemically and geometrically, a potassium channel "sees" the Ba^{2+} cation as a divalent K^+ ion (Jiang and MacKinnon 2000). However, although the size allows barium to fit into the selectivity filter of the channel, its doubled charge defines tighter binding. Therefore, binding of Ba^{2+} to the channel's filter prevents the rapid flow of K^+ (Jiang and MacKinnon 2000). In fact, the Ca^{2+}-activated K^+ channel was shown to be forced to close with a single Ba^{2+} ion inside the pore. Furthermore a Ba^{2+} ion inside the closed channel was trapped and cannot escape until the channel was opened (Miller 1987).

Since the trapping of barium inside the channel and its ability to exit to the external side were strongly dependent on the potassium concentration on both sides of the membrane, the existence of three K^+ ion sites (the external lock-in site, the enhancement site that is located closer to the barium-binding site, and the internal lock-in site located between the position of Ba^{2+} and the internal entryway) was proposed (Neyton and Miller 1988). The presence of K^+ at the external lock-in site obstructs the outward movement of barium, whereas occupancy of both, the external lock-in and the enhancement, sites by K^+ would destabilize Ba^{2+} and speed its exit to the inside (Neyton and Miller 1988). The internal lock-in site is occupied by K^+ with the affinity of ~10 mM, being also not very selective for K^+ when compared with Na^+ (Neyton and Miller 1988). In agreement with this model, structural analysis of the Rb^+-saturated KcsA K^+ channel equilibrated with solutions containing barium chloride revealed that there were four distinct Rb^+-binding sites inside the channel. These Rb^+-binding sites contained one outer, two inner, and one cavity ions. The outer ion was near the extracellular entryway and the inner ion was closer to the cavity and was shown to be present at either of two positions, closer to the inner ion or closer to the outer ion. Ba^{2+} resides at a single location within the selectivity filter, being located at the location of the inner ion closest to the central cavity (Jiang and MacKinnon 2000).

Inhibition of the Na+/K(+)-Pump in Mast Cells

When mast cells are stimulated (both in a IgE-directed and non-IgE-directed way), they release potent mediators of inflammation (e.g., histamines), thereby playing an important role in the pathogenesis of disease states in which the inflammatory response contributes to the development of the clinical symptoms (Knudsen 1995). Mast cells contain Na+/K(+)-pump that is able to respond

to changes in the intracellular sodium concentration and that is inhibited by lanthanides and several divalent cations, including barium (Knudsen 1995).

Barium Inhibition of Kir2 Channels

Inward rectifier K^+ (Kir2) channel is present in a number of excitable and non-excitable cell types, such as cardiac muscle, skeletal muscle, some neurons, epithelial cells, and vascular endothelial cells. In cardiac, neurons, and other excitable tissues, these channels stabilize the membrane potential until a threshold potential can be reached. The Kir2 conductance, which is qualitatively dependent on the membrane potential and extracellular K^+ concentration, is inhibited by barium (Park et al. 2008).

Barium Activation of the Ca^{2+}-Activated and Voltage-Dependent BK-Type K^+ Channel

The Ca^{2+}-activated and voltage-dependent big K^+ channel (BK-type channel also known as Maxi-K or slo1 channel) is characterized by the large conductance of K^+ ions through the cell membrane and encodes negative feedback regulation of membrane voltage and Ca^{2+} signaling. Here, depolarization of the membrane voltage and increased intracellular Ca^{2+} levels both cause BK channels to open, which hyperpolarizes the membrane and closes voltage-dependent channels, including Ca^{2+} channels, reducing Ca^{2+} influx into the cell. BK channels are found virtually in all excitable and non-excitable tissues, with the exception of heart, and play a number of crucial roles in regulation of smooth muscle tone and neuronal excitability, for example, being involved in controlling the contraction of smooth muscles and electrical tuning of hair cells in the cochlea. BK channel represents a homo-tetramer of the channel forming α-subunits (each being the product of the *KCNMA1* gene) decorated by modulatory β-subunits (encoded by *KCNMB1*, *KCNMB2*, *KCNMB3*, or *KCNMB4* genes). BK α-subunit is a large modular protein containing seven transmembrane segments (residues 1–343) and a large intracellular C-terminal domain (residues 344–1113). In the transmembrane N-terminal part, there are several functional segments, such as a unique transmembrane region (S0) that precedes the 6 transmembrane segments (S1–S6) conserved in all voltage-dependent K^+ channels and comprising a voltage-sensing domain (S1–S4) and a K^+ channel pore domain (S5, selectivity filter, and S6). A cytoplasmic C-terminal domain (CTD) consisting of a pair of RCK regions (RCK1, residues 344–613, and RCK2, residues 718–1056) that are connected by a long linker and assemble into an octameric gating ring on the intracellular side of the tetrameric channel, in addition to regulating the pore directly, may also modulate the voltage sensor (Yuan et al. 2010). The CTD contains a high-affinity binding site for Ca^{2+}, called "calcium bowls," encoded within the RCK2 domain of each monomer (Zhou et al. 2012). Furthermore, RCK1 contain a second high-affinity Ca^{2+}-binding site. Therefore, one tetrameric BK channel contains eight Ca^{2+}-binding sites that contribute to regulation by Ca^{2+}.

Early analysis of the divalent cation selectivity of the BK-channel Ca^{2+}-binding sites revealed that Ca^{2+} and Sr^{2+} were effective at the Ca^{2+} bowl, and Ca^{2+}, Cd^{2+}, and Sr^{2+} acted through the RCK1 domain, whereas divalent cations of smaller ionic radius, such as Mn^{2+}, Co^{2+}, Mg^{2+}, and Ni^{2+}, were ineffective or only weakly effective at either of the higher-affinity sites (Zeng et al. 2005). It was shown recently that Ba^{2+}, which is typically considered as a specific blocker of potassium channels, is also able to activate BK channel via specific binding to the Ca^{2+}-bowl site (Zhou et al. 2012). Since ionic radius of Ba^{2+} is larger than that of Sr^{2+} and Ca^{2+}, this finding provided a valuable support to the hypothesis that ionic radius is an important determinant of selectivity differences among different divalent cations observed for each Ca^{2+}-binding site of the BK channels (Zhou et al. 2012).

Cross-References

- ▶ Barium, Physical and Chemical Properties
- ▶ Calmodulin
- ▶ EF-Hand Proteins
- ▶ Potassium Channel Diversity, Regulation of Potassium Flux across Pores
- ▶ Potassium Channels, Structure and Function

References

Armstrong CM, Taylor SR (1980) Interaction of barium ions with potassium channels in squid giant axons. Biophys J 30:473–488

Bernatchez G, Talwar D, Parent L (1998) Mutations in the EF-hand motif impair the inactivation of barium currents of the cardiac alpha1C channel. Biophys J 75:1727–1739

Chang LS, Chen CY, Wu TT (2003) Functional implication with the metal-binding properties of KChIP1. Biochem Biophys Res Commun 311:258–263

Curran T, Morgan JI (1986) Barium modulates c-fos expression and post-translational modification. Proc Natl Acad Sci USA 83:8521–8524
Doyle DA, Morais Cabral J, Pfuetzner RA, Kuo A, Gulbis JM, Cohen SL, Chait BT, MacKinnon R (1998) The structure of the potassium channel: molecular basis of K^+ conduction and selectivity. Science 280:69–77
Gilly WF, Armstrong CM (1982) Divalent cations and the activation kinetics of potassium channels in squid giant axons. J Gen Physiol 79:965–996
Jiang Y, MacKinnon R (2000) The barium site in a potassium channel by x-ray crystallography. J Gen Physiol 115:269–272
Knudsen T (1995) The Na+/K(+)-pump in rat peritoneal mast cells: some aspects of regulation of activity and cellular function. Dan Med Bull 42:441–454
Kursula P, Majava V (2007) A structural insight into lead neurotoxicity and calmodulin activation by heavy metals. Acta Crystallogr Sect F Struct Biol Cryst Commun 63:653–656
Miller C (1987) Trapping single ions inside single ion channels. Biophys J 52:123–126
Neyton J, Miller C (1988) Potassium blocks barium permeation through a calcium-activated potassium channel. J Gen Physiol 92:549–567
Orr R, Kinkead R, Newman R, Anderson L, Hoey EM, Trudgett A, Timson DJ (2012) FhCaBP4: a *Fasciola hepatica* calcium-binding protein with EF-hand and dynein light chain domains. Parasitol Res 111:1707–1713
Park WS, Han J, Earm YE (2008) Physiological role of inward rectifier K(+) channels in vascular smooth muscle cells. Pflugers Arch 457:137–147
Werman R, Grundfest H (1961) Graded and all-or-none electrogenesis in anthropod muscle. J Gen Physiol 44:997–1027
Yuan P, Leonetti MD, Pico AR, Hsiung Y, MacKinnon R (2010) Structure of the human BK channel Ca^{2+}−activation apparatus at 3.0 A resolution. Science 329:182–186
Zeng XH, Xia XM, Lingle CJ (2005) Divalent cation sensitivity of BK channel activation supports the existence of three distinct binding sites. J Gen Physiol 125:273–286
Zhou Y, Zeng XH, Lingle CJ (2012) Barium ions selectively activate BK channels via the Ca^{2+}-bowl site. Proc Natl Acad Sci USA 109:11413–11418

Barium(II) Transport in Potassium(I) and Calcium(II) Membrane Channels

J. Preben Morth and Harmonie Perdreau
Centre for Molecular Medicine Norway (NCMM), Nordic EMBL Partnership, University of Oslo, Oslo, Norway

Synonyms

Ba; Barium

Definition

Barium is an alkaline earth metal that can be used as a substrate analogue of other alkaline earth metals (e.g., calcium) and alkali metals (e.g., potassium) in electrophysiology and membrane transport researches.

Background

Barium is a chemical element from the group 2 of alkaline earth metals, with symbol Ba and atomic number 56. The name barium originates from Greek *barys*, meaning "heavy," and though the chemical has been known for centuries, it was initially isolated in 1808 by the English chemist Sir Humphrey Davy.

Barium is the fourteenth most abundant element in the Earth's crust and is estimated to constitute about 0.05% of the elemental mass. Nevertheless, Ba is not found in its pure form (a soft silvery-white metal) in nature due to its high reactivity with oxygen and water. The most common naturally occurring barium minerals are barite (barium sulfate, $BaSO_4$) and witherite (barium carbonate, $BaCO_3$).

Physical and Chemical Properties

Barium belongs to the same family as the well-known magnesium (Mg) and calcium (Ca) metals with which it shares certain ▶ physical and chemical properties:

- Relatively soft metal with a shiny silvery-white color
- Harder, denser, and higher melting point than sodium and potassium
- High reactivity with oxygen and water (but less than alkali metals from group 1)
- Oxidation number of +2

The biological applications of barium are limited since $BaSO_4$ have low solubility in water (0.0024 g/100 mL at 20°C). The free Ba^{2+} ions are highly toxic and have been used as rodenticides and pesticides. Incidences of human poisonings by soluble barium salts are rare; however, isolated cases have been reported, in particular for people living or working near high-risk areas like heavy industrial sites. Barium poisoning can notably induce a rapid hypokalemia, resulting in nausea, diarrhea, cardiac problems,

and muscular spasms/paralysis. Patients are then treated by potassium administration (Smith and Gosselin 1976).

Despite its toxicity, barium chloride ($BaCl_2$) is the most commonly used barium salt as its solubility in water reaches 35.8 g/100 mL at 20°C. $BaCl_2$ is particularly used in brine purification, pigment synthesis, and salt manufacturing. In laboratories, this barium salt is used as a test for sulfate ions, as it reacts with these ions to produce a white precipitate of barium sulfate.

There are seven naturally occurring barium isotopes, the most abundant being ^{138}Ba (71.7%). About a dozen radioactive isotopes of barium are also known, but they present very short half-lives (from several milliseconds to several seconds), and none of them has any practical commercial application. The only notable exception is ^{133}Ba which has a half-life of 10.51 years and is used as a standard source for gamma-ray detectors in nuclear physics studies.

Clinical Applications

Barium compounds are usually toxic and not used in any clinical studies. The only exception is barium sulfate, used for its density, insolubility, and X-ray opacity as a radiocontrast agent for imaging the human gastrointestinal tract. This form of barium, insoluble in water or human fluids, does not bioaccumulate. "Barium meals" and "barium enemas" are then used for radiologic examination of patients with swallowing disorders, polyps, inflammatory bowel diseases, colorectal cancers, etc. (Ott 2000).

Scientific Applications

Because of its toxicity, the use of barium in scientific approaches is somewhat limited. Barium chloride is yet utilized in electrophysiological studies as a substrate analogue of other alkaline earth metals (e.g., calcium) and alkali metals (e.g., potassium). The common stock and working solutions are 1 M $BaCl_2$ and 10–100 nM $BaCl_2$, respectively.

Study of Potassium (K) Channels

Ba^{2+} ions are well-known efficient K^+ channel (▶ Potassium Channels, Structure and Function) blockers, and they are widely used in electrophysiological and structural studies as a probe to investigate the permeation mechanisms of these channels.

Neyton and Miller showed in 1988 (Neyton and Miller 1988a, b), through single-channel studies of Ca^{2+}-activated K^+ (BK) channels, that barium ions have a size that allow them to enter inside the pore. Because of their charges, Ba^{2+} ions bind tightly and prevent the flow of K^+ in the narrow pore of BK channels. They also showed that barium is a reversible blocker effective from either side of the membrane and sensitive to the presence of K^+ ions in the pore. Indeed, it is observed that in the presence of low extracellular concentrations of K^+ ions (0.01 mM), Ba^{2+} ions mainly dissociate to the external solution, while in the presence of higher K^+ ion concentrations (500 mM), dissociation to the internal solution is favored. These properties were attributed to two distinct K^+ ion binding sites and classified the K^+ channels as "long-pore channels," constituted of multiple ions in single file inside a long and narrow pore.

For scientific experimental usage today, the blockade properties of Ba^{2+} ions are used to understand the ion selectivity of K^+ channels. Indeed, K^+ channels are able to conduct K^+ ions at nearly diffusion-limited rates and, at the same time, to prevent Na^+ ions from conducting. A number of studies are about the necessary properties of ions (i.e., size, charge) and channels to recognize each other.

A recent structural and thermodynamic study of *Streptomyces lividans* K^+ channel (KcsA) revealed that two Ba^{2+} ions can bind the channel by an exothermic reaction (Lockless et al. 2007). They proposed that the ion/channel selectivity is achieved by the size of the ion and the structure of the ion-binding site. K^+ and Ba^{2+} ions have indeed different electric field strengths at their surface but nearly the same size: The ionic radius of Ba^{2+} (1.35 Å) is very close to that of K^+ (1.33 Å), whereas the radii of Ca^{2+} (0.99 Å) and Na^+ (0.95 Å) are smaller. Furthermore, the ion-binding sites of KcsA are created by eight oxygen ligands and appropriately sized for K^+/Ba^{2+} ions and not for Na^+ ions. Figure 1 presents the crystal structure of KcsA in complex with Ba^{2+} ions.

Study of Calcium (Ca) Channels

The basic mechanism of Ca^{2+} channels (▶ Bacterial Calcium Binding Proteins) is complex because it

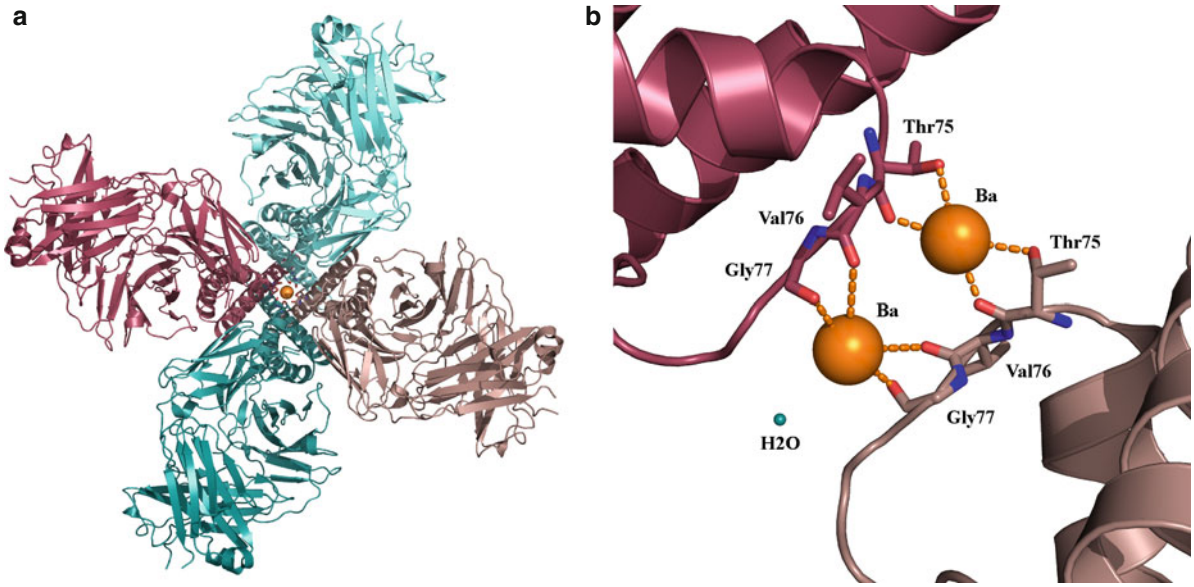

Barium(II) Transport in Potassium(I) and Calcium(II) Membrane Channels, Fig. 1 Biological assembly of Streptomyces lividans K^+ channel (KcsA) in complex with barium chloride. (**a**) Assumed biological molecule composed of four partners. (**b**) Interacting residues in the metal binding site, only two partners are represented. The figure was generated with Protein Data Bank identification code: 2ITD. Using the PyMOL Molecular Graphics System, Version 1.3, Schrödinger, LLC

depends on the presence or absence of extracellular Ca^{2+} ions:

- When Ca^{2+} ions are present (physiological conditions), the channels are selective (▶ Calcium Ion Selectivity in Biological Systems) and exclude other cations.
- When Ca^{2+} ions are absent, the channels become permeable to Ba^{2+} and other divalent and monovalent cations.

In contrast to the K^+ channel, the Ca^{2+} channel pore has a relatively wide diameter of 6 Å which allows, in absence of the high-affinity Ca^{2+} ions, the conduction of other ions, mainly depending on their size (McCleskey and Almers 1985).

Thereby, Ba^{2+} ions can be used, according to the experimental conditions:

- To reduce the contamination by K^+ currents and to obtain a more specific result in the study of Ca^{2+} channels. For example, Almog et al. replaced Ca^{2+} ions (2 mM) in the application solution with Ba^{2+} ions (5 mM) for the characterization of voltage-gated Ca^{2+} channels, because of the similarity of the activation curves with Ca^{2+} or Ba^{2+} (Almog and Korngreen 2009).
- To differentiate Ca^{2+} channel types. Indeed, inward currents are 2-fold larger with Ba^{2+} than Ca^{2+} for L-channels, whereas they are quite comparable for T-channels (Hess and Tsien 1984; Huguenard 1996).
- To unravel the ion selectivity mechanism of the different Ca^{2+} channels. For instance, subtle differences can be shown between Ca^{2+} and Ba^{2+} permeations in T-type channels, more particularly in the presence of Mg^{2+} ions (Serrano et al. 2000).

Cross-References

- ▶ Barium, Physical and Chemical Properties
- ▶ Calcium Ion Selectivity in Biological Systems
- ▶ Calcium-Binding Proteins, Overview
- ▶ Potassium Channels, Structure and Function

References

Almog M, Korngreen A (2009) Characterization of voltage-gated Ca(2+) conductances in layer 5 neocortical pyramidal neurons from rats. PLoS One 4(4):e4841

Hess P, Tsien RW (1984) Mechanism of ion permeation through calcium channels. Nature 309(5967):453–456

Huguenard JR (1996) Low-threshold calcium currents in central nervous system neurons. Annu Rev Physiol 58:329–348

Lockless SW, Zhou M, MacKinnon R (2007) Structural and thermodynamic properties of selective ion binding in a K^+ channel. PLoS Biol 5(5):e121
McCleskey EW, Almers W (1985) The Ca channel in skeletal muscle is a large pore. Proc Natl Acad Sci USA 82(20):7149–7153
Neyton J, Miller C (1988a) Discrete Ba^{2+} block as a probe of ion occupancy and pore structure in the high-conductance Ca^{2+} – activated K^+ channel. J Gen Physiol 92(5):569–586
Neyton J, Miller C (1988b) Potassium blocks barium permeation through a calcium-activated potassium channel. J Gen Physiol 92(5):549–567
Ott DJ (2000) Accuracy of double-contrast barium enema in diagnosing colorectal polyps and cancer. Semin Roentgenol 35(4):333–341
Serrano JR, Dashti SR, Perez-Reyes E, Jones SW (2000) Mg(2+) block unmasks Ca(2+)/Ba(2+) selectivity of alpha1G T-type calcium channels. Biophys J 79(6):3052–3062
Smith RP, Gosselin RE (1976) Current concepts about the treatment of selected poisonings: nitrite, cyanide, sulfide, barium, and quinidine. Annu Rev Pharmacol Toxicol 16:189–199

Barium, Physical and Chemical Properties

Timothy P. Hanusa
Department of Chemistry, Vanderbilt University, Nashville, TN, USA

Synonyms

Alkaline-earth metal; Atomic number 56

Definition

The heaviest nonradioactive member of the alkaline-earth elements (atomic number 56), barium is a soft, silvery, highly reactive metal. Its compounds have various uses, particularly in drilling fluids, paints, glasses, and pyrotechnics, but all soluble compounds of barium are toxic to mammals. The insoluble barium sulfate is used as a radiocontrast agent in medical imaging.

Background

Barium is a member of the alkaline-earth family of metals (Group 2 in the periodic table). It is a relatively common element, ranking approximately 14th in natural abundance in the Earth's crust; it is more plentiful than, for example, sulfur or zinc. The free metal does not occur in nature, but is found combined in minerals such as barite (barium sulfate, $BaSO_4$) (Fig. 1), or less commonly, in witherite (barium carbonate, $BaCO_3$). The density of such compounds (i.e., $BaSO_4$, 4.5 g cm^{-3}; $BaCO_3$, 4.3 g cm^{-3}) has long been reflected in their names; barite, for example, was at one time known as *terra ponderosa*, heavy spar, or barytes (from the Greek βαρύς *barys*, meaning "heavy"). Barium oxide (BaO, 5.7 g cm^{-3}) was similarly called *baryta*, and barium hydroxide ($Ba(OH)_2$), baryta water. When Sir Humphry Davy first isolated the metal by electrolysis of a mixture of barium oxide and mercuric oxide in 1808, he used the stem of the word baryta to form the name of the element. (Ironically, the name is not as appropriate for barium itself; the density of the metal (3.51 g cm^{-3}) is less than half that of iron, and it is only 30% more dense than aluminum.) The most important commercial source of barium is barite; its production in recent decades has varied between 6 and 8 million tons/year. Over half the world's supply comes from China, with India, the USA, and Morocco together providing about one quarter of the total.

Isotopes

Naturally occurring barium comprises six stable isotopes; ^{138}Ba is the most common (72%), followed by ^{137}Ba (11%) and ^{136}Ba (7.9%) (Table 1). One other naturally occurring isotope (^{130}Ba, 0.11%) undergoes decay by double electron capture; its half-life (7×10^{13} year) is many times the age of the universe, however, and can be considered stable for practical purposes. The synthetic isotopes are radioactive with far shorter half-lives, with mass numbers ranging from 114 to 153. The isotope with the longest half-life (^{133}Ba, 10.5 year) is used as a gamma reference source. The next longest-lived isotope (^{140}Ba) has a half-life of only 13 days, and it, along with ^{141}Ba (18 min) and ^{139}Ba (83 min), played a key role in the discovery of nuclear fission by Hahn, Strassman, and Meitner in 1938. They found that after the ^{235}U nucleus split under neutron bombardment, the three barium isotopes were detectable among the fission products. Some use has been made of $^{131}Ba/^{131}Cs$ (half-lives of 11.5 and 9.7 days, respectively) in radiation treatments (prostate brachytherapy).

Barium, Physical and Chemical Properties, Fig. 1 Sand-encrusted blades of barite ($BaSO_4$) form *rose rock*, the official state rock of Oklahoma

Barium, Physical and Chemical Properties, Table 1 Selected isotopes of barium

Nuclide	Nat. abund (%)	Nuclear spin	Half-life
^{130}Ba	0.106%	0	7×10^{13} year
^{131}Ba	–	+1/2	11.5 days
^{132}Ba	0.101%	0	stable
^{133}Ba	–	+1/2	10.51 year
^{134}Ba	2.42%	0	stable
^{135}Ba	6.59%	+3/2	stable
^{136}Ba	7.85%	0	stable
^{137}Ba	11.2%	+3/2	stable
^{138}Ba	71.7%	0+	stable
^{139}Ba	–	−7/2	83.1 min
^{140}Ba	–	0	12.75 days
^{141}Ba	–	−3/2	18.3 min
^{142}Ba	–	0	10.6 min

Properties of the Metal

Various physical and chemical properties of barium are listed in Table 2. Barium is a lustrous, silvery metal that is relatively soft (Mohs hardness of 1.5). It crystallizes in a body-centered cubic lattice with $a = 5.028$ Å. It readily oxidizes when exposed to air, and must be protected from oxygen during storage. One of the few applications for elemental barium takes advantage of this property; thin films of the metal serve as getters in vacuum and cathode ray tubes, and chemically remove traces of oxygen that otherwise could cause tube failure. Barium also forms an alloy with nickel that finds use in automobile spark plug electrodes, and it is a component of Frary metal, an alloy of lead, calcium, and barium that has been used as a bearing metal.

Barium, Physical and Chemical Properties, Table 2 Atomic and physical properties of barium

Atomic number	56	E° for $M^{2+}(aq) + 2e^- \rightarrow M(s)$	−2.91 V
Number of naturally occurring isotopes	7	Melting point	727°C
Atomic mass	137.33	Boiling point	1,870°C
Electronic configuration	$[Xe]6s^2$	Density (20°C)	3.51
Ionization energy (kJ mol^{-1})	502.7 (1st); 965 (2nd)	ΔH_{fus} (kJ mol^{-1})	7.8
Metal radius	2.22 Å	ΔH_{vap} (kJ mol^{-1})	136
Ionic radius (6-coordinate)	1.35 Å	Electrical resistivity (20°C)/ μohm cm	34

General Properties of Compounds

Barium exclusively displays the +2 oxidation state in its compounds. The metal is highly electropositive ($\chi = 0.89$ on the Pauling scale; 0.97 on the Allred-Rochow scale; cf. 0.93 and 1.01, respectively for sodium), and with a noble gas electron configuration for the Ba^{2+} ion ($[Xe]6s^0$), the metal-ligand interactions are usually viewed as electrostatic. To a first approximation, the bonding can be considered as nondirectional, and strongly influenced by ligand packing. The structures of barium compounds with multidentate and sterically bulky ligands can be highly irregular.

It has been clear since the 1960s that a more sophisticated analysis of bonding than that provided by simple electrostatics must be used with some compounds of the heavy alkaline-earth metals. The gaseous Group 2 dihalides (MF_2 (M = Ca, Sr, Ba), MCl_2 (M = Sr, Ba), $BaBr_2$, BaI_2) (Hargittai 2000), for example, are nonlinear, contrary to the predictions of electrostatic bonding. An argument based on the "reverse polarization" of the metal core electrons by the ligands has been used to explain their geometry, an

analysis that makes correct predictions about the ordering of the bending for the dihalides (i.e., Ca < Sr < Ba; F > Cl > Br > I). The "reverse polarization" analysis can be recast in molecular orbital terms; that is, bending leads to a reduction in the antibonding character in the HOMO.

An alternative explanation for the bending in ML_2 species has focused on the possibility that metal *d* orbitals might be involved. Support for this is provided by calculations that indicate a wide range of small molecules, including MH_2, MLi_2, $M(BeH)_2$, $M(BH_2)_2$, $M(CH_3)_2$, $M(NH_2)_2$, $M(OH)_2$, and MX_2 (M = Ca, Sr, Ba) should be bent, owing partially to the effect of metal d-orbital occupancy. The energies involved in bending are sometimes substantial (e.g., the linearization energy of $Ba(NH_2)_2$ is placed at ca. 28 kJ mol^{-1}) (Kaupp and Schleyer 1992). Spectroscopic confirmation of the bending angles in most of these small molecules is not yet available, however.

The standard classification of alkali and alkaline-earth ions as hard (type a) Lewis acids leads to the prediction that ligands with hard donor atoms (e.g., O, N, halogens) will routinely be preferred over softer (type b; P, S, Se) donors. This is generally true, but studies have demonstrated that the binding of s-block ions to "soft" aromatic donors can be quite robust; for example, the gas-phase interaction energy of two barium atoms with benzene to form the $[Ba(C_6H_6)Ba]$ complex is calculated to be exothermic with a bond energy $D_e[Ba–(C_6H_6)Ba]$ of 162.0 kJ mol^{-1} (Diefenbach and Schwarz 2005). Furthermore, it has been suggested that the toxicity of certain barium compounds may be related to the ability of Ba^{2+} to coordinate to "soft" disulfide linkages, even in the presence of harder oxygen-based residues (Murugavel et al. 2001).

The Ba^{2+} ion is large (the 6-coordinate radius is 1.35 Å) and approximately the same size as potassium (1.38 Å) and polyatomic cations such as NH_4^+ and PH_4^+. Coordination numbers in barium compounds are typically high; a 12-coordinate barium center exists in the $[Ba(NO_3)_6]^{4-}$ ion, for example. In the presence of sterically compact ligands (e.g., -NH_2, -OMe, halides), extensive oligomerization or polymerization will occur, leading to the formation of nonmolecular compounds of limited solubility or volatility. However, sterically bulky ligands can be used to produce compounds with low coordination numbers and improved solubility; barium is only 3-coordinate in $\{Ba[N(SiMe_3)_2]_2\}_2$, for example (Fig. 2) (Westerhausen 1998).

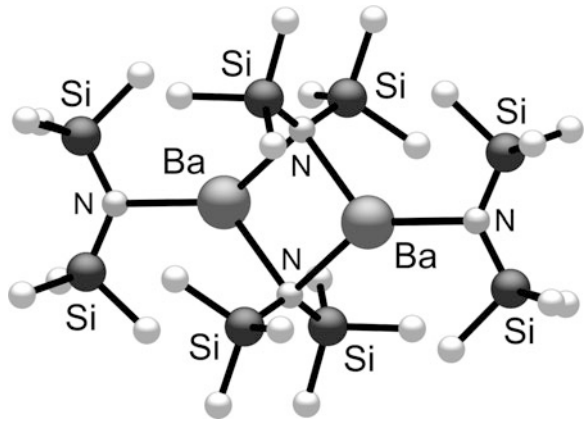

Barium, Physical and Chemical Properties, Fig. 2 Solid state structure of $\{Ba[N(SiMe_3)_2]_2\}_2$

Barium, Physical and Chemical Properties, Table 3 Bond energies in diatomic barium molecules

Ba–E	Enthalpy (kJ mol^{-1})
Ba–H	176 ± 15
Ba–O	562 ± 13
Ba–S	400 ± 19
Ba–F	587 ± 7
Ba–Cl	436 ± 8
Ba–Br	363 ± 8
Ba–I	321 ± 6

The strengths of common barium-element bonds are listed in Table 3. These are for gas-phase species, and so must be used with caution in comparison to the solid state. Bonds to oxygen and fluorine are the strongest that barium forms, and are comparable to those of some early transition metals (e.g., Mo–O = 560 kJ mol^{-1}; V–F = 590 kJ mol^{-1}).

Common Reactions and Compounds of Barium

With Barium-Oxygen Bonds

In addition to its reaction with oxygen at room temperature, barium burns in air to yield a mixture of white barium oxide, BaO, barium nitride, Ba_3N_2, and the peroxide, BaO_2 (1–3). Barium oxide is cleanly made

by heating barium carbonate, $BaCO_3$, and is a high melting solid (1,923°C) with a rock salt lattice that reacts with CO_2 in the reverse of the reaction used to prepare it (4). For a time in the nineteenth century, the reaction of barium oxide with air at 500°C was used to produce the peroxide on an industrial scale (the Brin process); BaO_2 could be subsequently heated at 700°C to release oxygen (5). Prior to the introduction of low-temperature air fractionation, this was a major method for producing oxygen. The oxide finds use today in fluorescent lamps as an electrode coating to enhance electron release.

$$2Ba(s) + O_2(g) \rightarrow 2BaO(s) \quad (1)$$

$$Ba(s) + O_2(g) \rightarrow BaO_2(s) \quad (2)$$

$$3Ba(s) + N_2(g) \rightarrow Ba_3N_2(s) \quad (3)$$

$$BaO(s) + CO_2(g) \rightarrow BaCO_3(s) \quad (4)$$

$$2BaO(s) + O_2(g) \rightleftarrows 2BaO_2(s) \quad (5)$$

About 75% of all barium carbonate produced goes into the manufacturing of specialty glass. The addition of barium increases the refractive index of glass, but unlike lead oxide, it does not increase the dispersion. Before the introduction of lanthanide-containing glasses in the 1930s, this property was critically important in the design of lenses that would minimize astigmatic aberrations. Barium-containing glass is also used to provide radiation shielding in cathode ray and television tubes, although the voltage in such devices must be controlled to avoid secondary emission of X-rays.

Barium and barium oxide react with water to form the hydroxide, $Ba(OH)_2$, and in the case of barium, also hydrogen gas (H_2) (6, 7). Barium hydroxide, which crystallizes as the octahydrate, $Ba(OH)_2 \cdot 8H_2O$, is readily soluble in water (38 g L^{-1}), and is similar to the alkali metal hydroxides in its base strength.

$$Ba(s) + 2H_2O(g) \rightarrow Ba(OH)_2(aq) + H_2(g) \quad (6)$$

$$BaO(s) + H_2O(l) \rightarrow Ba(OH)_2(aq) \quad (7)$$

Barium sulfate (barita) is the main commercial source of barium, although the metal will react with sulfuric acid to form the sulfate (8), and it can be formed from an exchange reaction (e.g., 9). The latter works because of the sulfate's low solubility in water ($K_{sp} = 1.1 \times 10^{-10}$), which causes it to precipitate from solution. Barium sulfate itself is not the direct source of most barium compounds, but it is converted to the soluble sulfide BaS by heating with carbon (10) or hydrogen. The sulfide is then used to prepare other barium derivatives.

$$Ba(s) + H_2SO_4(l) \rightarrow BaSO_4(s) + H_2(g) \quad (8)$$

$$BaCl_2(aq) + Na_2SO_4(aq) \rightarrow BaSO_4(s) + 2NaCl(aq) \quad (9)$$

$$BaSO_4 + 2C(s) \rightarrow BaS(s) + 2CO_2(g) \quad (10)$$

The density of $BaSO_4$ is exploited in its largest industrial use (approx. 80% of world consumption), that of a component in water-based drilling fluid. The sulfate is also used as a pigment in paints (where it is known as *blanc fixe*, i.e., "permanent white"), either alone or in combination with titanium dioxide or zinc sulfide. It finds some use as a filler for rubber or paper, and its insolubility makes it valuable as a radiocontrast agent in medical imaging (see Section "General Properties of Compounds").

Barium nitrate, and to a lesser extent barium chlorate, is used to create a green color in fireworks and other pyrotechnics. Mixed with thermite (aluminum/metal oxide mixture), a small percentage of sulfur and a binder, barium nitrate forms Thermate-TH3, which is used in incendiary grenades.

The technique of chemical vapor deposition (CVD; sometimes abbreviated as MOCVD [metalorganic chemical vapor deposition]) has been under intensive development for the s-block elements, and particularly the alkaline-earth metals, since the late 1980s (Pierson 1999). The production of complex oxides of barium, such as the perovskite-based titanate $BaTiO_3$ and superconducting cuprates (e.g., $YBa_2Cu_3O_{7-x}$) has been one focus of this research. Barium titanate is a ferroelectric ceramic that is used in capacitors, as a piezoelectric material, and in nonlinear optical applications. The high-temperature superconductors have a variety of applications, including use in Josephson junctions and in current-carrying cable.

Simple metal alkoxides and acac derivatives are usually unsuitable as precursors to electronic materials, and even specially modified compounds have difficulties with deposition. For example, fluorinated

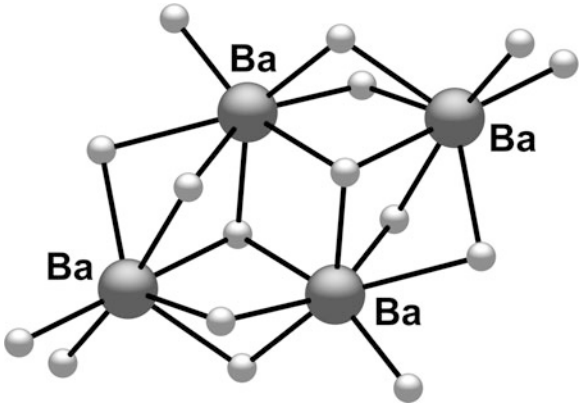

Barium, Physical and Chemical Properties, Fig. 3 Barium-oxygen core of $Ba(tmhd)_2$; in the solid state, the material is a tetrametallic compound. Carbon and hydrogen atoms have been omitted for clarity

compounds are favored for their increased volatility, but their use can lead to the deposition of metal fluorides that contaminate the deposited oxides and require extra processing to remove. Early reports on the thermal behavior of the widely used barium oxide precursor $Ba(tmhd)_2$ (tmhd = 2,2,6,6-tetramethylheptane-3,5-dionate anion, Fig. 3) indicated that ca. 25–40% of the material remained unsublimed under oxide-forming conditions. Such problems were later found to be the result of using partially decomposed or impure material; with the pure compound, only a 5–6% residue remains after heating to 410°C (Drake et al. 1993).

With Barium-Sulfur Bonds

Barium sulfide can be formed from the reaction of barium sulfate with hydrogen (11), but the original and most important method uses carbon as the reducing agent (10). Like the oxide, it possesses a rock salt crystal structure, and is soluble in water. A particular crystalline form of barite found near Bologna, Italy in the early seventeenth century was dubbed "Bologna stone." When strongly heated with charcoal (which formed the sulfide), the material was phosphorescent, and glowed for a time after exposure to bright light. The phenomenon was so unusual that it attracted the attention of many scientists of the day, including Galileo. Barium sulfide was thus the first synthetic phosphor, a property associated with its being a wide band-gap (3.9 eV) semiconductor. Cerium-doped BaS remains of interest as a phosphor for electroluminescent devices (Braithwaite and Weaver 1990).

$$BaSO_4 + 4H_2(950^\circ C) \rightarrow BaS(s) + 4H_2O(g) \quad (11)$$

With Barium-Halogen Bonds

All four halides of barium are known; BaF_2 has the CaF_2 lattice type, $BaBr_2$ and BaI_2 display the $PbCl_2$ lattice, and $BaCl_2$ can crystallize in either type. They are not formed commercially from the metal and halogens, but rather from displacement reactions. BaF_2, for example, is formed from barium carbonate; the insolubility of the fluoride ($K_{sp} = 1.8 \times 10^{-7}$) drives the reaction (12). Barium chloride is made by the neutralization of barium hydroxide with HCl in water (13); the dihydrate product $BaCl_2 \cdot 2H_2O$ can be heated to leave the anhydrous $BaCl_2$. Industrially, $BaCl_2$ can be made from the high-temperature fusion of barium sulfide and calcium chloride (14); the barium chloride is removed with water, leaving the less soluble calcium sulfide behind. Barium bromide can be made from barium carbonate or barium sulfide (15, 16). Barium iodide can be made exactly as the bromide (17), but it is also formed by the reaction of BaH_2 with ammonium iodide in pyridine (18).

$$BaCO_3(aq) + 2NH_4F(aq) \rightarrow BaF_2(s) + (NH_4)_2CO_3(aq) \quad (12)$$

$$Ba(OH)_2 + 2HCl(aq) \rightarrow BaCl_2(aq) + 2H_2O \quad (13)$$

$$BaS + CaCl_2 \rightarrow BaCl_2(s) + CaS(s) \quad (14)$$

$$BaCO_3 + 2HBr(aq) \rightarrow BaBr_2(aq) + H_2O + CO_2(g) \quad (15)$$

$$BaS + HBr \rightarrow BaBr_2 + H_2S(g) \quad (16)$$

$$BaCO_3 + 2HI(aq) \rightarrow BaI_2(aq) + H_2O + CO_2(g) \quad (17)$$

$$BaH_2 + 2NH_4I(aq) \rightarrow BaI_2(aq) + 2NH_3(g) + H_2(g) \quad (18)$$

Although brittle and rather soft (Mohs hardness = 3), crystalline barium fluoride is used to make optical lenses and windows for infrared spectroscopy, as it is suitably transparent from roughly 150 nm

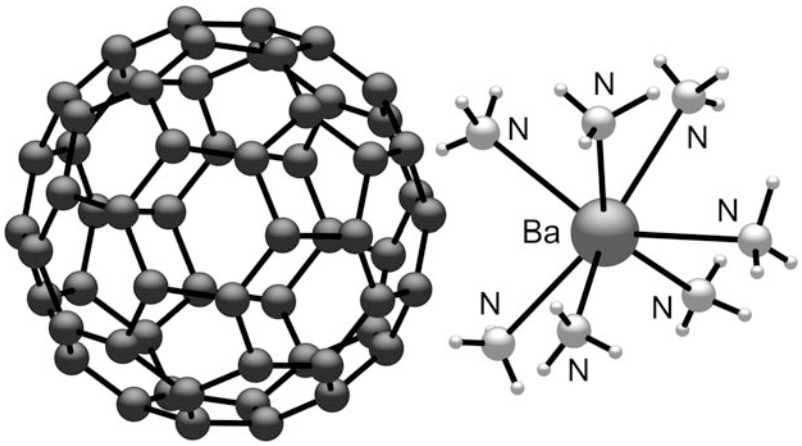

Barium, Physical and Chemical Properties, Fig. 4 Solid state structure of $[Ba(NH_3)_7]^{2+}[C_{60}]^{2-}$

(ultraviolet) to 12 μm (infrared). Barium fluoride is also a fast scintillator material for detecting X-rays, gamma rays, alpha and beta particles, and neutrons.

Barium hydride, which is made by the high temperature reaction of elemental barium and hydrogen (19), can be fused with the barium halides to produce the barium hydride halides BaHX (X = Cl, Br, I). An alternative method of preparation is to heat elemental barium and a barium halide in a hydrogen atmosphere at 950°C (20). The BaHX compounds have the PbClF crystal structure, and melt without decomposition at high temperatures (e.g., mp of BaHCl is 850°C).

$$Ba(s) + H_2(g) \rightarrow BaH_2(s) \quad (19)$$

$$Ba(s) + BaX_2(s) + H_2(g) \rightarrow 2BaHX(s)\ (X = Cl, Br, I) \quad (20)$$

With Barium-Nitrogen Bonds

Barium dissolves in liquid ammonia to give a deep blue-black solution that yields a copper colored ammoniate, $Ba(NH_3)_6$, on evaporation. With time, the ammoniate will decompose to form the amide (21). In the presence of the carbon fullerenes C_{60} and C_{70}, however, the $[Ba(NH_3)_n]^{2+}$ cations (n = 7, 9) are generated from barium in liquid ammonia. The X-ray crystal structure of $[Ba(NH_3)_7]C_{60}{\bullet}NH_3$ reveals a monocapped trigonal antiprism around the metal (Ba–N = 2.85–2.94 Å), with an ordered C_{60} dianion (Fig. 4) (Himmel and Jansen 1998).

$$Ba(NH_3)_6(s) \rightarrow Ba(NH_2)_2(s) + 4NH_3(s) + H_2(g) \quad (21)$$

Whereas the parent amide $Ba(NH_2)_2$ possesses an ionic lattice, replacement of the hydrogen atoms with groups of increasing size leads to molecular complexes. Such amido complexes are versatile reagents, and can be used to prepare other main-group and transition metal complexes. The chemistry of $Ba[N(SiMe_3)_2]_2$ (Fig. 2) has been reviewed (Westerhausen 1998).

With Barium-Carbon Bonds

Barium compounds with bonds to carbon (organobarium complexes) are relatively rare species. Owing to the largely ionic character of the bonding in barium compounds, all are reactive species, and decompose in the presence of air and moisture. They are formed by a variety of methods, often involving exchange reactions (e.g., (22)) (Hanusa 2007). Some organobarium species can function as initiators for polymerization reactions and serve as precursors to oxides under CVD conditions. The bis(cyclopentadienyl) metallocenes usually display "bent" (nonlinear) geometries (Fig. 5), similar to the bent gas-phase dihalides; related issues in their metal-ligand bonding (e.g., reverse polarization effects, d-orbital participation) may be involved.

$$2K[C_5R_5] + BaI_2(s) \rightarrow (C_5R_5)_2Ba + 2KI(s) \quad (22)$$

Biological Features of Barium Chemistry

The soluble salts of barium are toxic in mammalian systems. They are absorbed rapidly from the gastrointestinal tract and are deposited in the muscles, lungs, and bone. At low doses, barium acts as a muscle

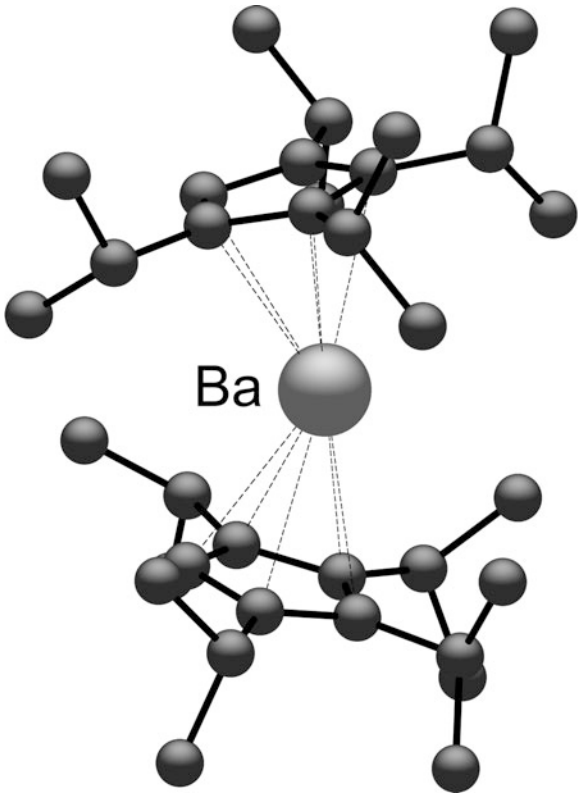

Barium, Physical and Chemical Properties, Fig. 5 Solid state structure of $[C_5(i\text{-}Pr)_4H]_2Ba$. The molecule is "bent," with an angle between the cyclopentadienyl ring planes of 153°

stimulant; at higher doses, barium affects the nervous system, eventually leading to paralysis. Oral doses of barium cause vomiting and diarrhea, followed by decreased heart rate and elevated blood pressure. Higher doses result in cardiac irregularities, tremors, and difficult or labored breathing. Death can occur from cardiac and respiratory failure. A single 0.8 g dose of barium chloride can be fatal to a 70 kg human. The similar size of the barium and potassium ions (1.35 Å and 1.38 Å, respectively), is thought to be the major source of the toxicity. Barium may interfere in the functioning of ▶ potassium channels, and the symptoms of barium poisoning are characteristic of the effects observed with a drop in serum potassium levels.

Industrial workers exposed to barium dust, usually in the form of barium sulfate or carbonate, may develop a benign pneumoconiosis referred to as "baritosis." Although it results in incidences of hypertension, baritosis is unusually reversible once the source of exposure is removed.

An important medical application of barium is the use of a slurry of the sulfate known as a "barium meal." When swallowed, the material coats the lining of the gastrointestinal tract, allowing for improved imaging by X-ray techniques. The minimal toxicity of barium sulfate is a consequence of its low solubility, and the ingested material is rapidly excreted.

Cross-References

- ▶ Barium(II) Transport in Potassium(I) and Calcium (II) Membrane Channels
- ▶ Potassium Channels, Structure and Function

References

Braithwaite N, Weaver G (1990) Electronic materials. Butterworth, London

Diefenbach M, Schwarz H (2005) High-electron-density C_6H_6 units: stable ten-electron benzene complexes. Chem Eur J 11:3058–3063

Drake SR et al (1993) Group IIA metal β-diketonate complexes; the crystal structure of $[Sr_3(tmhd)_6(Htmhd)]\bullet C_6H_5Me\bullet C_5H_{12}$ and $[Ba_4(tmhd)_8]$ (Htmhd = 2,2,6,6-tetramethylheptane-3,5-dione). J Chem Soc, Dalton Trans 2883–2890

Hanusa TP (2007) Alkaline-earth metals: beryllium, magnesium, calcium, strontium, and barium. In: Crabtree RH, Mingos DMP (eds) Comprehensive organometallic chemistry-III, vol 2. Elsevier, Oxford, pp 67–152

Hargittai M (2000) Molecular structure of metal halides. Chem Rev 100:2233–2301

Himmel K, Jansen M (1998) Synthesis and single-crystal structure analysis of $[Ba(NH_3)_7]C_{60}\bullet NH_3$. Inorg Chem 37:3437–3439

Kaupp M, Schleyer PVR (1992) The structural variations of monomeric alkaline earth MX_2 compounds (M = Ca, Sr, Ba; X = Li, BeH, BH_2, CH_3, NH_2, OH, F). An ab initio pseudopotential study. J Am Chem Soc 114:491–497

Murugavel R et al (2001) Reactions of 2-mercaptobenzoic acid with divalent alkaline earth metal ions: synthesis, spectral studies, and single-crystal X-ray structures of calcium, strontium, and barium complexes of 2,2´-dithiobis(benzoic acid). Inorg Chem 40:6870–6878

Pierson HO (1999) Handbook of chemical vapor deposition: principles, technology, and applications. Noyes, Norwich

Westerhausen M (1998) Synthesis, properties, and reactivity of alkaline earth metal bis[bis(trialkylsilyl)amides]. Coord Chem Rev 176:157–210

Behavior of Aluminum in Biological Systems

- ▶ Aluminum, Biological Effects

Berylliosis

▶ Beryllium as Antigen

Beryllium (Be) Exposure in the Workplace

▶ Beryllium as Antigen

Beryllium as Antigen

Vladimir N. Uversky
Department of Molecular Medicine, University of South Florida, College of Medicine, Tampa, FL, USA

Synonyms

Berylliosis; Beryllium (Be) exposure in the workplace; Beryllium sensitization (BeS); Beryllium-induced disease; Chronic beryllium disease (CBD); Contact allergy to beryllium

Definition

Beryllium exposure can have adverse health effects, starting from the contact allergy to Be and ending with the chronic beryllium disease (CBD) that leads to physiologic impairment and need for immunosuppressive medications, or even with the lung cancer.

Some Physicochemical Properties and Commercial Use

The chemical element beryllium is the fourth element in the chemical periodic table with the symbol of Be, atomic number of 4, and atomic weight of the 9.0122. Beryllium is a typical steel-gray metal, which in its free form exists as a strong, brittle, and lightweight alkaline earth metal. Beryllium is a relatively rare element in both the universe and in the crust of the Earth (it has a concentration of 2–6 parts per million (ppm) in the Earth's crust), being naturally found only in combination with other elements in minerals. It is almost always divalent in its compounds. Among the notable gemstones that contain beryllium are beryl (the precious forms of which are aquamarine, bixbite, and emerald) and chrysoberyl.

Its lightweight and unique chemical and physical properties make beryllium a highly desirable component with a wide use in high-technology industries, such as aerospace, ceramics, electronics, and defense. For example, when alloyed to aluminum, cobalt, copper, iron, and nickel, Be increases hardness and resistance to corrosion of the corresponding alloys. Since beryllium is nonmagnetic, tools made of this metal are used by naval or military explosive ordnance disposal teams for work on or near naval mines, since these mines commonly have magnetic fuzes. Beryllium-based instruments are also used to tune the highly magnetic klystrons, magnetrons, traveling wave tubes, and other gears, that are used for generating high levels of microwave power in the transmitters. In magnetic resonance imaging (MRI) machines, many maintenance and construction materials contain beryllium. Also, due to its high thermal stability, thermal conductivity, flexural rigidity, and low density (1.85 times that of water), beryllium has multiple structural applications and is considered as a unique aerospace material utilized in construction of high-speed aircrafts, missiles, various space vehicles, and communication satellites. Furthermore, due to its low density and atomic mass, beryllium is relatively transparent to X-rays and other forms of ionizing radiation. These properties make Be the most common window material for the X-ray equipment and in particle physics experiments. Finally, the high thermal conductivities of beryllium and beryllium oxide have led to their use in heat transport and heat-sinking applications (http://en.wikipedia.org/wiki/Beryllium).

Beryllium Exposure and Health Risks

Beryllium is not known to be necessary or useful for either plant or animal life. The commercial use of beryllium is challenged due to the toxicity of this metal. Since beryllium is chemically similar to

magnesium, it can replace magnesium in some proteins, causing their malfunction (Emsley 2001). Although small amounts (approximately 35 μm) of beryllium are found in the human body, this content is not considered to be harmful (Emsley 2001).

Beryllium exposure primarily occurs through inhalation of the beryllium-containing dusts by workers involved in manufacturing the Be-containing products. It is estimated that approximately 200,000 current and at least one million total workers have been exposed to beryllium in the United States alone (Henneberger et al. 2004). In some people, beryllium exposure can cause a chronic life-threatening allergic disease, the chronic beryllium disease (CBD) (also known as berylliosis). Beryllium and beryllium compounds are also considered as category I carcinogens (http://en.wikipedia.org/wiki/Beryllium). Some of the consequences of the beryllium exposure are considered below.

Contact Allergy to Beryllium and Acute Beryllium Disease

Acute inhalation of large amounts of dust or fumes contaminated with beryllium over a short time or short and heavy exposure to beryllium might produce acute beryllium disease, which results from an irritant response at high exposure levels and which may take several forms, such as contact dermatitis, conjunctivitis, gingivitis, stomatitis, nasopharyngitis, tracheobronchitis, and pneumonitis. Severities of damage and recovery times are different for different forms of the acute beryllium disease and depend on the exposure level. Information on the acute beryllium disease is mostly based on the materials available at the Canadian Centre for Occupational Health and Safety web site (http://www.ccohs.ca/oshanswers/diseases/beryllium.html).

Contact dermatitis is an inflammation of the skin that is accompanied by itching, redness, rashes, swelling, and blisters. These symptoms appear on the exposed areas of the body, especially on the face, neck, arms, and hands. Skin effects (lesions, ulcerations, wart-like bumps) can also develop if beryllium penetrates into cuts or scratches. The membrane that covers the front of the eye can become inflamed in association with dermatitis. Beryllium may also cause conjunctivitis in occupationally exposed workers. Splashes of beryllium solutions may also burn the eyes causing fluid accumulation and reddening around the eyes. Conditions reflecting contact dermatitis usually improve a few weeks after the exposure ends.

Besides skin, beryllium may act on mucous membranes of oral cavities. As a result, persons with dental implants made from alloys including beryllium may develop gingivitis, stomatitis, and asymptomatic local sensitivity to beryllium.

Nasopharyngitis is an inflammation of the nose and throat. Symptoms include pain, swelling, and bleeding of the nose. This condition clears up 3–6 weeks after exposure ends.

Tracheobronchitis is an inflammation of the windpipe and the airways beyond it. Symptoms are coughing and discomfort, and tightness of the chest. Recovery takes about 1 month.

Acute beryllium inhalation can cause pneumonitis, which is an inflammation of the lungs confined to the walls of the air sacs. Pneumonitis is the most serious of the acute effects from the beryllium exposure. It varies in severity and can result in death. However, fatal cases are rare, and recovery is usually complete in about 6 months. Symptoms of acute beryllium pneumonitis are coughing, breathing difficulties, tightness of the chest, appetite and weight loss, and general weakness and tiredness.

Allergic reactions to beryllium in patients subjected to the skin-patch tests were considered as rather rare. However, recent systematic study on the patients with patch test reactions to beryllium chloride revealed that contact allergy to beryllium chloride may not be as unusual as the literature suggested (Toledo et al. 2011).

Beryllium Sensitization

Beryllium sensitization is an allergic reaction to beryllium that can develop after a person breathes beryllium dust or fumes. Here, beryllium acts as an antigen that induces a hypersensitive cellular immune response. Beryllium sensitization is not a disease, and sensitized people may not have symptoms. However, beryllium sensitization represents a potential foundation for both skin effect and chronic beryllium disease (CBD) associated with the secondary beryllium exposures. In fact, beryllium sensitization and CBD are both caused by the beryllium exposure and can be found based on the results of the beryllium lymphocyte proliferation test (BeLPT) (Newman et al. 2005). Since approximately 50% of individuals with beryllium sensitization have chronic beryllium disease at the time of their initial clinical evaluation, it was hypothesized that most

beryllium-sensitized workers will eventually develop CBD (Newman et al. 2005). The hypothesis was supported by a longitudinal cohort study of a group of individuals with beryllium sensitization but without the initial evidence of CBD. The study showed that CBD developed in 31% of sensitized individuals within an average follow period of 3.8 years (range, 1.0–9.5 years), whereas 69% remained beryllium sensitized without disease after an average follow-up time of 4.8 years (range, 1.7–11.6 years) (Newman et al. 2005). This high probability of CBD development in originally asymptotic beryllium-exposed workers and the fact that beryllium is retained in lungs long after the actual exposure clearly suggested that beryllium sensitization is an adverse health effect that merits medical follow-up (Newman et al. 2005).

Chronic Beryllium Disease (CBD)

Inhalation of small amounts of beryllium-containing dusts or fumes contaminated with beryllium over a long time can lead to the development of berylliosis or chronic beryllium disease (CBD), which is an immunologically mediated granulomatous lung disease that could result from the inhalation of airborne beryllium particles. CBD is definitely a product of industrialization, since for the first time, this disease in the form of chemical pneumonitis was reported in Europe in 1933 and in the United States in 1943 (http://en.wikipedia.org/wiki/Beryllium). Symptoms of the disease can take up to 5 years to develop. It is estimated that about a third of the CBD patients die, whereas the survivors are left disabled (Emsley 2001).

CBD is characterized by the presence of noncaseating granulomatous inflammation primarily affecting the lung, although other organs may be involved (Fontenot and Kotzin 2003). There are several hallmarks of the CBD, such as the accumulation of Be-specific $CD4^+$ T cells in the lung (the healthy human lung contains few lymphocytes, whereas the lungs of patients with CBD are characterized by the accumulation of a remarkably large number of Be-responsive $CD4^+$ T cells; that is, by the $CD4^+$ T cell alveolitis (Saltini et al. 1989)), persistent lung inflammation, and the development of lung fibrosis (Falta et al. 2010). Because the histopathologic features of CBD resemble those of lung sarcoidosis, a disease in which abnormal collections of chronic inflammatory cells (granulomas) also form nodules in lungs, the CBD diagnosis is complicated and depends on the detection of a Be-specific immune response in blood and/or lung and the presence of noncaseating granulomas and/or mononuclear cell inflammation on a biopsy specimen (Falta et al. 2010). It was pointed out that the frequency of antigen-specific T cells in blood can serve as a noninvasive biomarker to predict disease development and severity of the Be-specific $CD4^+$ T-cell alveolitis (Martin et al. 2011).

Since the susceptibility to this disease depends on the nature of the exposure and the genetic predisposition of the individual (see below), this ailment develops in 2–16% of subjects exposed to the beryllium at the workplace (Falta et al. 2010). It is recognized now that the activation and accumulation of Be-responsive $CD4^+$ T cells in the lungs of the CBD patients is linked to the genetic alterations in the major histocompatibility complex class II (MHCII) molecules, which generally are implicated in susceptibility to various immune-mediated diseases. MHCII proteins are the protein/peptide receptors (T-cell receptors, TCRs) found only on antigen-presenting cells. The human MHC class II molecules (human leukocyte antigen complexes, HLA) are encoded by three different isotypes, HLA-DR, -DQ, and -DP, each being highly polymorphic. CBP-related MHCII molecules are from the HLA-DP isotype. These receptors are composed of two subunits, DPα and DPβ, each having two domains, α_1 and α_2 and β_1 and β_2, with the domains α_1 and β1 forming a recognition module, heterodimer that contains the peptide-binding groove, and with the domains α_2 and β_2 acting as transmembrane domains that anchor the MHC class II molecule to the cell membrane (Abbas and Lichtman 2009). MHCII subunits are encoded by the *HLA-DPA1* and *HLA-DPB1* loci found in the *MHCII* (or *HLA-D*) region located within the human chromosome 6 (http://en.wikipedia.org/wiki/HLA-DP). CBD predisposition is linked to *HLA-DP* alleles that contain a glutamic acid at position 69 of the β-chain (βGlu69) (Falta et al. 2010; Richeldi et al. 1993).

Here is a brief description of the development of the beryllium-induced granulomatous response. As it was already mentioned, CBD patients are characterized by the presence of the large amounts of Be-responsive $CD4^+$ T cells that contain Be-specific TCRs. Besides these Be-specific TCRs, the Be-responsive $CD4^+$

T lymphocytes express markers of previous activation and exhibit an effector memory T cell phenotype (Saltini et al. 1990; Fontenot et al. 2002). Recognition of beryllium by such memory $CD4^+$ T cells promotes their clonal proliferation and secretion of the T helper 1 (Th1)-type cytokines, such as interleukin-2 (IL-2), interferon-γ (IFN-γ), and tumor necrosis factor-α (TNF-α) (Fontenot et al. 2002). Then, IFN-γ and TNF-α promote macrophage accumulation, activation, and aggregation, resulting in the initiation of the granulomatous response (Falta et al. 2010).

Obviously, the existence of Be-specific TCRs (i.e., some mutant forms of MHCII) is crucial for the initiation of this process. In agreement with this hypothesis, *DPB1* alleles with βGlu69 mutation were shown to be strongly associated with disease susceptibility (Falta et al. 2010; Richeldi et al. 1993), since approximately 80% of patients with CBD were characterized by the presence of βGlu69-containing *DPB1* alleles (Falta et al. 2010), and since βGlu69-containing *DPB1* alleles were shown to be a serious risk factor for the development of Be sensitization and not simply a marker of progression from sensitization to disease (Falta et al. 2010). Furthermore, since these same alleles were capable of presenting beryllium to pathogenic $CD4^+$ T cells, and since beryllium recognition required the presence of βGlu69, it was proposed that a single polymorphic amino acid might dictate beryllium presentation and, more importantly, disease susceptibility (Falta et al. 2010). However, the fact that ~20% CBD patients do not possess a βGlu69-containing *HLA-DPB1* allele suggests that some other mutations in the MHCII molecules can be important for the genetic susceptibility to CBD (Falta et al. 2010).

The existing structural data on the HLA-DP2 in complex with a peptide derived from the HLA-DR α-chain (pDRA) revealed that the binding groove of the HLA-DP2 βGlu69 variant is characterized by the presence of the unique acidic pocket flanked by leucine residues at the positions 4 and 7 of the pDRA and the β-chain α-helix and was composed of three DP2 β-chain amino acids that contribute to the net negative surface charge of this pocket: βGlu68 and βGlu69 from the β-chain α-helix and βGlu26 from the floor of the peptide-binding groove (Dai et al. 2010). These findings clearly indicated that the acidic pocket induced by the βGlu69 mutation should be considered as the beryllium binding site (Falta et al. 2010). This hypothesis was supported by the fact that the mutated HLA-DP2 molecules that contained point substitutions at the positions βGlu26 and βGlu68 did not activate beryllium-specific T cells (Dai et al. 2010).

Therefore, existing data strongly suggest that the acidic pocket of the HLA-DP2 binding groove is the beryllium binding site. Formation of this pocket as a result of the βGlu69 mutation in the HLA-DP2 protein provides an explanation for the genetic linkage of HLA-DP2 to the development of granulomatous inflammation in the Be-exposed worker and therefore represents a molecular basis for better understanding of the beryllium-induced disease immunopathogenesis.

Beryllium Exposure and Lung Cancer

The topic of the potential carcinogenicity of beryllium is full of controversies. Early epidemiological and animal studies suggested that the occupational exposure to beryllium might cause lung cancer (Schubauer-Berigan et al. 2011). However, a recent systematic review of epidemiologic studies on cancer among workers exposed to beryllium showed that the available evidence does not support a conclusion that a causal association has been established between occupational exposure to beryllium and the risk of cancer (Boffetta et al. 2012). One of the major reasons for this discrepancy is the lack of adequate analysis of confounding factors in early studies. For example, some excess mortality from lung cancer was detected in the large cohort of patients with the beryllium exposure, which was partially explained by confounding by tobacco smoking and urban residence (Boffetta et al. 2012). Similarly, a weight-of-evidence analysis of the 33 animal studies and 17 epidemiologic studies showed that the evidence for carcinogenicity of beryllium is not as clear as suggested by previous evaluations, because of the inadequacy of the available smoking history information, the lack of well-characterized historical occupational exposures, and shortcomings in the animal studies (Hollins et al. 2009). Therefore, it was concluded that the studies of beryllium disease patients did not provide independent evidence for the carcinogenicity of beryllium and the results from other studies did not

support the hypothesis of an increased risk of lung cancer or any other cancer associated with the occupational exposure to beryllium (Boffetta et al. 2012).

Cross-References

► Beryllium, Physical and Chemical Properties

References

Abbas AK, Lichtman AH (2009) Basic Immunology. Functions and disorders of the immune system, 3rd edn. Saunders/Elsevier, Philadelphia

Boffetta P, Fryzek JP, Mandel JS (2012) Occupational exposure to beryllium and cancer risk: a review of the epidemiologic evidence. Crit Rev Toxicol 42:107–118

Dai S, Murphy GA, Crawford F, Mack DG, Falta MT, Marrack P, Kappler JW, Fontenot AP (2010) Crystal structure of HLA-DP2 and implications for chronic beryllium disease. Proc Natl Acad Sci USA 107:7425–7430

Emsley J (2001) Nature's Building blocks: an A-Z guide to the elements. Oxford University Press, Oxford

Falta MT, Bowerman NA, Dai S, Kappler JW, Fontenot AP (2010) Linking genetic susceptibility and T cell activation in beryllium-induced disease. Proc Am Thorac Soc 7:126–129

Fontenot AP, Canavera SJ, Gharavi L, Newman LS, Kotzin BL (2002) Target organ localization of memory CD4(+) T cells in patients with chronic beryllium disease. J Clin Invest 110:1473–1482

Fontenot AP, Kotzin BL (2003) Chronic beryllium disease: immune-mediated destruction with implications for organ-specific autoimmunity. Tissue Antigens 62:449–458

Henneberger PK, Goe SK, Miller WE, Doney B, Groce DW (2004) Industries in the United States with airborne beryllium exposure and estimates of the number of current workers potentially exposed. J Occup Environ Hyg 1:648–659

Hollins DM, McKinley MA, Williams C, Wiman A, Fillos D, Chapman PS, Madl AK (2009) Beryllium and lung cancer: a weight of evidence evaluation of the toxicological and epidemiological literature. Crit Rev Toxicol 39(Suppl 1):1–32

Martin AK, Mack DG, Falta MT, Mroz MM, Newman LS, Maier LA, Fontenot AP (2011) Beryllium-specific CD4+ T cells in blood as a biomarker of disease progression. J Allergy Clin Immunol 128(1100–1106):e1101–e1105

Newman LS, Mroz MM, Balkissoon R, Maier LA (2005) Beryllium sensitization progresses to chronic beryllium disease: a longitudinal study of disease risk. Am J Respir Crit Care Med 171:54–60

Richeldi L, Sorrentino R, Saltini C (1993) HLA-DPB1 glutamate 69: a genetic marker of beryllium disease. Science 262:242–244

Saltini C, Kirby M, Trapnell BC, Tamura N, Crystal RG (1990) Biased accumulation of T lymphocytes with "memory"-type CD45 leukocyte common antigen gene expression on the epithelial surface of the human lung. J Exp Med 171:1123–1140

Saltini C, Winestock K, Kirby M, Pinkston P, Crystal RG (1989) Maintenance of alveolitis in patients with chronic beryllium disease by beryllium-specific helper T cells. N Engl J Med 320:1103–1109

Schubauer-Berigan MK, Deddens JA, Couch JR, Petersen MR (2011) Risk of lung cancer associated with quantitative beryllium exposure metrics within an occupational cohort. Occup Environ Med 68:354–360

Toledo F, Silvestre JF, Cuesta L, Latorre N, Monteagudo A (2011) Contact allergy to beryllium chloride: report of 12 cases. Contact Dermatitis 64:104–109

Beryllium Sensitization (BeS)

► Beryllium as Antigen

Beryllium, Physical and Chemical Properties

Fathi Habashi
Department of Mining, Metallurgical, and Materials Engineering, Laval University, Quebec City, Canada

Beryllium is the first member of the alkaline earths but its chemical properties are more similar to aluminum – a property described as "diagonal similarities" (Fig. 1) as discussed below. Beryllium is an expensive metal used in small and specialized industries. Its dust and fumes as well as vapours of its compounds are poisonous to inhale. Its compounds have sweet taste that is why it was initially called "glucinium." It is fabricated by powder metallurgy techniques because coarse grains tend to develop in the castings causing brittleness and low tensile strength. About 10 % of the metal is used in the metallic form, 80 % in form of beryllium–copper alloys (containing about 2 % Be), or other master alloys, and the remaining 10 % is used as a refractory oxide. In the metallic form it is used as a moderator to slow down fast neutrons in nuclear reactors because of its low atomic weight and low neutron

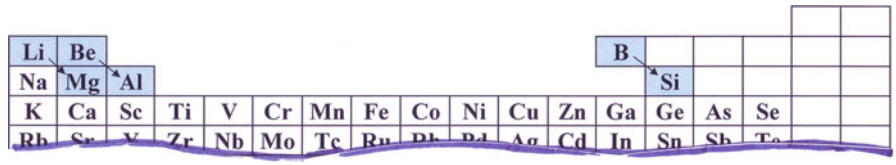

Beryllium, Physical and Chemical Properties, Fig. 1 Diagonal similarities in the periodic table

cross section. As an alloy with copper, it is particularly important in springs because such alloys possess high elasticity and great endurance.

Physical Properties

Atomic number	4
Atomic weight	9.0122
Relative abundance in the Earth's crust, %	6×10^{-4}
Atomic radius, pm	112.50
Atomic volume at 298 K, cm^3/mol	4.877
Crystal structure	
At 293 K	Hexagonal closest packed
At 1,523 K	Body-centered cubic
Melting point, °C	1,287
Boiling point, °C	2,472
Transformation point, °C	1,254
Density	
At 298 K. g/cm^3	1.8477
At 1,773 K, g/cm^3	1.42
Heat of fusion, J/g	1,357
Heat of transformation, J/g	837
Vapor pressure	
At 500 K	5.7×10^{-29}
At 1,000 K	4.73×10^{-12}
At 1,560 K	4.84×10^{-6}
Specific heat	
At 298 K, J g^{-1} K^{-1}	1.830
At 700 K, J g^{-1} K^{-1}	2.740
Thermal conductivity at 298 K, W m^{-1} K^{-1}	165 ± 15
Linear coefficient of thermal expansion, 298–373 K, K^{-1}	11.5×10^{-6}
Electrical resistivity at 298 K, Ω m	4.31×10^{-8}
Volume contraction on solidification	3%

Because of its low density beryllium is considered a light metal. It transmits X-rays well because of its low atomic number. Relatively long-wave gamma rays cause beryllium to emit neutrons, on account of a (InlinemediaObject γ, n) reaction.

Chemical Properties

Beryllium is a typical metal; it has the electronic structure 2, 2 and hence when it loses its two outer electrons it will have the electronic structure of the inert gas helium. Although beryllium is almost always divalent in its compounds, it is more similar to aluminum than to magnesium or calcium. For example, like aluminum, it is amphoteric: it dissolves in dilute nonoxidizing mineral acids, accompanied by hydrogen evolution and salt formation and is also attacked by aqueous hydroxide accompanied by hydrogen evolution and beryllate formation. Beryllium ion precipitates by alkali to form beryllium hydroxide, $Be(OH)_2$, which dissolves in excess alkali. Beryllium chloride, $BeCl_2$, is volatile and has a covalent bond like aluminum chloride, $AlCl_3$.

In humid air and water vapor, beryllium forms a strongly adhering surface layer of oxide that prevents further oxidation up to about 600°C. Above 600°C oxidation takes place. Beryllium is an excellent reducing agent because of its great affinity for oxygen:

$$Be + {}^1/_2O_2 \rightarrow BeO$$

At temperatures >900°C, it reacts violently with nitrogen or ammonia to form beryllium nitride, Be_3N_2. However, it does not react with hydrogen even at high temperatures. Below 500–600°C beryllium is not attacked by dry carbon dioxide and is attacked only very slowly by moist carbon dioxide. Beryllium powder reacts with fluorine at room temperature, and at elevated temperatures it reacts with chlorine, bromine, and iodine and with sulfur, selenium, and tellurium vapor; in each case, beryllium burns with a flame.

The adhering oxide film protects beryllium from attack by both cold and hot water. It also protects cold

beryllium from attack by oxidizing acids. Since most beryllium compounds have a highly exothermic heat of formation, beryllium reduces the salts and the borates and silicates of many metals. For example, the only halides that are stable toward beryllium are those of the alkali metals and magnesium; all others are reduced by beryllium. Molten alkali-metal hydroxides react explosively with beryllium.

Beryllium is very reactive in the liquid state, reacting with most oxides, nitrides, sulfides, and carbides, including those of magnesium, calcium, aluminum, titanium, and zirconium.

References

Habashi F (2003) Metals from Ores. An Introduction to Extractive Metallurgy, Métallurgie Extractive Québec, Québec City, Canada. Distributed b Laval University Bookstore "Zone". www.zone.ul.ca

Petzow G et al (1997) In: Habashi F (ed) Handbook of extractive metallurgy. Wiley, Weinheim, pp 955–980

Beryllium-Induced Disease

▶ Beryllium as Antigen

Bestatin, N-[(2 S, 3R)-3-Amino-2-hydroxy-4-phenylbutyryl]-L-leucin

▶ Zinc Aminopeptidases, Aminopeptidase from Vibrio Proteolyticus (Aeromonas proteolytica) as Prototypical Enzyme

Biarsenical Fluorescent Probes

Artur Krężel
Department of Protein Engineering, Faculty of Biotechnology, University of Wrocław, Wrocław, Poland

Synonyms

Bisarsenical probes; FlAsH-EDT_2; Fluorescent arsenical helix/hairpin binder; ReAsH-EDT_2

Definition

Fluorescent biarsenical probes refer to chemical agents that are built on fluorescent platforms with two proton to arsenic substitutions at certain positions that are capped with two molecules of 1,2-ethanedithiol. The probes remain nonluminescent until protein conjugation when they became highly fluorescent. Due to stability of arsenic-sulfur bond, biarsenical probes have very high affinity to four cysteine residues, which may be genetically introduced to proteins as a short sequence appropriately spaced (e.g., CCPGCC) or by incorporation into secondary structure elements.

Principles of the Biarsenical Labeling Strategy

Many of the chemistry-driven strategies used for monitoring, controlling, and modifying protein functions require small fluorescent probes that are selectively attached to the protein of interest. The probe conjugation is mostly achieved by single or multiple amino acid residue chemical labeling. From all functional groups being modified with probes such as carboxylic, hydroxyl, amine, and thiol group (R-SH), the last one is the most applicable due to its low natural abundance and relatively high reactivity (Hermanson 2008). Additionally, successful usage of the probe in vivo requires unique amino acid sequence or unique structural motif in the target protein. In 1998 R.Y. Tsien and coworkers presented a new fluorescent protien labeling strategy that use the biarsenical fluorescein derivative, FLASH-EDT_2 (fluorescein arsenical helix/hairpin binder). Later, they introduced a new probe based in biarsenical modification of resorufin (ReAsH-EDT_2) as well as other less known probes (Tsien 2005). These probes, having two arsenic atoms at position 4′ and 5′ capped with small protectants – 1,2-ethanedithiol (EDT) or 2,3-dimercaptopropanol (BAL) – possess ultrahigh affinity for short tetracysteine sequence appropriately spaced with two amino acids (CCXXCC: TC tag), uncommon in naturally occurring proteins (Jakobs et al. 2008). TC tag has significantly higher affinity to biarsenical platforms than the two protecting molecules (Fig. 1). New genetically encoded biarsenical probe recognition tag has been optimized several times to date to obtain the most efficient sequence in terms of conjugate stability and fluorescent properties. The most important advantage of biarsenical labeling strategy is that EDT-protected probes are usually cell permeable (require less than 1 h incubation) and practically

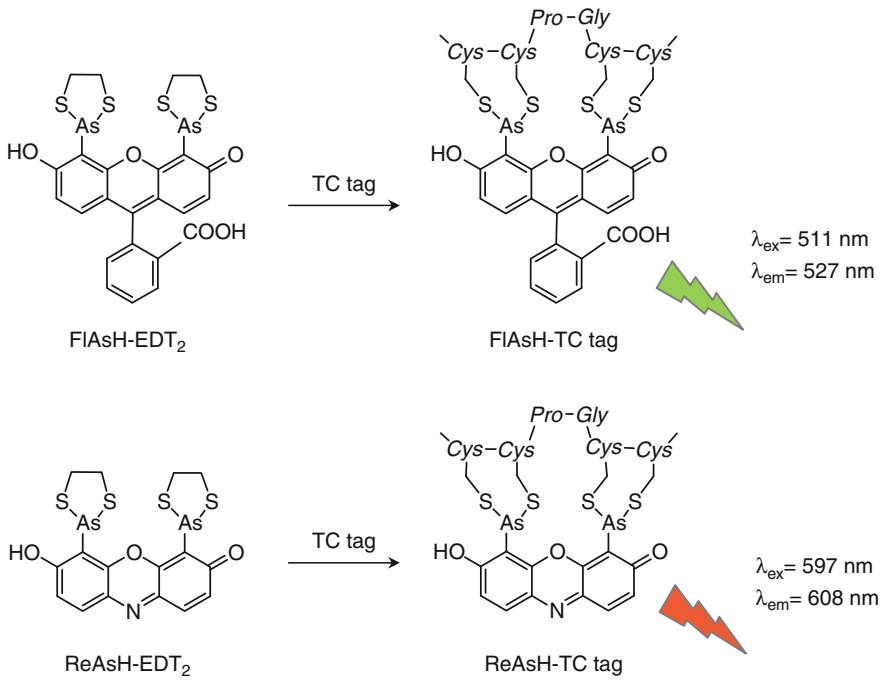

Biarsenical Fluorescent Probes, Fig. 1 Structures of the most frequently used biarsenical probes for fluorescent labeling of protein with tetracysteine tag (TC tag); *green* FlAsH-EDT_2 and *red* ReAsH-EDT_2

nonfluorescent, which significantly decreases the background when they are used for fluorescent microscopy imaging, compared to other fluorescent probes. Biarsenical EDT-protected probes became highly fluorescent when they bind to TC tags both in vitro and in vivo, and its fluorescence is more than 50,000 times higher than that of protected probe. Moreover, fluorescent conjugation in the cell is relatively fast (typically a couple of minutes) which makes this strategy one of the most important on the market. However, there are a number of proteins with vicinal thiols in the cell that may nonspecifically coordinate biarsenical probes with lower affinity than TC tags and increase the background causing lower signal to noise ratio. The administration of EDT-protected biarsenicals to TC-tagged proteins in the presence of the protectant prevents poisoning of other cellular proteins with vicinal or surface-exposed thiols. In vitro addition of excess of protectants (typically 0.25–1 mM) to biarsenical complex with TC-tagged protein results in immediate decrease of the fluorescence due to reverse reaction.

Besides some drawbacks of the fluorescent labeling strategy, one of the most attractive feature of this methodology is low molecular weight of the fluorescent moiety and affinity tag (typically less than 2 kDa), which is much lower compared to fluorescent proteins family (FPs), luciferase, β-galactosidase, β-lactamase, and many other protein reporters (Crivat and Tarasaka 2012).

Design of New Biarsenical Probes

Currently, there are many known biarsenical probes based on various fluorescent dyes with different chemical and spectral properties. New ones are still developing. Synthesis of the most popular biarsenical probes relies on two plain steps. The first one is mercuration reaction (proton substitution with mercury) of fluorescein or resorufin at positions 4′ and 5′. Biarsenical product is received by transmetalation reaction with arsenic(III) chloride followed by addition of dithiol protectant (Adams and Tsien 2008). Green (FlAsH) and red (ReAsH) moieties differ not only in spectral properties but also in reactivity. The red probe represents higher reactivity which is explained by lower molecular weight. This probe gives much faster response; however, its quantum yield is significantly lower when compared to the green probe.

FlAsH-EDT_2 and ReAsH-EDT_2 probes are significantly different and do not cover research requirements for new probes with novel or intermediate spectral or chemical properties. Simple proton substitution with

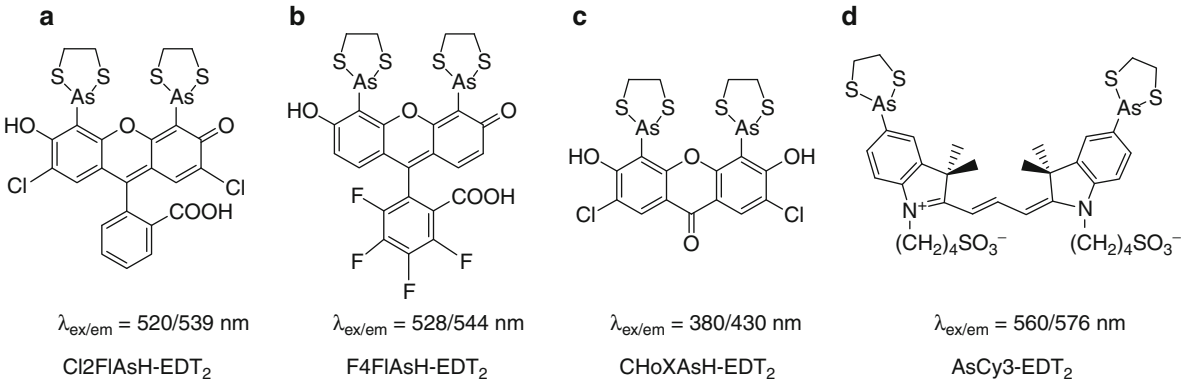

Biarsenical Fluorescent Probes, Fig. 2 Examples of multicolor EDT-protected biarsenical probes built on various types of fluorescent platforms: (**a**) 2′7′-dichlorofluorescein – $Cl2FlAsH\text{-}EDT_2$; (**b**) 3,4,5,6-tetrafluorofluorescein – $F4FlAsH\text{-}EDT_2$; (**c**) 2,7-dichloro-3,6-dihroxyxanthone – $ChoXAsH\text{-}EDT_2$; (**d**) Cy3 platform

chlorine or fluorine atoms at position 2′ and 7′ of fluorescein molecule resulted in new derivatives $F2FlAsH\text{-}EDT_2$ and $Cl2FlAsH\text{-}EDT_2$, respectively (Fig. 2). Halogenated biarsenical probes demonstrate higher absorbance, quantum yield, and Stokes shift, higher photostability, reduced pH dependence, and significantly different excitation and emission energies. Similarly, halogenation at positions 3–6 results in a new set of biarsenical probes: $F4FlAsH\text{-}EDT_2$, $Cl4FlAsH\text{-}EDT_2$. Blue and red shifts of new probes make them ideal tool for FRET pair constructions when attached to certain protein positions (Pomorski and Krężel 2011). Usage of 3,6-dihydroxy-xanthone and its 2,7-dichloro derivative allowed to construct blue biarsenical probes $HoXAs\text{-}EDT_2$ and $CHoXAs\text{-}EDT_2$, respectively. Although, they have been used for FRET pair construction with fluorescent proteins, their stability is significantly lower compared to $FlAsH\text{-}EDT_2$ and $ReAsH\text{-}EDT_2$ probes. The design of new biarsenicals is not only limited to fluorescein and resorufin derivatives that posses conserved interarsenic distance ~ 4.8 Å. Usage of Cy3 platform for preparation of biarsenical derivative ($AsCy3\text{-}EDT_2$) resulted in significantly increased interarsenic distance of ~ 14.5 Å (Fig. 2). The elongated distance requires different TC tag with longer spacer, CCKAEAACC. This probe exhibits extremely rapid response (<15 s) toward affinity tag and has a very high extinction coefficient ($1.8 \times 10^5\ M^{-1}\ cm^{-1}$), which makes the probe a very attractive tool in terms of the level of brightness ($\varepsilon \times \Phi = 5 \times 10^4\ M^{-1}\ cm^{-1}$).

Some of the biarsenical products, such as rhodamines, are nonfluorescent even when bound to TC tags. Another example is biarsenical fluorescein spirolactams SplAsH (Spirolactam Arsenical Hairpin binder). These chemicals can be used as convenient site-specific handles for attaching other chemicals or other fluorescent probes.

The biarsenical probes built on 5(6)-carboxyfluorescein ($CrAsH\text{-}EDT_2$) or 5(6)-aminofluorescein ($aminoFlAsH\text{-}EDT_2$) bring enormous possibilities in utilizing the biarsenical chemistry. Usage of relatively highly reactive carboxylic or amine group allows to design another generation of dual or multifunctional biarsenical probes. Classic application was done by immobilization of $CrAsH\text{-}EDT_2$ onto amine-agarose resin for use in protein purification. Another successful applications were based on coupling of $CrAsH\text{-}EDT_2$ moiety with Ca(II) chelator (Calcium Green $FlAsH\text{-}EDT_2$, CaGF) and photocrosslinker (TRAP) for measuring available Ca(II) signals in neurons and protein-protein interactions linkage, respectively. Multifunctional derivatives were also achieved by conjugation of biotin ($biotinFlAsH\text{-}EDT_2$) and AlexaFluor 568 ($AF568\text{-}FlAsH\text{-}EDT_2$) to biarsenical platforms (Pomorski and Krężel 2011).

Tetracysteine Tags

The biarsenical affinity tag (TC tag) was originally designed in such a way to maintain coordination properties of two As(III) with highest possible affinity. To build a rigid structure, an α-helical motif based on

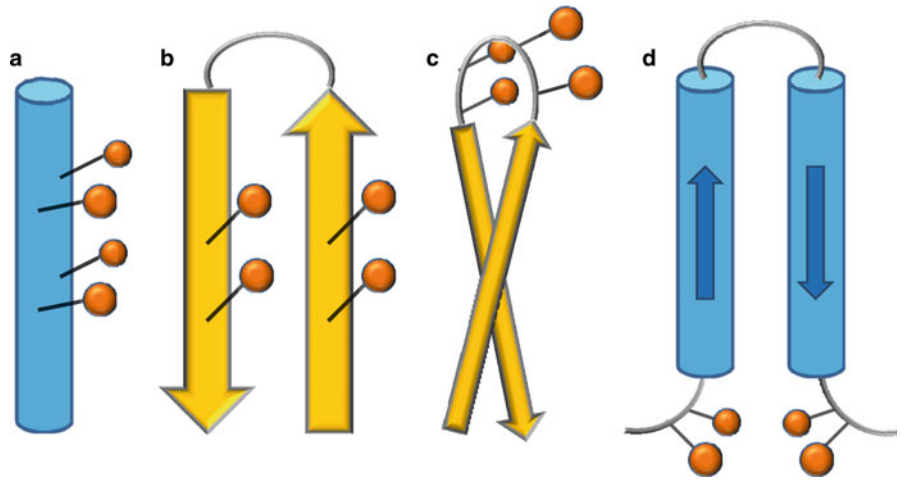

Biarsenical Fluorescent Probes, Fig. 3 The comparison of TC motifs successfully incorporated into protein structures. (**a**) α-Helix, (**b**) β-strand, (**c**) protein loop, (**d**) protein split/bipartite motif. *Yellow spheres* demonstrate exposed cysteine residues essential for efficient biarsenical conjugation

$W(EAAAR)_n$ sequence was applied in the case of the first biarsenical-protein conjugate. Four alanine to cysteine residue substitutions in α-helix formed a convenient coordination environment for biarsenical moiety in a characteristic parallelogram. Further studies showed that truncation of the original 18 amino acid peptide to shorter α-helix and substitution of ER to other helical amino acid did not significantly affect complex properties. However, use of helical-breaking proline residue in PG sequence resulted in formation of a much more stable complex. CCPGCC sequence reflects in high rate formation of the complex and has high affinity for biarsenicals ($K_d = 4$ pM). Additional optimization of the TC tag relied on optimization of flanking amino acids performed using high-throughput genetic screens and fluorescence-activated cell sorting. The optimized sequence FLNCCPGCCMEP indicates higher quantum yield and dithiol resistance in case of FlAsH-EDT_2 and ReAsH-EDT_2 probes. Improved fluorescent properties were explained by NMR studies that showed strong interaction of the N-terminal part of the TC tag with biarsenical moiety of the probe. FLNCCPGCCMEP sequence is so far the most frequently used TC tag for protein conjugation with biarsenical fluorescent probes (Adams and Tsien 2008).

The biarsenical labeling of proteins is significantly limited due to the fact that one TC tag may bind various biarsenical probes at the same moment if they are available. This fact limited multicolor use of the methodology. However, in a few studies, it has been shown that diversification of TC tags reflects in different probe affinities. Green FlAsH-EDT_2 was shown to selectively label CCPGCC sequence, while ReAsH-EDT_2 tends to label CCKACC sequence. The orthogonal labeling in vivo may be achieved by usage of CCPGCC sequence and its optimized version, FLNCCPGCCMEP, together with proper dithiol washing. The latter sequence tends to bind with ReAsH-EDT_2, while short tag is selectively labeled with FlAsH-EDT_2. In some cases, TC tandem sequence (TC_n tag) may improve fluorescent brightness; however, it reflects in higher cysteine residues' oxidation tendency and significant increase in molecular weight of the affinity tag (Pomorski and Krężel 2011).

Essential requirement for biarsenical labeling technology is not to disturb protein structure, activity, and other functions of the protein, unless so desired. The easiest way to incorporate TC tag to the protein is an addition of the TC sequence to protein terminus that form N- or C-terminal fusion. This approach allows protein labeling, even when protein structure is unknown, and its immediate illumination. Since TC tag was originally designed to be a part of α-helix, there is a possibility to place TC motif into this structure as continuous sequence (Fig. 3). α-Helix may be also be elongated to introduce TC motif in such a manner to not disturb protein structure. The placement of TC motif to β-structure requires usually knowledge about 3D structure of the protein of interest. In this case, the most efficient fluorescence or complex affinity is usually achieved in several trials with cysteine residue placement. The most frequent structural motif of the protein used for TC environment design is protein loop. It may be based on a loop already present in protein or may be added into protein

chain turns or domain connections. This approach is frequently used together with bioinformatic prediction of protein structure. One should remember that TC motif based on protein loop may differ from other loops and strongly depends on surrounding amino acids. Another type of tetracysteine coordination environment is built on protein splits and bipartite motifs (Scheck and Schepartz 2011). There are several ways to bind a probe using such coordination environment (Fig. 3). One includes the placement of four cysteine residues into two different a-helices in 2 × 2 Cys mode. Similarly, protein loops and β-strands may be structurally arranged in such a manner to form TC environment. Bipartite architecture of TC motif is very important in protein science, allowing one to study protein-protein interactions, oligomerization, activity, protein structure recognition, etc.

Although CCXXCC sequence and generally speaking TC motif is uncommon in naturally occurring proteins, there are some studies showing high affinity to nonrecombinant proteins, such as bacterial protein family SlyD or RBSS domain of human PML-PARα oncoprotein.

Protein Imaging with Biarsenical Fluorescent Probes

The main application of the biarsenical probes is visualization of the specific protein, that have an appropriate TC tag. Since the tag and probe are small sized, they have been used for imaging of proteins whose function or location is disrupted when fused with fluorescent proteins. Some of the early works indicated that unspecific binding to naturally occurring thiols prevented successful usage of the probes; however, recently published protocol shows that insufficient washing with dithiol protectant can lead to poor results (Hoffmann et al. 2010). However, one should keep in mind that different sequence-probe pairs have limited dithiol resistance and very high concentration can lead to probe release from sequence. Also high protectant concentration can also lead to cell detachment. The extracellular proteins as well as those located in endoplasmic reticulum and Golgi apparatus are oxidized, so in order for the probe to attach to TC tag, the cysteines have to be reduced first. In the first case, use of membrane-impermeant biarsenical probe such as CrAsH-EDT_2 or sFlAsH-EDT_2 is recommended. Although it has been shown that biarsenical probes can cause some toxicity in mitochondria, it was numerously stated that staining did not affect cell viability or cause cell death. It was previously mentioned that there is a strategy for orthogonal labeling of different TC sequences in the same cell, but it is also possible to perform pulse-chase experiments, where current population of TC-tagged proteins is stained with one probe, e.g., FlAsH-EDT_2, and then after additional incubation, the new pool of tagged protein is visualized using second biarsenical probe, e.g., ReAsH-EDT_2. This approach allows tracking of the fate of the protein and shows how new pool of the protein is incorporated into cellular structures. Additionally, ReAsH/DAB/OsO_4 strategy allows to gain ultrastructural information on the protein location. TC tag was added to GFP in order to develop multi-resolution tag, which combines GFP's excellent contrast with ReAsH's ability to generate singlet oxygen. The examples of biarsenical probes application include monitoring of mitochondrial proteins during apoptosis, study of protein translocation in response to the stimuli, or receptor trafficking. Additionally, since the probes attach very fast once TC tag is present, they can be used for visualization of the mRNA translation in vivo. The application of the probes for protein imagining is not only limited to mammalian cells, but can be also applied in bacteria and yeast. In this case, due to different nature of the cell's outer barrier, the biarsenical probes do not enter the cell so readily as with mammalian cells; however, there are published methods that allow their convenient use. It was shown that the biarsenical probes have negative effect on the doubling time of *S. cerevisiae* but there are many successful examples of their usage. Examples of application include study of spatial and temporal dynamics of flagellar filament protein in *E. coli* multicellular communities or labeling of secretion effectors of pathogenic bacteria during invasion of mammalian cells. The utilization of biarsenical probes was most successful in case of virus proteins, since the fluorescent proteins tend to disrupt their function. The probes allowed tracking of absorption, entry, and uncoating of vesicular stomatis virus. HIV-1 integrase was tracked in 4D. Also HIV Gag protein was thoroughly studied using biarsenical probes. There are also examples of successful imaging of proteins in plant cells and *Dictyostelium* (Pomorski and Krężel 2011).

Other Applications of Biarsenical Probes

Advantages of protein labeling with biarsenical probes are mostly based on their fluorescence switch feature,

low molecular weight, and almost unlimited possibilities to use them to site-controlled protein conjugation. The last advantage opens enormous application possibilities in protein science both in vitro and in vivo. In early study FlAsH-EDT_2 was used as a reporter of folding state of the cellular CRABP I protein in vivo. Incorporation of TC motif in appropriate place of the protein and its subsequent conjugation with biarsenical probe functions as protein denaturation indicator. By measuring fluorescence changes, one may control the protein denaturation progress, mechanism, as well its kinetics. Based on similar conformational changes, aggregation of α-synuclein was studied in living cells. FlAsH-based fluorescence was also used to recognize different β-amyloid oligomeric states. The usage of biarsenical probes is limited not only to dramatic conformational changes during protein denaturation or aggregation. In most examples studied so far, conformational changes were related to protein activity and its function upon various stimuli. The first structural studies were performed on calmodulin, where Ca(II)-induced structural changes monitored by FlAsH moiety led to increase fluorescence ~40%. In later study, more environmental sensitive ReAsH-EDT_2 with fluorescence anisotropy showed that distinct conformations of helix A are formed in response to Ca(II) binding to N- and C-terminal sites. Studies performed on calmodulin example proved that FlAsH moiety can be applied in single molecule anisotropy measurement to probe protein dynamics on a nanosecond scale.

Since TC tags allow precise location of small fluorophores like no other method, they have been widely used for FRET applications, where protein conformational changes are measured. Usage of FlAsH moiety for FRET pair constructions gave better resolution than previously often used FITC. Biarsenical probes were mostly used to replace fluorescent proteins as donors or acceptors in FRET. This approach has several advantages over FP-FP pair, such as reduced size, no FRET control before probe addition, and variety of colors of the probes. Use of the biarsenical probes overcomes the probel of obligatory dimerization of some FPs. There are several examples where FP-biarsenical pair was used to observe conformational changes of G-protein coupled receptors (GPCRs) such as changes induced by activation of human A_{2A} adenosine receptor and mouse α_{2A} adrenergic receptor. FRET between FlAsH and CFP or FlAsH and YFP was shown to give better signal amplitude compared to previously used CFP-YFP pair. Moreover, FlAsH moiety was utilized together with conventional fluorescent probe, such as Alexa Fluor 488, to investigate ligand-induced movement of C-terminal part of β_2-adrenoceptor relative to the cytoplasmic end of transmembrane helix 6 of this protein.

One of the very attractive and powerful applications of biarsenical probes is the control of protein activity. Since biarsenical probes can be placed at desired protein place, they can function as molecular switch of protein functions, such as allosteric inhibitor or activator. Tests on mutants with differently placed TC tag revealed that tag location can have various effect on protein activity (e.g., V_{max}, K_m) upon biarsenical conjugation when compared to WT protein. In one of the first examples, TC environment was introduced into loops of protein tyrosine phosphatase (PTP) to find the most efficient regulatory site. One of the investigated mutants showed 12 × reduced catalytic efficiency. Alternatively, FlAsH-EDT_2 was applied to mimic the inhibitory effect of Cd(II) on renal Na^+/glucose co-transporter and its mutants, providing evidence that endogenous CXXC is responsible for transporter sensitivity toward Cd(II). Next application related to protein control activity was achieved by chromophore/fluorescence-assisted light inactivation (CALI/FALI). Biarsenical probes were found to be better inactivators than FPs. Study on molecular mechanism of calmodulin inactivation by FlAsH CALI revealed that singlet oxygen causes methionine oxidation that leads to destruction of protein structure and histidine oxidation which can form cross-links within calmodulin-MLCK peptide complex. In latter study ReAsH moiety was proved to generate more singlet oxygen species under strong irradiation. TC-tagged connexin43 in gap junctions was 95% inactivated after only 25 s light exposure when conjugated with ReAsH.

The affinity of biarsenical probes to its affinity tag is so efficient that protein complexes may be observed in SDS-PAGE gels. The detection limit depends on protein but reaches even as little as 1 ng. Naturally occurring bacterial chaperone SlyD has the ability to bind biarsenical probes and may be used as internal mass marker of ~27 kDa. Biarsenical labeling was also used

in capillary electrophoresis techniques with detection limit of as little as 10^{-20} mol of FlAsH-TC complex. The tight binding of TC motif to biarsenical probe has led to the invention of affinity purification systems with immobilized biarsenical platforms. Due to reversible complex formation, TC-tagged proteins are eluted from beads with a solution of EDT or less odorous DMPS.

Since biarsenical fluorescent probes bind to TC tag with 1:1 stoichiometry, it can be used in fluorescence anisotropy (polarization) experiments. It allows, e.g., time-resolved monitoring of proteolytic reaction that can be used in high-throughput systems. Biarsenical probes can also be used as reporter for gene therapy. In the first study that compared usage of different genetically encoded reporters, TC-tagged proteins were expressed as well as WT and did not affect cell growth. Similarly, FlAsH-EDT_2 can be used to monitor real-time protein synthesis or gene expression.

Cross-References

- ▶ Arsenic-Induced Stress Proteins
- ▶ As
- ▶ Cadmium, Effect on Transport Across Cell Membranes
- ▶ Calcium in Nervous System
- ▶ Calcium Signaling
- ▶ Calmodulin
- ▶ Mercury, Physical and Chemical Properties
- ▶ Osmium, Physical and Chemical Properties

References

Adams SR, Tsien RY (2008) Preparation of the membrane-permeant biarsenicals FlAsH-EDT_2 and ReAsH-EDT_2 for fluorescent labeling of tetracysteine-tagged proteins. Nat Protoc 3:1527–1534

Crivat G, Tarasaka JW (2012) Imaging proteins inside cells with fluorescent tags. Trends Biotechnol 30:8–16

Hermanson GT (2008) Bioconjugate techniques. Academic, Amsterdam

Hoffmann C, Gaietta G, Zürn A, Adams SR, Terrillon S, Ellisman MH, Tsien RY, Lohse MJ (2010) Fluorescent labeling of tetracysteine-tagged proteins in intact cells. Nat Protoc 5:1666–1677

Jakobs S, Andresen M, Wurm CA (2008) "FlAsH" protein labeling. In: Miller LW (ed) Probes and tags to study biomolecular function: for proteins, RNA, and membranes. Wiley-VCH, Weinheim, pp 73–88

Pomorski A, Krężel A (2011) Exploration of biarsenical chemistry – challenges in protein research. Chembiochem 12:1152–1167

Scheck RA, Schepartz A (2011) Surveying protein structure and function using bis-arsenical small molecules. Acc Chem Res 44:654–665

Tsien RY (2005) Building and breeding molecules to spy on cells and tumors. FEBS Lett 579:927–932

Bicarbonate

▶ Zinc and Iron, Gamma and Beta Class, Carbonic Anhydrases of Domain Archaea

Bilayer

▶ Chromium and Membrane Cholesterol

Bind

▶ Calcium-Binding Protein Site Types

Binding of Fluorescent Proteins at Gold Nanoparticles

▶ Gold Nanoparticles and Fluorescent Proteins, Optically Coupled Hybrid Architectures

Binding of Platinum to Metalloproteins

▶ Platinum Interaction with Copper Proteins
▶ Platinum-Containing Anticancer Drugs and proteins, interaction

Binding of Platinum to Proteins

▶ Platinum (IV) Complexes, Inhibition of Porcine Pancreatic Phospholipase A2

Binding Site: Binding Motif

▶ Magnesium Binding Sites in Proteins

Binuclear Mixed-Valent Electron Transfer Copper Center

▶ Cytochrome c Oxidase, CuA Center

Biodistribution of Gold Nanomaterials

▶ Gold Nanomaterials as Prospective Metal-based Delivery Systems for Cancer Treatment

Bioinformatics

▶ Zinc-Binding Proteins, Abundance

Bioinspired Materials

▶ Silicateins

Biological Activity

▶ Lanthanides, Toxicity

Biological Copper Acquisition

▶ Biological Copper Transport

Biological Copper Transport

David L. Huffman and Alia V. H. Hinz
Department of Chemistry, Western Michigan University, Kalamazoo, MI, USA

Synonyms

Biological copper acquisition; Copper trafficking in eukaryotic cells

Definition

Biological copper transport describes the acquisition and delivery of Cu(I) to cellular destinations, as well as the removal of excess Cu(I). Eukaryotic cells transport Cu(I) via permeases, metallochaperones, Cu(I)-specific pumps, and accessory factors responsible for *holo*protein maturation. Key cellular challenges include the prevention of deleterious adventitious reactions and the facile (i.e., rapid) movement of Cu(I) in transit. Inborn errors of certain genes in these pathways are linked to Wilson's disease, Menkes disease, ALS (Lou Gehrig's disease), and cytochrome c oxidase deficiency.

A Copper Requirement

Copper has been refined and processed by humans since the dawn of civilization but its role in living processes was only appreciated in the twentieth century. The vital processes of respiration, iron uptake, neurotransmitter synthesis, and free radical detoxification all include enzymes with copper cofactors. Copper deficiency is rare since we typically acquire sufficient copper in our diets.

Copper: A Double-Edged Sword

While copper is a necessary cofactor for certain enzymes, excess copper is toxic. Copper toxicity occurs by several different mechanisms. Cu(I) can disproportionate into Cu(0) and Cu(II) in aqueous solution. Additionally, Cu(I) is also able to react with

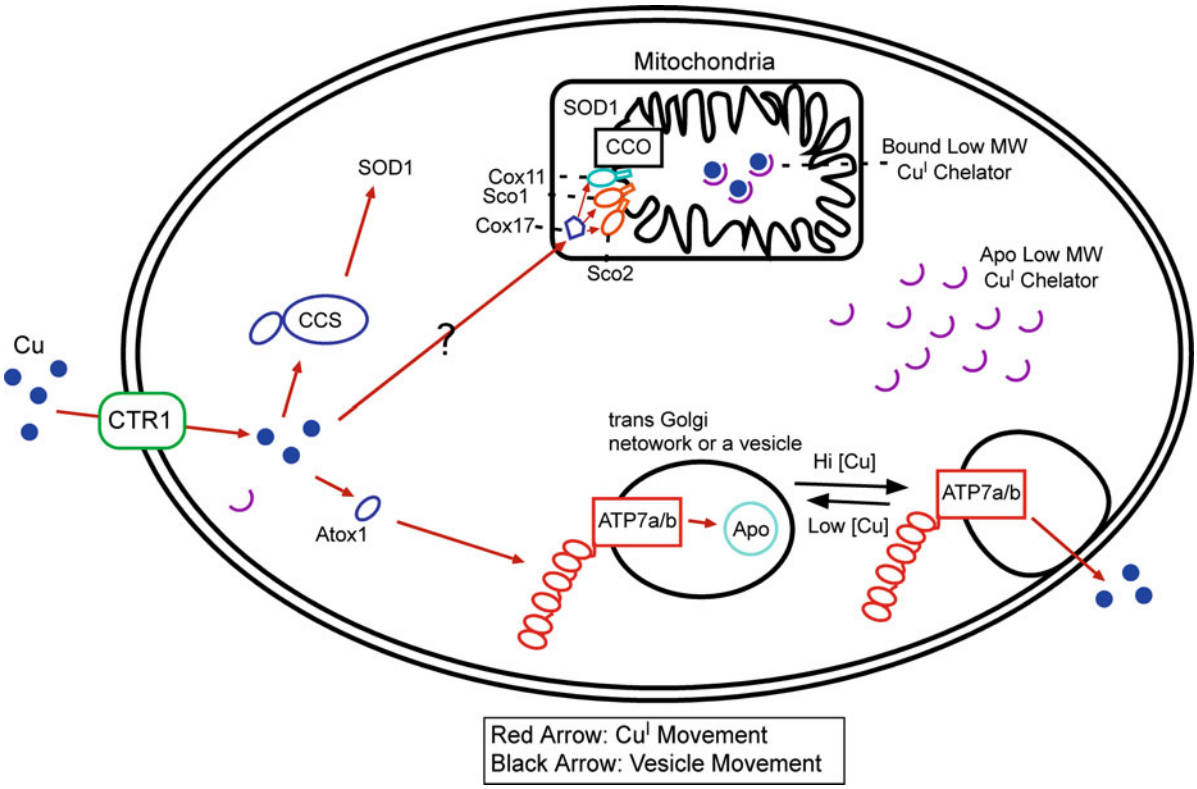

Biological Copper Transport, Fig. 1 Entry of Cu(I) (●) into the cell is mediated by Ctr1, a Cu permease. The chaperone for superoxide dismutase (CCS) delivers Cu to SOD. The metallochaperone Atox1 delivers Cu to ATP7a (Menkes) and ATP7b (Wilson) proteins, then Cu is pumped into the trans-Golgi network for incorporation into apoprotein. Under high copper conditions, ATP7a/b traffics toward the cell surface for expulsion of Cu. The metallochaperone Cox17 delivers Cu to Sco1, Cox11, and Sco2, for metallation of cytochrome c oxidase (CCO) from a matrix pool of Cu that is bound to a low molecular weight ligand

molecular oxygen to produce the superoxide anion or with hydrogen peroxide to produce the hydroxyl radical via Fenton-like chemistry. Both the superoxide anion and the hydroxyl radical are highly reactive and can damage nucleic acids, lipids, and proteins. Lastly, excess Cu(I) or Cu(II) can coordinate with the sites that are meant for other metal ions, thus altering the metal allocation of the system. Therefore, the cell must meticulously maintain proper copper ion levels (termed "homeostasis") to ensure that enough copper is available for the proteins that require it while preventing excess copper from accumulating (Huffman and O'Halloran 2001). This is achieved by carefully controlling the movement of copper from the moment it enters the cell until it reaches its ultimate destination (Fig. 1).

Copper(I) Coordination Chemistry

Biologically utilized oxidation states of copper include both Cu(I) and Cu(II), and the coordination preferences differ for these two oxidation states; however, Cu(I) is the form that is encountered in the copper delivery pathways. Cu(I) typically prefers softer ligands, such as the sulfur in cysteine or methionine, and can be found in digonal, trigonal, and tetrahedral environments in mononuclear coordination complexes. From an energetic standpoint, Cu(I) is less expensive to transport than Cu(II), but the chemical reactivity of Cu(I) poses a significant problem. The cell solves this issue by providing ligands that satisfy the coordination preferences of Cu(I), thus stabilizing the monovalent oxidation state of copper.

Mononuclear Cu(I) complexes within copper trafficking proteins are usually digonal or trigonal (Boal and Rosenzweig 2009), provided by thiols on the surface of the protein spatially arranged to provide facile transfer to a copper site of similar or greater affinity for Cu(I) (Xiao et al. 2011). Typically a digonal site is housed in a conserved MXCXXC motif, but the coordination sphere can be expanded by an exogenous ligand or another protein-based ligand. Interestingly, Cu(I) clusters with a nuclearity of 2–4 have been detected as in vitro metallochaperone crystal structures, usually at a dimer or trimer interface (Banci et al. 2010), and their in vivo relevance is not known. The repertoire of copper trafficking proteins has expanded with other cysteine-containing motifs (Robinson and Winge 2010), especially with the assembly factors for cytochrome c oxidase (CcO) found in the mitochondria, including Cox17, Sco1, Sco2, and Cox11, demonstrating the versatility and wealth of Cu(I) coordination.

Copper(I) Permeases

Ctr1, a membrane protein that is conserved among many organisms and part of the Ctr family, plays a significant role in the import of Cu(I) into the cell (Kim et al. 2008). Ctr1 has several distinct domains, including three transmembrane domains, a MX_3M element in the second transmembrane domain, a cluster of cysteine and histidine residues in the C terminus, and multiple methionine residues in the N terminus. The MX_3M element has been shown to be vital for copper uptake, with mutation of the methionine to alanine or serine resulting in decreased copper uptake. Electron microscopy and two-dimensional crystallography studies have indicated that Ctr1 is functionally active as a homotrimer in the membrane, with a putative pore forming between the interfaces of the subunits to allow Cu(I) to traverse the membrane and enter the cell (De Feo et al. 2007). A multiple Met-containing motif is becoming a common theme in extracytosolic Cu(I) acquisition, including prokaryotic metallo-oxidases, a term coined by Daniel J. Kosman. The FRE family of metalloreductases and Steap proteins are candidates for the reduction of Cu(II) to Cu(I) on the cell surface, facilitating uptake with the Cu(I) permeases. Through a process of endocytosis, Ctr1 can also relocalize to intracellular vesicles to decrease Cu(I) uptake (Kim et al. 2008).

Metallochaperones

Prior to the mid-1990s, metalloproteins were believed to acquire their metal cofactors directly by encountering metal ions that had diffused into the cell. Since then it has been found that proteins, termed "metallochaperones," bind and deliver specific metal ions, including copper, to target proteins. Given the potentially devastating effects of excess copper, cells have developed mechanisms for preventing the accumulation of unbound, excess copper. The amount of free copper in the cell at any one point in time is very low, with estimates of less than one free atom per cell (Huffman and O'Halloran 2001).

Metallochaperones That Target P_{IB}-Type ATPases

The single domain metallochaperones are small proteins, approximately 7–8 kD. The most studied of these proteins, yeast Atx1, contains a ferrodoxin fold ($\beta\alpha\beta\beta\alpha\beta$) that binds Cu(I) in a conserved MXCXXC motif (Fig. 2) between the first beta sheet and alpha helix of the protein (Boal and Rosenzweig 2009). Atx1 delivers copper to Ccc2a, an N-terminal cytosolic domain of a P_{1B}-type ATPase, named Ccc2 that possesses a ferrodoxin fold as well. The interaction between Atx1 and Ccc2a is copper-dependent and also depends upon a complex interaction interface, consisting of basic residues in Atx1 and acidic residues in Ccc2a as well as a surface complementarity (Banci et al. 2010). During the copper transfer process between Atx1 and Ccc2a a trigonal copper complex is formed as observed by NMR studies, provided by two cysteine thiolates from one protein and one from its partner; mutagenesis studies followed by NMR titrations indicate that the most predominant intermediate possesses one thiolate from Atx1 and two from Ccc2a. The human homolog of Atx1, Atox1 (or Hah1), functions in a similar way. In the trans-Golgi, Atox1 delivers copper to the N-terminal metal-binding domains of ATP7a or ATP7b (also P_{1B}-type ATPases), which in turn pumps copper across a membrane concomitant with ATP hydrolysis.

Atox1 forms NMR-observable complexes with copper-binding domains 1, 2, and 4 (e.g., Fig. 3) of ATP7b and domains 1 and 4 of ATP7a (Banci et al. 2010). Insights into the nature of this complex is

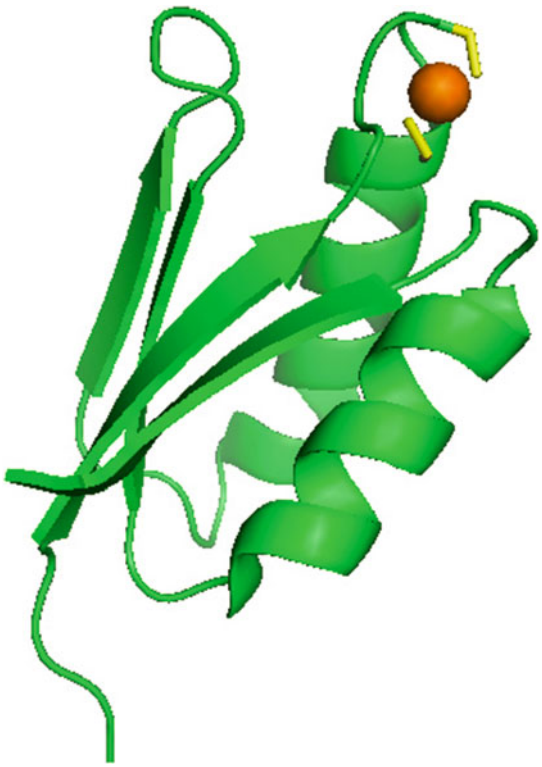

Biological Copper Transport, Fig. 2 Solution NMR structure of the yeast metallochaperone Cu^{I}-Atx1, PDB ID 1FD8, with ferrodoxin fold (*green*), cysteine thiolates (*yellow*), and digonal Cu (*orange sphere*) site

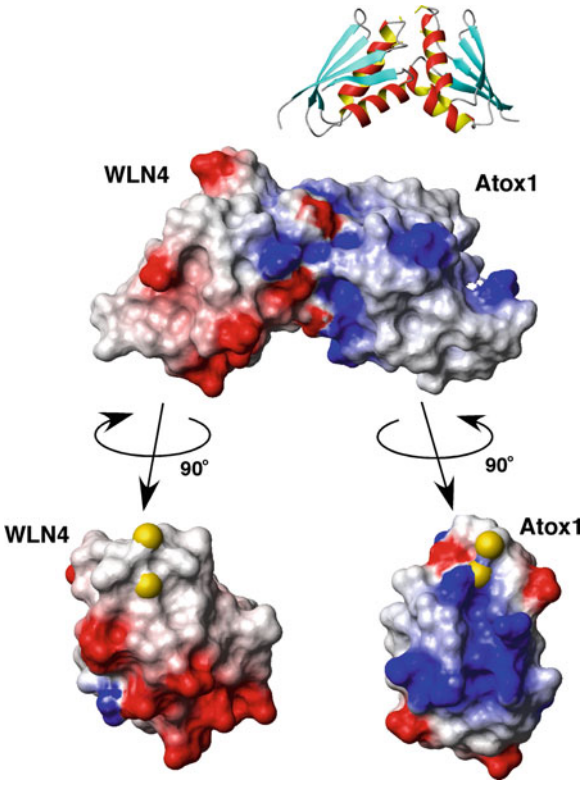

Biological Copper Transport, Fig. 3 Model of Cu-dependent complex formation between HMBD 4 of ATP7b, WLN4, and the human metallochaperone Atox1, based on the structure of Atx1/Cu/Ccc2a (PDB ID 2GGP) and NMR titrations. Potential surface of WLN4 shows array of acidic residues that interact with complementary basic surface of Atox1

provided by the X-ray structures of the metal-bridged homodimers Hg(II)-$[Atox1]_2$ (PDB ID 1FE4), Cd(II)-$[Atox1]_2$ (PDB ID 1FE0), Cu(I)-$[Atox1]_2$ (PDB ID 1FEE), the X-ray and NMR structures of the Cd-bridged heterodimer Atox1-Cd(II)-MNK1 (PDB ID 3CJK and 2K1R), and the NMR structure of the Cu(I)-bridged Atx1-Ccc2a heterodimer (PDB ID 2GGP). This review focuses on eukaryotes, but many other structures exist for homologues of these proteins, in archea, bacteria, and cyanobacteria (Boal and Rosenzweig 2009; Banci et al. 2010).

Metallochaperones That Target SOD1

The only identified protein of this class to date is CCS. Under copper limiting conditions, this protein transports copper to Cu, Zn superoxide dismutase (SOD1), an enzyme that detoxifies the reactive superoxide anion and protects the cell from oxidative damage (Leitch et al. 2009). CCS (*c*opper *c*haperone for *S*OD) is found in yeast and other eukaryotes and located primarily in the cytoplasm, though a small amount is found in the inner membrane space of the mitochondria where SOD is believed to neutralize any superoxide inadvertently produced by the electron transport chain.

At 30–32 kD and with three functionally distinct domains, the CCS proteins are larger and more complex than their single domain counterparts. Domain I is found at the amino terminus and has a ferrodoxin fold like yeast Atx1, including the MXCXXC motif used for copper binding. Displaying a similar sequence homology to SOD, Domain II binds to SOD to properly orientate the protein (Fig. 4) and facilitate the copper transfer, but is not believed to actually bind copper. Domain III, located at the carboxy terminal and possessing a conserved CXC

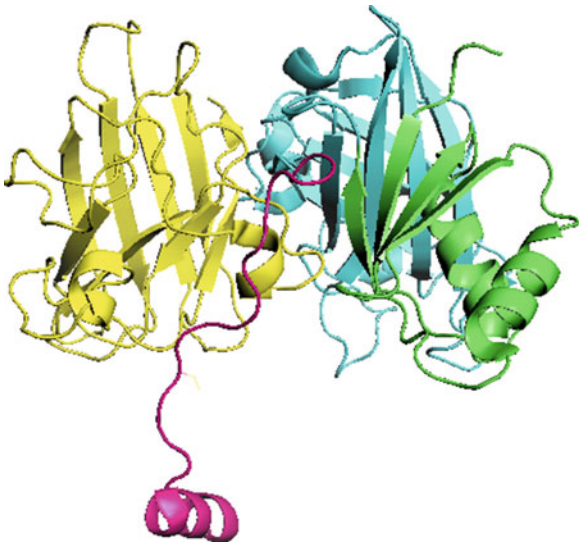

Biological Copper Transport, Fig. 4 Crystal structure of the complex between yeast CCS and yeast Cu,Zn SOD1 (*yellow*), PDB ID 1JK9. Domain I of CCS is *green*, SOD-like Domain II is *blue*, and Domain III containing the CXC motif is *pink*

motif, acts in conjunction with Domain I to transfer the copper to SOD (Leitch et al. 2009). The similarity of specific domains to other proteins with which they interact is a common theme in copper trafficking proteins.

Copper(I)-Pumping Enzymes

The copper transporting P_{IB}-type ATPases are commonly referred to as Cu(I) pumps, powered by ATP hydrolysis (Lutsenko et al. 2007). Though they are found in prokaryotes as well as eukaryotes, the human homologues differ by the presence of six high-affinity copper-binding sites (HMBD) at the N-terminus of ATP7a and ATP7b (Fig. 5). This provides an entropic driving force for copper capture and thereby increases the local concentration of copper in the vicinity of the transmembrane copper-binding sites. The apparent trafficking of ATP7b and ATP7a as a function of intracellular copper concentration and the interaction of the N-terminus of the protein with the actuator (A) and the ATP-binding domain point to a sophisticated role for the N-terminus (Lutsenko et al. 2007). The HMBD functions to capture copper and transduce conformational changes to other cytosolic facing domains. Each HMBD possesses the conserved MXCXXC motif and ligates one atom of Cu(I) in a distorted linear arrangement via the sulfur atoms in the cysteines. These proteins, in response to elevated cytosolic copper concentrations, translocate from the trans-Golgi network to vesicles that ferry copper to the plasma membrane for extracellular release. The 650 amino acid N-terminal domain interacts with other cytosolic facing domains, including the actuator (A) domain and the ATP-binding domain (comprised of the nucleotide binding N- and phosphorylation P-subdomains) (Lutsenko et al. 2007). Copper-binding domains 5 and 6, WLN5-6, function as a unit in solution and rotate little with respect to one another (Banci et al. 2010), whereas domains 3 and 4 are mobile with respect to one another.

The N-terminal copper-binding sites of ATP7a and ATP7b can obtain Cu(I) from the metallochaperone Atox1 or from low molecular weight chelators (Banci et al. 2010). The exchange of copper between sites has been determined empirically and a low barrier for copper transfer exists, as in the Atx1-Ccc2a paradigm. One question that has not been addressed is the rate of copper movement between sites in the N-terminal of ATP7b. The three-dimensional structure has not yet been solved for full-length ATP7a or ATP7b, but NMR structures exist for a number of the metal-binding domains as well as the A domain and the N domain. The way in which the cytosolic facing domains of these ATPases interact is not yet known, but clues have been garnered from cryoEM structures (PDB ID: 2VOY, 3J08, 3J09) of *Archaeoglobus fulgidus* CopA and from the X-ray structure of *Legionella pneumophila* CopA (PDB ID: 3RFU, Fig. 6), gram negative bacterial P_{IB}-type ATPases. Neither of these structures has pinpointed the exact location of the N-terminal copper-binding domain (HMBD), but it coincides with the position of the N-terminal portion of the A-domain in the SERCA1 structure, just prior to the M1 helix.

The six HMBD of ATP7a and ATP7b are spatially separated, suggesting that different portions of the N-terminus interact with discrete portions of the other cytosolic-facing domains. For example in ATP7b, domain 6 of WLN5-6 would occupy the same position as the N-terminal HMBD of CopA, but WLN1-4 is separated by 57 disordered residues from WLN5-6, and therefore WLN1-4, interacts at different positions on the cytosolic surface *or* it functions only to acquire copper from the Atox1 metallochaperone. The exact

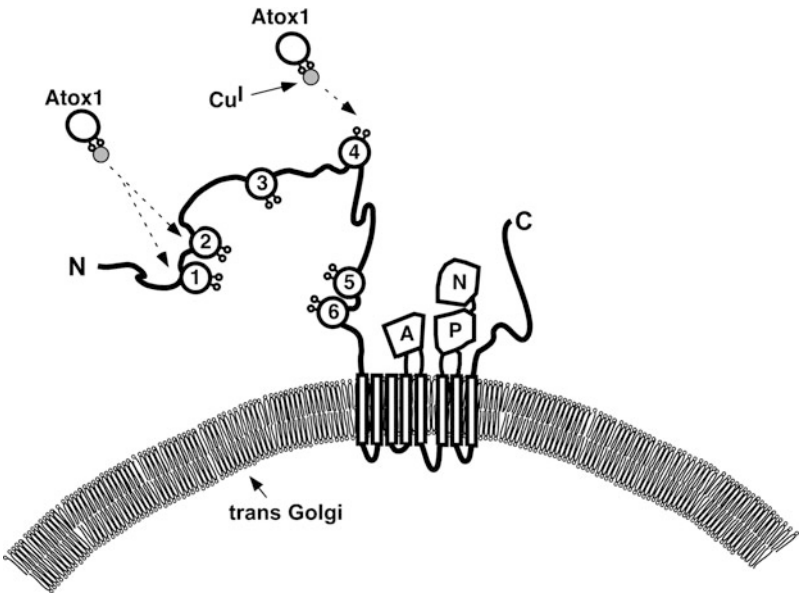

Biological Copper Transport, Fig. 5 Cartoon of ATP7b (ATP7a has similar topology), showing the interaction, observed by NMR, of Cu^{I}-Atox1 with domains one, two, and four. Cytosolic domains include the 650 residue N-terminus with six HMBD, the A (actuator), N (nucleotide binding), P (phosphorylation) domains, and the 90 residue C terminus. ATP7b has eight transmembrane helices

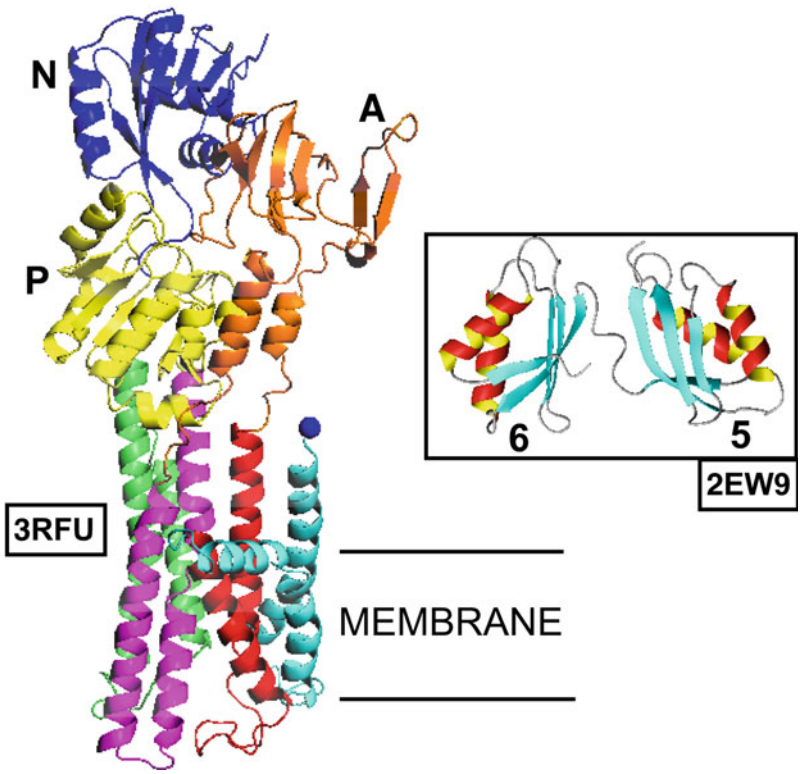

Biological Copper Transport, Fig. 6 Crystal structure of *Legionella pneumophila* CopA (PDB ID 3RFU) copper-transporting P_{IB}-type ATPase. The most N-terminal resolved feature (HMBD is disordered) is Val74 (*blue sphere*). The first two transmembrane (TM) helices MA and MB are shown in *blue*, TM helices M1 and M2 in *red*, A (actuator) domain in *orange*, TM helices M3 and M4 in *magenta*, P (phosphorylation) in *yellow*, N (nucleotide binding) in *blue*, and TM helices M5 and M6 in *green*. Membrane spanning portion is indicated by *bars*. The solution structure of WLN5-6 (PDB ID 2EW9) consisting of two HMDB is shown for visual comparison. The human homolog, ATP7b (or ATP7a), has six HMBD, whereas CopA has one

function of the N-terminal domains has been a matter of discussion, and like the structures of the bacterial homologues, they are likely more mobile than the rest of the structure. Do they simply regulate the function of the enzyme *or* do they have a role in passing Cu(I) to the binding sites at and within the membrane? Perhaps the HMBDs function *both* to capture Cu(I) and also possess a regulatory role. The low free concentration

of copper in the cytosol suggests a role of the HMBD in copper acquisition. Does the Atox1 metallochaperone directly pass copper to binding sites in the membrane portion of the enzyme? The trafficking of ATP7a and ATP7b and the role of the N- and C-termini in this process facilitate removal of copper from the cytosol, and the possession of six HMBDs likely aids this process. Several groups have shown that ATP7a and ATP7b undergo kinase-mediated phosphorylation at specific sites within the N-terminus and C-terminus, and this event has an effect on the trafficking of these proteins (Inesi 2011). Cisplatin, the most widely prescribed chemotherapeutic agent, binds to the copper-binding site of Atox1 (PDB ID 3IWL), and also interacts with the N-terminus of ATP7b; detoxification of cisplatin by proteins of the copper trafficking pathway is an area of active investigation.

Mitochondrial Copper Handling Proteins

The only mitochondrial cuproenzymes identified to date are Cu,Zn SODI and cytochrome c oxidase (CcO). Both utilize distinct metallochaperones to acquire their copper. Cu,Zn SODI is supplied with copper from CCS (Leitch et al. 2009), a metallochaperone discussed above. Several proteins are involved in transporting copper to CcO, a large, transmembrane complex that is the final enzyme in the mitochondrial electron transport chain (Robinson and Winge 2010). CcO synthesis and metallation occurs in the mitochondria, though how exactly the copper enters the mitochondria after it has entered the cell is still being elucidated. From a mitochondrial matrix pool, Cu(I) is acquired by Cox17, a small, hydrophilic protein in the intermembrane space that can bind between one and four Cu(I) atoms. Cox17 then transfers Cu(I) to two intermembrane associated proteins, Cox11 and Sco1 (Robinson and Winge 2010). Cox11 transfers Cu(I) to the mononuclear Cu_B site on Cox1 of CcO, while Sco1 transfers Cu(I) to the dinuclear Cu_A site on Cox2 of CcO. How Cox17 acquires Cu(I) is an area of much interest. It was originally thought that since Cox17 is present in both the cytosol and the intermembrane space of the mitochondria, Cox17 was shuttling Cu(I) from the cytosol to the mitochondria. However, an experiment in which Cox17 was tethered revealed that the protein did not need to leave the mitochondria in order to supply Cu(I) to CcO. Perhaps Cox17 is supplied Cu(I) by a small, copper-binding ligand that is present in both the cytosol and the mitochondrial matrix (Robinson and Winge 2010).

Conclusion

The cellular requirement for copper dictates the need for uptake, distribution, and export pathways, carefully handled by task-specific proteins at each checkpoint. Details about the mechanism and structures of these proteins are continuing to emerge, and the way in which copper trafficking proteins interact with each other. Insights are being gained by the development of exciting new methods to track copper ions in situ. The binding affinity of copper to these proteins has been under intense investigation, but unanswered questions remain about the rates of copper transfer. Areas of future study include (1) copper delivery to, and regulation of the P_{IB}-type ATPases, (2) and the maintenance of mitochondrial copper pools.

Acknowledgments DLH gratefully acknowledges support from the National Science Foundation (CAREER 0645518) and AVHH acknowledges Western Michigan University Graduate Student Research Fund.

Cross-References

- ▶ Copper-Binding Proteins
- ▶ Copper, Biological Functions
- ▶ Copper, Physical and Chemical Properties
- ▶ Copper-Zinc Superoxide Dismutase and Lou Gehrig's Disease
- ▶ Metallothioneins and Copper

References

Banci L, Bertini I, McGreevy KS, Rosato A (2010) Molecular recognition in copper trafficking. Nat Prod Rep 27:695–710, http://www.ncbi.nlm.nih.gov/entrez/query.fcgi?cmd=Retrieve&db=PubMed&dopt=Citation&list_uids=20442960

Boal AK, Rosenzweig AC (2009) Structural biology of copper trafficking. Chem Rev 109:4760–4779, http://www.ncbi.nlm.nih.gov/entrez/query.fcgi?cmd=Retrieve&db=PubMed&dopt=Citation&list_uids=19824702

De Feo CJ, Aller SG, Unger VM (2007) A structural perspective on copper uptake in eukaryotes. Biometals 20:705–716, http://www.ncbi.nlm.nih.gov/entrez/query.fcgi?cmd=Retrieve&db=PubMed&dopt=Citation&list_uids=17211682

Huffman DL, O'Halloran TV (2001) Function, structure, and mechanism of intracellular copper trafficking proteins. Annu Rev Biochem 70:677–701, http://www.ncbi.nlm.nih.gov/entrez/query.fcgi?cmd=Retrieve&db=PubMed&dopt=Citation&list_uids=11395420

Inesi G (2011) Calcium and copper transport ATPases: analogies and diversities in transduction and signaling mechanisms. J Cell Commun Signal 5:227–237. http://www.ncbi.nlm.nih.gov/entrez/query.fcgi?cmd=Retrieve&db=PubMed&dopt=Citation&list_uids=21656155

Kim BE, Nevitt T, Thiele DJ (2008) Mechanisms for copper acquisition, distribution and regulation. Nat Chem Biol 4:176–185, http://www.ncbi.nlm.nih.gov/entrez/query.fcgi?cmd=Retrieve&db=PubMed&dopt=Citation&list_uids=18277979

Leitch JM, Yick PJ, Culotta VC (2009) The right to choose: multiple pathways for activating copper, zinc superoxide dismutase. J Biol Chem 284:24679–24683, http://www.ncbi.nlm.nih.gov/entrez/query.fcgi?cmd=Retrieve&db=PubMed&dopt=Citation&list_uids=19586921

Lutsenko S, Barnes NL, Bartee MY, Dmitriev OY (2007) Function and regulation of human copper-transporting ATPases. Physiol Rev 87:1011–1046, http://www.ncbi.nlm.nih.gov/entrez/query.fcgi?cmd=Retrieve&db=PubMed&dopt=Citation&list_uids=17615395

Robinson NJ, Winge DR (2010) Copper metallochaperones. Annu Rev Biochem 79:537–562. http://www.ncbi.nlm.nih.gov/entrez/query.fcgi?cmd=Retrieve&db=PubMed&dopt=Citation&list_uids=20205585

Xiao Z, Brose J, Schimo S, Ackland SM, La Fontaine S, Wedd AG (2011) Unification of the copper(I) binding affinities of the metallo-chaperones Atx1, Atox1, and related proteins: detection probes and affinity standards. J Biol Chem 286:11047–11055. http://www.ncbi.nlm.nih.gov/entrez/query.fcgi?cmd=Retrieve&db=PubMed&dopt=Citation&list_uids=21258123

Biological Effect

▶ Lanthanides, Toxicity

Biological Effect of Vanadium

▶ Vanadium in Live Organisms

Biological Functions of $Ca2^+$ in Mitochondria

▶ Calcium and Mitochondrion

Biological Implications: Cell Death

▶ Hexavalent chromium and DNA, biological implications of interaction

Biological Implications: Chromosomal Aberrations

▶ Hexavalent chromium and DNA, biological implications of interaction

Biological Implications: Genomic Instability

▶ Hexavalent chromium and DNA, biological implications of interaction

Biological Implications: Mutagenesis

▶ Hexavalent chromium and DNA, biological implications of interaction

Biological Methane Oxidation Catalyst

▶ Particulate Methane Monooxygenase

Biology

▶ Tungsten in Biological Systems

Biomacromolecular Coordination of Germanium

▶ Rubredoxin, interaction with germanium

Biomarker

▶ Lanthanides, Luminescent Complexes as Labels

Biomarkers for Cadmium

Walter C. Prozialeck
Department of Pharmacology, Midwestern University, Downers Grove, IL, USA

Synonyms

Cadmium: Cd; Cd^{2+}

Definitions

Cadmium (*Cd*): Is an important industrial agent and environment pollutant that is a major cause of kidney disease in many regions of the world.

Nephrotoxicity/proximal tubule: The proximal tubule is the primary target of Cd toxicity in the kidney. Injury of proximal tubule epithelial results in increases in urine volume and excretion of low-molecular-weight proteins, amino acids, glucose, and electrolytes. These effects of Cd may result from even low levels of exposure and are often irreversible.

Biomarkers: The United States National Institutes of Health have broadly defined the term "biomarker" as a "characteristic that is objectively measured and evaluated as an indicator of normal biological processes, pathogenic processes, or pharmacologic responses to a therapeutic intervention." In this entry, the topic of Cd biomarkers will be considered from a more narrow perspective, as "any substance or molecule that can serve as an indicator of the functional state or level of toxic injury in the kidney."

Biological implications: Biomarkers have proven to be useful tools for evaluating Cd exposure and nephrotoxicity in human populations as well in laboratory studies on animals. However, many fundamental issues regarding the selection of markers and definition of their critical levels have yet to be fully resolved. Recent studies have provided hope that new and even more sensitive biomarkers of Cd-induced kidney injury can be developed.

Cadmium Overview

Cd as an Environmental Health Problem

Cd is an important industrial agent and a widespread environmental pollutant that currently ranks seventh on the United States Environmental Protection Agency's priority list of hazardous substances. Cd is normally found at low concentrations throughout the lithosphere but has become increasingly concentrated in the biosphere through smelting, mining, agriculture, and industrial activities of humans. As a stable, divalent cation, Cd is not biodegradable and persists in the environment for long periods of time. Despite efforts by many agencies to reduce the usage of Cd, Cd pollution continues to be a major public health problem in many regions of the world (for reviews see ATSDR 2008; Jarup and Akesson 2009).

Workers in smelting industries or industries that utilize Cd and its compounds can be exposed in the workplace by inhaling Cd oxide fumes or Cd-contaminated dust. The general population is more likely to be exposed by the ingestion of Cd-contaminated food or water (ATSDR 2008; Jarup and Akesson 2009). In addition, tobacco contains large amounts of Cd and is a major source of exposure among smokers (ATSDR 2008).

Depending on the dose, route, and duration of exposure, Cd can damage various organs including the lung, liver, kidney, and bone (ATSDR 2008; Jarup and Akesson 2009), and it is carcinogenic (ATSDR 2008). With the chronic, low-level patterns of exposure that are common in human populations, the kidney is the primary target of toxicity, where Cd accumulates in the epithelial cells of the proximal tubule, resulting in a generalized reabsorptive dysfunction that is characterized by polyuria, glucosuria, and low-molecular-weight proteinuria (Jarup and Akesson 2009; Prozialeck and Edwards 2010).

The nephrotoxic actions of Cd are, to a great extent, a consequence of the unique toxicokinetics of Cd in the body (for reviews see ATSDR 2008; Prozialeck and Edwards 2010). Following respiratory exposure, Cd is efficiently absorbed from the lung; up to 40–60% of inhaled Cd reaches the systemic circulation. With oral

exposure, the absorption of Cd from the gastrointestinal tract is considerably lower (only 5–10%). However, with long-term exposure, even this low level of absorption from the gastrointestinal tract can lead to systemic accumulation of Cd and subsequent toxicities.

Cd is initially transported to the liver where it is taken up by hepatocytes. In the hepatocytes, Cd induces the synthesis of metallothionein, which binds Cd. However, over time, the Cd-metallothionein complex can be released into the bloodstream. Even though the complex is nontoxic to most organs, it can be filtered at the glomerulus and taken up by the epithelial cells of the proximal tubule. Thus, Cd-metallothionein can have the paradoxical effect of facilitating the delivery of Cd from the liver to the kidney. In addition, Cd in plasma binds to a variety of other proteins as well as low-molecular-weight thiols, such as cysteine and glutathione. The Cd that is associated with the low-molecular-weight compounds is filtered at the glomerulus and be taken up by epithelial cells of the proximal tubule. In addition, there is some evidence for the uptake of ionic Cd^{2+} through metal ion transporters in the proximal tubule. Regardless of the form or speciation of Cd that is present in the bloodstream, Cd eventually accumulates in the epithelial cells of the proximal tubule.

Monitoring of Human Populations

The monitoring of human populations for early signs of Cd exposure and toxicity has posed a major challenge (Bernard 2004; Prozialeck and Edwards 2010). Intuitively, it might seem that the most direct way to monitor levels of Cd exposure would be to simply measure blood or urinary levels of Cd. However, this issue is greatly complicated by the tendency of Cd to be sequestered in organs such as liver and kidney. While blood levels of Cd can yield information regarding recent exposures, they often do not provide information regarding the total body burden of Cd or the severity of injury in specific target organs. Likewise, the monitoring and interpretation of data on urinary levels of Cd are not as straightforward as one might expect. With low, or even moderate, levels of exposure, any Cd that is filtered at the glomerulus is almost completely reabsorbed by epithelial cells of the proximal tubule; little or no Cd is excreted in the urine. It is only when the body burden of Cd is fairly large and/or kidney injury begins to appear that urinary excretion of Cd increases significantly. As a result of these limitations in interpreting data on blood and urinary levels of Cd, investigators have utilized various biomarkers to assess levels of Cd exposure and toxicity. As a result of Cds tendency to accumulate in epithelial cells of the proximal tubule, the kidney is, in effect, a sentinel of Cd exposure. Consequently, the most useful biomarkers of Cd exposure and toxicity have been markers of the various effects of Cd in the kidney.

This entry will highlight some of the urinary biomarkers that have proven to be most useful in monitoring Cd exposure and toxicity in human populations and in experimental animals. In addition, novel markers that appear to offer increased sensitivity will be described. All of the biomarkers that will be described represent different events in the pathophysiology of Cd-induced kidney injury. With continuous exposure, the levels of Cd in the proximal tubule cells continue to increase until a critical threshold concentration of about 150–200 μg/g of tissue is reached. The classic view is that as this threshold concentration is approached, the cells undergo oxidative stress that leads to injury and either necrotic or apoptotic cell death (reviewed by Prozialeck and Edwards 2010). The cellular injury causes alterations in proximal tubule function as well as the shedding of injured cells and cytosolic contents into the urine. The shedding of dead or injured cells triggers a repair process in which neighboring noninjured cells dedifferentiate in a process known as epithelial-mesenchymal transformation. The dedifferentiated cells migrate to the denuded area of the basement membrane and replace the injured cells.

Biomarkers of Cd Nephrotoxicity

As noted previously, the traditional urinary biomarkers that have been used to monitor Cd toxicity reflect various steps in this sequence of pathologic events. These urinary markers can be classified into four broad categories: (1) Cd-binding proteins such as metallothionein; (2) low-molecular-weight proteins; (3) proteins and enzymes derived from the brush border, intracellular organelles, or the cytosol of proximal tubule epithelial cells; and (4) proteins expressed in response to cellular injury. Figure 1 shows the typical patterns for the urinary excretion of each of these classes of markers along with a timeline describing

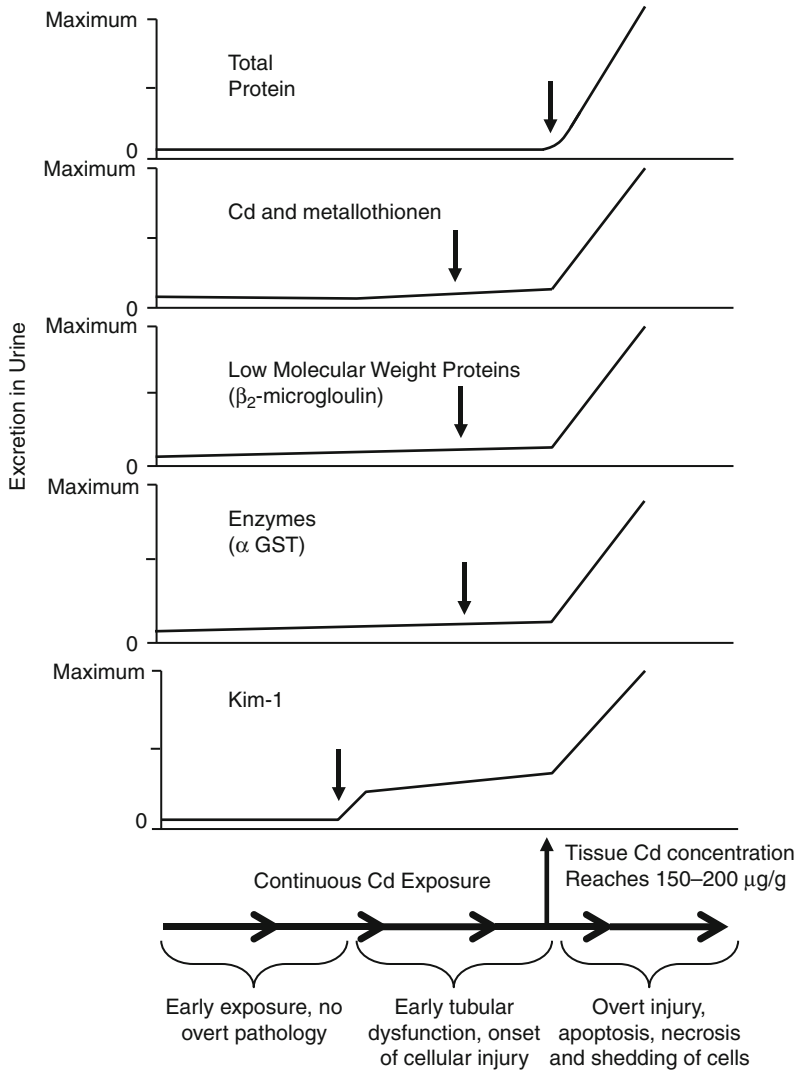

Biomarkers for Cadmium, Fig. 1 Patterns of urinary excretion of representative markers of Cd exposure and toxicity. The graphs show the general patterns for the urinary excretion of various classes of biomarkers of Cd-induced kidney injury. These are not the results of single experiments but rather depict the general results of a wide variety of studies (reviewed in Prozialeck and Edwards 2010 and Shaikh and Smith 1986). The y-axis shows the relative urinary excretion of the various markers (0 to maximum), and the x-axis indicates the relative duration of Cd exposure. The actual time frame for the various events depends on the level of Cd exposure. In humans who are exposed to low levels of Cd, the time frame can involve years of exposure. With higher levels of exposure that are used in experimental animals, the same events can occur in weeks. The *bracketed comments* at the *bottom* describe the stages of exposure and proximal tubular injury. The *downward arrows* (↓) indicate the point at which excretion of each marker usually becomes significantly elevated

specific pathophysiologic events in the proximal tubule. Reference will be made to this figure as each of the classes of markers is described below.

Cd and Metallothionein

The urinary excretion of Cd and metallothionein can serve as markers of both Cd exposure and of Cd-induced proximal tubule injury (Bernard 2004; Prozialeck and Edwards 2010; Shaikh and Smith 1986). During early stages of exposure, circulating Cd which is bound to low-molecular-weight molecules such as metallothionein, cysteine, or glutathione in the plasma is filtered at the glomerulus and efficiently taken up by the epithelial cells of the proximal tubule. Only extremely small amounts are excreted in the urine. During this stage of exposure (labeled as "Early exposure" in the timeline in the figure), the presence of Cd or metallothionein in the urine most likely results from the normal turnover and shedding of epithelial cells and is a reflection of the level of Cd exposure and the body burden of Cd (Prozialeck and Edwards 2010). However, over time, the concentration of Cd in the epithelial cells increases to the point that Cd injures the cell and/or disrupts tubular reabsorptive processes. At this stage (labeled "Intermediate exposure" in the figure), the excretion of Cd and metallothionein begins to increase in a linear manner. However, as the intracellular levels of Cd increase further, more of the epithelial cells begin to die and slough off. At this point, the urinary excretion of Cd

and metallothionein increases markedly (Prozialeck and Edwards 2010; Shaikh and Smith 1986). This surge in the urinary excretion of Cd and metallothionein coincides with the onset of polyuria and proteinuria. Thus, the early, linear phases of Cd and metallothionein excretion are a reflection of Cd exposure, whereas the later increases in excretion are a reflection of Cd-induced tubular injury.

The World Health Organization, United States Environmental Protection Agency and other agencies have established guidelines for the monitoring of populations for Cd exposure and for Cd exposure limits (ATSDR 2008; Huang 2004; World Health Organization (WHO) 2000). Even though there are variations among the standards from these different agencies, some generalizations can be made. The blood levels of Cd in nonexposed populations are typically less than 0.5 μg/L. Blood levels higher than 1.0 μg/L are generally indicative of Cd exposure; levels higher than 5 μg/L are considered hazardous. Urinary levels of Cd in nonexposed populations are usually below 0.5 μg/g creatinine; values above 1–2 μg/g are indicative of exposure or elevated body burden. The critical urinary Cd concentration that is associated with the onset of renal injury is usually about 2–10 μg/g creatinine, which corresponds to a renal cortical Cd concentration of about 150–200 μg/g tissue (Prozialeck and Edwards 2010). It should be emphasized that these generalizations are derived from consensus-based standards from various regulatory agencies. However, there is evidence that even lower urinary levels of Cd may be associated with adverse effects (for review see Prozialeck and Edwards 2010). With regard to metallothionein, the critical urinary level that is associated with the onset of overt kidney injury is about approximately 300 μg/g creatinine (Chen et al. 2006; Shaikh and Smith 1986).

It should be noted that the majority of studies on which these standards/recommendations are based involved the measurement of total urinary metallothionein; they did not differentiate/identify specific metallothionein isoforms. There are currently four known isoforms of metallothionein. Although the relationships between urinary excretion of Cd and these different metallothionein isoforms have not been established, there are a few reports indicating possible differential effects of Cd on the expression of the different isoforms. The application of using specific isoforms of metallothionein as biomarkers of Cd exposure remains to be fully explored.

Low-Molecular-Weight Proteins

The second category of Cd urinary biomarkers includes a variety of low-molecular-weight proteins such as β_2-microglobulin, Clara cell protein (CC-16), α_1-microglobulin, retinol-binding protein, and vitamin D–binding protein. These low-molecular-weight proteins are present in plasma and are small enough to be easily filtered at the glomerulus. Under normal circumstances, these filtered proteins are efficiently reabsorbed by the proximal tubule and are not excreted to any great extent in the urine (Bernard 2004; Prozialeck and Edwards 2010). However, as Cd accumulates in the proximal tubule, absorption of these proteins becomes impaired, and the proteins begin to appear in the urine. Of these proteins, β_2-microglobulin has been most widely employed as a standard marker for monitoring the early stages of Cd exposure and toxicity in humans. Urinary levels of β_2-microglobulin of 1,000 μg/g creatinine (or greater) are considered to indicate specific renal injury. This level is typically associated with urinary Cd of greater than 5 μg/g creatinine. For population monitoring, a cutoff value of 300 μg/g β_2-microgobulin/creatinine has been used (Huang 2004). However, other investigators have recommended lower critical exposure levels (Uno et al. 2005). Even though β_2-microglobulin has proven to be a very useful biomarker, its lack of stability in acidic urine can be problematic.

As with β_2-microglobulin, increased levels of retinol-binding protein are suggestive of impairment of tubular reabsorptive function. Unlike β_2-microglobulin, however, retinol-binding protein is stable in acidic urine, and no special preservative or alkaline treatment is required (for review see Prozialeck and Edwards 2010).

Proximal Tubule–Derived Enzymes

Some of the most extensively used markers of Cd-induced proximal tubule injury have been enzymes that are expressed in proximal tubule epithelial cells. A variety of enzymes including: N-acetyl-β-D-glucosaminidase (NAG), lactate dehydrogenase (LDH), alkaline phosphatase, and more recently, alpha-glutathione-S-transferase (α-GST) have been studied in this context. The appearance of these enzymes in urine is classically thought to result from the leakage of intracellular contents when necrotic proximal tubule epithelial cells lose their membrane integrity and/or slough off into the urine (Vaidya et al. 2008).

NAG has proven to be especially useful in the monitoring of human populations. NAG is a lysosomal enzyme that exists as multiple isoforms. Both forms A and B are expressed in kidney. However, the B form, which is more abundant in the proximal tubule, is regarded as the more sensitive and reliable marker of Cd-induced injury. However, assays that do not differentiate between the two isoforms can also yield useful results. Several epidemiologic studies have shown that NAG outperforms other traditional markers (Jin et al. 1999; Moriguchi et al. 2009; Noonan et al. 2002; Suwazono et al. 2006). However, it is also noteworthy that it does not perform as well in animal (rat) models of Cd nephrotoxicity (Prozialeck and Edwards 2010). One major advantage of NAG for large-scale population studies is that it is relatively stable in nonpreserved urine.

Recent studies suggest that α-GST may also be especially useful early marker of Cd-induced kidney injury. Garcon et al. (2007) reported that α-GST was a sensitive indicator of kidney injury in workers who had been exposed to Pb and Cd. Results of studies from our laboratories showed that α-GST was a more sensitive marker of kidney injury than NAG in a rat model of Cd-induced kidney injury (Prozialeck and Edwards 2010).

Miscellaneous Markers of Proximal Tubule Dysfunction, Amino Acids, Glucose, Na^+, K^+, and Ca^{2+}

In addition to its effects on these protein biomarkers, Cd causes a generalized proximal tubule dysfunction that results in an increase in the urinary excretion of amino acids, Na^+, K^+, PO_4^-, and Ca^{2+} (Shaikh and Smith 1986). Even though these effects are characteristic of Cd nephrotoxicity, the urinary excretion of these substances can be influenced by many factors other than Cd exposure (Shaikh and Smith 1986). In general, these substances have not been widely applied in the monitoring of human populations for early signs of Cd exposure. One notable exception, however, is Ca^{2+}, which has been shown to be a reliable indicator of Cd-induced proximal dysfunction in exposed human subjects (Wu et al. 2001).

Injury Response Proteins

Most of the traditional biomarkers of Cd nephrotoxicity are based on the assumption that Cd causes necrotic or apoptotic cell death of proximal tubule epithelial cells. However, an increasing volume of evidence indicates that the early stages of Cd toxicity involve changes in proximal tubule cell adhesion and function that occur before the onset of cell death (Prozialeck et al. 2009a; Prozialeck and Edwards 2010). In addition, several recent studies indicate that the onset of Cd-induced kidney injury may be preceded by changes in specific markers of metallothionein expression, immune function, and glucose metabolism (for review see Prozialeck and Edwards 2010). Together, these recent findings raise the possibility of identifying more specific and earlier biomarkers of Cd exposure and toxicity. One of the more promising urinary markers that have been described recently is kidney injury molecule-1 (Kim-1).

Kim-1 is a transmembrane protein that is not detectable in normal kidney but is expressed at high levels in the proximal tubule after ischemic or toxic injury (Vaidya et al. 2008). Kim-1 acts as a regulator of cell adhesion and endocytosis in regenerating cells of the injured tubule as they reform a functional epithelial barrier. This process is associated with the proteolytic cleavage of the ectodomain of Kim-1 into the urine. The ectodomain is stable in urine and has been shown to be a sensitive marker of renal injury induced by a variety of agents (Vaidya et al. 2008).

In studies utilizing a rat model of Cd-induced kidney injury, Kim-1 outperformed traditional urinary markers (Prozialeck et al. 2007; Prozialeck et al. 2009a, 2009b). Kim-1 was detected in the urine 4–5 weeks before the onset of proteinuria and 2–5 weeks before the appearance of other markers such as metallothionein and CC-16. Other studies showed that the Cd-induced increase in Kim-1 expression occurred at a time when there was little or no evidence of either necrosis or apoptosis of proximal tubule epithelial cells (Prozialeck et al. 2009b). The fact that Kim-1 can be detected at a time before lethal injury to proximal tubule epithelial cells has occurred may be especially significant. Perhaps, with earlier detection via Kim-1, it may be possible to reverse, or at least more effectively treat, Cd-induced kidney injury. In light of this possibility, studies on the utility of Kim-1 as marker of Cd toxicity in humans are certainly warranted.

Markers of Glomerular Injury

While the proximal tubule is the primary target of Cd-induced kidney injury, there is evidence that Cd can also affect the glomeruli. Changes in classic markers of

glomerular dysfunction such as BUN and serum or urinary creatinine are generally not seen during the early or mild stages of Cd-induced kidney injury (Prozialeck and Edwards 2010). However, other investigators have reported associations between Cd exposure and alterations (in glomerular function). For example, Weaver et al. (2011) have recently reported significant increases in creatinine clearance in subjects exposed to Cd and Pb. At present, the relative contributions and relationship of glomerular injury and proximal tubule injury to these finding remain unclear.

Summary and Perspective

Biomarkers have proven to be useful tools for evaluating Cd exposure and nephrotoxicity in human populations as well in laboratory studies on animals. While many fundamental issues regarding the selection of markers and definition of their critical levels have yet to be fully resolved, recent studies have provided hope that new and even more sensitive Cd biomarkers can be developed.

Cross-References

- ▶ Cadmium Absorption
- ▶ Cadmium and Metallothionein
- ▶ Cadmium and Oxidative Stress
- ▶ Cadmium and Stress Response
- ▶ Cadmium Exposure, Cellular and Molecular Adaptations
- ▶ Cadmium, Effect on Transport Across Cell Membranes
- ▶ Cadmium Transport
- ▶ Cadmium, Physical and Chemical Properties

References

ATSDR (2008) Toxicological profile for cadmium. http://www.atsdr.cdc.gov/cercla/toxprofiles/tp5.html

Bernard A (2004) Renal dysfunction induced by cadmium: biomarkers of critical effects. Biometals 17:519–523

Chen L, Jin T, Huang B et al (2006) Critical exposure level of cadmium for elevated urinary metallothionein–an occupational population study in China. Toxicol Appl Pharmacol 215:93–99

Garcon G, Leleu B, Marez T et al (2007) Biomonitoring of the adverse effects induced by the chronic exposure to lead and cadmium on kidney function: usefulness of alpha-glutathione S-transferase. Sci Total Environ 377:165–172

Huang J (2004) Chinese National health standards for occupational exposure to cadmium and diagnostic criteria of occupational chronic cadmium poisoning. Biometals 17(5):511. doi:10.1023/B:BIOM.0000045833.30776.84

Jarup L, Akesson A (2009) Current status of cadmium as an environmental health problem. Toxicol Appl Pharmacol 238:201–208

Jin T, Nordberg G, Wu X et al (1999) Urinary N-acetyl-beta-D-glucosaminidase isoenzymes as biomarker of renal dysfunction caused by cadmium in a general population. Environ Res 81:167–173

Moriguchi J, Inoue Y, Kamiyama S et al (2009) N-acetyl-beta-D-glucosaminidase (NAG) as the most sensitive marker of tubular dysfunction for monitoring residents in non-polluted areas. Toxicol Lett 190:1–8

Noonan CW, Sarasua SM, Campagna D et al (2002) Effects of exposure to low levels of environmental cadmium on renal biomarkers. Environ Health Perspect 110:151–155

Prozialeck WC, Edwards JR (2010) Early biomarkers of cadmium exposure and nephrotoxicity. Biometals 23:793–809

Prozialeck WC, Vaidya VS, Liu J et al (2007) Kidney injury molecule-1 is an early biomarker of cadmium nephrotoxicity. Kidney Int 72:985–993

Prozialeck WC, Edwards JR, Lamar PC et al (2009a) Expression of kidney injury molecule-1 (Kim-1) in relation to necrosis and apoptosis during the early stages of Cd-induced proximal tubule injury. Toxicol Appl Pharmacol 238:306–314

Prozialeck WC, Edwards JR, Vaidya VS et al (2009b) Preclinical evaluation of novel urinary biomarkers of cadmium nephrotoxicity. Toxicol Appl Pharmacol 238:301–305

Shaikh ZA, Smith LM (1986) Biological indicators of cadmium exposure and toxicity. Experientia Suppl 50:124–130

Suwazono Y, Sand S, Vahter M et al (2006) Benchmark dose for cadmium-induced renal effects in humans. Environ Health Perspect 114:1072–1076

Uno T, Kobayashi E, Suwazono Y et al (2005) Health effects of cadmium exposure in the general environment in Japan with special reference to the lower limit of the benchmark dose as the threshold level of urinary cadmium. Scand J Work Environ Health 31:307–315

Vaidya VS, Ferguson MA, Bonventre JV (2008) Biomarkers of acute kidney injury. Annu Rev Pharmacol Toxicol 48:463–493

Weaver VM, Kim NS, Jaar BG et al (2011) Associations of low-level urine cadmium with kidney function in lead workers. Occup Environ Med 68(4):250–256

World Health Organization (WHO) (2000) Cadmium. http://www.euro.who.int/document/aiq/6_3cadmium.pdf

Wu X, Jin T, Wang Z et al (2001) Urinary calcium as a biomarker of renal dysfunction in a general population exposed to cadmium. J Occup Environ Med 43:898–904

Biomedical Application

- ▶ Gold Nanomaterials as Prospective Metal-based Delivery Systems for Cancer Treatment

Biomedical Plausibility of Exposure and Mechanism of Action

► Mercury and Alzheimer's Disease

Biomimicry

► Silicateins

Biomineralization

► Silicateins

Biomineralization of Gold Nanoparticles from Gold Complexes in *Cupriavidus Metallidurans* CH34

► Gold Biomineralization in Bacterium Cupriavidus metallidurans

Biomonitoring

► Arsenic in Tissues, Organs, and Cells

Biosensors

► Silicon Nanowires

Biosilica

► Silicateins

Biosynthesis of Selenoproteins

► Selenoproteins and the Biosynthesis and Activity of Thyroid Hormones

Bisarsenical Probes

► Biarsenical Fluorescent Probes

Bismuth in Brain

► Bismuth in Brain, Distribution

Bismuth in Brain, Distribution

Agnete Larsen
Department of Biomedicine/Pharmacology Health, Aarhus University, Aarhus, Denmark

Synonyms

Bismuth in brain

Definitions

Encephalopathy: This term involves a large group of transient or permanent brain disorders with very diverse etiologies. Among other causes it can be mentioned metabolic alterations, bacterial, food poisoning, trauma, hypoxia, pharmacological, etc. When unresolved, encephalopathies lead to neurodegeneration. The hallmark of encephalopathy is mental alteration, impairment of cognitive functions, lethargy, confusion, tremors, seizures, convulsions, and others.

Autometallography: This method is used for the imaging of metal-containing clusters in tissues sections. This methodology involves the reduction of silver ions from a silver donor e.g., silver lactate (Ag^{+}) to metallic silver (Ag^{0}) by metals such as bismuth in the presence of a developer. In consequence, Ag^{0} is

deposited in the site where the metal of interest is located and those deposits can be photographed by both light and electron microscopies.

In contrast to many other heavy metals, bismuth is generally considered a safe or even "green" heavy metal. Due to the chemical and physical properties of the metal, bismuth is often used as a replacement of lead and mercury in many industrial settings, and in 2004, the industrial use of bismuth reached a yearly consumption of as much as 5,000 t (Palmieri 2004). Possible source of human bismuth exposure include the widespread use of bismuth in cosmetics and as the soft metal has excellent ballistic qualities, bismuth shotgun pellets are a known source of direct bismuth exposure to wild life especially wounded game animals which might live on for prolonged periods exposed to fragments from shotgun pellets (Pamphlett et al. 2000; Stoltenberg 2004).

Medical use of bismuth dates back more than a 100 years (The Lancet 1857) but even in this millennium, bismuth compounds are still in use for gastrointestinal disorders such as the well-known US over-the-counter remedy Pepto-Bismol. Bismuth salts have also been shown to have a bacteriostatic effect on the ulcer-generating bacteria *Heliocobacter pylori* (Rokkas and Sladen 1988; Stoltenberg et al. 2001a). Modern medical use also includes bismuth adjuvants for chemotherapy (Tiekink 2002). Reported side effects to bismuth pharmaceuticals include gingival discoloration, erythema, and osteopathy. More dangerous side effects are nephropathy and a potentially fatal encephalopathic condition (Slikkerveer and de Wolff 1989). Bismuth encephalopathy is characterized by a series of neuropsychiatric changes such as emotional changes, insomnia, and changes in eating habits followed by confusion and motor dysfunctions stretching from tremors and ataxia to myoclonus and overt convulsions (Bes et al. 1976). Though sometimes fatal, this encephalopathic state is most often reversible within a few weeks after cessation of bismuth exposure. Most available knowledge regarding the pathogenesis of bismuth encephalopathy dates back to an epidemic incident taking place in France and neighboring countries in the 1970s. During this episode, approximately 1,000 cases of bismuth-induced encephalopathies were reported. The epidemic occurred at a time and place at which the use of bismuth compounds for various gastrointestinal disorders was quite high and with great individual variation however despite the high number of patients evaluations of the incidence expect that only 0.1% of all bismuth consumers were affected. There was no apparent relationship between disease susceptibility, bismuth blood values, or the amount or period of bismuth ingestion, and the pathogenesis of the disease is still far from unraveled and it thus remains unclear if it was a random clustering or if unknown environmental factors contributed (Martin-Bouyer 1978; Martin-bouyer et al. 1981).

Following the epidemic, Ross and coworkers (1988) set out to create an animal (mouse) model for bismuth encephalopathy and much of our knowledge of the distribution of bismuth in brain tissue is derived from this model. The model is based on intraperitoneal injections of bismuth subnitrate (2,500 mg/kg) functioning as a permanent deposit for bismuth liberation. Using this model, many mice display neurotoxic features similar to the human condition, reaching a brain Bi level (~8 ppm) similar to the one reported in deceased patients. In a later bismuth distribution study, the model was modified to a single injection, giving raise to brain Bi levels of 1–5 ppm within a 1–4-week period of exposure (Ross et al. 1994).

Applying atomic absorption spectrometry (AAS), Ross and coworkers could show that given blood-borne bismuth exposure, there is a clear pattern of regional difference in bismuth content throughout the brain. In these studies, it was evident that the highest accumulation of bismuth is found in the olfactory bulb and subsequently the hypothalamus. The olfactory bulb is seldom examined but a high degree of hypothalamic accumulation has been reported also in more qualitative studies (Pamphlett et al. 2000; Larsen et al. 2005).

Other areas with relatively high quantitative bismuth concentration were the septum region and the brain stem containing approximately half the concentration of the olfactory bulb. Outside these regions, the amount of bismuth accumulation was relatively small compared to the olfactory bulb and the hypothalamus. About a third of the maximal olfactory bulb concentration was found in tissue samples from the spinal cord and a little less in the thalamus and cerebellum. The by far lowest bismuth concentrations were seen in cortical areas and the striatum, e.g., in the temporal cortex the bismuth concentration was about one seventh of concentration seen in the olfactory bulb (1 ppm to 7.1 ppm respectively). It should be noted that the regional distributions seen here have also been

reported on intraperitoneal exposure to water-soluble bismuth compounds (Ross et al. 1994).

In their 1994 and 1996 articles (Ross et al. 1994; Larsen et al. 2005), the Ross group also purposed a technique for in situ bismuth visualization, the autometallographic silver enhancement technique (AMG), later to be refined by Danscher and Stoltenberg (Ross et al. 1996; Stoltenberg and Danscher; Stoltenberg et al. 2007). With AMG around 96% of injected bismuth can be visualized (Stoltenberg et al. 2007). Using AMG, Ross could confirm distinct regional differences in bismuth distribution with olfactory bulb and hypothalamus exhibiting the highest amount of AMG-detectable bismuth accumulation. Overall, the regional staining pattern showed little inter-animal variation in the Ross studies; however, some inter-animal variation in AMG-staining intensity was evident and this phenomenon is supported in other animal studies (Pamphlett et al. 2000; Larsen et al. 2005). The AMG study made by Ross depicted a regional distribution of bismuth centered around and gradually spreading from the circumventricular organs (CVOs), i.e., it was evident that the accumulations of bismuth present decreased as the distance to the CVO increased (Ross et al. 1994, 1996). The lack of the blood–brain barrier allowed the way in for the blood-borne bismuth exposure, e.g., the high amount of bismuth in the hypothalamus seems associated to the near presence to fenestrated blood vessels. In accordance with this, a very high amount of bismuth is seen in the vessels and the underlying lamina and in areas with only minor bismuth accumulations, most metals seem to be captured within the vasculature (Ross et al. 1994, 1996). However, throughout the brain, a high amount of bismuth accumulations was also seen in lysosomes in both neurons and glia (Pamphlett et al. 2000; Stoltenberg 2004; Ross et al. 1994, 1996). The choroid plexus was also characterized by a very high amount of bismuth in the epithelia, corresponding to morphological findings of alteration in the ventricular system with hydrocephalus as a striking feature in the murine model. The neuronal staining was most evident in larger neurons especially in the brain stem. Other animal studies also reported that large motor neuron is a center for bismuth accumulation (Pamphlett et al. 2000; Ross et al. 1994). The cerebellum, especially the Purkinje cells (especially those close to the fourth ventricle), is also described as among the neurons most heavily loaded with AMG-detectable bismuth. The only human study (Stoltenberg et al.) employing AMG on brain slices from six victims of bismuth encephalopathies also confirmed metal accumulations in both neuron and glia with cerebellum as one of the "hot spots." Unlike the mouse model, this study did however find equally large mainly neuronal accumulations in thalamus and neocortex, areas of lesser bismuth content in the rodent model of encephalopathy. In one human sample, a widely distributed bismuth pattern was seen involving also areas like the hippocampus, indicating that bismuth accumulation takes place in any brain region depending on the amount of metal present. Retrograde axonal transport of bismuth occurs both within the CNS and from the periphery into spinal cord (Ross et al. 1994; Stoltenberg et al. 2001b) and both such active transport and the mode of entry will also affect the distribution patterns as seen, e.g., following direct intercranial exposure in which the highest amount of bismuth accumulation is seen in the vicinity of a bismuth implant (Stoltenberg et al. 2003).

To sum up, the presently available information on bismuth distribution indicates that bismuth uptake is affected by the mode of entry, i.e., blood-borne intra via fenestrated blood vessels contra intra-muscularly or intra-cranially, with CVO-near accumulation of especially the hypothalamus as a heavily loaded area. Olfactory bulb with its projection to the periphery is another central area of accumulation. Additionally, cerebellar Purkinje cells and large sensory and especially motor neurons in the brain stem seem prone to bismuth accumulation. Bismuth can be found not only in vasculature but also in glia cells, many of them astrocytes in the white matter as well as in neurons. The ependyma of the choroid plexus also contains a high amount of bismuth. On the ultrastructural level, cellular bismuth inclusions are seen in lysosomal-like structures of both glia and neurons as well as extracellular in basement membranes. Blood concentration of bismuth shows a high degree of intrapersonal variation, and even in the laboratory setting, there are differences in the degree of neuronal accumulation between individuals, although the regional pattern of distribution remains the same for many types of bismuth exposure. Especially with regard to the concentration of bismuth in larger, mainly motor neurons and the choroid plexus, the distribution of bismuth shows similarity to other heavy metals such as silver and mercury (Møller-Madsen 1993; Cassano et al. 1969; Rungby and Danscher 1983).

Cross-References

- ▶ Germanium, Toxicity
- ▶ Germanium, Physical and Chemical Properties
- ▶ Germanium-Containing Compounds, Current Knowledge and Applications

References

Bes A et al (1976) Toxic encephalopathy due to bismuth salts. Rev Med Touluse 12:801–813

Cassano GB et al (1969) The distribution of inhaled mercury (Hg^{203}) vapors in the brain of rats and mice. J Neuropathol Exp Neurol 28:214–255

Larsen A et al (2005) In vivo distribution of bismuth in the mouse brain; influence of long-term survival and intracranial placement on the uptake and transport of bismuth in neuronal tissue. Basic Clin Pharmacol Toxicol 97(3):188–196

Martin-Bouyer B (1978) Poisoning by orally administred bismuth salts. Gastrointest Clin Biol 2(4):349–356

Martin-bouyer G et al (1981) Epidemiological study of encephalopathies following bismuth administration per os. Characteristics of intoxicated subjects: comparison with control group. Clin Toxicol 11:1277–1283

Møller-Madsen B (1993) Localization of mercury in CNS of the ratII interperitoneal injection of methylmercuric chloride (CH_3HgCl) and mercuric chloride ($HgCl_2$). Toxicol Appl Pharmacol 103:303–323

Palmieri Y (2004) About bismuth. htpp://www.bismuth.be/bismuthpdf

Pamphlett R et al (2000) Tissue Uptake of bismuth from shotgun pellets. Envion Res 82(3):258–262

Rokkas T, Sladen GE (1988) Bismuth: effects on gastritis and peptic ulcer. Scand J Gastroentral Suppl 142:82–86

Ross JF et al (1988) Characterization of a murine model for human bismuth encephaloapathy. Neurotoxicoly 9:581–586

Ross JF et al (1994) Highest brain bismuth levels and neuropathology are adjeacent to fenestrated blood vessels in mouse brain after intraperitonal dosing of bismuth subnitrate. Toxicol Appl Pharmacol 124:191–200

Ross JF et al (1996) Distribution of bismuth in the brain: intraperitoneal dosing of bismuth subnitratein mice: implications for the route of entry of xenobiotic metals into the brain. Brain Res 725:137–154

Rungby J, Danscher G (1983) Localization of exogenous silver in brain and spinal cord of silver exposed rats. Acta Neuropathol 60:92–98

Slikkerveer A, de Wolff FA (1989) Pharmacokinetices and toxicity of bismuth compounds. Toxicol Manag Rev 4:303–323

Stoltenberg M (2004) Bismuth. Some aspects of localization, transport and pathological effects of metalic bismuth and bismuth salts with special emphasis o nits neurotoxicity to man and experimental animals. Thesis, University of Aarhus, Denmark

Stoltenberg M, Danscher G. Histochemical differentiation of autometallographically traceable metals (Au, Ag, Bi, Zn): Protocols for chemical removal of separate autometallographic metal clusters in Epon Sections. Histochem J 32:645–652

Stoltenberg M et al Autometallographic tracing of bismuth in human brain autopsies. J Neuropathol Exp Neurol 60:705–710

Stoltenberg M et al (2001) Histochemical tracing of bismuth in *Heliocobacter pylori* after in vitro exposure to bismuth citrate. Scand J Gastroenterol 36(2):144–148

Stoltenberg M et al (2001) Retrograde axonal transport of bismuth. An autometallograhic study. Acta Neuropathol 101:123–128

Stoltenberg M et al (2003) In vivo cellular uptake of bismuth ions from shotgun pellets. Histol Histopathol 18(3):781–785

Stoltenberg M, Juhl S, Danscher G (2007) Bismuth ions are metabolized into autometallographic traceable bismuth-sulphur quantum dots. Eur J Histochem 51(1):53–57

The Lancet (1857). 2:185–187

Tiekink ER (2002) Antimony and bismuth compounds in oncology. Crti Rev Oncol 42(3):217–224

Bismuth, Interaction with Gastrin

Graham S. Baldwin
Department of Surgery, Austin Health, The University of Melbourne, Heidelberg, VIC, Australia

Definition

The peptide hormone gastrin was originally identified as a stimulant of acid secretion, but is now known to also act as a growth factor in the gastrointestinal tract (Dockray et al. 2001). Gastrin is synthesized as a precursor of 101 amino acids (*preprogastrin*) which, on removal of the signal peptide of 21 amino acids, yields *progastrin* (80 amino acids). Proteolytic processing in antral G cells in the stomach generates a number of intermediate peptides, including *glycine-extended gastrin*$_{17}$ (Ggly), which has the sequence ZGPWLEEEEEAYGWMDFG. Transamidation of the C-terminal glycine yields the C-terminal amidated phenylalanine characteristic of *amidated gastrin* (Gamide). Both Ggly and Gamide are independently active, via different receptors, in the gastrointestinal tract.

Basic Characteristics

Iron: Interaction with Gastrin

Fluorescence experiments have revealed that both Ggly and Gamide bind two ferric ions with high affinity (K_d = 0.6 μM, pH 4.0) in aqueous solution (Baldwin et al. 2001), via the carboxylate groups in the side chains of Glutamates 7, 8, and 9 (Pannequin et al. 2002).

Progastrin also binds two ferric ions, and the ferric ion–progastrin complex is very stable, with a half-life of 117 ± 8 days at pH 7.6 and 25°C (Baldwin 2004).

Binding of ferric ions is essential for the biological activities of Ggly in vitro. Mutation of Glutamate 7 of Ggly to Alanine reduced the stoichiometry of ferric ion binding from 2 to 1, and completely abolished biological activity in cell proliferation and migration assays (Pannequin et al. 2002). The iron chelator desferrioxamine also completely blocked Ggly activity in cell proliferation and migration assays in vitro (Pannequin et al. 2002) and in the colorectal mucosa in vivo (Ferrand et al. 2010). The minimum biologically active Ggly fragments are the heptapeptides LEEEEEA and EEEEEAY, and their activity is still dependent on ferric ions (He et al. 2004). Interestingly, mutation of Glutamate 7 of Gamide to Alanine had no effect on the biological activity of Gamide, even though the stoichiometry of ferric ion binding was again reduced from 2 to 1, presumably because the receptors for Ggly and Gamide are distinct (Pannequin et al. 2004a).

Bismuth: Interaction with Gastrin

Bi^{3+} ions also bind to Ggly, although with lower affinity than Fe^{3+} ions (K_d = 5.8 ± 1.4 μM, pH 4.0) (Pannequin et al. 2004b). NMR spectroscopy indicated that, as with Fe^{3+} ions, binding was via the carboxylate groups in the side chains of Glutamates 7, 8 and 9. Because the Bi^{3+}–Ggly complex is not recognized by the Ggly receptor, Bi^{3+} ions act as competitive inhibitors in both cell proliferation and migration assays in vitro (Pannequin et al. 2004b). In contrast Bi^{3+} ions did not reduce the binding of Gamide to its receptor, or inhibit the biological activity of Gamide.

Physiological Significance

Bismuth salts have been used for many years for the treatment of gastrointestinal disorders such as ulcers and diarrhea (Gorbach 1990). The direct anti-bacterial effect of Bi^{3+} ions on the gastric bacterium *Helicobacter pylori* provided the rationale for the use of bismuth salts, in combination with inhibitors of gastric acid production and with antibiotics, in the treatment of *H. pylori*–induced ulcers (Houben et al. 1999). The recognition of the ability of Bi^{3+} ions to inhibit the biological activity of Ggly suggests that bismuth salts may also interfere with the potentiation by Ggly of the Gamide-induced secretion of gastric acid (Chen et al. 2000). Since non-amidated gastrins like Ggly appear to act as growth factors for colorectal cancer (Aly et al. 2004), inhibition of Ggly activity by Bi^{3+} ions may offer a novel and selective therapy for this all too common disease.

References

Aly A, Shulkes A, Baldwin GS (2004) Gastrins, cholecystokinins and gastrointestinal cancer. Biochim Biophys Acta 1704:1–10

Baldwin GS, Curtain CC, Sawyer WH (2001) Selective, high-affinity binding of ferric ions by glycine-extended gastrin(17). Biochemistry 40:10741–10746

Baldwin GS (2004) Properties of the complex between recombinant human progastrin and ferric ions. The Protein Journal 23:65–70

Chen D, Zhao CM, Dockray GJ et al (2000) Glycine-extended gastrin synergizes with gastrin 17 to stimulate acid secretion in gastrin-deficient mice. Gastroenterology 119:756–765

Dockray GJ, Varro A, Dimaline R et al (2001) The gastrins: their production and biological activities. Annu Rev Physiol 63:119–139

Ferrand A, Lachal S, Bramante G et al (2010) Stimulation of proliferation in the colorectal mucosa by gastrin precursors is blocked by desferrioxamine. Am J Physiol Gastrointestinal and Liver Physiology 299:G220–G227

Gorbach SL (1990) Bismuth therapy in gastrointestinal diseases. Gastroenterology 99:863–875

He H, Shehan BP, Barnham KJ et al (2004) Biological activity and ferric ion binding of fragments of glycine-extended gastrin. Biochemistry 43:11853–11861

Houben MH, van de Beek D, Hensen EF et al (1999) A systematic review of *Helicobacter pylori* eradication therapy–the impact of antimicrobial resistance on eradication rates. Aliment Pharmacol Ther 13:1047–1055

Pannequin J, Barnham KJ, Hollande F et al (2002) Ferric ions are essential for the biological activity of the hormone glycine-extended gastrin. J Biol Chem 277:48602–48609

Pannequin J, Tantiongco JP, Kovac S et al (2004a) Divergent roles for ferric ions in the biological activity of amidated and non-amidated gastrins. J Endocrinol 181:315–325

Pannequin J, Kovac S, Tantiongco JP et al (2004b) A novel effect of bismuth ions: selective inhibition of the biological activity of glycine-extended gastrin. J Biol Chem 279:2453–2460

Bismuth, Interaction with Transferrin

Graham S. Baldwin

Department of Surgery, Austin Health, The University of Melbourne, Heidelberg, VIC, Australia

Definition

Transferrin is an abundant serum glycoprotein of molecular mass 80 kDa (kilodaltons) (Wally and

Buchanan 2007). Sequence similarity between the N- and C-terminal lobes of the molecule indicates that transferrin has evolved by duplication of an ancestral gene. Each lobe binds a single ferric ion with high affinity, via the side chains of two tyrosines, a histidine, and an aspartic acid. The remaining two ligands in the distorted octahedral binding site are provided by the synergistic anion bicarbonate. Transferrin is responsible for the transport of iron around the body, and delivers iron to target cells via interaction with the transferrin receptor TfR1. A related protein, lactoferrin, is found in milk and other secreted fluids, where its ability to bind iron tightly limits bacterial growth.

Basic Characteristics

Binding of Bismuth by Transferrins

In the presence of bicarbonate, bismuth ions bind to both ferric ion–binding sites of transferrin (Li et al. 1996; Sun et al. 1999, 2001). Binding to the C-terminal lobe is tighter than to the N-terminal lobe (Li et al. 1996; Sun et al. 1999), and the affinity of the C-terminal site for bismuth ions (K_d(Dissociation constant) $= 1.5 \times 10^{-17}$ M) is greater than for the binding of ferric ions ($K_d = 1 \times 10^{-16}$ M) at I = 0.2 M, 298 K (Miquel et al. 2004). Lactoferrin also binds two bismuth ions, but in this case the affinity is weaker than for ferric ions (Zhang et al. 2001).

Interaction with the Transferrin Receptor

Bismuth-loaded transferrin is recognized by the transferrin receptor TfR1, although the interaction is considerably weaker ($K_d = 4 \times 10^{-6}$ M) than for iron-loaded transferrin ($K_d = 2.3 \times 10^{-9}$ M) at I = 0.2 M, 310 K (Miquel et al. 2004). Further studies with human cell lines will be required to establish whether or not the interaction with the transferrin receptor TfR1 is responsible for the cellular uptake of bismuth ions.

References

Li H, Sadler PJ, Sun H (1996) Unexpectedly strong binding of a large metal ion (Bi^{3+}) to human serum transferrin. J Biol Chem 271:9483–9489

Miquel G, Nekaa T, Kahn PH et al (2004) Mechanism of formation of the complex between transferrin and bismuth, and interaction with transferrin receptor 1. Biochemistry 43:14722–14731

Sun H, Li H, Mason AB et al (1999) N-lobe versus C-lobe complexation of bismuth by human transferrin. Biochem J 337(Pt 1):105–111

Sun H, Li H, Mason AB et al (2001) Competitive binding of bismuth to transferrin and albumin in aqueous solution and in blood plasma. J Biol Chem 276:8829–8835

Wally J, Buchanan SK (2007) A structural comparison of human serum transferrin and human lactoferrin. Biometals 20:249–262

Zhang L, Szeto KY, Wong WB et al (2001) Interactions of bismuth with human lactoferrin and recognition of the Bi (III)-lactoferrin complex by intestinal cells. Biochemistry 40:13281–13287

Bismuth, Physical and Chemical Properties

Fathi Habashi
Department of Mining, Metallurgical, and Materials Engineering, Laval University, Quebec City, Canada

Bismuth is a metalloid of no useful mechanical properties. It is mainly used as an alloying component in fusible alloys. Only one stable isotope, ^{209}Bi, is known, but there are several unstable isotopes (^{199}Bi–^{215}Bi). Isotopes with mass number > 210 are found in the natural decay chains of radioactive elements. Isotopes with mass number < 208 have been formed in nuclear transformations. The volume of the molten metal increases by about 3% on solidification.

Physical Properties

Atomic number	83
Atomic weight	208.98
Relative abundance in Earth's crust,%	2×10^{-5}
Atomic radius, nm	0.18
Density at 20°C, g/cm^3	9,790
Melting point, °C	271.40
Boiling point, °C	1,564
Crystal system	Rhombohedral
Lattice constant, nm	$a = 0.47457$
	$\alpha = 57.24°$
Latent heat of fusion, J/mol	11,280
Latent heat of vaporization, J/mol	178,632
Coefficient of linear expansion, K^{-1}	13.5×10^{-6}

(*continued*)

Electrical resistivity, μΩ cm	
At 0°C	106.8
At 1,000°C	160.2
Specific heat at 25°C, J mol^{-1} K^{-1}	25.5
Thermal conductivity, J s^{-1} m^{-1} K^{-1}	
At 0°C	8.2
At 300°C	11.3
At 400°C	12.3
Vapor pressure, bar	
At 893°C	1.013×10^{-3}
At 1,053°C	1.013×10^{-2}
At 1,266°C	1.013×10^{-1}
Surface tension, mN/m	
At 300°C	376
At 400°C	370
At 500°C	363
Absorption cross section for thermal neutrons, m^2/atom	$(3.4 \pm 0.2) \times 10^{-30}$
Hardness, Brinell, N/mm^2	184
Hardness, Mohs	2.5
Poisson's ratio	0.33
Shear modulus, MPa	12,400
Modulus of elasticity, GPa	338
Viscosity, MPa·s	
At 300°C	1.65
At 350°C	1.49
At 400°C	1.37
At 500°C	1.19
At 600°C	1.06

Chemical Properties

Bismuth does not oxidize in dry air. Liquid bismuth is covered by an oxide film of Bi_2O_3 that protects it from further oxidation. In most compounds, bismuth has a +3 oxidation state. Bismuth is precipitated by hydrolysis on dilution or partial neutralization:

$$BiCl_3 + H_2O \rightarrow Bi(OH)Cl_2 + HCl$$

$$Bi(OH)Cl_2 \rightarrow BiOCl + HCl$$

or by cementation with iron turnings:

$$2BiCl_3 + 3Fe \rightarrow 3FeCl_2 + 2Bi$$

Bismuthine, BiH_3, is a colorless gas unstable at room temperature decomposing to bismuth and hydrogen. Bismuth is precipitated as Bi_2S_3 from slightly acidic solution with H_2S. The precipitate is brown black and soluble in strong acids and hot dilute nitric acid. Yellow-green Bi_2S_3 precipitates from alkaline solution on addition of Na_2S.

References

Habashi F (2001) Arsenic, antimony, and bismuth production. In: Encyclopedia of materials: science & technology, pp 332–336

Krüger J et al (1997) In: Habashi F (ed) Handbook of extractive metallurgy. Wiley, Weinheim, pp 845–871

Blood Clotting

▶ Calcium-Binding Proteins, Overview

Blood Clotting Impairments as Result of Zinc Disorders

▶ Zinc in Hemostasis

Blood Clotting Proteins

Sheryl R. Bowley, Mingdong Huang, Barbara C. Furie and Bruce Furie
Division of Hemostasis and Thrombosis, Beth Israel Deaconess Medical Center, Harvard Medical School, Boston, MA, USA

Synonyms

EGF-like domain: epidermal growth factor-like domain; *Gla*: Γ-carboxyglutamic acid; *Procofactors*: procoagulant cofactors

Definitions

Coagulation: blood clotting

Gla: γ-carboxyglutamic acid is formed by post-translational addition of a carboxyl group to the γ-carbon of glutamic acid

Thrombosis: formation of a blood clot inside a blood vessel, obstructing the flow of blood through the circulatory system

Procofactors: proteins whose binding to another coagulation protein requires proteolytic cleavage for full activity of the complex

Tenase complex: a complex formed by the assembly of factors IXa and VIIIa on a cell membrane that converts factor X to active factor Xa

Prothrombinase complex: a complex formed by the association of factors Va and Xa on a cell membrane that converts prothrombin to thrombin

EGF-like domain: a protein domain conserved through evolution that includes an N-terminal two-stranded beta-sheet followed by a loop and a short C-terminal two-stranded beta-sheet

Blood coagulation is an important host defense mechanism that maintains the integrity of the vascular system in response to injury. To prevent excessive bleeding after vascular injury, platelets rapidly bind to the subendothelium to form the initial platelet plug. This is followed by a series of reactions involving the conversion of soluble blood coagulation proteins from their proenzyme forms to serine proteases and the proteolytic activation of plasma-derived procofactors to active cofactors. This culminates in the production of thrombin which catalyzes the formation of the fibrin clot that stabilizes the initial platelet plug. Many of these enzymatic reactions are calcium dependent and occur on negatively charged cellular surfaces.

The extrinsic pathway, responsible for rapid and efficient coagulation in vivo, includes vitamin K–dependent proteins, plasma and cellular cofactors and enzymes. The vitamin K–dependent proteins (prothrombin, factor VII, factor IX, and factor X) contain γ-carboxyglutamic acid residues essential for calcium-dependent membrane binding. The posttranslational carboxylation of glutamic acid residues is mediated by the γ-carboxylase in the presence of vitamin K, oxygen, and carbon dioxide during protein biosynthesis. Indeed, vitamin K deficiency results in impaired blood clotting. Plasma procofactors, factor V and factor VIII, serve as cofactors for two vitamin K–dependent serine proteases, factor Xa and factor IXa, respectively. Both procofactors are activated proteolytically by thrombin and require calcium to maintain productive association between different domains.

The key to initiation of the extrinsic pathway is the cellular cofactor tissue factor (TF), an integral membrane protein that is constitutively expressed by certain cells within the vessel wall and cells surrounding blood vessels (Furie and Furie 2008). Upon exposure to plasma, TF binds factor VII and its active form factor VIIa. The TF/VIIa complex activates both factor IX and factor X to factor IXa and factor Xa, respectively. Factor IXa assembles on membrane surfaces with its active cofactor, factor VIIIa in the presence of calcium. The factor IXa/factor VIIIa complex, referred to as the "tenase" complex, converts factor X to active factor Xa. Similarly, factor Xa binds to its cofactor active factor Va bound on membrane surfaces in the presence of calcium to form the "prothrombinase" complex that converts the enzymatically inactive prothrombin to its enzyme form thrombin. Thrombin mediates the conversion of the soluble plasma protein fibrinogen into monomeric fibrin molecules that rapidly polymerize to form the insoluble fibrin clot. The fibrin clot is further reinforced by covalent cross-linking between fibrin molecules by factor XIIIa. As with other proenzymes, factor XIII is activated to factor XIIIa by thrombin and requires calcium as a cofactor.

Vitamin K–Dependent Blood Coagulation Proteins

Prothrombin

Prothrombin is a plasma glycoprotein with a molecular weight of 72,000 Da. The most abundant of the vitamin K–dependent blood coagulation proteins, it circulates as a single polypeptide chain zymogen. Ten γ-carboxyglutamic acid residues are located in the Gla domain, a region that anchors the protein to membranes in the presence of calcium ions. γ-Carboxyglutamic acid is generated as a vitamin K–dependent post-translational modification of glutamic acid during protein biosynthesis. Adjacent to the Gla domain are two kringle domains, important for protein complex formation with factor Va. The C-terminal region of prothrombin is the catalytic domain that includes the proteolytic site involved in its conversion from a zymogen to an active enzyme, thrombin. Prothrombin is converted to thrombin by the prothrombinase complex, factor Xa, and factor Va bound on a cell membrane exhibiting exposed phosphatidylserine.

The calcium ions in the Gla domain are mostly bound internally to stabilize the omega loop that characterizes all Gla domains in the vitamin K–dependent

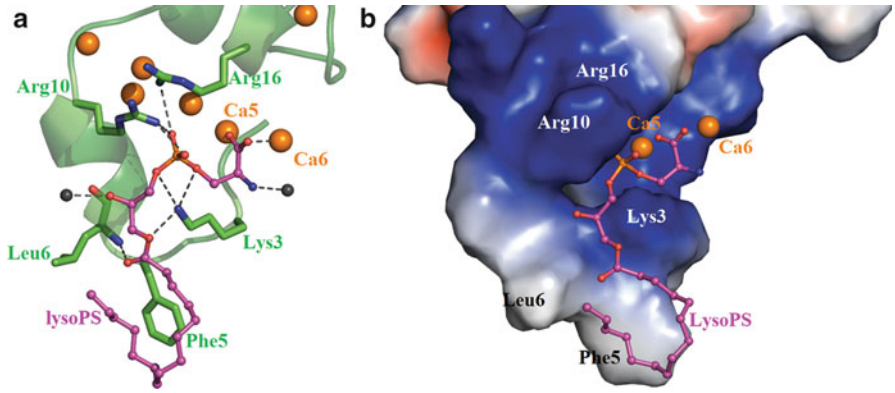

Blood Clotting Proteins, Fig. 1 *Gla domain of prothrombin.* (**a**) Calcium ions (*orange spheres*) in the Gla domain of prothrombin form electrostatic interactions with the serine head group of lysophosphoserine, lysoPS (*magenta*). The phosphate group interacts with positively charged lysine and arginine side chains (Huang et al. 2003). (**b**) The calcium-dependent conformational transition via the Gla domain of prothrombin leads to exposure of hydrophobic residues forming an external patch (*gray area*) that align with fatty acid tails in the membrane

proteins (Soriano-Garcia et al. 1992). In the presence of calcium ions, the serine head group of the acidic phospholipid, phosphatidylserine, of an activated cell membrane, forms electrostatic interactions with the γ-carboxyglutamic acid-calcium network in the Gla domain of prothrombin, allowing the substrate to bind the membrane and the prothrombinase complex (Fig. 1a) (Huang et al. 2003). A calcium-dependent conformational transition in the prothrombin Gla domain leads to exposure of a hydrophobic patch (e.g., amino acids Phe5, Leu6, and Val9 in bovine prothrombin) that aligns with fatty acid tails in the membrane (Fig. 1b) (Huang et al. 2003).

Factor VII

Factor VII, a protein with a molecular weight of 50,000 Da, circulates in plasma in two forms: the dominant albeit inactive zymogen factor VII and a trace amount of enzymatically active factor VIIa. Typical of vitamin K–dependent blood coagulation proteins, factor VII contains a Gla domain with ten γ-carboxyglutamic acid residues. Adjacent to the Gla domain are two epidermal growth factor (EGF)-like domains, followed by the serine protease domain with an active site homologous to trypsin and chymotrypsin. Tissue factor, an integral membrane protein expressed on the plasma membrane of many cells, can bind either factor VII or factor VIIa in a calcium-dependent manner. The tissue factor/factor VIIa complex initiates blood coagulation via activation of factor IX and factor X to their active enzyme forms.

The structure of the complex of the active site–inhibited factor VIIa and the extracellular domain of tissue factor has been determined by X-ray crystallography (Fig. 2) (Banner et al. 1996). Salient features of this complex include extensive "embracing" of extended conformations of one protein by the other. The structure also shows the Gla domain with seven bound calcium ions. Factor VII binds to negatively charged membranes via the Gla domain in a reversible and calcium-dependent manner. The structure of the calcium-stabilized Gla domain is homologous to that of prothrombin, factor X, and factor IX. Of the two EGF domains of factor VII, only EGF1 binds calcium ions. The EGF1, together with the protease domain, serves as the main site of contact with tissue factor. The serine protease domain also binds a single calcium ion. Zinc binding to the protease domain inhibits the enzymatic activity of factor VIIa.

Factor IX

Factor IX has a molecular weight of 56,000 Da and consists of a Gla domain, two adjacent EGF domains, and a serine protease domain. The Gla domain contains 12 γ-carboxyglutamic acid residues that bind calcium ions crucial for interaction with membranes. Factor IX is activated to its serine protease form, factor IXa, by either the tissue factor/factor VIIa complex or factor XIa, in the presence of calcium ions. Factor IXa and factor VIIIa assemble to form a membrane surface–bound tenase complex that activates factor X to factor

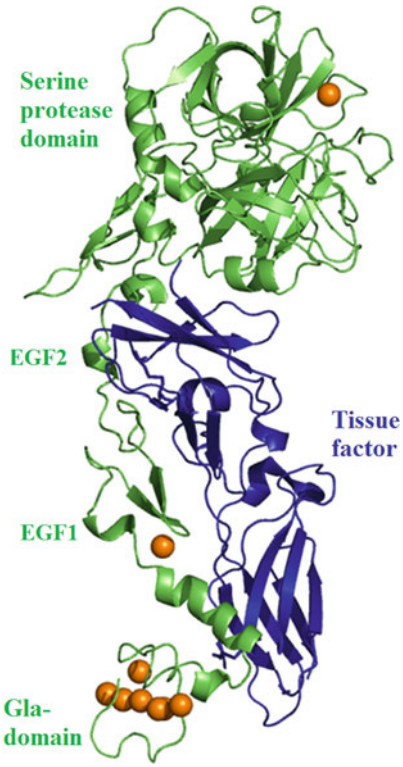

Blood Clotting Proteins, Fig. 2 *Domain organization of vitamin K–dependent proteins*. The structure of the complex of active site–inhibited factor VIIa and the extracellular domain of tissue factor shows the domain organization of factor VIIa (Banner 2006). Interaction with tissue factor involves mostly the EGF1 domain and the serine protease domain of factor VIIa. Factor VII binds to negatively charged phospholipid membranes via the Gla domain. Calcium ions are shown as *orange spheres*

Xa in the presence of calcium ions. Defective activity or deficiency of factor IX due to mutation of the gene is the cause of hemophilia B.

The Gla domain of factor IX binds both internal calcium ions as well as calcium ions on the protein surface (Huang et al. 2004). The crystal structures of the Gla domain confirm the similarity of this domain in all of the vitamin K–dependent proteins involved in blood coagulation. The Gla domain of factor IX undergoes two metal-dependent conformational transitions. The calcium-stabilized conformer expresses a phospholipid-binding site that is located in the Gla domain at the amino terminus of the protein. Factor IXa, but not factor IX, binds to factor VIIIa on the surface of activated platelets via the second EGF domain and the serine protease domain. The first EGF-like domain has a high-affinity calcium-binding site that includes a β-hydroxyaspartic acid. The post-translational modification of this aspartic acid, however, is not required for factor IX function.

Factor X

Factor X, with a molecular weight of 56,000 Da, contains a Gla domain, two EGF domain, and a serine protease domain. The Gla domain of factor X includes 11 γ-carboxyglutamic acid residues and has marked structural homology with other Gla domains. The Gla domain binds Ca^{2+}, exposing a membrane binding site which is a prerequisite for anchoring the vitamin K–dependent blood clotting proteins to membranes. The N-terminus of the Gla domain shows little stable structure in the absence of Ca^{2+}. The two EGF domains are important for binding factor Va.

Factor X is activated to factor Xa by either the tissue factor/factor VIIa complex or by the factor IXa/factor VIIIa complex in the presence of phospholipid membranes and calcium ions. Factor Xa then associates with factor Va on the membrane surface to form the prothrombinase complex. This complex activates prothrombin to thrombin in the presence of calcium ions.

Procofactors

Factor VIII

Factor VIII is a plasma glycoprotein that is synthesized as a single polypeptide precursor with domains organized as A1–A2–B–A3–C1–C2. Intracellular proteolytic cleavage at the B–A3 junction or within the B-domain produces forms of factor VIII that circulate in the blood: a light chain (A3–C1–C2, 80,000 Da) and a heterogeneous heavy chain with a molecular weight varying between 90,000 Da (A1–A2) and 200,000 Da (A1–A2–B). Further proteolysis between the A1 and A2 domains by thrombin results in the generation of active factor VIII. The activated cofactor forms a complex with factor IXa on membrane surfaces to activate factor X during blood coagulation. Defects in the factor VIII gene that lead to diminished or absent factor VIII activity cause a bleeding disorder, hemophilia A.

The three-dimensional structures of the human factor VIII C2 domain (Pratt et al. 1999) and the B-domain-deleted human factor VIII (Ngo et al. 2008, Shen et al. 2008) have been determined by

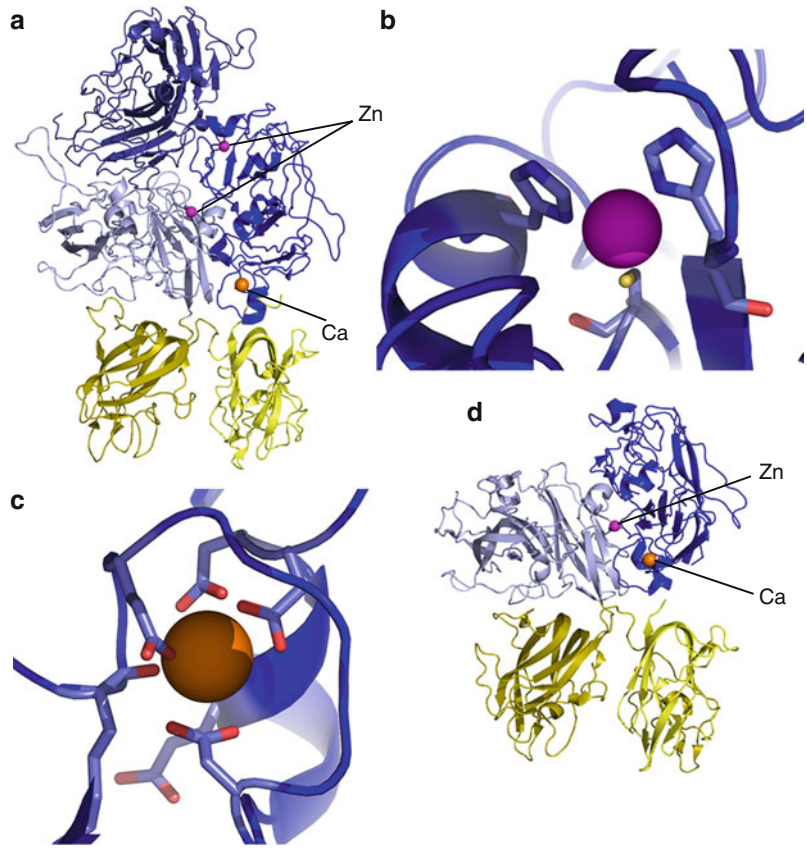

Blood Clotting Proteins, Fig. 3 *Structures of procofactors*. (**a**) The three-dimensional structure of B-domain-deleted human factor VIII showing a triangular heterotrimer of the A domains (*blue*) stacked on two smaller globular C domains (*yellow*)(Ngo et al. 2008). Factor VIII proteins bind copper ions (*magenta spheres*) and calcium ions (*orange spheres*). (**b**) The copper ion in the A1 domain of factor VIII is coordinated by two His residues and a single Cys. (**c**) The A1 domain of factor VIII contains a single calcium-binding site coordinated by Glu and Asp side chains as well as the backbone carbonyl of a Lys and a Glu. (**d**) Bovine-activated protein C–inactivated factor Va has a similar domain structure as factor VIII (Adams et al. 2004)

X-ray crystallography (Fig. 3a). The B-domain has no apparent function with regard to the procoagulant activity of factor VIII. The overall structure of the B-domain-deleted factor VIII has been described as a triangular heterotrimer of the A domains stacked on two smaller globular C domains. Each C domain projects loops containing hydrophobic and basic residues that likely contribute to the interaction of factor VIII with the membrane. The A1, A2, and A3 domains resemble a typical cupredoxin fold. Two copper ions are present within the A1 and A3 domains that are homologous to the copper-binding motif in ceruloplasmin, the major copper-carrying protein in the blood. Both of the copper ions in the A1 and A3 domains are coordinated by two His residues and a single Cys (Fig. 3b). The strategic locations of these copper ions likely maintain the structural integrity of the interdomain interface and enhance subunit affinity. The A1 domain also contains a single calcium-binding site defined by Glu and Asp side chains as well as the backbone carbonyl of a Lys and a Glu (Fig. 3c). This calcium ion may be important in the maintenance of the C2-A1 domain interface, thus promoting the active conformation of factor VIII.

Factor V

Plasma-derived factor V is synthesized in the liver and circulates as a single 330,000 Da polypeptide chain. Factor V and factor VIII share the same A1–A2–B–A3–C1–C2 multidomain architecture, with the A and C domains in the two proteins sharing approximately 40% homology. Proteolytic removal of the B-domain produces factor Va composed of a 105,000 Da heavy chain (A1–A2 domains) and a 74,000 or 71,000 Da light chain (A3–C1–C2 domains) that are held together by a single calcium ion and hydrophobic interactions. In a calcium-dependent manner, factor Va assembles with factor Xa on membrane surfaces and enhances the rate at which factor Xa cleaves prothrombin to thrombin. Factor Va is inactivated by activated protein C through cleavage adjacent to Arg 506, leading to the release of the A2 domain. The Arg506Gln

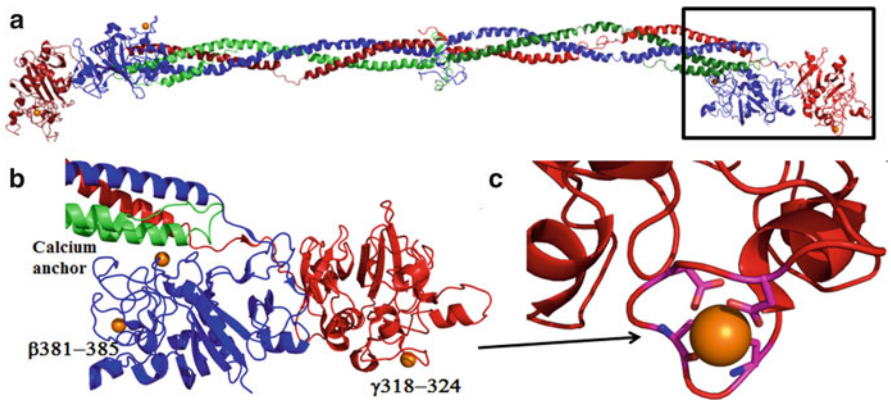

Blood Clotting Proteins, Fig. 4 *Calcium-binding sites in fibrinogen*. (**a**) Fibrinogen has a trinodular structure with calcium-binding sites in the distal globular region of the molecule (Kollman et al. 2009). (**b**) The β-chain (*blue*) and γ-chain (*red*) contain homologous calcium (*orange spheres*) binding sites. Another calcium-binding site is located at the junction where all three chains meet. This calcium ion appears to anchor the globular region of the molecule to the coiled-coil region. (**c**) The high-affinity calcium-binding site in the γ-chain has an EF-hand binding motif

mutation, known as factor V_{Leiden}, is associated with thrombosis due to inefficient inactivation of factor Va.

Only the C2 domain crystal structure has been determined for human factor V. While the multidomain structure of human factor V is yet to be determined, the crystal structure of activated protein C–inactivated bovine factor Va (Factor Vai) has revealed important details regarding factor V function (Fig. 3d). The bovine factor Vai structure reveals a domain arrangement similar to the human factor VIII structure, albeit missing the A2 domain due to APC-mediated inactivation. In contrast to factor VIII, the bovine factor Vai has a single copper ion coordinated by two His residues and an Asp residue. This copper ion is located within the buried surface between the A1 and A3 domains and likely provides additional structural stabilization of the interface but no ascertained functional role. The A1 domain also contains a high-affinity calcium-binding site. This calcium site may be critical for the packing of the A3 domain against the A1 domain (Adams et al. 2004).

Fibrinogen and Factor XIII

Fibrinogen, the most abundant plasma blood coagulation protein, has a molecular weight of 340,000 Da and consists of three pairs of nonidentical polypeptide chains, $(A\alpha,B\beta,\gamma)_2$. These chains are folded into three distinct structural regions: two distal globular regions linked by coiled-coil connectors to one central region forming a trinodular structure (Fig. 4a). Thrombin catalyzes the conversion of fibrinogen into fibrin monomer. Fibrin monomers self-assemble, polymerizing in an orderly sequence leading to the formation of fibrin strands.

Calcium ions enhance fibrin polymerization to produce thicker fibers and modulate fibrinogen susceptibility to proteolytic enzymes. Calcium-binding sites in fibrinogen have been identified in the crystal structure (Fig. 4b). The γ-chain has a high-affinity calcium-binding site located in the γ318–324 loop with amino acid sequence homology to the EF-hand in calmodulin (Fig. 4c) (Kollman et al. 2009). This calcium-binding site influences fibrinogen-mediated platelet aggregation and imparts protection to fibrinogen from proteolytic degradation. Since the γ- and β-chain polypeptides are homologous, there is a corresponding calcium-binding site located in the β381–385 loop for which function has yet to be ascertained. Another calcium ion–binding site involves two β-chain Asp residues and a γ-chain Glu residue. This site serves as an anchor between the β-globular region and the coiled-coil connector. This calcium may also impact access to tissue plasminogen activator–binding sites, a protein involved in the breakdown of clots (Weisel 2005).

Factor XIII, a plasma glycoprotein transglutaminase of 320,000 Da molecular weight, is a tetramer consisting of two catalytic A subunits and two carrier B subunits (A_2B_2). The activated form, factor XIIIa, stabilizes the fibrin clot by catalyzing covalent cross-linking between Glu and Lys residues in the

fibrin molecule. In the presence of calcium, factor XIII is activated by thrombin-mediated cleavage of the activation peptides from the A subunits. The carrier subunits then dissociate from the catalytic subunits, leading to a conformational change that unmasks the catalytic site. The X-ray crystal structure of factor XIII A_2 showed a single major Ca^{2+}-binding site in each A subunit (Komaromi et al. 2011).

Cross-References

- ▶ Calcium-Binding Protein Site Types
- ▶ Calcium-Binding Proteins, Overview
- ▶ Calcium in Biological Systems
- ▶ EF-Hand Proteins
- ▶ Zinc in Hemostasis

References

Adams TE, Hockin MF, Mann KG, Everse SJ (2004) The crystal structure of activated protein C-inactivated bovine factor Va: implications for cofactor function. Proc Natl Acad Sci USA 101:8918–8923

Banner DW, D'Arcy A, Chene C, Winkler FK, Guha A, Konigsberg WH, Nemerson Y, Kirchhofer D (1996) The crystal structure of the complex of blood coagulation factor VIIa with soluble tissue factor. Nature 380:41–46

Furie B, Furie BC (2008) Mechanisms of thrombus formation. N Engl J Med 359:938–949

Huang M, Rigby AC, Morelli X, Grant MA, Huang G, Furie B, Seaton B, Furie BC (2003) Structural basis of membrane binding by Gla domains of vitamin K-dependent proteins. Nat Struct Biol 10:751–756

Huang M, Furie BC, Furie B (2004) Crystal structure of the calcium-stabilized human factor IX Gla domain bound to a conformation-specific anti-factor IX antibody. J Biol Chem 279:14338–14346

Kollman JM, Pandi L, Sawaya MR, Riley M, Doolittle RF (2009) Crystal structure of human fibrinogen. Biochemistry 48:3877–3886

Komaromi I, Bagoly Z, Muszbek L (2011) Factor XIII: novel structural and functional aspects. J Thromb Haemost 9(1):9–20

Ngo JC, Huang M, Roth DA, Furie BC, Furie B (2008) Crystal structure of human factor VIII: implications for the formation of the factor IXa-factor VIIIa complex. Structure 16:597–606

Pratt KP, Shen BW, Takeshima K, Davie EW, Fujikawa K, Stoddard BL (1999) Structure of the C2 domain of human factor VIII at 1.5 Å resolution. Nature 402:439–442

Shen BW, Spiegel PC, Chang CH, Huh JW, Lee JS, Kim J, Kim YH, Stoddard BL (2008) The tertiary structure and domain organization of coagulation factor VIII. Blood 111:1240–1247

Soriano-Garcia M, Padmanabhan K, de Vos AM, Tulinsky A (1992) The Ca^{2+} ion and membrane binding structure of the Gla domain of Ca-prothrombin fragment 1. Biochemistry 31:2554–2566

Weisel JW (2005) Fibrinogen and fibrin. Adv Protein Chem 70:247–299

Blood Platelets

- ▶ Nanosilver, Next-Generation Antithrombotic Agent

Blue Copper Protein

- ▶ Plastocyanin

Blue Copper Proteins

- ▶ Monocopper Blue Proteins

BOR1 – Borate Transporter Protein

- ▶ Boron, Biologically Active Compounds

Borane

- ▶ Amine-Boranes

Borano-Amine

- ▶ Amine-Boranes

Boric Acid Transport

- ▶ Atr1, Boron Exporter in Yeast

Boron and Aquaporins

Gerd Patrick Bienert and François Chaumont
Institut des Sciences de la Vie, Universite catholique de Louvain, Louvain-la-Neuve, Belgium

Synonyms

Aquaporin-mediated boron transport; Boron channel; Major intrinsic proteins and boron transport

Definition

Aquaporins or major intrinsic proteins (MIPs) are transmembrane channel proteins, which facilitate the passive and bidirectional diffusion of water and a variety of small and noncharged compounds across biological membranes. Aquaporins are found in organisms of all kingdoms of life and are present in all main subcellular membrane systems. The substrate specificity/spectra of aquaporins are highly isoform-dependent. Some plant isoforms were shown to facilitate the transmembrane diffusion of boric acid, the most frequent chemical boron species that organisms have to deal with. All organisms face the challenge to handle considerable variations in the concentration of metalloids they are exposed to, in terms of either the demand to acquire sufficient amounts for their metabolism or, conversely, the necessity to extrude them to prevent toxicity. This is achieved through homeostatic processes that require, among others, aquaporin-mediated transport across membranes at the cellular level.

Essentiality and Roles of Boron in Living Organisms

In the past years, a large number of studies have demonstrated that boron (B) is an essential or at least beneficial element for animals and humans (reviewed in Hunt 2007). Boron is crucial for vertebrate development as boron deprivation resulted in abnormal or necrotic embryonic phenotypes. Molecular mechanisms and functions underlying boron demand are unknown. Interestingly, although the molecular targets are likely to be different in animal and plant metabolism, boron seems to be highly needed at early stages of tissue differentiation (Goldbach et al. 2007).

Plant biology can be seen as the pioneering research field driving advances in the understanding of biological boron handling and roles. This is due to the fact that the essential role of boron in plants was already established more than 80 years ago (Warington 1923). An adequate nutritional boron status is essential for plants in general and for high yield and crop quality in particular, as boron deficiency causes many disadvantageous morphological, physiological, and biochemical alterations (reviewed in Goldbach et al. 2007; Marschner 2011). These defects mainly result in rapid cessation of root elongation and reduced vegetative growth and fertility.

Underlying molecular mechanisms for most of the negative effects are still a matter of speculation. The only known molecular function of boron in plants is its role in cross-linking apiose residues from rhamnogalacturonan II moieties of pectin and, therefore, sustaining cell-wall integrity and functioning (reviewed in Miwa et al. 2010).

Despite its complex chemistry and a large range of binding forms, boron is exclusively found as borates in most soils. Bioavailable boron species are solely boric acid ($B(OH)_3$) and the borate anion ($B(OH)_4^-$) which stay in chemical equilibrium ($B(OH)_3 + H_2O = B(OH)_4^- + H^+$) at a pKa of 9.25. In most soils and at physiological pH ranges in organisms, the equilibrium is greatly shifted toward boric acid. Therefore, the chemistry of boron in soils and organisms is very simple. For plants, boron is the only essential microelement which was shown to be mainly taken up as an uncharged boric acid molecule but not in an ionic form. This represents a peculiarity of plant boron management in plant nutrition (Marschner 2011).

Membrane Permeability to Boric Acid

The undissociated boric acid molecule was initially thought to cross the membrane by simple diffusion because it is among the smallest of all metalloid species. Furthermore, the amount of boron species taken up by plants in physiological uptake assays was closely correlated to boric acid concentrations in the medium (Miwa and Fujiwara 2010). However, permeability coefficients of plant membranes for boric acid were lower than predicted. For instance, the permeability

coefficient of plasma membrane from squash roots was one to two orders of magnitudes smaller than the values obtained in experiments using liposomes made of different artificial lipid compositions (Dordas et al. 2000). The low permeability coefficient values for boric acid could not meet plant boron demand and uptake rates, respectively. In addition, physiological studies have suggested the existence of channel-mediated facilitated diffusion as well as energy-dependent active transport systems for boron (Miwa and Fujiwara 2010). It was hypothesized that boric acid transport occurred via aquaporins (see below), as the application of aquaporin inhibitors (mercuric chloride and phloretin) to plasma membrane vesicles of squash roots partially inhibited boron uptake (Dordas and Brown 2001). Accordingly, the expression of a PIP (plasma membrane intrinsic protein) aquaporin from maize in *Xenopus laevis* oocytes resulted in an increased boron permeability of the plasma membrane further suggesting the involvement of aquaporins in transmembrane boric acid transport in plants.

Aquaporins Are Important Players in the Uptake and Distribution of Boron in Plants

In a complete set of studies including direct uptake assays *in planta*, functional tests in heterologous expression systems, and physiological and molecular genetic studies in *Arabidopsis thaliana*, Fujiwara and coworkers solved the long-standing puzzle of boron transport in plants by independently identifying two types of transport proteins regulating the uptake and redistribution of boron: the aquaporin nodulin-26-like intrinsic proteins (NIPs) and the BOR transport proteins (Takano et al. 2002, 2006). Members of the BOR transporter family have similarities to anion exchange proteins and represent active efflux transporters for borate anions. NIPs belong to the aquaporin or MIP family (▶ Aquaporins and Transport of Metalloids). Under boron-limited conditions, the spatially coordinated action of AtNIP5;1 conducting boric acid uptake and AtBOR1 ensuring borate efflux into the xylem was shown to be essential for the flux of boron from the soil to the shoot in *A. thaliana* (Miwa and Fujiwara 2010). AtNIP5;1 mediates the diffusion of boric acid through root endodermis cells and provides the substrate for AtBOR1, which is localized in proximal plasma membrane domains of pericycle cells. Nutrient export from pericycle cells that surround the vascular tissues is part of the xylem-loading process for subsequent long-distance transport and distribution of nutrients to the shoot. Such a spatial cooperation between an import (NIP-mediated) and an export (BOR-mediated) function of boron transporters may also be expected in other tissues or cell types since the transport of this uncharged molecule cannot benefit from the plasma membrane electrochemical gradient (Miwa and Fujiwara 2010). Similar cooperative work of a passive NIP channel and an active efflux transporter (Lsi2) was also shown to be crucial to regulate the uptake and allocation of the beneficial metalloid species silicic acid in rice (*Oryza sativa*) (▶ Silicon and Aquaporins). Characterization of NIP-mediated boron transport processes has shown that other NIP isoforms including OsNIP3;1, AtNIP5;1, and AtNIP6;1 constitute passive boric acid channels playing key roles in boron transport under boron-limiting conditions (Miwa and Fujiwara 2010; Tanaka et al. 2008). Interestingly, quantitative PCR analyses showed that *OsNIP3;1*, *AtNIP5;1*, and *AtNIP6;1* are consistently upregulated under low boron supply suggesting that plants (1) perceive their boron status and (2) actively regulate NIP-mediated transport processes at the transcriptional level to ensure boron homeostasis (Miwa et al. 2010). Altogether, these data clearly support the idea that NIP aquaporins are crucial for boron uptake and allocation in both monocot and eudicot plant species.

However, boron uptake under boron-deficient conditions is not the only challenge for plants. Bioavailable soil boron concentrations are very important for plant fitness, as the range between boron deficiency and toxicity is very narrow compared to many other nutrients. Excess of boron supply, which can occur during dry periods, in irrigated fields of arid areas or in (over-) fertilized fields, was shown to rapidly lead to leaf necrosis and growth inhibition. Plants have therefore to carefully regulate boron transport processes and cope with both boron deficiency and toxicity during the growth period.

Plant tolerance mechanisms against an excess of boron in soils also seem to involve NIP aquaporins. *HvNIP2;1* gene from barley (*Hordeum vulgare*) is associated to a quantitative trait locus (QTL) conferring boron tolerance. A significantly lowered expression of *HvNIP2;1* under high-boron conditions was shown to prevent toxic boron influx into the root of a boron-tolerant barley cultivar compared to a nontolerant one (Schnurbusch et al. 2010).

NIPs can be classified into three subgroups: NIPIs, NIPIIs, and NIPIIIs based on the amino acid residue composition of the aromatic/Arginine selectivity filter of aquaporins which represents the narrowest part of the channel path (▶ Aquaporins and Transport of Metalloids). The physicochemical properties of these residues are involved in the determination of the substrate specificity of the MIP pore. Until now, all boric acid-permeable NIP aquaporins belong to either the NIPII or NIPIII subgroup (Miwa and Fujiwara 2010).

Other Aquaporins and Their Role in Plant Boron Transport

In addition to NIPs, other members of the aquaporin family might also be involved in boron transport. For instance, expression of maize ZmPIP1;1 in *X. laevis* oocytes resulted in an increased boron permeability (Dordas et al. 2000) and heterologous expression of *Solanaceae* XIPs and barley PIPs in *Saccharomyces cerevisiae* yeast mutants resulted in an increased sensitivity of yeast toward boron (Bienert et al. 2011; Fitzpatrick and Reid 2009). XIPs possess striking similarities in their sequence and selectivity with members of the boron-permeable NIPII subgroup (Bienert et al. 2011). Interestingly, XIPs are absent from genomes of boron-deficiency-sensitive eudicot plants (e.g., species belonging to the genus of *Brassica*) and the low boron demanding and boron-deficiency-insensitive gramineous species such as wheat, barley rice, and maize. When boron efficiency was studied in Arabidopsis, the identified QTLs encompassed two *TIP* aquaporin genes, namely, *AtTIP3;1* and *AtTIP4;1* (Zeng et al. 2008). Additionally, the ectopic overexpression of the tonoplast and/or mitochondrial-localized aquaporin AtTIP5;1 in Arabidopsis conferred tolerance to boron toxicity, suggesting its capacity to transport boron and/or its involvement in boron regulation in physiological conditions (Pang et al. 2010). As the expression of *AtTIP5;1* is pollen-specific, its function in boron transport has a potentially high interest as pollen germination, pollen viability, and pollen tube growth of most plants are highly sensitive to boron deficiency (Marschner 2011). Nevertheless, physiologically relevant roles of TIPs, PIPs, and XIPs in boron transport remain to be resolved.

Aquaporins and BOR Transporters from Organisms Other than Plants Are Involved in Boron Transport Processes

Knowledge on boron transport processes in organisms other than plants is scarce. Nevertheless, the discovery of AtBOR1 and AtNIP5;1 encouraged the search and characterization of homologous transport proteins in other organisms. In *S. cerevisiae* ScBor1p (a BOR transport protein) and ScFps1p (an aquaglyceroporin) seem to have similar roles as AtBOR1 and AtNIP5;1 in borate efflux and boric acid influx, respectively (Nozawa et al. 2006). HsNaBC1 in humans (a Na^+-coupled borate cotransporter) which is the mammalian homolog of AtBOR1 catalyzes the uptake of borate across the plasma membrane, coupled to the Na^+ gradient. The importance of the boron transporter HsNaBC1 is supported by the fact that *NaBC1* knocked-out cell lines stop to develop and proliferate (Park et al. 2004). It is expected that mammals possess, besides NaBC1 transporter, a high-capacity efflux system for boron as a surplus of boron in the diet leads to massive excretion of this compound via the urine. It is tempting to speculate that such massive flux is mediated by aquaglyceroporins releasing boric acid out of the cells.

Concluding Remarks

NIPs of several plant species have been demonstrated to be involved in boric acid uptake and allocation. Boron demand varies a lot between plant species. Therefore, a detailed molecular and physiological characterization of different NIP isoforms will allow a more complete understanding of the mechanisms regulating boron transport in different plant species. Furthermore, it has to be resolved whether aquaporins of organisms other than plants play a similar important role in boron transport processes as NIPs do.

Funding

This work was supported by grants from the Belgian National Fund for Scientific Research (FNRS), the Interuniversity Attraction Poles Programme–Belgian Science Policy, and the "Communauté française de Belgique–Actions de Recherches Concertées." GPB was supported by a grant from the FNRS.

Cross-References

- ▶ Arsenic and Aquaporins
- ▶ Aquaporins and Transport of Metalloids
- ▶ Selenium and Aquaporins
- ▶ Silicon and Aquaporins

References

Bienert GP, Bienert MD, Jahn TP et al (2011) Solanaceae XIPs are plasma membrane aquaporins that facilitate the transport of many uncharged substrates. Plant J 66:306–317

Dordas C, Brown PH (2001) Evidence for channel mediated transport of boric acid in squash (*Cucurbita pepo*). Plant Soil 235:95–103

Dordas C, Chrispeels MJ, Brown PH (2000) Permeability and channel-mediated transport of boric acid across membrane vesicles isolated from squash roots. Plant Physiol 124: 1349–1362

Fitzpatrick KL, Reid RJ (2009) The involvement of aquaglyceroporins in transport of boron in barley roots. Plant Cell Environ 32:1357–1365

Goldbach HE, Huang L, Wimmer MA (2007) Boron functions in plants and animals: recent advances in boron research and open questions. Springer, Dordrecht

Hunt CD (2007) Dietary boron: evidence for essentiality and homeostatic control in humans and animals. Springer, Dordrecht

Marschner H (2011) Marschner's Mineral Nutrition of Higher Plants. Academic, London

Miwa K, Fujiwara T (2010) Boron transport in plants: co-ordinated regulation of transporters. Ann Bot 105:1103–1108

Miwa K, Tanaka M, Kamiya T et al (2010) Molecular mechanisms of boron transport in plants: involvement of Arabidopsis NIP5;1 and NIP6;1. Landes Bioscience-Springer, New York

Nozawa A, Takano J, Kobayashi M et al (2006) Roles of BOR1, DUR3, and FPS1 in boron transport and tolerance in *Saccharomyces cerevisiae*. FEMS Microbiol Lett 262: 216–222

Pang Y, Li L, Ren F et al (2010) Overexpression of the tonoplast aquaporin AtTIP5;1 conferred tolerance to boron toxicity in Arabidopsis. J Genet Genomics 37:389–397

Park M, Li Q, Shcheynikov N et al (2004) NaBC1 is a ubiquitous electrogenic Na+ −coupled borate transporter essential for cellular boron homeostasis and cell growth and proliferation. Mol Cell 16:331–341

Schnurbusch T, Hayes J, Hrmova M et al (2010) Boron toxicity tolerance in barley through reduced expression of the multifunctional aquaporin HvNIP2;1. Plant Physiol 153: 1706–1715

Takano J, Noguchi K, Yasumori M et al (2002) Arabidopsis boron transporter for xylem loading. Nature 420:337–340

Takano J, Wada M, Ludewig U et al (2006) The Arabidopsis major intrinsic protein NIP5;1 is essential for efficient boron uptake and plant development under boron limitation. Plant Cell 18:1498–1509

Tanaka M, Wallace IS, Takano J et al (2008) NIP6;1 is a boric acid channel for preferential transport of boron to growing shoot tissues in Arabidopsis. Plant Cell 20:2860–2875

Warington K (1923) The effect of boric acid and borax on the broad bean and certain other plants. Ann Bot 37:629–672

Zeng C, Han Y, Shi L et al (2008) Genetic analysis of the physiological responses to low boron stress in Arabidopsis thaliana. Plant Cell Environ 31:112–122

Boron Channel

- ▶ Boron and Aquaporins

Boron Efflux Pump

- ▶ Atr1, Boron Exporter in Yeast

Boron Stress Tolerance, YMR279c and YOR378w

Ahmet Koc and İrem Uluisik
Department of Molecular Biology and Genetics,
Izmir Institute of Technology,
Urla, İzmir, Turkey

Synonyms

ATR1 paralogs in yeast; The role of ATR1 paralogs in boron stress response

Definition

The essentiality of boron for plants has been known for about 90 years. And it is also necessary for the growth and development of various species. Boron deficiency and toxicity is associated with several defects in these organisms. Thus, regulation of the boron intake and efflux is essential. Transporters constitute an important place in this sense.

There are several genes that play a role in boron transport and tolerance. The first identified boron transporter was *Arabidopsis thaliana BOR1* and homologs of

BOR1 were found in many organisms (Takano et al. 2002). The yeast homolog of *BOR1 (YNL275W)* was the first identified gene related with boron metabolism. It is localized to the plasma membrane and has an efflux function (Takano et al. 2007). Dur3 and Fps1 were suggested to have roles in boron tolerance in yeast, but the mechanism in which these genes function is not clear (Nozawa et al. 2006). Atr1 was characterized in 2009 as the main boron exporter in yeast *Saccharomyces cerevisiae*. It is regulated strictly by the boron treatment. Both yeast Bor1 and Atr1 were shown to reduce the intracellular boron concentrations. The study also revealed that *S. cerevisiae* genome contains two *ATR1* paralogs. Bioinformatic analysis showed that the paralogs *YMR279C*, *YOR378W*, and *ATR1* have 70% similarity in their sequences (Kaya et al. 2009). Both genes belong to DHA2 family of drug:H + antiporters like Atr1 (Sa-Correia et al. 2009). Thus it is thought that these genes may play a role in boron tolerance mechanisms as well.

Deletion of either of these genes did not result in sensitivity to boron. The N-terminal regions of these genes were found to be heterogeneous. They are not controlled by the same transcription factors suggesting they probably function in response to different stresses. In addition, wild-type cells carrying *YMR279C* gene can grow in the presence of toxic amount of (150 mM) boric acid; however, the overexpression of *YOR378W* had no effect on the growth of cells. To examine the role of *YMR279C* in boron stress response, intracellular boron levels were measured and found out that *YMR279C* expressing wild-type and *ymr279cΔ* cells has 60% and 40% intracellular boron, respectively. Thus, Ymr279c has a potential to be a boron transporter that can pump out boron from the cell; however, Yor378w does not have a role in boron stress (Bozdag et al. 2011).

Cross-References

▶ Atr1, Boron Exporter in Yeast

References

Bozdag GO, Uluisik I et al (2011) Roles of ATR1 paralogs YMR279c and YOR378w in boron stress tolerance. Biochem Biophys Res Commun 409(4):748–751

Kaya A, Karakaya HC et al (2009) Identification of a novel system for boron transport: atr1 is a main boron exporter in yeast. Mol Cell Biol 29(13):3665–3674

Nozawa A, Takano J et al (2006) Roles of BOR1, DUR3, and FPS1 in boron transport and tolerance in *Saccharomyces cerevisiae*. FEMS Microbiol Lett 262(2): 216–222

Sa-Correia I, dos Santos SC et al (2009) Drug:H(+) antiporters in chemical stress response in yeast. Trends Microbiol 17(1):22–31

Takano J, Noguchi K et al (2002) Arabidopsis boron transporter for xylem loading. Nature 420(6913):337–340

Takano J, Kobayashi M et al (2007) *Saccharomyces cerevisiae* Bor1p is a boron exporter and a key determinant of boron tolerance. FEMS Microbiol Lett 267(2): 230–235

Boron Toxicity

▶ Atr1, Boron Exporter in Yeast

Boron Transport in Yeast

▶ Atr1, Boron Exporter in Yeast

Boron, Biologically Active Compounds

Leonid Breydo
Department of Molecular Medicine, Morsani College of Medicine, University of South Florida, Tampa, FL, USA

Synonyms

AI-2 – autoinducer 2; BOR1 – borate transporter protein; RGII – rhamnogalacturonan II

Definition

Boron-containing compounds are primarily utilized by bacteria as quorum autoinducers and by plants as components of the cell wall. Many synthetic organoboron compounds are used as enzyme inhibitors.

Boron, Biologically Active Compounds, Fig. 1 Structure of RGII, a boron-containing polysaccharide present in the plant cell walls (**1**)

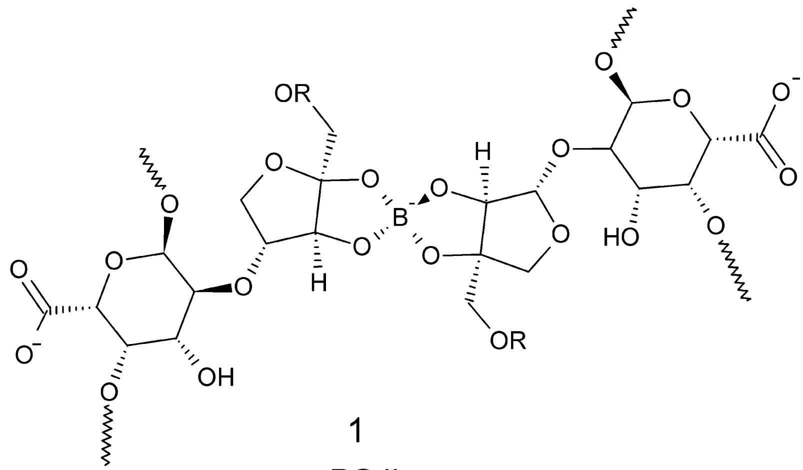

1

RG II

Introduction

Boron is a ubiquitous element in rocks, soil, and water; its average concentration ranging from 1 mg/kg in water to 100 mg/kg in rocks. Boron is electron-poor and prefers to form tetracoordinate complexes with "hard" nucleophiles. In physiological environment, it is present in +3 oxidation state, usually in the form of borate anion or borate esters. Borate anions form stable complexes with organic acids, polysaccharides, and other biopolymers. Usually borate complexes two hydroxyl groups (either a diol or a hydroxycarboxylic acid) to form a borate diester. Since boron can bind four ligands, in many cases, borate esters cross-link two organic molecules together.

Boron in Plants

Boron is a required nutrient for plants. Its main role is structural: a borate-cross-linked polysaccharide rhamnogalacturonan II (RGII) is an important component of cell walls (O'Neill et al. 2004). Rhamnogalacturonan II (RGII) is a structurally complex pectic polysaccharide. It is a 5–10 kDa polysaccharide composed primarily of D-galactose along with 11 other glycosyl residues (O'Neill et al. 2004). It was later discovered that it exists as a dimer covalently cross-linked by a borate diester (Fig. 1). Cross-linking of RGII is required for the formation of a three-dimensional pectic network in the cell walls and thus for normal plant development. Cross-linking is accelerated by divalent metal ions that are believed to bind to polysaccharides bringing them closer together. There is considerable evidence that RGII is present in cell walls of all gymnosperms and angiosperms. Interestingly, boron-cross-linked RGII is a major component of red wine (about 150 mg/l) where it complexes the majority of heavy metal ions present in wine (Pellerin and O'Neill 1998).

Boron uptake in plants is controlled by BOR1, a borate transporter (Takano et al. 2002). It is analogous to bicarbonate transporter, and its overexpression allows the plant to survive in low boron environment. Boron deficiency leads to significant problems with plant growth as the tissues of boron-deficient plants are often brittle and contain cells that do not expand normally.

Boron in Bacteria

Boron-containing compound also plays a role in quorum sensing in bacteria (Federle 2009). Quorum sensing is the process of cell-to-cell communication in bacteria. It allows bacterial populations to coordinate gene expression and increases the effectiveness of biofilm formation, antibiotic production, and other communal responses to the environment (Miller and Bassler 2001). It is accomplished via exchange of small molecules called autoinducers. These molecules are ligands for cytoplasmic or membrane-bound receptors that act as transcriptional regulators upon ligand binding. If ligand concentration is high enough, its

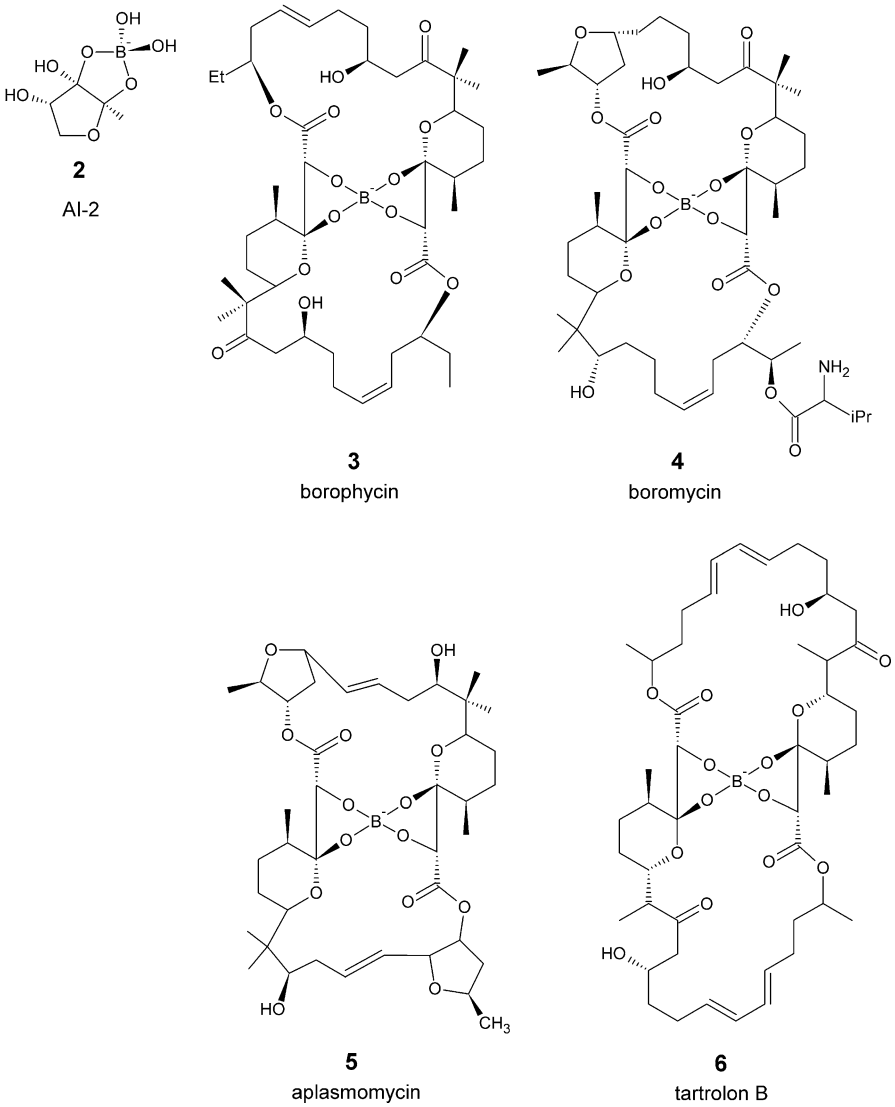

Boron, Biologically Active Compounds, Fig. 2 Boron-containing natural products: AI-2, an autoinducer of bacterial quorum sensing (**2**); antibiotics borophycin (**3**), boromycin (**4**), aplasmomycin (**5**), and tartrolon B (**6**)

receptor activates transcription of several genes including the one for the enzyme producing the autoinducer (Hodgkinson et al. 2007). Most autoinducers are specific to a single bacterial species while some are produced by a large number of species. AI-2 is one of those multi-species autoinducers. It actually corresponds to either of two diastereomers of 2-methyl-2,3,3,4-tetrahydroxytetrahydrofuran (THMF) that are formed by cyclization of a linear precursor. S-diastereomer of this compound exists as a borate diester while R-diastereomer is not boronated because its hydroxyl groups are in trans-configuration (Federle 2009). Borate diester is synthesized in a reaction of S-THMF with boric acid. Usage of S- versus R-diastereomer of AI-2 depends on the bacterial species. In the bacteria that use S-enantiomer of AI-2, signaling is significantly accelerated by addition of 10–100 μM boric acid (Chen et al. 2002). Upon uptake, AI-2 is phosphorylated and binds to a transcriptional repressor LsrR, releasing it from DNA and activating transcription of several genes (Xavier and Bassler 2005). Boronate ester likely stabilizes this autoinducer since in its absence, THMF is prone to isomerization, reductive elimination, and oligomerization via acetal formation (Dembitsky et al. 2011). Synthetic boron-containing analogs of AI-2 have been prepared, and some of them inhibit biofilm formation at micromolar concentrations (Dembitsky et al. 2011).

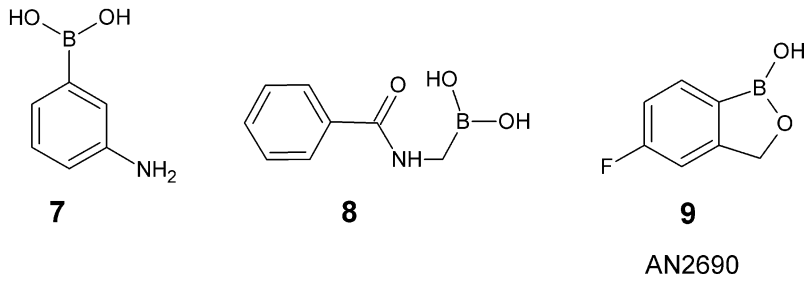

Boron, Biologically Active Compounds, Fig. 3 Boronic acids (**7**, **8**) and other boron-containing enzyme inhibitors (**9**)

Bacteria and fungi synthesize a variety of antibiotics to compete with other microorganisms. These natural products have been the source of many commercial antibiotics and drugs against other diseases such as cancer. Since boric acid is abundant in nature, boron is incorporated in some of these antibacterial natural products (Dembitsky et al. 2011). All known boron-containing antibiotics are polyketide antibiotics that contain a boronate diester bound to four hydroxyls (Fig. 2). These antibiotics include borophycin, boromycin, aplasmomycin, tartrolon B, and several of their derivatives. These antibiotics act as ionophores increasing permeability of the cell membranes for cations. Removal of boron from aplasmomycin resulted in loss of its ionophore activity, and this activity could be restored by addition of boric acid (Chen et al. 1980). It is likely that the role of boronate diester in these antibiotics is to maintain vicinal cis-diols in a specific conformation and increase their stability.

Boron in Animals

Boric acid and most organoboron compounds are nontoxic to humans with LD_{50} at 6 g/kg. In fact, boron is an essential or at least beneficial element in animals. Presence of specific borate transporter (a homolog of BOR1 in plants) in the human proteome indicates the importance of this element. Congenital endothelial dystrophy type 2, a rare form of corneal dystrophy, is associated with mutations in borate transporter, causing loss of function of this protein (Vithana et al. 2006).

Several physiological roles for boron in animals have been proposed although its exact function is unknown. Boron is important for calcium and magnesium metabolism. For example, low boron diet leads to poor absorption of calcium and magnesium and bone abnormalities (Armstrong et al. 2000). In addition, studies have shown the importance of boron-containing compounds in embryonic development in animals with low levels of borate leading to high percentage of necrotic embryos (Fort et al. 2002). It is also possible that borate diesters of galactose derivatives perform similar functions in animal membranes as RGII performs in the plant cell walls. Specifically, it has been proposed that borate diester–cross-linked polysaccharides stabilize lipid rafts and enhance membrane binding by GPI anchors of membrane proteins (Brown et al. 2002).

Biological Activity of Synthetic Organoboron Compounds

Structure of boronic acid resembles a transition state for the ester and amide hydrolysis. Thus, boronic acids such as **7** and **8** (Fig. 3) are effective inhibitors of hydrolytic enzymes (serine proteases, β-lactamases, and others) acting as transition state analogs (Dembitsky et al. 2011). In addition, high affinity of boron for oxygen ligands enables organoboron compounds such as boroxazole AN2690 (Fig. 3) to inhibit other enzymes. Boroxazoles similar to AN2690 inhibit leucyl t-RNA synthetase by forming stable adducts with oxygen atoms in the enzyme's active site (Rock et al. 2007).

Conclusions

Chemical properties of boron (stable (+3) oxidation state and ability to form strong covalent complexes with cis-diols and other oxygen ligands) drive the biological activity of this element. Stabilization of cis-diols is crucial to boron's role in both plants and bacteria. Its role in animals is not well understood but may involve the same chemistry. Many synthetic boron-containing compounds function as effective enzyme inhibitors.

Cross-References

- ▶ Atr1, Boron Exporter in Yeast
- ▶ Boron-containing Compounds, Regulation of Therapeutic Potential
- ▶ Boron Stress Tolerance, YMR279c and YOR378w

References

Armstrong TA, Spears JW, Crenshaw TD, Nielsen FH (2000) Boron supplementation of a semipurified diet for weanling pigs improves feed efficiency and bone strength characteristics and alters plasma lipid metabolites. J Nutr 130:2575–2581

Brown PH, Bellaloui N, Wimmer MA, Bassil ES, Ruiz JH, Pfeffer H, Dannel F, Romheld V (2002) Boron in plant biology. Plant Biol 4:205–223

Chen TS, Chang CJ, Floss HG (1980) Biosynthesis of the boron-containing antibiotic aplasmomycin. Nuclear magnetic resonance analysis of aplasmomycin and desboroaplasmomycin. J Antibiot (Tokyo) 33:1316–1322

Chen X, Schauder S, Potier N, Van Dorsselaer A, Pelczer I, Bassler BL, Hughson FM (2002) Structural identification of a bacterial quorum-sensing signal containing boron. Nature 415:545–549

Dembitsky VM, Al Quntar AA, Srebnik M (2011) Natural and synthetic small boron-containing molecules as potential inhibitors of bacterial and fungal quorum sensing. Chem Rev 111:209–237

Federle MJ (2009) Autoinducer-2-based chemical communication in bacteria: complexities of interspecies signaling. Contrib Microbiol 16:18–32

Fort DJ, Rogers RL, McLaughlin DW, Sellers CM, Schlekat CL (2002) Impact of boron deficiency on *Xenopus laevis*: a summary of biological effects and potential biochemical roles. Biol Trace Elem Res 90:117–142

Hodgkinson JT, Welch M, Spring DR (2007) Learning the language of bacteria. ACS Chem Biol 2:715–717

Miller MB, Bassler BL (2001) Quorum sensing in bacteria. Annu Rev Microbiol 55:165–199

O'Neill MA, Ishii T, Albersheim P, Darvill AG (2004) Rhamnogalacturonan II: structure and function of a borate cross-linked cell wall pectic polysaccharide. Annu Rev Plant Biol 55:109–139

Pellerin P, O'Neill MA (1998) The interaction of the pectic polysaccharide Rhamnogalacturonan II with heavy metals and lanthanides in wines and fruit juices. Analusis 26:32–36

Rock FL, Mao W, Yaremchuk A, Tukalo M, Crepin T, Zhou H, Zhang YK, Hernandez V, Akama T, Baker SJ et al (2007) An antifungal agent inhibits an aminoacyl-tRNA synthetase by trapping tRNA in the editing site. Science 316:1759–1761

Takano J, Noguchi K, Yasumori M, Kobayashi M, Gajdos Z, Miwa K, Hayashi H, Yoneyama T, Fujiwara T (2002) Arabidopsis boron transporter for xylem loading. Nature 420:337–340

Vithana EN, Morgan P, Sundaresan P, Ebenezer ND, Tan DT, Mohamed MD, Anand S, Khine KO, Venkataraman D, Yong VH et al (2006) Mutations in sodium-borate cotransporter SLC4A11 cause recessive congenital hereditary endothelial dystrophy (CHED2). Nat Genet 38:755–757

Xavier KB, Bassler BL (2005) Regulation of uptake and processing of the quorum-sensing autoinducer AI-2 in *Escherichia coli*. J Bacteriol 187:238–248

Boron: Physical and Chemical Properties

Fathi Habashi
Department of Mining, Metallurgical, and Materials Engineering, Laval University, Quebec City, Canada

Boron is a metalloid of no useful mechanical properties but used as an alloying element in steel. It is the second hardest element after diamond and is an essential plant nutrient. Relatively large quantities of amorphous boron are used as additives in pyrotechnic mixtures, solid rocket propellant fuels, and explosives. High-purity boron (>99.99%) is used in electronics. It is used as a ppm additive for germanium and silicon to make *p*-type semiconductors. Crystalline high-purity boron is used in thermistors. Boron filaments have been developed as reinforcing material for light-weight, stiff composites for use in commercial and military aircraft recently replaced by graphite filaments. In nuclear technology thin films of boron are used in neutron counters. Boron powder dispersed in polyethylene castings is used for shielding against thermal neutrons. The isotope boron-10 has a large neutron absorption cross section and is used as a control for nuclear reactors, as a shield for nuclear radiation, and in instruments used for detecting neutrons.

Boron compounds are extensively used in the manufacture of borosilicate glasses which have low coefficient of expansion hence can resist thermal shock, known under the trade name Pyrex. The borax bead test is a historical method of qualitative analysis for metals invented by Berzelius in 1812 and is based on the solubility of metal oxides in borax glass to give a distinctive color.

Physical Properties

There are several allotropic forms of boron. The β-rhombohedral form is the thermodynamically stable

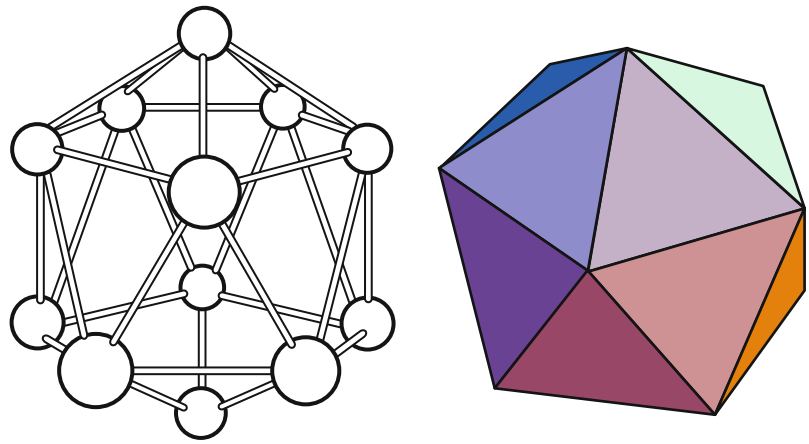

Boron: Physical and Chemical Properties, Fig. 1 Elemental boron, B_{12}, and the icosahedron

modification at all temperatures. Amorphous boron slowly converts to the β-rhombohedral form at ≈1,200°C and to α-rhombohedral boron above 1,500°C. Any type of boron recrystallizes in β-rhombohedral structure when heated above the melting point and cooled. In the stable modification, boron forms an icosahedron, B_{12}, in which the atoms are connected together by a covalent bond (Fig. 1). An icosahedron is a polyhedron having 12 vertices, 30 edges, and 20 equivalent equilateral triangle faces.

Atomic number	5
Atomic weight	10.811
Melting point, °C	2,050 ± 50
Sublimation point, °C	2,550
Density, g/cm^3	
Amorphous, at 20°C	2.3
β-rhombohedral, at 20°C	2.35
α-rhombohedral, at 20°C	2.46
Liquid at melting point	2.99
Solid at melting point	2.13
Color	
Amorphous	Brown to gray
α-rhombohedral	Red to brown
β-rhombohedral	Lustrous gray black
Hardness (Knoop), kg/mm^2	
Crystallized from melt	2,390
Vapor deposited	2,690
Electrical resistivity at 300 K, Ω cm	
Amorphous	7.5×10^2
β-rhombohedral, single crystal	7×10^5
β-rhombohedral, polycrystalline	10^6–10^7
Heat capacity C_p,J K^{-1} mol^{-1}	
Amorphous at 300 K	12.054
β-rhombohedral at 300 K	11.166
Solid at melting point	33.955
Liquid at melting point	39.063
Entropy S at 298 K, J K^{-1} mol^{-1}	
Amorphous	6.548
β-rhombohedral	5.875
Enthalpy of fusion, ΔH_f, kJ/mol	50.2
Enthalpy of sublimation, ΔH_s, kJ/mol	572.7

(*continued*)

Chemical Properties

Boric acid, $B(OH)_3$ is a weak acid. Boron oxide, B_2O_3, like SiO_2 has the ability to dissolve metallic oxides to form borates and glasses which are difficult to crystallize. Boron hydrides are gases of the composition B_nH_{n+4} and B_nH_{n+6}, are known as boranes. They are easily oxidized with considerable energy liberation and have been studied for use as rocket fuels. Boron nitride, BN, a soft white powder, has a structure like graphite and similar lubricating properties at high temperature. When heated at high temperature and under pressure it becomes very hard like diamond.

References

Baudis U et al (1997) Boron. In: Habashi F (ed) Handbook of extractive metallurgy. Wiley-VCH, Weinheim, pp 1985–2063

Habashi F (2009) Boron. Its history and its position in the periodic table. In: Konuk A et al. (eds) Fourth international boron symposium, Eskişehir, Turkey, pp 355–363

Boronated Amine

► Amine-Boranes

Boron-containing Compounds, Regulation of Therapeutic Potential

Ion Romulus Scorei
Department of Biochemistry, University of Craiova, Craiova, DJ, Romania

Synonyms

Cellular control mechanism for therapeutic potential of boron-containing compounds; The molecular mechanisms of the therapeutic action of boron-containing compounds

Definition

Boron is a micronutrient element necessary for the growth and development of vascular plants, marine algae and algal flagellates, diatoms, and cyanobacteria. Although boron has not been yet shown to be an essential nutrient in animal cells, more data will probably support this role in the future.

Boron compounds with therapeutic potential are the inorganic or organic compounds that contain boron as an integral part of the molecule and possess interesting pharmacological properties like hypolipidemic, anti-inflammatory, anti-osteoporosis, and antineoplastic.

Introduction

Boron (B) has been shown to possess the following characteristics: (1) It is a cell signaling molecule. (2) It is a co-factor of the enzymes it regulates. (3) It is a nonenzymatic cofactor. (4) It plays both structural and functional roles, including electron transfer, redox sensing, and structural modules. (5) It plays a role in the cytoskeleton structure (Scorei 2012).

Various types of B-containing molecules already exist and have been investigated as therapeutic agents. These molecules include B-containing analogues of natural biomolecules; the antibacterial and antimalarial agent diazaborine; antibacterial oxazaborolidines; antibacterial diphenyl borinic esters; the antifungal benzoxaboroles; and a B-N bond containing an estrogen receptor modulator (Scorei and Popa 2010).

Boron contains an empty *p*-orbital which makes it a strong electrophilic compound and a Lewis acid. It can readily form dative bonds with nucleophiles and thus, it transforms from an uncharged, trigonal-planar structure to an anionic, tetrahedral structure. This feature allows it to form dative bonds with nucleophiles in enzyme-active sites, providing additional binding affinity. The attractive characteristics of boron have not been let unnoticed by the pharmaceutical industry and the use of boron in pharmaceuticals has been expanding. Except for the drug Bortezomib, the majority of B-containing compounds are currently used in the cancer treatment and they belong to the Boron Neutron Capture Therapy (BNCT) class. Identification of the bacterial quorum sensor autoinducer 2 (AI2) as a B-containing stable complex (Park et al. 2005), of the transporters responsible for efficient B uptake in animal cells, and of the borate ability to inhibit many enzyme systems represents the discoveries of the boron chemistry and constitutes the basis of new drugs with boron atom included.

The Use of Boron-Containing Compounds as Potential Therapeutics

Natural Boron Compounds

Boric Acid and Borate Esters

Boric acid (BA) is an astringent, mild disinfectant, and is good for eye wash. Sodium borate is used in cold creams, eye washes, and mouth rinses.

BA is an inhibitor of peptidases, proteases, proteasomes, arginase, nitric oxide synthase, and transpeptidases (Hunt 1996). The inhibition of serine protease and dehydrogenase activities can be explained by the BA capacity to bind OH groups from NAD and serine. It has been demonstrated that BA controls the proliferation of some cancer cell types (Barranco and Eckhert 2004). The Prostatic Serum Antigen (PSA) is a serine protease and a putative target for BA (Scorei and Popa 2010). Based on the PSA inhibition, the use of BA in the chemical therapy of prostate carcinoma has been proposed (Devirian and Volpe 2003).

A high dose of BA (1–50 mM) slows down the cell replication and induces apoptosis in both melanoma cells and MDA. Thus, the inhibition of cancer cells by BA involves a diversity of cellular targets, such as direct enzymatic inhibition, apoptosis, receptor binding, and

mRNA splicing. Recently, it has been experimentally demonstrated that 1 mM of BA inhibits the ZR-75-1 breast cancer cell line, but not the MCF-7 cell line (Meacham et al. 2010). The lack of BA-mediated inhibition of MCF-7 cellular growth could be caused by the presence of the "sodium-boron co-transporter (NaBC1)." This co-transporter exists on the cell surface and is able to pump out boron molecules from the cell, in exchange for Na^+ ions. This co-transporter is not present in the ZR-75-1 cells. ZR-75-1 is a nonmetastatic epithelial breast cancer cell line, which is estrogen/progesterone receptor–positive. MCF-7 is a metastatic epithelial cell line of breast cancer. These cells are positive for estrogen and progesterone receptors. If BA becomes an anticancer agent for breast cancer, these data will encourage women with increased cancer risk factors to raise their boron intake, in order to diminish the evolution of this disease (Scorei 2011).

Calcium fructoborate (CF) is a commercially marketed borate ester naturally found in fresh and dried fruits, vegetables, and herbs, as well as in wine or produced by chemical synthesis (Scorei and Popa 2010). CF is efficient in the treatment (as adjuvant) of osteoporosis and osteoarthritis (Scorei and Rotaru 2011). In addition, CF has shown inhibitory effects on MDA-MB-231 breast cancer cells. CF enters most likely the cell through a co-transport mechanism, via a sugar transporter. MDA-MB-231 is a metastatic cancer cell line and it is negative for the estrogen receptor expression. Inside cells, CF acts as an antioxidant and induces the over-expression of apoptosis-related proteins, and eventually apoptosis (Scorei and Rotaru 2011).

Boron Polyketides

Generally speaking, B-containing macrolides such as boromycin, borophycin, tartrolon B, and aplasmomycin are antibiotic borodiesters and act as ionophores (Dembitsky et al. 2002).

Boromycin is a natural bacteriocidal polyether-macrolide produced by *Streptomyces antibioticus*, with antibiotic activity against Gram-positive bacteria. It acts at the cell membrane level and affects cells by losing the intracellular potassium. It also disrupts selectively the cell cycle in some cancer cell types, making them sensitive to specific anticancer agents, albeit the mechanism of action against eukaryotic cells remains little understood. Boromycin was recently discovered to be a potent antihuman immune-deficiency virus (HIV) antibiotic. It strongly inhibits the replication of the clinically isolated HIV-1 strain and apparently blocks the release of infectious HIV particles from the cells chronically infected with HIV-1, by unknown mechanisms. Synthesis, biosynthesis, and biological activities of boromycin derivatives have been described and reviewed (Dembitsky et al. 2011).

Borophycin is a polyketide and it is extracted from the species of *Nostoc*. It was shown to have inhibitory effects on several cancer cell lines. The compound exhibits potent cytotoxicity against human epidermoid carcinoma (LoVo) and human colorectal adenocarcinoma (KB) cell lines (Scorei and Popa 2010).

Tartrolons are macrolides with a chemical structure related to boromycin and aplasmomycin. They have antiviral and antineoplastic chemotherapeutic properties. Tartrolon B acts against Gram-positive bacteria and notably, it strongly inhibits the growth of mammalian cells (mouse fibroblasts) in culture.

Aplasmomycin, secreted by *Streptomyces griseus*, has known inhibitory effects against Gram-positive bacteria and *Plasmodium berghei*. It has not yet been verified against cancer cells, but is similar in structure with tartrolons which have anticancer properties.

Synthetic Boron Compounds

Boranes are a large class of B-containing derivatives, relevant in cancer treatments. Amine-carboxyboranes are efficient antineoplastic and cytotoxic agents, with selective action against unicellular tumors and leukemia-derived solid tumors, lymphoma, sarcoma, and carcinoma. Amine-cyanoboranes and amine-carboxyboranes have previously been shown to inhibit the induced inflammation in rodents. Dicarba-closo-dodecaborane (carborane) is a novel class of androgen receptor antagonists, with a hydrophobic skeletal structure and possible antitumor activity. Amine-boranes have cytotoxic activity and are of potential use in BNCT. Trimethylamine cyanoborane (TACB) inhibits DNA and protein synthesis in Ehrlich ascite cells, gene regulation via chromatin phosphorylation and methylation.

Borinic esters are a class of boron-containing compounds that showed broad-spectrum antibacterial activity with minimum inhibitory concentrations (MIC). They have been designed and synthesized with low μ/mL range.

Boronic acids are potent and selective inhibitors for the migration and viability of the cancer cells.

From the structural point of view, boronic acids are trivalent boron-containing organic compounds that possess one alkyl substituent (i.e., a C–B bond) and two hydroxyl groups, to fill the remaining valences on the boron atom. Due to the easy interconversion of boronic acids between the neutral sp2 (trigonal planar substituted) and the anionic sp3 (tetrahedral substituted) hybridization states, the B-OH unit replaces the C = O bond, at a site where an acyl group transfer takes place (Groziak 2001).

Phenylboronic acid (PBA) and diphenylboronic esters (DPBE) are the most efficient types of boronic acid derivatives, which act as serine protease inhibitors. PBA is more efficient than BA and decreases the cancer cell viability in 8 days. Non-tumorigenic cells are at least five times less sensitive to PBA, at the effective dose for cancer cells. These data suggest that PBA could be a promising cancer treatment and could be used prophylactically. PBA shows a selective inhibition of breast and prostate cancer migration in vivo and of tumor metastasis in mice (McAuley et al. 2012).

The drug Bortezomib (PS-341) is a boronic acid derivative and a proteasome inhibitor, in other words a novel target in cancer therapy. It disrupts the regulation of cell cycle and induces apoptosis. Bortezomib has been approved by the US Food and Drug Administration for the treatment of patients with chemorefractory multiple myeloma and for some forms of non-Hodgkin's lymphoma (Paramore and Frantz 2003). In cell cultures, Bortezomib induces apoptosis in both hematologic and solid tumor malignancies, including myeloma, mantle cell lymphoma, cell lung cancer, ovarian cancer, pancreatic cancer, prostate cancer, and head and neck cancers. Good correlation was seen between the Bortezomib dose, proteasome inhibition, and positive modulation of serum PSA. This indicates that Bortezomib could be used efficiently in combination with radiation or chemotherapy, for controlling androgen-independent prostate cancer. Until now, clinical experiments with Bortezomib have demonstrated only a limited activity against solid tumors when it is used as a single agent. However, Bortezomib has demonstrated its activity either as a single agent or in combination with several other cytotoxic agents, such as 5-fluorouracil, irinotecan, gemcitabine, doxorubicin, and docetaxel, or with radiation, enhancing both chemotherapy- and radiation therapy (RT)-induced apoptosis.

Benzoxaboroles – derivatives of boronic acids – were first described over 50 years ago. However, most of them have recently been investigated due to their exceptional properties and wide applications. For instance, it has been recently discovered that 5-fluoro-1,3-dihydro-1-hydroxy-2,1-benzoxaborole (AN2690) is an efficient broad-spectrum antifungal agent. The potency of molecules is believed to arise from the ability of boron atoms to form a stable adduct with the oxygen atoms of the leucyl-tRNA synthetase, effectively inhibiting the enzyme. After the discovery of the excellent antifungal activity of the 5-fluoro-substituted benzoxaborole (AN2690) against onychomycosis, a systematic investigation of the medical applications of benzoxaboroles is conducted. Some of them are currently in preclinical and clinical trials (Baker et al. 2011).

Oxazaborolidines are compounds that possess a B-N bond, and are readily obtained from an amino alcohol and a boronic acid. Nevertheless, despite their ubiquity in organic synthesis, the effect of oxazaborolidines on bacterial adhesion, biofilm formation, or any other pharmacological activity has been recently known. Several representative oxazaborolidines have been synthesized and evaluated for their antibacterial activity against *S. mutans*, which is one of the most predominant bacteria in the etiology of dental caries (Dembitsky et al. 2011).

The Molecular Mechanisms of the Boron-Containing Compounds as Potential Therapeutics

Boron compounds like BA, borates, boranes, boronic esters, boronic acids, and borate esters influence many cellular processes. A short list includes B transport, cell growth, mitogen-activated protein kinase pathway, proteasomes, and apoptosis. Regarding the identification of the genes involved, most of the research work was realized on BA and borate esters versus B transport, and also on boronic-esters versus proteasomes. The mechanisms involved are largely unknown. The ratio between borate and BA and the pH are important in controlling the borate transport (Park et al. 2005). In yeasts, it is likely that the signal transduction pathways, with roles in B exchange, B resistance, and amino acid biosynthesis, share a common activator. Such work has not been realized

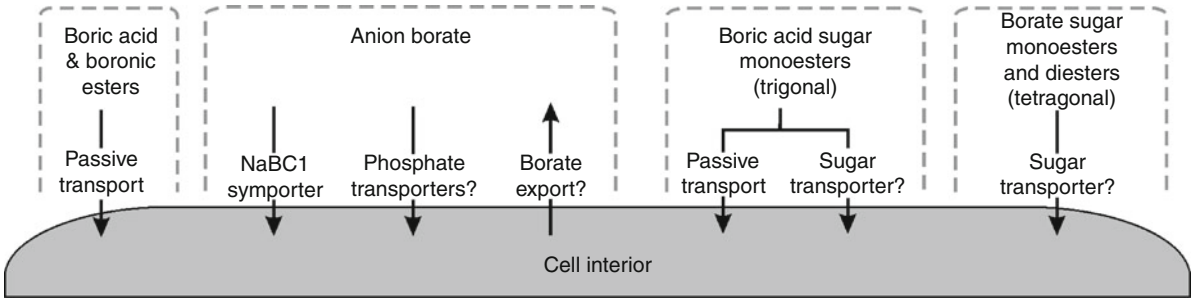

Boron-containing Compounds, Regulation of Therapeutic Potential, Fig. 1 Known and putative mechanisms for the transport of boron compounds (boric acid, borate, borate sugar esters, and boronic esters) into cells

yet on animal cells. If so, it would help decipher the interaction between B and cellular processes. Hence, the regulation of borates exporters may not be related to a redox process, but to a BA/borate speciation.

Boron as Signaling Molecule

One of the most exciting discoveries of the past years was the identification of the bacterial quorum sensor autoinducer 2 (AI2) as a B-containing stable complex (Dembitsky et al. 2011). Quorum sensing is a bacterial intercellular communication process that coordinates gene expression across cells, to initiate events such as bioluminescence, biofilm formation, production of virulence factors, etc. The B-containing autoinducer AI-2, a hydrated boric acid complex with a tetrahydroxydihydrofuran, was identified as ligand in an X-ray structure of the auto-sensor protein LuxP (Baker et al. 2011). Regulation of the quorum sensing as an approach to antimicrobial therapy was the subject of a recent review (Lowery et al. 2010).

Some main paradigms have been explored in developing the QS modulators as potential therapeutics: (1) interference with the signal synthase, (2) sequestration of the autoinducer, (3) antagonism of the receptor, with receptor antagonism having received the most attention to date for the discovery of QS modulators, (4) prevention of the signal secretion, and (5) inhibition of the downstream signaling events. Several arylboronic acids were found to inhibit AI-2-induced bioluminescence, with IC50 values of low or sub-micromolar concentrations.

Regulation of the Boron Transport in Cell

B is needed by cells in small amounts. In excess, BA and borate are toxic. Living cells regulate the internal concentration of borate, using specialized transporters, though the mechanism of regulation remains little understood.

Electrically neutral boron compounds can cross passively the membrane, while the borate anion is transported by aquaporins, such as APQ9, or by the specialized borate transporter, NABC1. Borate ions activate the mitogen-activated protein kinases pathway and stimulate the growth and the proliferation of human embryonic kidney 293 cells (Park et al. 2005). The B-transporter NaBCl controls the plasma borate levels in human kidney cells. The finding that low concentrations of borate activate the MAPK pathway and the knockdown of NaBC1 halted the cell growth and proliferation provide further evidence for the essential functional role of B in animal metabolism. Potential paths for the transport of B compounds in animal cells are summarized in Fig. 1.

B transporters practically limit the use of BA in cancer treatments. Some cancer cells have impaired ability to eliminate the excess of borate and are about five times more boron/apoptosis sensitive than the normal cells (Park et al. 2005).

Boron and the Enzymatic Activity

The mechanisms involving boron activity on human cells are based on the inhibition of a variety of enzymatic activities including serine proteases, cyt *b*5 reductase, dehydrogenase of xanthine oxidase, glutamyl transpeptidase, alkaline phosphatase, alcohol NAD-dehydrogenases, mRNA splicing and cell division, but also on receptor binding mimicry and on the induction of apoptosis. Borate forms complex between amino and hydroxy groups in proteins and targeting residues of lysine, glutamine, serine, hystidine, and proline. They also bind polyhydroxy compounds including sugars, such as mannitol, xylitol, sorbitol, glucose,

fructose, and ribose from NAD and FAD; phenols, such as catechol and pyrogallol; and α-hydroxy acids, such as 2-hydroxyisobutyric acid, salicylic acid, and *cis*-2-hydroxycyclopentanecarboxyric acid. The effect of borate as phosphate substituent might be also common, but it was less studied. Borate stabilizes the architecture and activity of alkaline phosphatase, protecting it from the oxidative stress. Boron was also shown to increase the resistance of heme-containing proteins, such as cyt *c* and metmyoglobin, to thermal stress, by increasing thermal stability to inactivation and resistance to denaturizing. These effects might be also due to boron protection of the 3D structure. Interestingly, cyt *b* is regulated by the boron concentration and inhibited when boron is above or below the optimal concentrations.

This fact has therapeutic implications, as boron can be used to stabilize the peroxide-sensitive heme proteins.

Boron and Proteasome Inhibition

Proteasomes are large protein complexes from eukaryotes, responsible for recycling ubiquitinated proteins. Proteasome alterations were associated to several diseases, such as cardiac dysfunction, cataract, neurodegenerative disorders, cachexia, and rheumatoid diseases. They have not been linked yet with cancer development. Several anti-apoptotic and proliferative signaling pathways require proteasomal activity. In the pro-oncogenic NF-κB pathway, which is activated and prevalent in the regulation of many tumor types, NF-κB proteins are kept in the inactive state by IκBs inhibitors. In order to remove this inhibition, IκBs have to be phosphorylated, polyubiquitylated, and then recycled by proteasome. The proper functioning of the proteasome complex seems to require boron within a specific concentration range. Less or more boron will inhibit the activity of proteasomes (Scorei 2012). In high concentration, boric acid and boronic acid slow down the carcinogenic progression, because they block the IκBs degradation, which in turn downregulates the NF-κB signaling. Bortezomib inhibits proteasomes through the formation of complexes with their active site. The relationship between apoptosis and the Bortezomib effects on cells is rather complex. The over-expression of the anti-apoptotic protein Bcl-2 in H460 cells does not affect the proteasomal activity, but decreases the effect of Bortezomib on apoptosis.

Boron-Containing Compounds as Inhibitors of Serine Proteases

Serine proteases, a large and functionally diverse class of proteolytic enzymes, are prominent therapeutic targets, due to their involvement in a host of physiological processes. They catalyze the peptide bond cleavage by acylation and deacylation of the active site serine residue, in a sequence that involves two tetrahedral intermediates. Peptide derivatives with electron-deficient ketones, aldehydes, boronic acids, and phosphonylating agents have been devised as analogues of the second tetrahedral intermediate, with their selectivity among the various proteases related to the substrate specificity. The expression of many of these proteases is thought to be linked with the pathogenicity of Gram-negative bacteria. This requires further studies to obtain more profound concepts. It has been shown that these enzymes facilitate the bacterial colonization of the skin and mucous membranes. Boronic acids are a very appealing class of serine proteases inhibitors.

Boron and Vitamin D3

Epidemiological studies have shown an inverse correlation between the exposure to solar radiation and breast cancer incidence and mortality (Scorei 2011). This was suggested to be linked with Vitamin D2 production. Vitamin D3 (calcitriol), a derivative of D2, has an important role in regulating the prostatic cell growth, with demonstrated effects on the prostate cancer cell line LNCaP31. Vitamin D3 arrests the cell cycle, induces apoptosis, and inhibits metastases. It also inhibits the proliferation of the prostate cancer cells. Its activity of tumor inhibition might be due to the induction of cyclin-dependent kinase inhibitor p21 and G1-G0 cell cycle arrest. This may explain the regression of the cancer cell growth in vitamin D3–treated rats. Vitamin D3 also initiates its own inactivation because it is able to induce the expression of a protein CYP24 that initiates the vitamin D3 catabolism, which is a mechanism present in the cells. It was shown that boron, in general, and fructoborate, in particular, increase the intracellular concentration of vitamin D3 (Scorei 2011). This effect might occur due to the fact that boron up-regulates the 25-hydroxylation step or suppresses the vitamin D3 catabolic pathway. Boron readily forms covalent complexes with *cis*-vicinal dihydroxy compounds and it is reasonable to assume that boron forms complexes with

24,25-dihydroxyvitamin D, the final product of the 25-OH-D reaction with 24-hydroxylase. This complex acts as a competitive inhibitor for the 24-hydroxylase reaction or as a downregulator for this enzyme. Boron may be an inhibitor for microsomal enzymes (24-hydroxylase and estradiol hydroxylases) that catalyze the insertion of the hydroxyl group vicinal to the existing hydroxyl groups in steroids. Consequently, the combinations between vitamin D3 and boron may become widespread in prostate cancer therapies.

Borate: Phosphate Similarities

A negative correlation has been reported to exist between the phosphate concentration and borate, in various types of cells from plants and in normal versus osteoporotic bones (Nielsen 2008). Borate was shown to enhance the phosphorylation. In human cells, it affects living cells via a mediator, putatively TNF-alpha, in which transduction signal involves a cascade of phosphorylations. Although many similarities exist in structure and activity between borate and phosphate, the borate: phosphate substitution and its effect was relatively little studied. Phosphate esters are important in cellular-energetic, biochemical activation, signal transduction, and conformational switching. The borate:phosphate similarity, combined with borate's ability to spontaneously esterify the hydroxyl groups, suggests that phosphate ester recognition sites on proteins might exhibit significant affinity for nonenzymatically formed borate esters. In normal cells, the borate:phosphate competition is little because phosphate is thousands of times more abundant and in some complexes, such as with cytidine-2′,3′ and RNAse, the affinity of phosphate is higher than that of borate. Will borate increase the effects of borate: phosphate similarity in phosphate-starved treatment? These results are consistent with the recent reports suggesting that in situ formation of borate esters, which mimic the corresponding phosphate esters, supports the enzyme catalysis (Gabel and London 2008).

Boron Esters as Anti-inflammatory Agents

The relationship between inflammation and cancer is realized through the elaboration of cytokines and growth factors, favoring the cancer cell growth, the induction of the COX-2, a protein that controls the synthesis of prostaglandins linked with tumor proliferation, and the generation of mutagenic reactive chemical species of oxygen and nitrogen (Nielsen and Meacham 2011). Cytokines produced during inflammation increase the expression of 5-lipoxygenase (5-LOX), leading to metabolites driving cancer development. Inhibiting 5-LOX metabolites triggers apoptosis in prostate cancer cells. Boron's anti-inflammatory activity may occur via the suppression of serine proteases released by inflammation-activated white blood cells, inhibition of leukotriene synthesis, reduction of reactive oxygen species generated during neutrophils respiratory burst, and suppression of T-cell activity and antibody concentrations. Boron inhibits the synthesis of arachidonic acid (AA)–derived eicosanoids, a class of pro-inflammatory prostaglandins. High boron intake leads to boron incorporation in membrane phospholipids, partially substituting AA-derived eicosanoids and increasing the abundance of the omega-3-derived eicosapentaenoic acid. The treatment with calcium fructoborate of the LPS-stimulated RAW264.7 macrophages inhibited the synthesis of the cytokines IL-1β and IL-6 and released the nitric oxide (NO). IL-1b, IL-6, and NO are inflammation mediators and researchers have proposed the use of CF as an anti-inflammatory agent (Scorei and Rotaru 2011).

Future Directions

Normal and Cancer Cell Boron Toxicity: A Novel Avenue in the Fight Against Cancer

The recommended daily dose of boron in humans is between 0.14 and 0.28 mg per day Kg body weight (bw). The 50% lethal dose of B as boric acid is of 2,660 mg per Kg bw. It is relatively close to that of the table salt (3,000 mg per Kg bw). For these reasons, B is not considered to be a toxic element (Baker et al. 2011). The daily doses of borate between 2.5 and 24.8 mg per kg bw, used in the past to treat epilepsy, were shown to have nonlethal side effects such as alopecia, and reversible side effects such as dermatitis, anorexia, and indigestion. In cell cultures, all cancer cells died at B concentrations varying from 1 to 50 mM boric acid. Non-cancer cells were shown to be about five times more resistant to B. No bibliographic evidence for a correlation between B exposure and carcinogenesis has been found, and no mutagenic effects have yet been reported for BA.

Based on the apoptosis measurements, some cancer cells were shown to be more sensitive to B than normal

cells (Scorei and Popa 2010). The BA sensitivity varies among different cancer cell lines and has shown that the sensitivity of the cultured cancer cells was negative correlated with the expression of the NaBC1 borate transporter. This indicates that apart from its borate import function, NaBC1 might be also used to regulate the level of the intracellular borate through export. These works were done in the range of 1–50 mM BA. Based on the fact that about 90% of boron is eliminated from the human body within 22–24 h, the above presented exposure treatments led to cancer cell apoptosis, corresponding to an approximate daily intake of B between 4.4 and 51.4 mg per Kg bw. This exposure is below the B toxic levels (see above) and is near the B exposure levels used in the past to treat epilepsy. For these reasons, B is a promising avenue for inducing apoptosis in some forms of cancer. B treatments are proposed to be the most efficient against cancer cell lines, showing an under-expression of NaBC1, when B is administered as nontoxic compounds such as boron sugar esters (BSE) or as BA. The BSE would be particularly more efficient against cancer cells that, unlike normal cells, also show an over-expression of the sugar transporters, glucose and fructose channels. Thus, cancer cells are exposed to an increased risk in the presence of B that enters masked, as a sugar derivative (Scorei and Rotaru 2011).

Boron and the Fight Against Osteoporosis

The trace element boron, previously thought to have no nutritional value, might play a key role in the fight against osteoporosis, the bone-thinning disease. B impacts steroid hormone metabolism in humans, affecting the levels of estrogens and testosterone. It has been hypothesized that B interacts with steroid hormones by facilitating the hydroxylation reactions and possibly by acting in some manner to protect steroid hormones from rapid degradation. Nielsen et al. reported that boron supplementation of 3 mg per day decreases urinary Ca and P excretion in humans. A significant increase in the concentration of plasma steroid hormones has also been demonstrated in rats and humans. The synthesis of vitamin D seems necessary, as well. It is believed that optimum boron supplementation regulates the catabolic enzymatic hydroxylation. Given all these effects of boron, it is not surprising that it is beneficial for the optimum calcium metabolism. This is very useful in the prevention of bone loss and generally in some disorders of unknown etiology such as osteoporosis. The latter exhibits disturbed major mineral metabolism and an impact on osteoarthritis by increasing the synthesis of corticosteroids. Recent results have shown that additional boron has a positive effect on the ostrich tibia growth and development, but a high dosage of boron has a negative effect. According to the present data, a boron supplementation of 200 mg/L in water represents the optimal dosage for bone development in ostrich chicks. The dietary boron supplements can increase the serum content of boron in osteoporotic rats to stimulate the bone formation and to inhibit the bone resorption, producing an obviously therapeutic effect against osteoporosis (Hosmane 2011).

Thus, boron supplements might be useful in the treatment of osteoporosis and in the maintenance of healthy women in the future.

Cross-References

- ▶ Amine-Boranes
- ▶ Atr1, Boron Exporter in Yeast
- ▶ Boron and Aquaporins
- ▶ Boron Stress Tolerance, YMR279c and YOR378w
- ▶ Boron, Biologically Active Compounds

References

Baker SJ, Tomshob JW, Benkovicc SJ (2011) Boron-containing inhibitors of synthetases. Chem Soc Rev 40:4279–4285

Barranco WT, Eckhert CD (2004) Boric acid inhibits human prostate cancer cell proliferation. Cancer Lett 216(1):21–29

Dembitsky VM, Smoum R, Al-Quntar AAA, Ali HA, Pergament I, Srebnik M (2002) Natural occurrence of boron-containing compounds in plants, algae and microorganisms. Plant Sci 163:931–942

Dembitsky VM, Al-Quntar AAA, Srebnik M (2011) Natural and synthetic small boron-containing molecules as potential inhibitors of bacterial and fungal quorum sensing. Chem Rev 111:209–237

Devirian T, Volpe S (2003) The physiological effects of dietary boron. Crit Rev Food Sci Nutr 43:219–223

Gabel SA, London RE (2008) Ternary borate-nucleoside complex stabilization by Ribonuclease A demonstrates phosphate mimicry. J Biol Inorg Chem 13(2):207–217

Groziak MP (2001) Boron therapeutics on the horizon. Am J Ther 8:321–328

Hosmane NS (ed) (2011) Boron science: new technologies and applications. CRC Press/Northern Illinois University, Dekalb

Hunt CD (1996) Biochemical effects of physiological amounts of dietary boron. J Trace Elem Exp Med 9(4):185–213

Lowery CA, Salzameda NT, Sawada D, Kaufmann GF, Janda KD (2010) Medicinal chemistry as a conduit for the modulation of quorum sensing. J Med Chem 53(21):7467–7489
McAuley EM, Bradke TA, Plopper GE (2012) Phenylboronic acid is a more potent inhibitor than boric acid of key signaling networks involved in cancer cell migration. Cell Adh Migr 5:382–386
Meacham S, Karakas S, Wallace A, Altun F (2010) Boron in human health: evidence for dietary recommendations and public policies. Open Miner Process J 3:36–53
Nielsen FH (2008) Is boron nutritionally relevant? Nutr Rev 66:183–191
Nielsen F, Meacham S (2011) Growing evidence for human health benefits of boron. J Evid Based Complement Alternat Med. doi:10.1177/2156587211407638
Paramore A, Frantz S (2003) Bortezomib. Nat Rev Drug Discov 2:611–612
Park M, Li Q, Shcheynikov N, Muallen S, Zeng W (2005) Borate transport and cell growth and proliferation: not only in plants. Cell Cycle 4(1):24–26
Scorei R (2011) Boron compounds in the breast cancer cells chemoprevention and chemotherapy. In: Gunduz E, Gunduz M (eds) Breast cancer – current and alternative therapeutic modalities. InTech, Rijeca, pp 91–114
Scorei R (2012) Is boron a prebiotic element? A mini-review of the essentiality of boron for the appearance of life on Earth. Orig Life Evol Biosph 42(1):3–17.
Scorei R, Popa R (2010) Boron-containing compounds as preventive and chemotherapeutic agents for cancer. Anti-Cancer Agents Med Chem 10:346–351
Scorei RI, Rotaru P (2011) Calcium fructoborate – potential anti-inflammatory agent. Biol Trace Elem Res 143(3):1223–1238

Botano-Remediation

► Lead and Phytoremediation

BSA-Coated AgNPs

► Colloidal Silver Nanoparticles and Bovine Serum Albumin

Burn Dressing

► Silver, Burn Wound Sepsis and Healing

Burn Wound Infection

► Silver, Burn Wound Sepsis and Healing

Burn Wound Reepithelialization

► Silver, Burn Wound Sepsis and Healing

Burn Wound Treatment

► Silver, Burn Wound Sepsis and Healing